

From: "Jeffrey Kimball" <JeffreyK@DNFSB.GOV>
To: "Sarah Gonzalez" <SHG1@nrc.gov>
Date: 10/29/2007 9:13:30 AM
Subject: Re: thanks

Sarah here is the subject report electronically, also the follow up report is also attached. In the comparison report the discussion is found on page 2-8, also the final EPRI PSHA report is clearly referenced so that work was out as final, see for example the references on page 4-10. I think I will try and sit in on the ACRS meeting on Thurs. Jeff

>>> "Sarah Gonzalez" <SHG1@nrc.gov> 10/29/2007 8:56 AM >>>
Hi Jeff,
Thanks so much for taking the time to talk to us this morning! We really appreciate it.
--Sarah

Hearing Identifier: Vogtle_Non_Public
Email Number: 8043

Mail Envelope Properties (475E55D4.HQGWDO01.TWGWPO04.200.2000004.1.101401.1)

Subject: Re: thanks
Creation Date: 10/29/2007 9:13:30 AM
From: "Jeffrey Kimball" <JeffreyK@DNFSB.GOV>

Created By: JeffreyK@DNFSB.GOV

Recipients

"Sarah Gonzalez" <SHG1@nrc.gov>

Post Office

TWGWPO04.HQGWDO01

Route

nrc.gov

Files

Size

Date & Time

MESSAGE

530

10/29/2007 9:13:30 AM

REI Comparison of LLNL and EPRI Hazard at SRS.pdf

2775276

12/11/2007 9:18:12 AM

REI Evaluation of SRS Seismic Hazard.pdf

2114231

12/11/2007 9:18:12 AM

Mime.822

6693324

12/11/2007 9:18:12 AM

Options

Priority: Standard

Reply Requested: No

Return Notification: None

None

Concealed Subject: No

Security: Standard

**COMPARISON AND ANALYSIS
OF ASSUMPTIONS IN
LLNL AND EPRI SEISMIC HAZARD STUDIES
FOR THE
SAVANNAH RIVER SITE**

Prepared for

**Westinghouse Savannah River Company
Aiken, South Carolina**

by

**Risk Engineering, Inc.
5255 Pine Ridge Road
Golden, Colorado**

March 22, 1990

CONTENTS

| <u>Section</u> | <u>Page</u> |
|--|-------------|
| 1 INTRODUCTION | 1-1 |
| 2 SEISMIC SOURCES AND SEISMICITY PARAMETERS | 2-1 |
| 2.1 LLNL Seismic Sources and Seismicity Parameters | 2-1 |
| 2.2 EPRI Seismic Sources and Seismicity Parameters | 2-4 |
| 2.3 Comparisons | 2-6 |
| 2.4 EFFECT ON CALCULATED HAZARD | 2-7 |
| 2.5 REFERENCES | 2-11 |
| 3 GROUND-MOTION ATTENUATION | 3-1 |
| 3.1 INTRODUCTION | 3-1 |
| 3.2 ATTENUATION FUNCTIONS FOR GROUND MOTIONS ON ROCK | 3-1 |
| 3.2.1 LLNL Attenuation Functions | 3-1 |
| 3.2.2 EPRI Attenuation Functions | 3-1 |
| 3.2.3 Comparison | 3-4 |
| 3.3 SOIL AMPLIFICATION MODELS | 3-8 |
| 3.3.1 LLNL Models | 3-8 |
| 3.3.2 EPRI Models | 3-8 |
| 3.3.3 Comparisons | 3-8 |
| 3.4 EFFECT OF ATTENUATION FUNCTIONS AND SITE FAC- TORS ON CALCULATED HAZARD | 3-9 |
| 3.5 REFERENCES | 3-11 |

| | | |
|-----|---|------|
| 4 | RECOMMENDATIONS | 4-1 |
| 4.1 | SEISMICITY MODELS | 4-1 |
| 4.2 | ATTENUATION FUNCTIONS FOR GROUND MOTIONS ON ROCK | 4-8 |
| 4.3 | SOIL AMPLIFICATION MODEL | 4-9 |
| 4.4 | REFERENCES | 4-10 |
| 5 | CONCLUSIONS | 5-1 |

LIST OF FIGURES

| <u>Figure</u> | | <u>Page</u> |
|---------------|--|-------------|
| 2-1 | Seismic sources that dominate the calculated hazard at the SRP site; base map for S-Expert 1. | 2-12 |
| 2-2 | Seismic sources that dominate the calculated hazard at the SRP site; base map for S-Expert 2. | 2-13 |
| 2-3 | Seismic sources that dominate the calculated hazard at the SRP site; base map for S-Expert 3. | 2-14 |
| 2-4 | Seismic sources that dominate the calculated hazard at the SRP site; base map for S-Expert 4. | 2-15 |
| 2-5 | Seismic sources that dominate the calculated hazard at the SRP site; base map for S-Expert 5. | 2-16 |
| 2-6 | Seismic sources that dominate the calculated hazard at the SRP site; base map for S-Expert 6. | 2-17 |
| 2-7 | Seismic sources that dominate the calculated hazard at the SRP site; base map for S-Expert 7. | 2-18 |
| 2-8 | Seismic sources that dominate the calculated hazard at the SRP site; base map for S-Expert 10. | 2-19 |
| 2-9 | Seismic sources that dominate the calculated hazard at the SRP site; base map for S-Expert 11. | 2-20 |
| 2-10 | Seismic sources that dominate the calculated hazard at the SRP site; base map for S-Expert 12. | 2-21 |
| 2-11 | Seismic sources that dominate the calculated hazard at the SRP site; base map for S-Expert 13. | 2-22 |
| 2-12 | Best-estimate hazard curves for the the S-Experts; Vogtle site. | 2-23 |
| 2-13 | Seismic sources that dominate the calculated hazard at the SRP site; Bechtel Team. | 2-24 |
| 2-14 | Seismic sources that dominate the calculated hazard at the SRP site; Dames and Moore Team. | 2-25 |

| | | |
|------|--|------|
| 2-15 | Seismic sources that dominate the calculated hazard at the SRP site; Law Team. | 2-26 |
| 2-16 | Seismic sources that dominate the calculated hazard at the SRP site; Rondout Team. | 2-27 |
| 2-17 | Seismic sources that dominate the calculated hazard at the SRP site; Weston Team. | 2-28 |
| 2-18 | Seismic sources that dominate the calculated hazard at the SRP site; Woodward-Clyde Team. | 2-29 |
| 2-19 | Median hazard curves for the the EPRI Teams; SRP site. | 2-30 |
| 3-1 | Comparison of predicted peak acceleration by the LLNL and EPRI attenuation equations. Predictions are shown for m_b 5 and 7. | 3-6 |
| 3-2 | Comparison of response spectra predicted by the SOG and LLNL attenuation equations. Predictions are shown for an epicentral distance of 25 km and for m_b 5 and 7. | 3-7 |
| 3-3 | LLNL median site-amplification factors. | 3-12 |
| 3-4 | Site-amplification factors used by G-Expert 5. | 3-13 |
| 3-5 | EPRI site amplification factors for 1-Hz spectral velocity (5% damping), for the 5 site categories. | 3-14 |
| 3-6 | EPRI site amplification factors for 2.5-Hz spectral velocity (5% damping), for the 5 site categories. | 3-15 |
| 3-7 | EPRI site amplification factors for 5-Hz spectral velocity (5% damping), for the 5 site categories. | 3-16 |
| 3-8 | EPRI site amplification factors for 10-Hz spectral velocity (5% damping), for the 5 site categories. | 3-17 |
| 3-9 | EPRI site amplification factors for 25-Hz spectral velocity (5% damping), for the 5 site categories. | 3-18 |
| 3-10 | EPRI site amplification factors for peak ground acceleration, for the 5 site categories. | 3-19 |
| 3-11 | Median hazard curves for each LLNL attenuation function; SRP zonations and seismicity parameters by the EPRI Teams. | 3-20 |
| 3-12 | Median hazard curves for each EPRI attenuation function; SRP zonations and seismicity parameters by the EPRI Teams. | 3-21 |
| 3-13 | Hazard curves for each LLNL attenuation function; SRP zonation and best-estimate seismicity parameters by S-Expert 6. | 3-22 |

| | | |
|------|---|------|
| 3-14 | Hazard curves for each EPRI attenuation function; SRP zonation and best-estimate seismicity parameters by S-Expert 6. | 3-23 |
| 3-15 | Hazard curves for each LLNL attenuation function; SRP zonation and best-estimate seismicity parameters by S-Expert 2. | 3-24 |
| 3-16 | Hazard curves for each EPRI attenuation function; SRP zonation and best-estimate seismicity parameters by S-Expert 2. | 3-25 |
| 4-1 | Seismicity of region around SRP, as contained in the EPRI catalog | 4-11 |
| 4-2 | Comparison of observed seismicity in the Charleston area (50 km radius) with the models of seismicity specified by the LLNL Experts | 4-12 |
| 4-3 | Comparison of observed seismicity in the Charleston area (50 km radius) with the models of seismicity specified by the EPRI Teams | 4-13 |
| 4-4 | Comparison of observed seismicity in the Charleston area (50 km radius) with the characteristic model of seismicity | 4-14 |
| 4-5 | Effect of the characteristic magnitude distribution on the calculated hazard; Rondout Team. | 4-15 |
| 4-6 | Results from the statistical analysis of the geographic distribution of earthquakes within source 18 by LLNL Expert 6 | 4-16 |

LIST OF TABLES

| <u>Table</u> | | <u>Page</u> |
|--------------|---|-------------|
| 2-1 | Summary of Dominant LLNL Seismic Sources and their Parameters | 2-3 |
| 2-2 | Summary of Dominant EPRI Seismic Sources and Their Parameters | 2-5 |
| 2-3 | Base-Case Parameter Values | 2-7 |
| 2-4 | Effect of Seismological Assumptions on Calculated Hazard (cases where Charleston source dominates the hazard) | 2-9 |
| 2-5 | Effect of Seismological Assumptions on Calculated Hazard (cases where host source dominates the hazard) | 2-10 |
| 3-1 | LLNL Peak Acceleration Models | 3-2 |
| 3-2 | LLNL Spectral Velocity Models | 3-3 |
| 3-3 | EPRI Ground Motion Attenuation Models | 3-5 |
| 3-4 | Effect of G-Expert 5 on Hazard Calculated by LLNL | 3-10 |
| 4-1 | Summary of Historical Earthquakes in the Charleston Region | 4-3 |
| 4-2 | Completeness Period and Activity Rates for the Charleston Source | 4-4 |
| 4-3 | Recommended LLNL and EPRI Seismicity Models | 4-7 |

Section 1
INTRODUCTION

Two state-of-the art seismic hazard studies have been recently performed for the Savannah River Plant (SRP). One study was performed by the Lawrence Livermore National Laboratory (LLNL) and used the inputs and methodology developed by LLNL (supported by the U.S. Nuclear Regulatory Commission). The other study was performed by the firm of Jack Benjamin and Associates and used the inputs and methodology developed by the Electric Power Research Institute (EPRI; sponsored by the Seismic Owners' Group, a group of eastern U.S. electric utilities.)

Although the LLNL and EPRI methodologies differ in how the inputs are parametrized and in computational details, the two methodologies are equivalent. That is, given the same input they will produce essentially the same output. Differences between the LLNL and EPRI results are due to differences in the input assumptions (e.g., geometries of seismic zones, seismicity and maximum magnitudes, and ground-motion attenuation).

This report compares the key assumptions in each study, quantifies the effects of the various assumptions on the calculated hazard, and recommends a set of assumptions to use in the evaluation of seismic hazard at SRP.

Section 2

SEISMIC SOURCES AND SEISMICITY PARAMETERS

2.1 LLNL SEISMIC SOURCES AND SEISMICITY PARAMETERS

The LLNL seismic-hazard calculations use the seismic sources and seismicity parameters developed by 11 panelists (the S-Experts). Figures 1 through 11 show the seismic sources that dominate the calculated hazard at the SRP site for each S-Expert.

To characterize his uncertainty on the existence and parameters of each seismic source, each expert specified his confidence that the source exists, and specified probability distributions for the source's seismicity parameters (i.e., activity rate, b value, and maximum magnitude). This analysis will focus on the S-Experts' base map and best-estimate parameter values.

Figure 2-12 shows the PGA hazard curves for the Vogtle site, obtained using the S-Expert's best-estimate parameters. There are very large differences among these hazard curves, especially for accelerations above 0.5 g. In particular, the three highest hazard curves are considerably higher than the other eight hazard curves.

Table 2-1 contains a summary description of the LLNL seismic sources that dominate the calculated hazard at SRP for each S-Expert. (The ordering of S-Experts follows their calculated hazards at 0.6 g, as shown in Figure 2-12.)

The description of each source contains the best-estimate values of parameters that determine seismic hazard from that source, namely, distance to site, activity rate, rate per unit area, Richter's b value, and maximum magnitude. These values were obtained or derived from values in Volume 1 of (1).

Both the rate and rate per unit area are included because rate is an indication of contribution to hazard from small, distant sources, whereas rate per unit area is an indicator of contribution to hazard from large, nearby sources (especially for the host zone). The quantities in Table 2-1 explain the large differences in seismic hazards calculated using inputs from the various S-Experts.

The inputs from S-Expert 6 produce the highest calculated hazards. This hazard comes from a Charleston source that covers most of South Carolina and adjacent areas of Georgia, and

contains the site. Furthermore, S-Expert 6 assigned high values of maximum magnitude and activity rate this source, relative to other S-Experts.

The inputs from S-Expert 2 produce the second highest calculated hazards. Most of this hazard is contributed by the Charleston source, which has the highest maximum magnitude (7.5) and activity rate, and the lowest b value (0.67).

The inputs from S-Expert 11 produce the third highest calculated hazards. This hazard comes from a large regional source that contains the site, as well as the Charleston area.

The inputs from S-Experts 3 and 12 produce the lowest calculated hazards. These two experts drew host sources that cover southern South Carolina, exclusive of Charleston, and adjacent areas in Georgia and North Carolina. This region has very low seismic activity, which results in a low rate per unit area for the host zones.

In summary, the S-Experts that predict the highest hazard of SRP assume either that the Charleston seismic zone, with a maximum magnitude of 7.0 or higher, extends to the site, or that the Charleston source has a maximum magnitude of 7.5, a low b value, and a high activity rate.

Table 2-1
Summary of Dominant LLNL Seismic Sources and their Parameters

| S-Expert | Source No. | Source Description | % Contribution to Hazard (0.6g) [†] | Min. Distance to Site (km) | Rate ($m_b > 5$) (events/year) | Rate($m_b > 5$)/Area events/year/degree ² | b | Maximum Magnitude (m_b) |
|----------|------------|--|--|----------------------------|----------------------------------|--|------|-----------------------------|
| 6 | 13 | Charleston, extends to site [‡] | 100 | 0 | 3.3×10^{-2} | 4.3×10^{-3} | 0.85 | 7.3 |
| 2 | 30 | Charleston | 81 | 99 | 1.5×10^{-1} | 9.7×10^{-2} | 0.67 | 7.5 |
| | 29 | Host zone | 18 | 0 | 2.8×10^{-2} | 3.4×10^{-3} | 0.88 | 6.5 |
| 11 | 8 | S.E. Coastal Plain | 100 | 0 | 5.6×10^{-2} | 1.6×10^{-3} | 0.70 | 7.0 |
| 5 | 9 | Charleston | 95 | 76 | 1.7×10^{-1} | 1.2×10^{-1} | 1.08 | 7.25 |
| | 10 | Host Zone | 4 | 0 | 2.3×10^{-2} | 1.1×10^{-3} | 1.28 | 5.75 |
| 4 | 10 | Charleston | 98 | 30 | 7.6×10^{-2} | 3.7×10^{-2} | 0.92 | 6.8 |
| 7 | 10 | Charleston | 69 | 129 | 1.8×10^{-2} | - | 1.10 | 7.3 |
| | 8 | Host Zone | 29 | 0 | 1.3×10^{-2} | 1.3×10^{-3} | 1.10 | 6.0 |
| 1 | 1 | Host Zone | 76 | 0 | 6.9×10^{-2} | 8.3×10^{-4} | 1.30 | 6.44 |
| | 2 | Charleston | 22 | 147 | 5.4×10^{-2} | - | 1.06 | 6.67 |
| 10 | 4 | Host Zone | 82 | 0 | 3.2×10^{-2} | 9.1×10^{-4} | 1.00 | 6.0 |
| | 15 | Charleston | 16 | 122 | 1.7×10^{-2} | - | 0.70 | 7.0 |
| 13 | 9 | Charleston | 72 | 63 | 1.6×10^{-2} | 9.3×10^{-3} | 0.91 | 6.7 |
| | CZ17 | Background | 26 | 0 | 2.6×10^{-2} | 6.9×10^{-4} | 1.15 | 5.8 |
| 12 | 23 | Host Zone | 67 | 0 | 2.9×10^{-3} | 6.7×10^{-4} | 0.90 | 6.0 |
| | 23A | Charleston | 32 | 119 | 1.1×10^{-2} | 2.7×10^{-2} | 0.90 | 6.9 |
| 3 | 9 | Charleston | 83 | 49 | 1.4×10^{-2} | 1.7×10^{-2} | 0.89 | 6.8 |
| | 8 | Host Zone | 17 | 0 | 2.6×10^{-3} | 3.2×10^{-4} | 1.19 | 6.4 |

[†] Source: (2); contributions for S-Expert 11 were obtained from Vol. 3 of (1)

[‡] Base configuration (60% weight). The second configuration (30% weight) is essentially identical to the base configuration in the vicinity of the site.

2.2 EPRI SEISMIC SOURCES AND SEISMICITY PARAMETERS

The EPRI seismic-hazard calculations use the seismic sources and seismicity parameters developed by six earth-science teams (the Teams). Figures 13 through 18 show the EPRI seismic sources identified by each team in the region around Charleston.

To characterize his uncertainty on the existence and parameters of each seismic source, each team specified its confidence that the source exists (i.e., the probability of activity P^a), and specified probability distributions for the source's seismicity parameters.

Figure 2-19 shows the median PGA hazard curves obtained using the inputs from the six Teams. Differences among the six Teams are much smaller than those among the LLNL S-Experts.

Table 2-2 contains a summary description of the EPRI seismic sources that dominate the calculated hazard at SRP for each Team. Table 2-2 differs from Table 2-1 in that it includes the activity probability P^a , because the EPRI Teams used P^a different from 1 to characterize alternative hypotheses about the seismic sources near SRP.

Table 2-2 indicates that, for all Teams, the major contributor to the hazard is a host zone (i.e., a source that contains the site). This does not imply, however, that the Charleston seismicity has no effect on the hazard calculated using the EPRI inputs. Sources such as Woodward-Clyde source 29 and Law source 22 contain both Charleston and the SRP site; these sources represent interpretations that allow Charleston-size earthquakes outside the immediate vicinity of Charleston.

All EPRI teams specify similar rates per unit area and b values for the dominant sources. Maximum magnitudes are also similar, except for the Dames and Moore Team.

Table 2-2 also contains those sources that represent the Team's localized interpretations of the Charleston seismic zone, even though most of these sources do not contribute significantly to the hazard at SRP. The EPRI teams assign to these sources rates between 2×10^{-4} and 6×10^{-4} events/year, b -values near 1.0 and maximum magnitudes between 6.6 and 7.1.

In summary, all but one of the EPRI Teams obtain consistent estimates of the hazard at SRP. This hazard is dominated by seismic sources that contain the site.

Table 2-2

Summary of Dominant EPRI Seismic Sources and Their Parameters

| Team | Source Number | Source Description | Prob. of Activity | % Contribution to Hazard (0.56 g) | Min. Distance to Site (km) | Rate ($m_b > 5$) (events/yr.) | Rate($m_b > 5$)/Area (events/yr./deg. ²) | b | Max. Magnitude |
|----------------|---------------|---|---------------------------------------|-----------------------------------|----------------------------|---------------------------------|--|----------------------|----------------|
| Rondout | 26 | S. Carolina | 1.00 | 99 | 0 | | 1.2×10^{-3} | 0.97 | 6.5 |
| | 24 | Charleston | 1.00 | 1 | 62 | 6.4×10^{-3} | 4.8×10^{-3} | 1.02 | 6.8 |
| Woodward-Clyde | B32 | Background | 0.69 | 45 | 0 | | 9.5×10^{-4} | 0.98 | 6.2 |
| | 29 | So. Carolina Grav. Saddle (contains Charleston) | 0.12 | 30 | 0 | | 1.0×10^{-3} | 1.00 | 7.0 |
| | | 29B | So. Carolina Grav. Saddle (config. 3) | 0.18 | 18 | 0 | | 1.3×10^{-3} | 0.93 |
| | 29A | So. Carolina Grav. Saddle (config. 2) | 0.31 | 7 | 5 | | 1.6×10^{-3} | 0.95 | 7.0 |
| | 30 | Charleston | 0.57 | 0 | 99 | 2.2×10^{-3} | 5.1×10^{-3} | 0.85 | 7.3 |
| Weston | C33 | Donut (26-25) | 0.85 | 98 | 0 | | 6.0×10^{-4} | 0.99 | 6.6 |
| | 25 | Charleston | 0.99 | 0 | 119 | 8.35×10^{-3} | | 0.95 | 6.6 |
| Law | 22 | Reactivated E. Seaboard (contains Charleston) | 0.27 | 40 | 0 | | 8.0×10^{-4} | 1.05 | 6.8 |
| | | M39 | Mafic Pluton | 0.43 | 38 | 68 | 3.9×10^{-4} | | 1.05 |
| | C09 | Mesozoic Basins | 0.27 | 12 | 0 | | 4.9×10^{-4} | 1.05 | 6.8 |
| | 35 | Charleston | 0.45 | 0 | 128 | 6.6×10^{-3} | | 1.03 | 6.8 |
| Bechtel | BZ4 | Atlantic Coast | 1.00 | 80 | 0 | | 2.7×10^{-4} | 1.06 | 7.1 |
| | BZ5 | S. Appalachians | 1.00 | 12 | 14 | | 1.5×10^{-3} | 0.90 | 6.0 |
| | H or N3 | Charleston | 0.95 | 2 | 93 | 6.9×10^{-3} | | 1.04 | 7.1 |
| Dames & Moore | 53 | S. Appalachians, Mobile Belt | 0.26 | 90 | 0 | | 7.4×10^{-4} | 1.04 | 5.6 |
| | 54 | Charleston | 1.00 | 8 | 63 | 6.6×10^{-3} | 5.1×10^{-3} | 1.01 | 6.6 |

Notes:

Rates per unit area for the host sources were computed from the most likely a and b values for the host 1-degree cell. Source: EPRI computer files containing seismicity parameters. Rates for the Charleston sources were computed from the most-likely a and b values.

The maximum magnitudes listed are the median values from the distributions specified by the Teams. Source: (3,4).

2.3 COMPARISONS

Observation of the seismicity parameters of the dominant sources in Tables 1 and 2 shows significant differences between the LLNL S-Experts and the EPRI teams. The most important differences are listed below.

- The rate of $m_b > 5$ earthquakes in the Charleston zone is higher (by one order of magnitude or more) for the LLNL S-Experts than for the EPRI teams.
- Some LLNL S-Experts (i.e., 2, 10 and 11) specify b -values of 0.7 for the Charleston zone. This value is significantly lower than those specified by the other S-Experts and by the EPRI Teams.
- Two LLNL S-Experts (i.e., 6 and 11) extend the Charleston source so that it includes the SRP site, thus assuming that Charleston-size earthquakes may occur at the site. Two EPRI Teams consider that hypothesis, but give it a low weight.
- LLNL S-Expert 2 assumes a maximum magnitude of 7.5 for the Charleston source. This value is considerably higher than values used by other S-Experts and by the EPRI teams.

The four differences listed above are significant contributors to the differences between the hazards calculated using the LLNL and EPRI inputs.

Among the numerous similarities between the LLNL and EPRI inputs, the following two are worth mentioning.

- A majority of LLNL S-Experts and EPRI Teams concur in their interpretation that the Charleston source does not extend to the SRP site.
- The LLNL S-Experts and EPRI Teams estimate similar rates per unit area, b values, and maximum magnitudes for the host zones (except for those Charleston zones that extend to the site).

Table 2-3
Base-Case Parameter Values

| Parameter | Charleston Source | Host Source |
|--|-----------------------|----------------------|
| Rate ($m_b > 5$) [events/yr] | 1.27×10^{-2} | — |
| $\frac{\text{Rate}(m_b > 5)}{\text{Area}}$ [events/yr/deg ²] | — | 8.5×10^{-4} |
| b | 0.95 | 1.05 |
| M_{\max} | 6.9 | 6.3 |

2.4 EFFECT ON CALCULATED HAZARD

To evaluate the effects of the various seismicity assumptions on the calculated hazard, we have varied each parameter individually and observed the variation in hazard. To this effect, we defined a base-case. The parameter values for the base-case were defined as the geometric average of the corresponding parameter values (given 50% weight to the LLNL Experts and 50% weight to the EPRI teams). Table 2-3 shows the base-case parameters for the Charleston source and for the host source.

For cases where the Charleston source dominates the hazard, each parameter of the Charleston source was varied individually. The effect of that parameter was evaluated by forming the ratio of the ratio of the following quantities.

- a. The hazard calculated by using all of the Expert's assumptions (including source geometries), to
- b. the hazard calculated by setting the parameter in question to its base-case value, while using the Expert's assumptions for all other parameters.

For Expert 6, the effect of assuming that the Charleston source extends to the site was evaluated by considering a base-case in which source 13 (see Fig. 2-6) was partitioned as follows:

- A "Charleston portion" of the source, which has the same rate per unit area, *b*-value, and maximum magnitude as the original source 13. The minimum distance of this source to the site is 70 km.
- A "host portion" of the source, which has the same parameters as the base-case host source.

Table 2-4 shows the hazard ratios obtained for cases where the Charleston source dominates the hazard.

For cases where the host source dominates the hazard, we followed a similar procedure, varying each parameter of the host source and observing the variation in hazard. Table 2-5 shows the corresponding hazard ratios.

Tables 2-4 and 2-5 indicate that the assumption by Experts 6 and 11 that a Charleston-type source extends to the site increases the hazard by a factor of 7 to 13. The high activity rates used by Experts 2, 5, and 4 increase the hazard by factors of 5 to 10. Hazard ratios for the remaining LLNL Experts and EPRI Teams are nearly equal to 1.0.

The above hazard ratios do not explain why Dames & Moore predicts much lower hazard than the other EPRI Teams (see Fig. 2-19). The explanation for this low hazard is that the host source (source 26) has an activity probability of 0.26. If source 26 is not active, there are no other significant local sources, and the hazard site is very low. Because this occurs with a probability of 0.74, the median hazard for the Dames & Moore team is very low.

Table 2-4
 Effect of Seismological Assumptions
 on Calculated Hazard
 (cases where Charleston source dominates the hazard¹)

| Expert/Team | Hazard Ratio (PGA=0.5g) | | | |
|----------------|-------------------------|-----|-----------|--|
| | Rate ($m_b > 5$) | b | M_{max} | Charleston Source extending to site |
| LLNL Expert 6 | — | 1.3 | 1.5 | 13 |
| LLNL Expert 2 | 8 | 1.9 | 2.9 | — |
| LLNL Expert 11 | — | 1.7 | 1.2 | 13 ² |
| LLNL Expert 5 | 10 | 0.7 | 2.0 | — |
| LLNL Expert 4 | 5 | 1.1 | 0.8 | — |
| LLNL Expert 7 | 1.1 | 0.7 | 1.7 | — |
| LLNL Expert 13 | 1.0 | 1.1 | 0.7 | — |
| LLNL Expert 3 | 0.9 | 1.1 | 0.8 | — |

| Expert/Team | Hazard Ratio (PGA=0.25g) | | | |
|----------------|--------------------------|-----|-----------|--|
| | Rate ($m_b > 5$) | b | M_{max} | Charleston Source extending to site |
| LLNL Expert 6 | — | 1.2 | 1.3 | 7.3 |
| LLNL Expert 2 | 8 | 1.9 | 2.3 | — |
| LLNL Expert 11 | — | 1.5 | 1.1 | 7.3 ² |
| LLNL Expert 5 | 10 | 0.7 | 2.0 | — |
| LLNL Expert 4 | 5 | 1.1 | 0.8 | — |
| LLNL Expert 7 | 1.1 | 0.7 | 1.4 | — |
| LLNL Expert 13 | 1.0 | 1.0 | 0.8 | — |
| LLNL Expert 3 | 0.9 | 1.1 | 0.9 | — |

¹Includes sources that contain Charleston and site

²Based on result obtained for Expert 6

Table 2-5
 Effect of Seismological Assumptions
 on Calculated Hazard
 (cases where host source dominates the hazard)

| Expert/Team | Hazard Ratio (PGA=0.5g) | | |
|----------------|--|----------|-----------|
| | $\frac{\text{Rate}(m_b > 5)}{\text{Area}}$ | <i>b</i> | M_{max} |
| LLNL Expert 1 | 1.0 | 0.8 | 1.1 |
| LLNL Expert 10 | 1.1 | 1.0 | 0.7 |
| LLNL Expert 12 | 0.9 | 1.1 | 0.6 |
| Rondout | 1.5 | 2.0 | 1.4 |
| Woodward-Clyde | 1.3 | 1.6 | 1.3 |
| Weston | 0.7 | 1.1 | 1.7 |
| Law | 0.7 | 1.0 | 1.7 |
| Bechtel | 0.6 | 1.1 | 1.6 |
| Dames & Moore | 0.9 | 1.0 | 0.7 |

| Expert/Team | Hazard Ratio (PGA=0.25g) | | |
|----------------|--|----------|-----------|
| | $\frac{\text{Rate}(m_b > 5)}{\text{Area}}$ | <i>b</i> | M_{max} |
| LLNL Expert 1 | 1.0 | 0.9 | 1.0 |
| LLNL Expert 10 | 1.1 | 1.0 | 0.8 |
| LLNL Expert 12 | 0.9 | 1.0 | 0.8 |
| Rondout | 1.5 | 1.9 | 1.1 |
| Woodward-Clyde | 1.3 | 1.4 | 1.1 |
| Weston | 0.7 | 1.0 | 1.3 |
| Law | 0.7 | 1.0 | 1.3 |
| Bechtel | 0.6 | 1.1 | 1.1 |
| Dames & Moore | 0.9 | 1.0 | 0.7 |

2.5 REFERENCES

1. D. L. Bernreuter, J. B. Savy, R. W. Mensing, and J. C. Chen. *Seismic Hazard Characterization of 69 Plant Sites East of the Rocky Mountains*. Technical Report NUREG/CR5250, UCID-21517, U. S. Nuclear Regulatory Commission, 1988.
2. J. B. Savy. *Seismic Hazard Characterization of the Savannah River Plant (SRP)*. Technical Report UCID-21596, Lawrence Livermore National Laboratory, November 1988.
3. *Seismic Hazard Methodology for the Central and Eastern United States*. Technical Report NP-4726-A, Electric Power Research Institute, July 1986. Vol. 1, Part 1: Methodology, Vol. 1, Part 2: Theory, Vol. 2: EQHAZARD Programmer's Manual, Vol. 3: EQHAZARD User's Manual, Vol. 4: Applications, Vols. 5 through 10: Tectonic Interpretations, Vol. 11: Nuclear Regulatory Commission Safety Review.
4. R. K. McGuire, G. R. Toro, and M. W. McCann. *EQHAZARD Primer*. Special Report NP101-46, Electric Power Research Institute, June 1989.

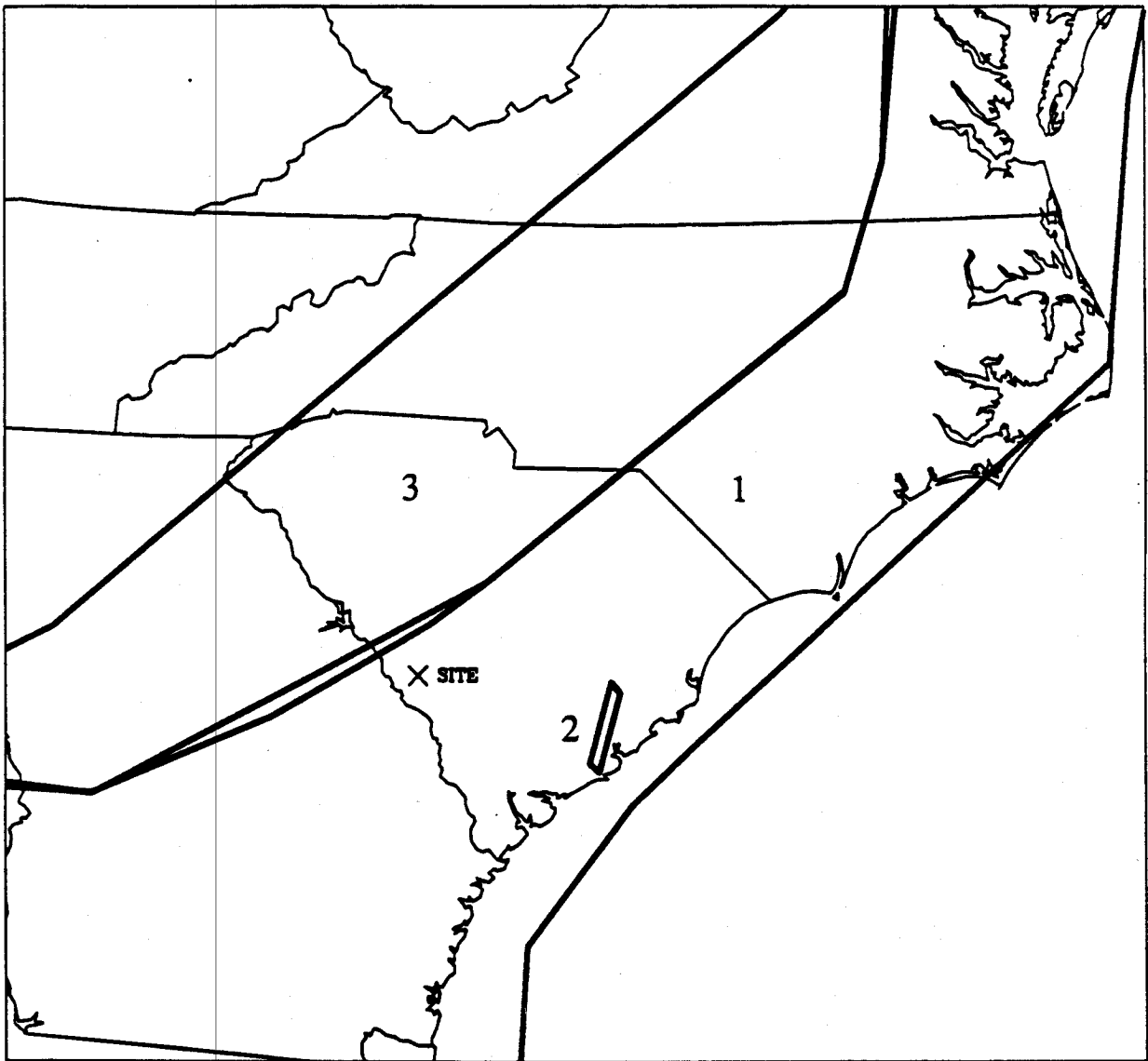


Figure 2-1. Seismic sources that dominate the calculated hazard at the SRP site; base map for S-Expert 1.

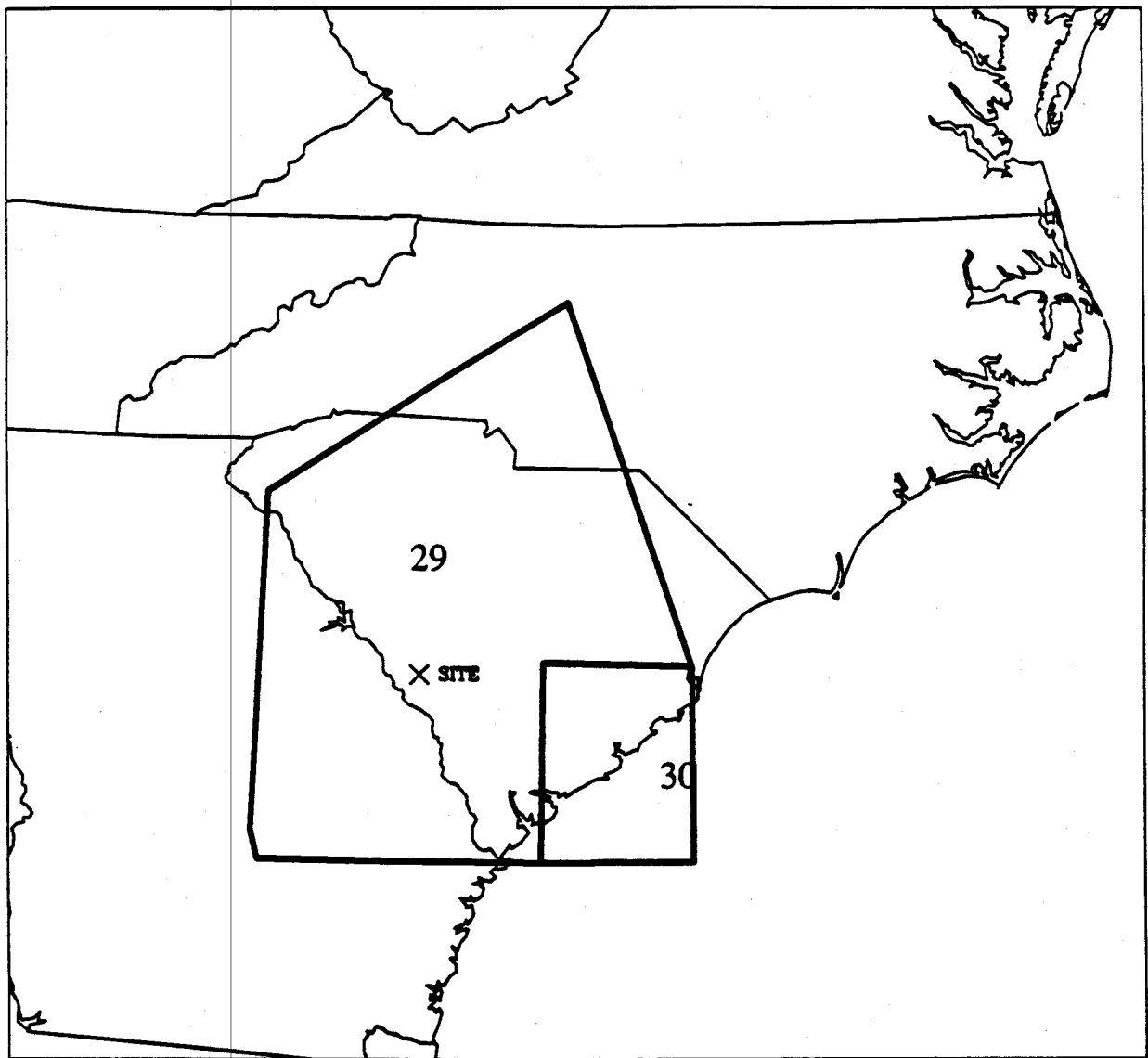


Figure 2-2. Seismic sources that dominate the calculated hazard at the SRP site; base map for S-Expert 2.

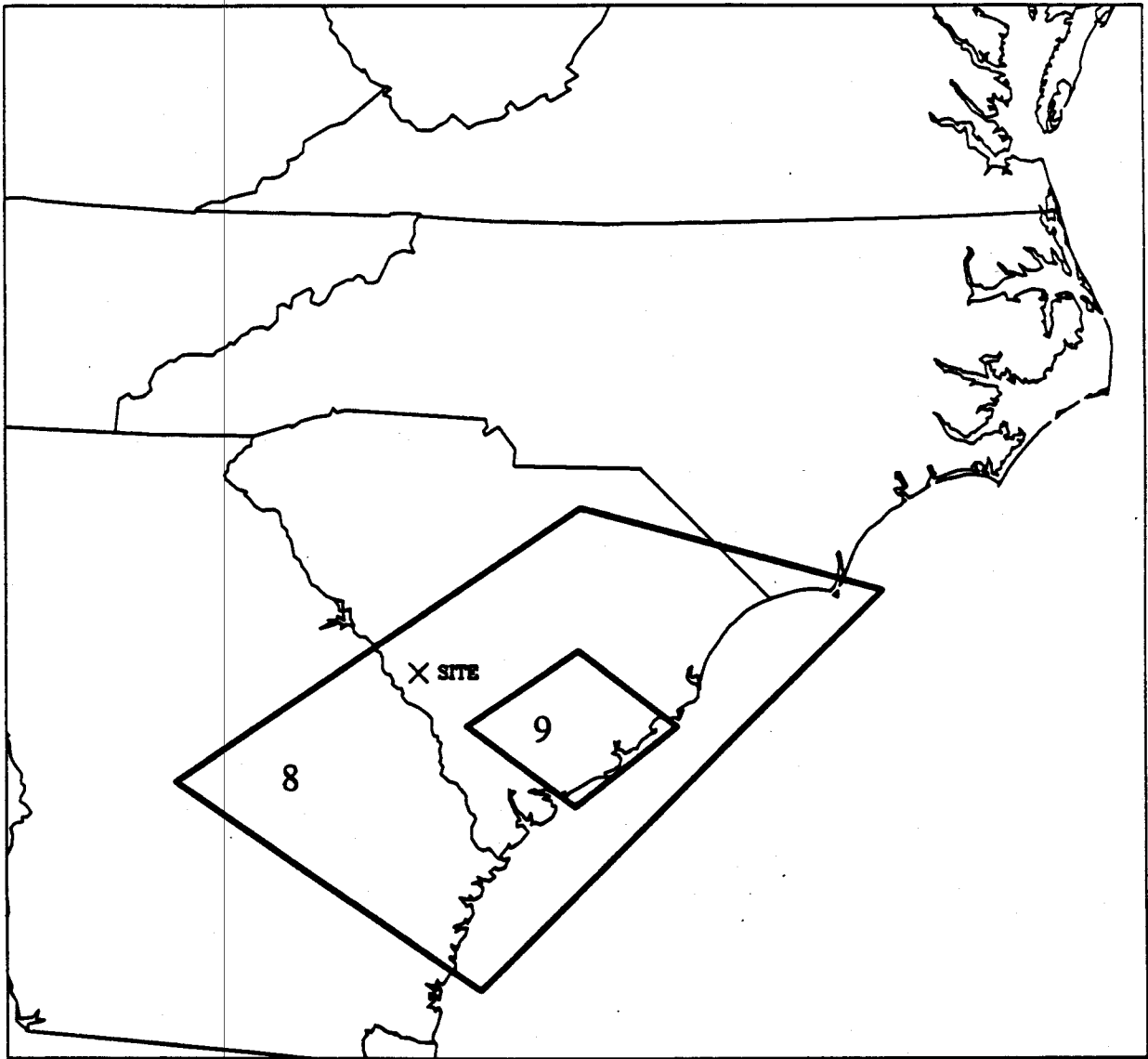


Figure 2-3. Seismic sources that dominate the calculated hazard at the SRP site; base map for S-Expert 3.

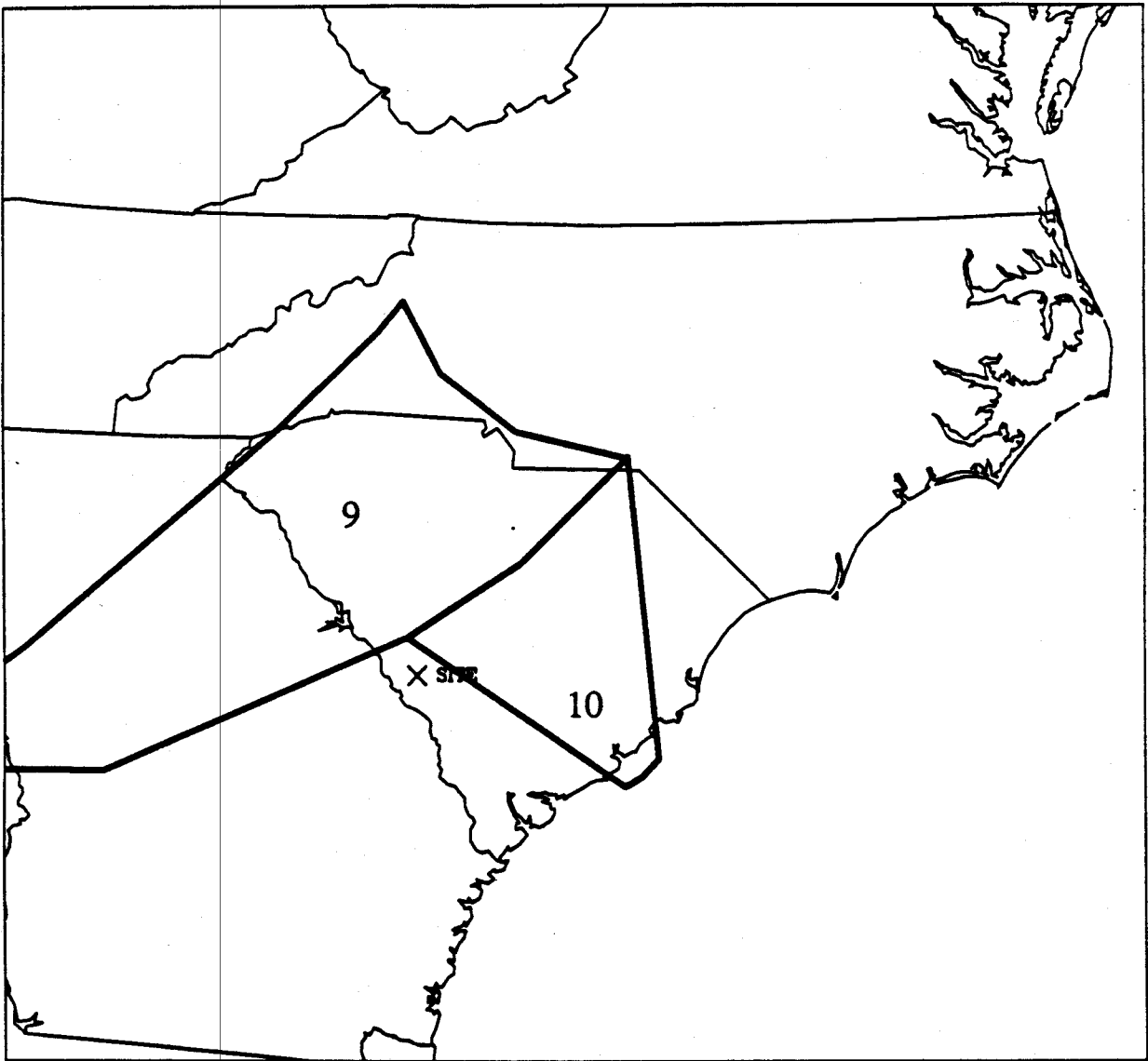


Figure 2-4. Seismic sources that dominate the calculated hazard at the SRP site; base map for S-Expert 4.

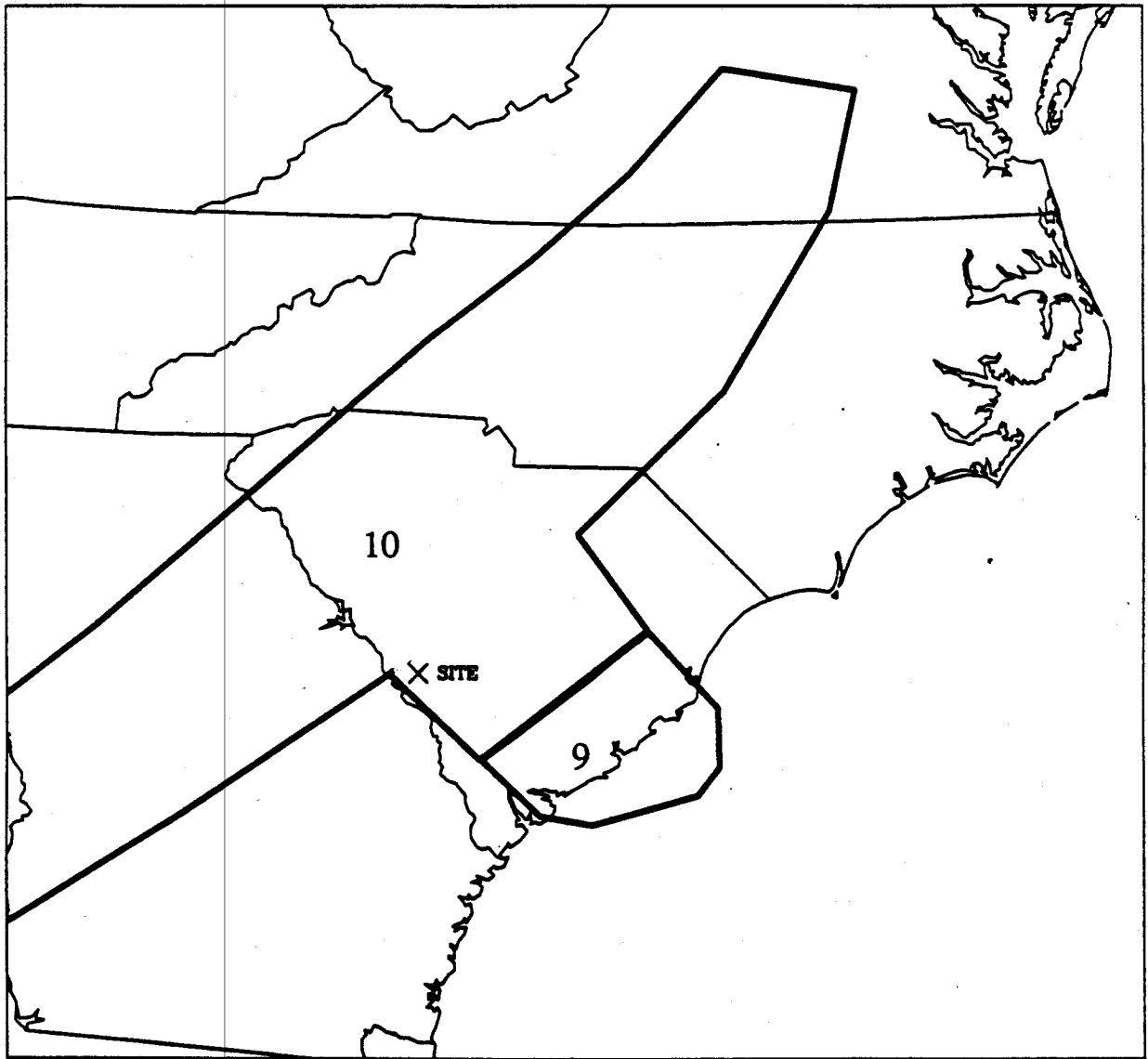


Figure 2-5. Seismic sources that dominate the calculated hazard at the SRP site; base map for S-Expert 5.

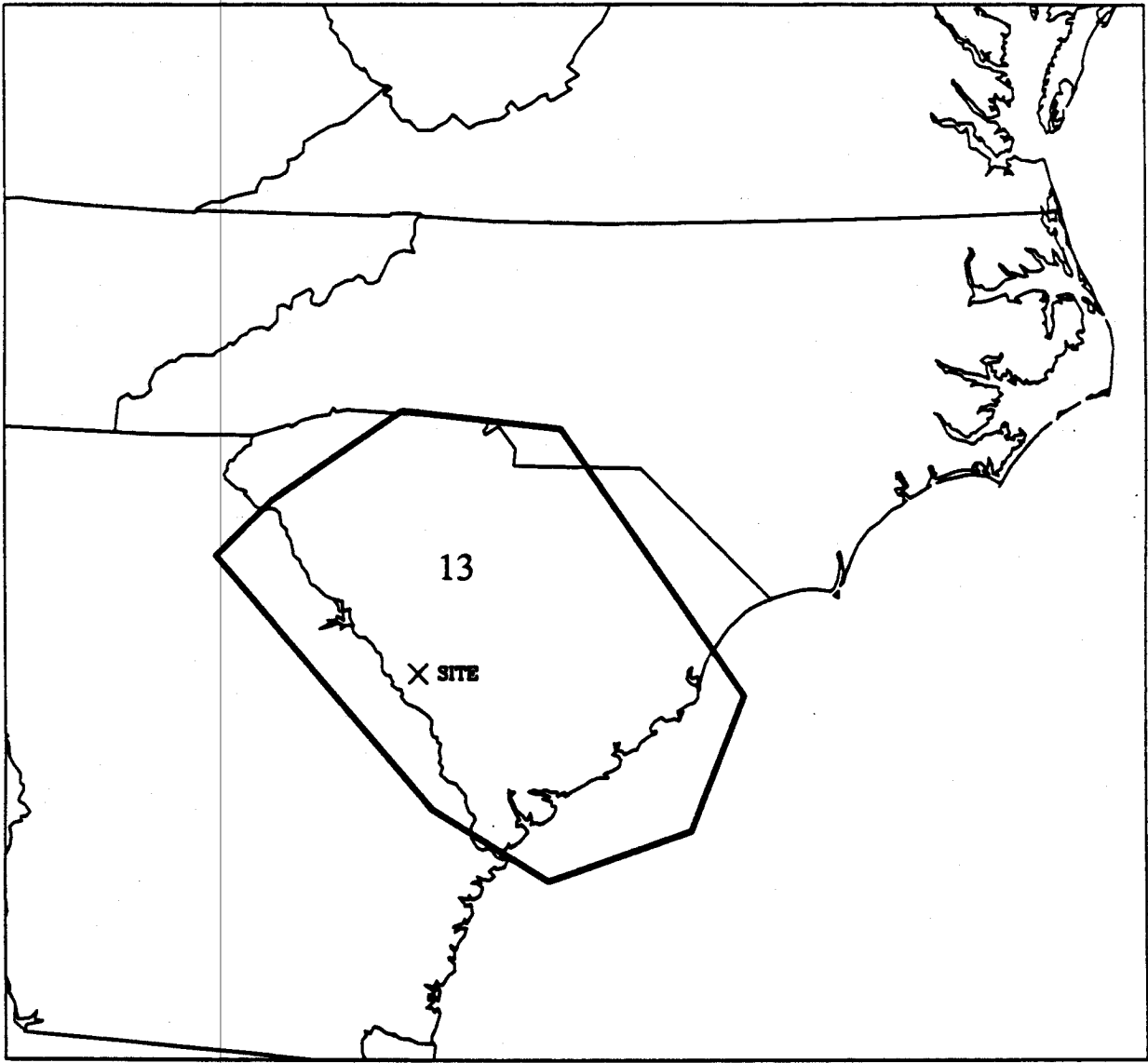


Figure 2-6. Seismic sources that dominate the calculated hazard at the SRP site; base map for S-Expert 6.

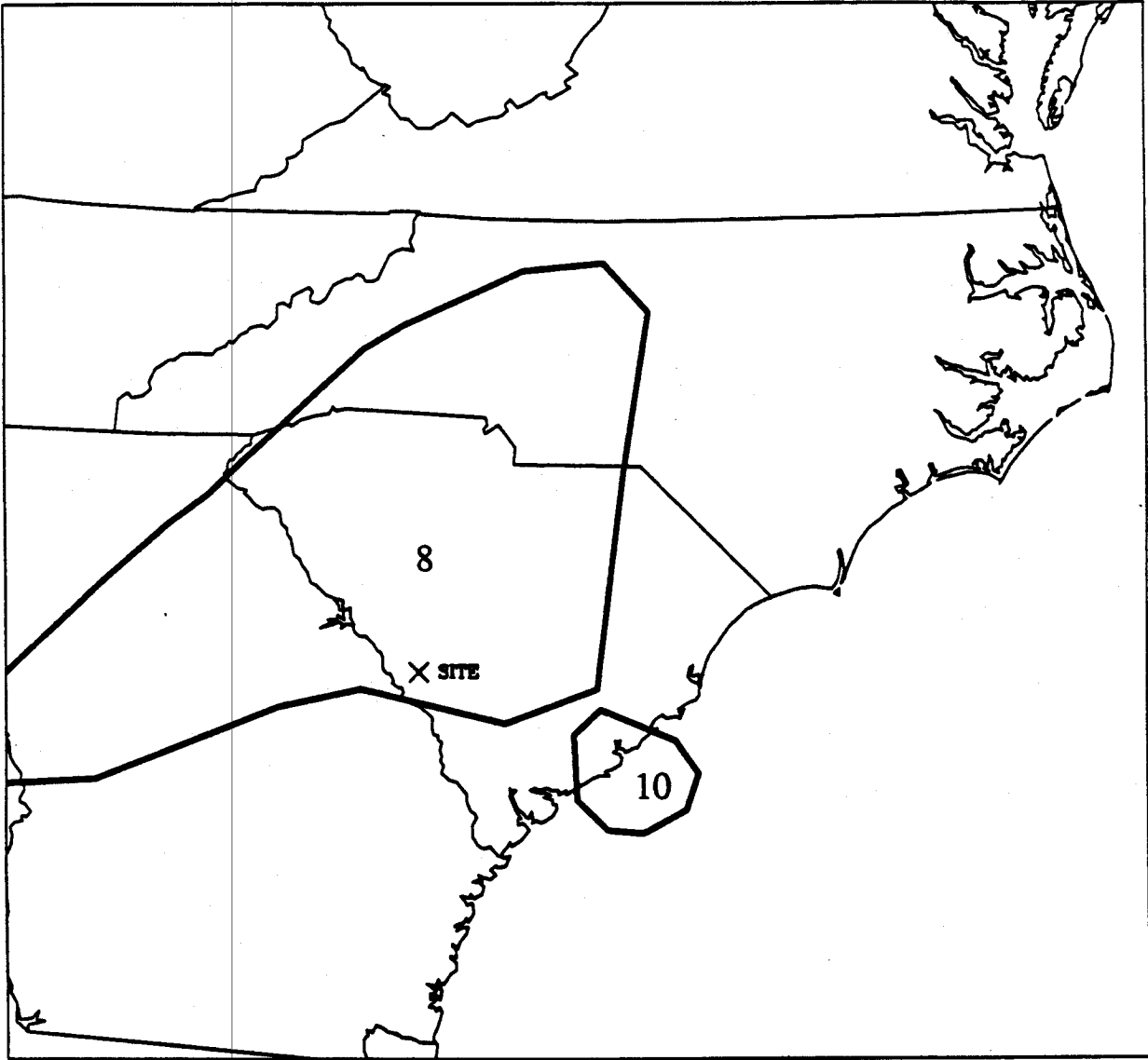


Figure 2-7. Seismic sources that dominate the calculated hazard at the SRP site; base map for S-Expert 7.

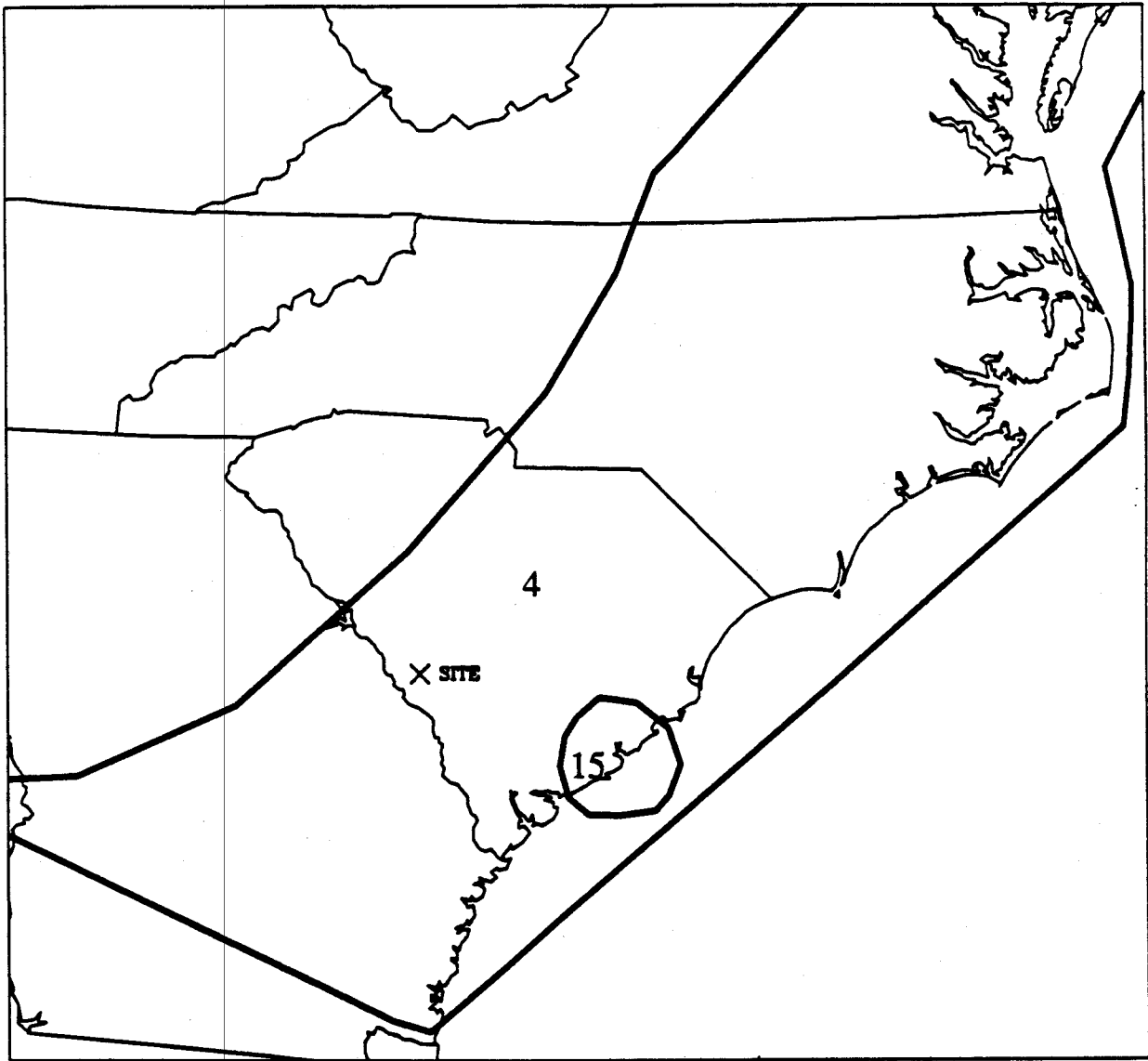


Figure 2-8. Seismic sources that dominate the calculated hazard at the SRP site; base map for S-Expert 10.

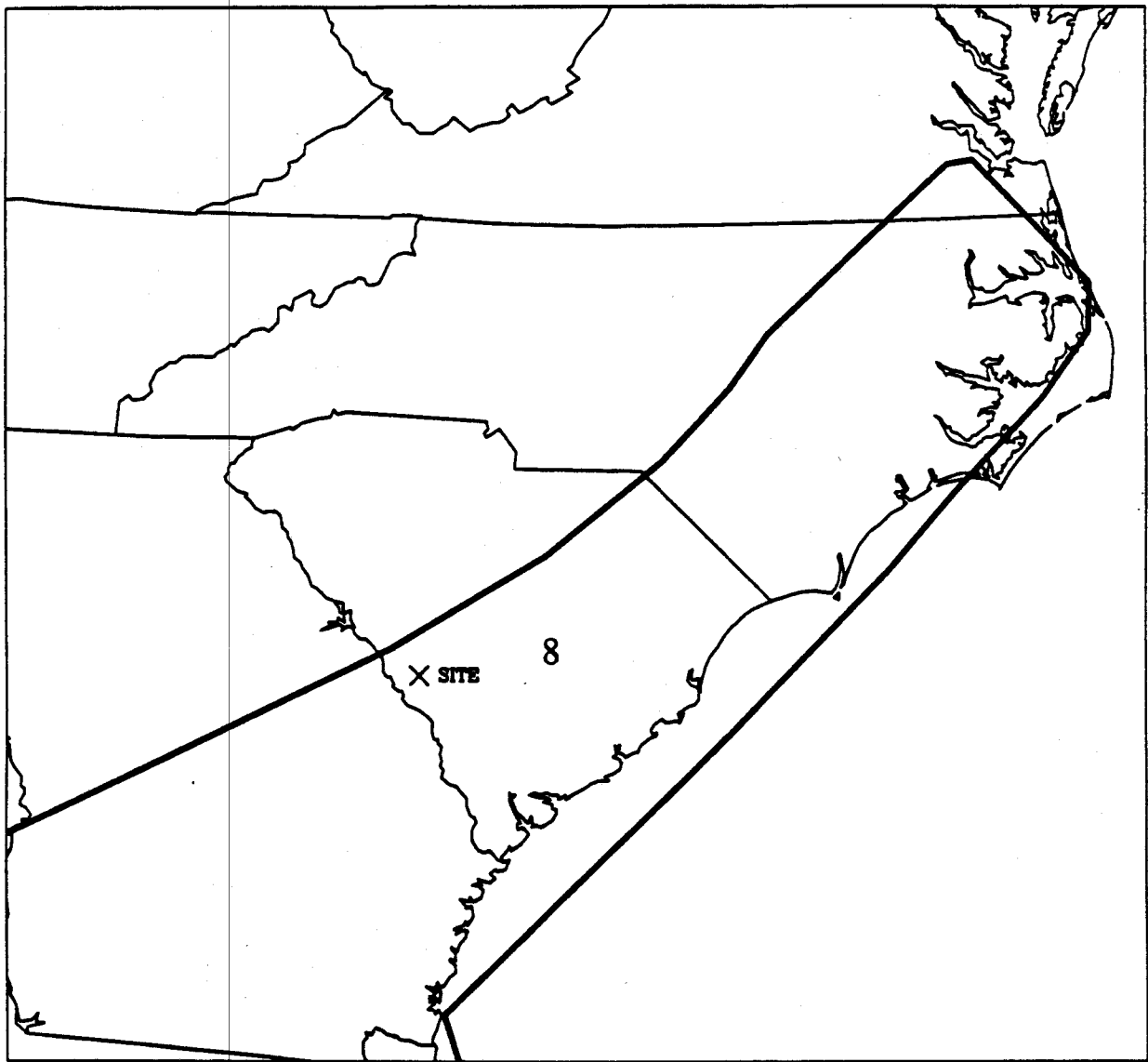


Figure 2-9. Seismic sources that dominate the calculated hazard at the SRP site; base map for S-Expert 11.

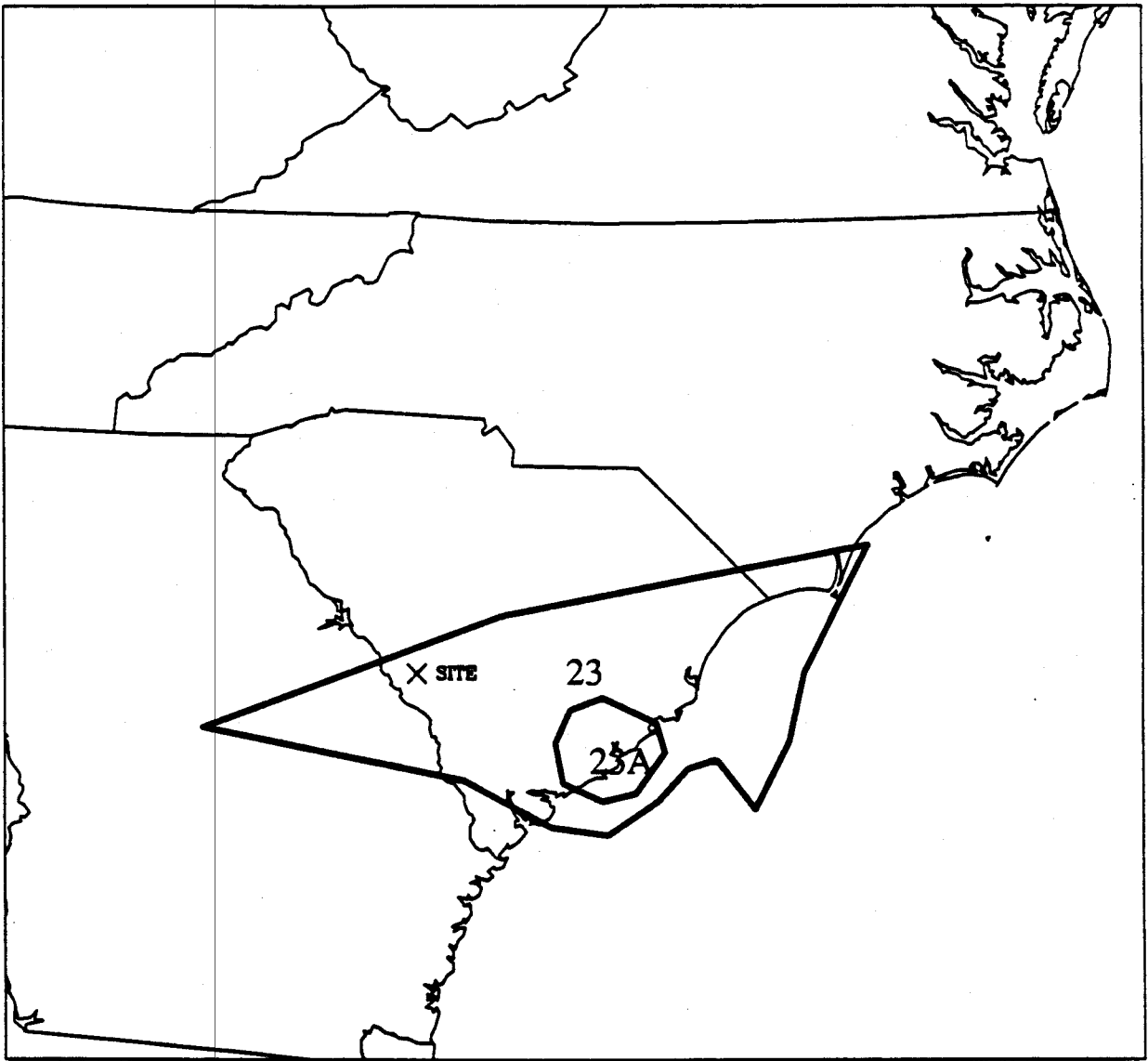


Figure 2-10. Seismic sources that dominate the calculated hazard at the SRP site; base map for S-Expert 12.

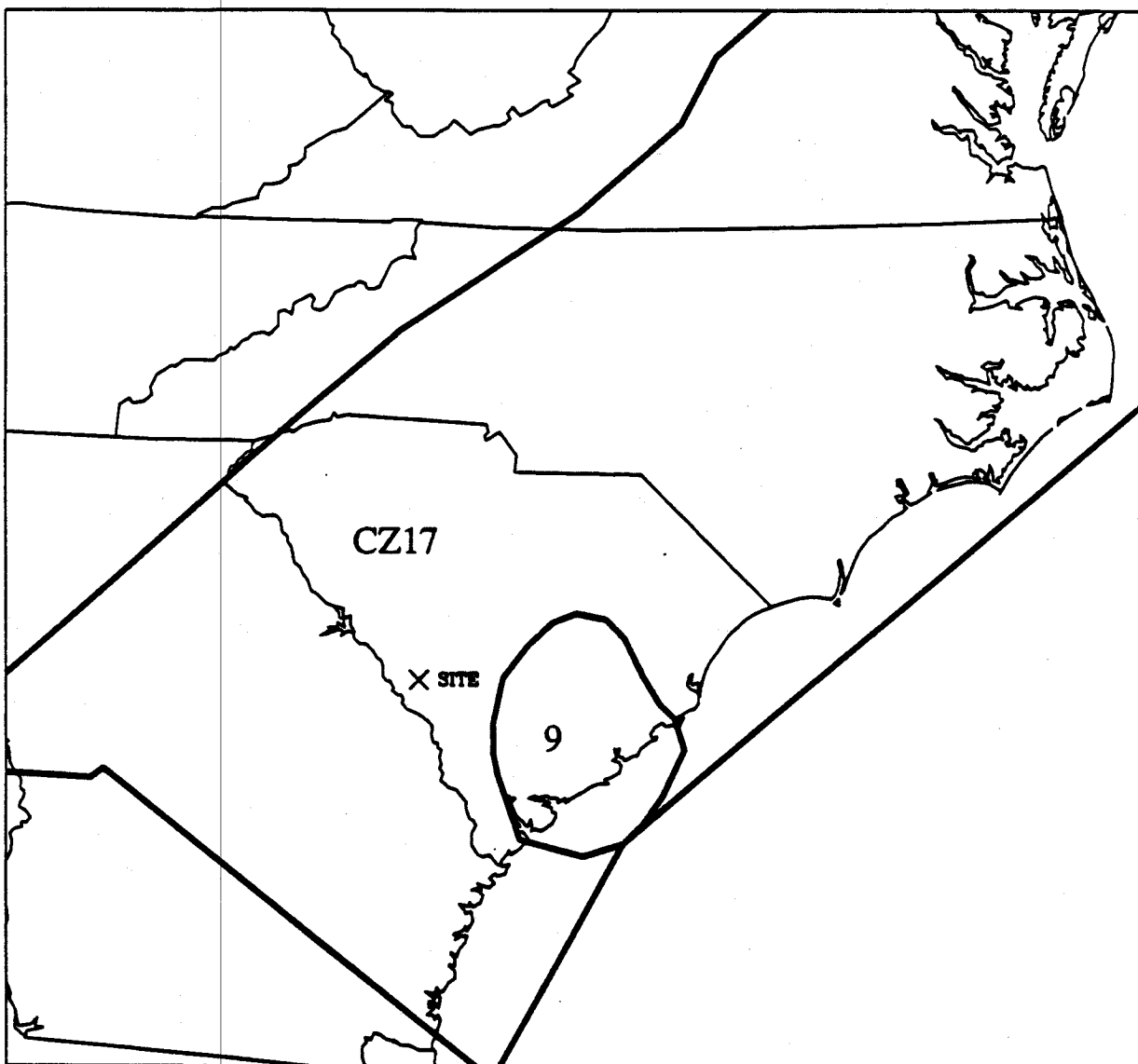


Figure 2-11. Seismic sources that dominate the calculated hazard at the SRP site; base map for S-Expert 13.

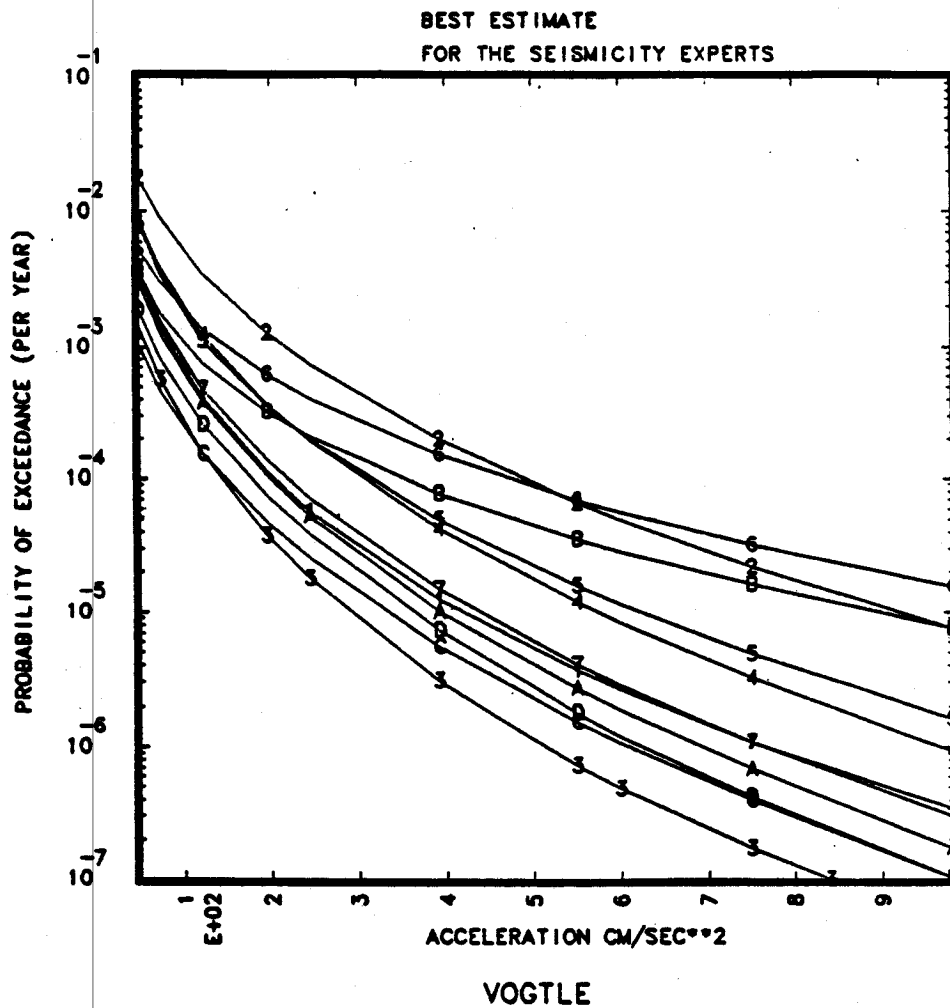


Figure 2-12. Best-estimate hazard curves for the the S-Experts; Vogtle site. (A: Expert 10, B: Expert 11, C: Expert 12, D: Expert 13.) Source: (1, Volume 3, page 202)

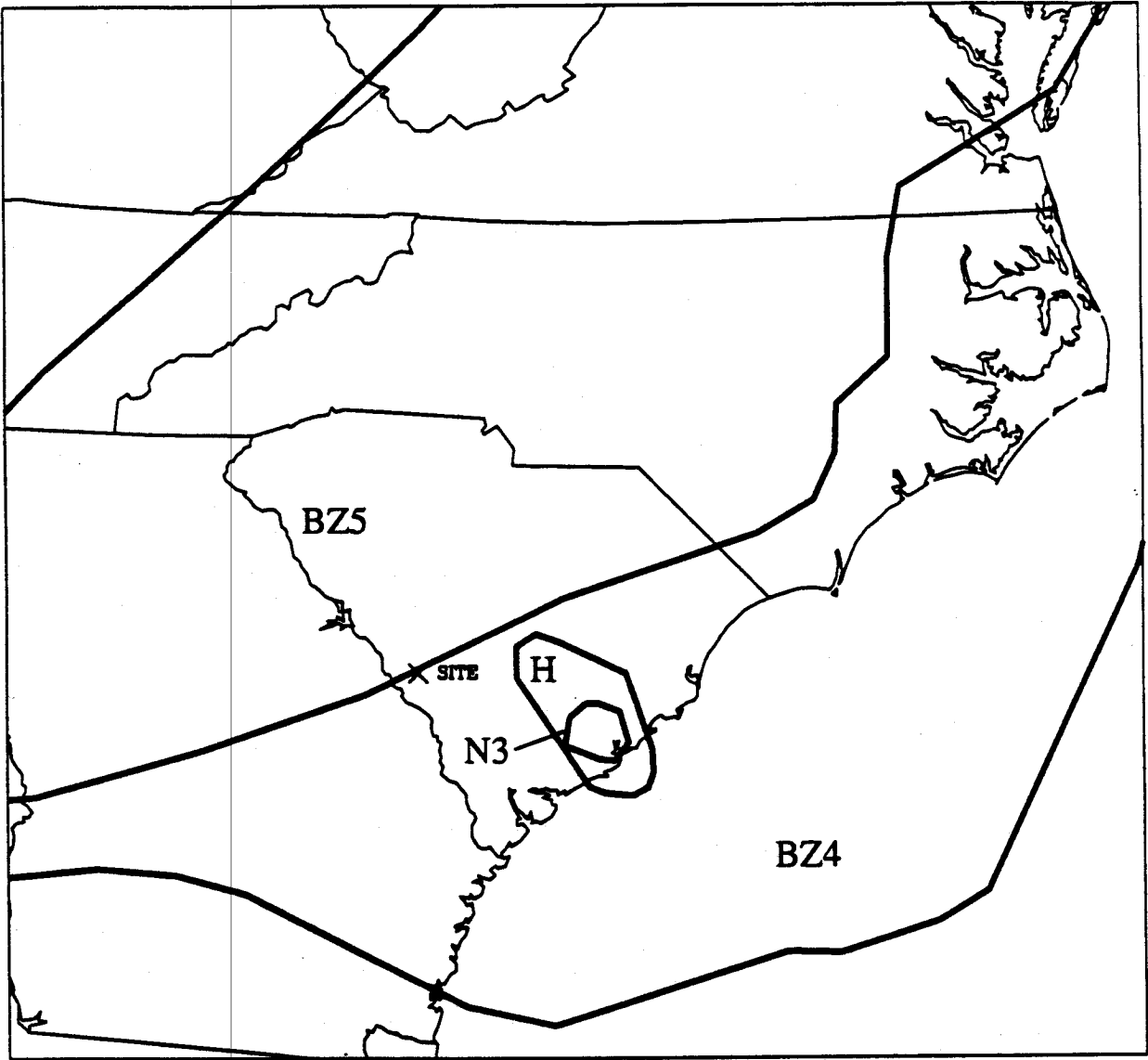


Figure 2-13. Seismic sources that dominate the calculated hazard at the SRP site; Bechtel Team.

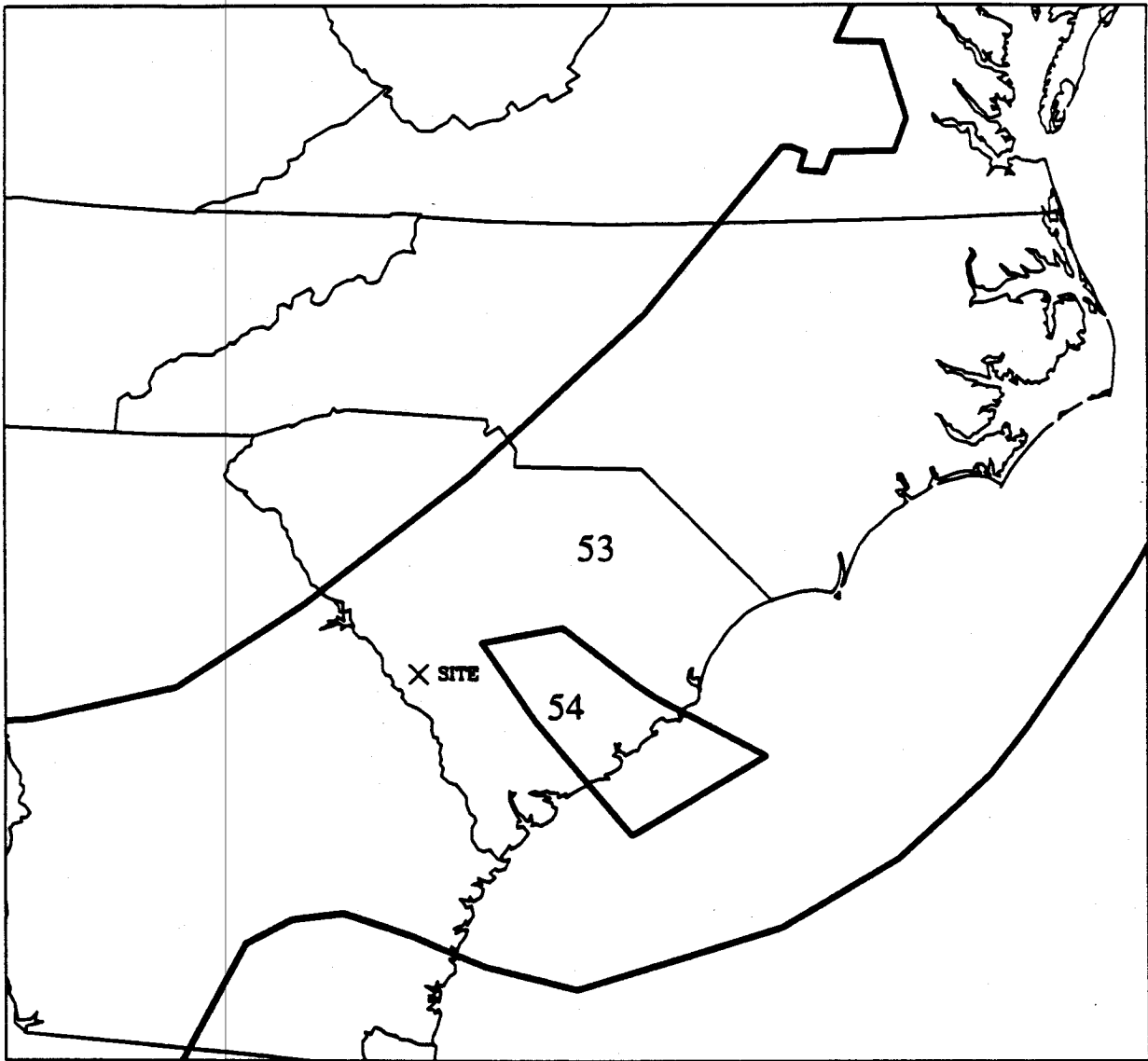


Figure 2-14. Seismic sources that dominate the calculated hazard at the SRP site; Dames and Moore Team.

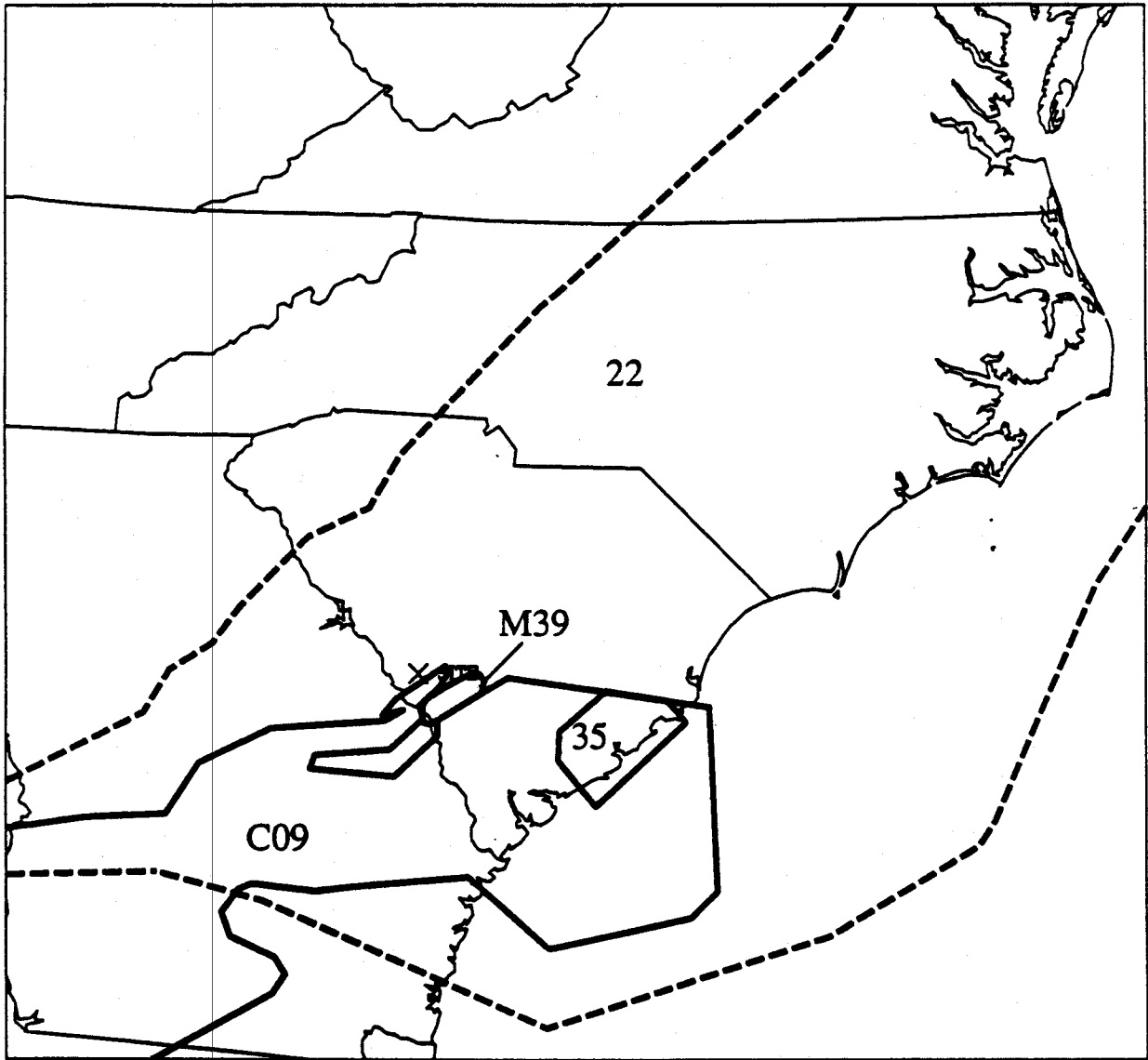


Figure 2-15. Seismic sources that dominate the calculated hazard at the SRP site; Law Team.

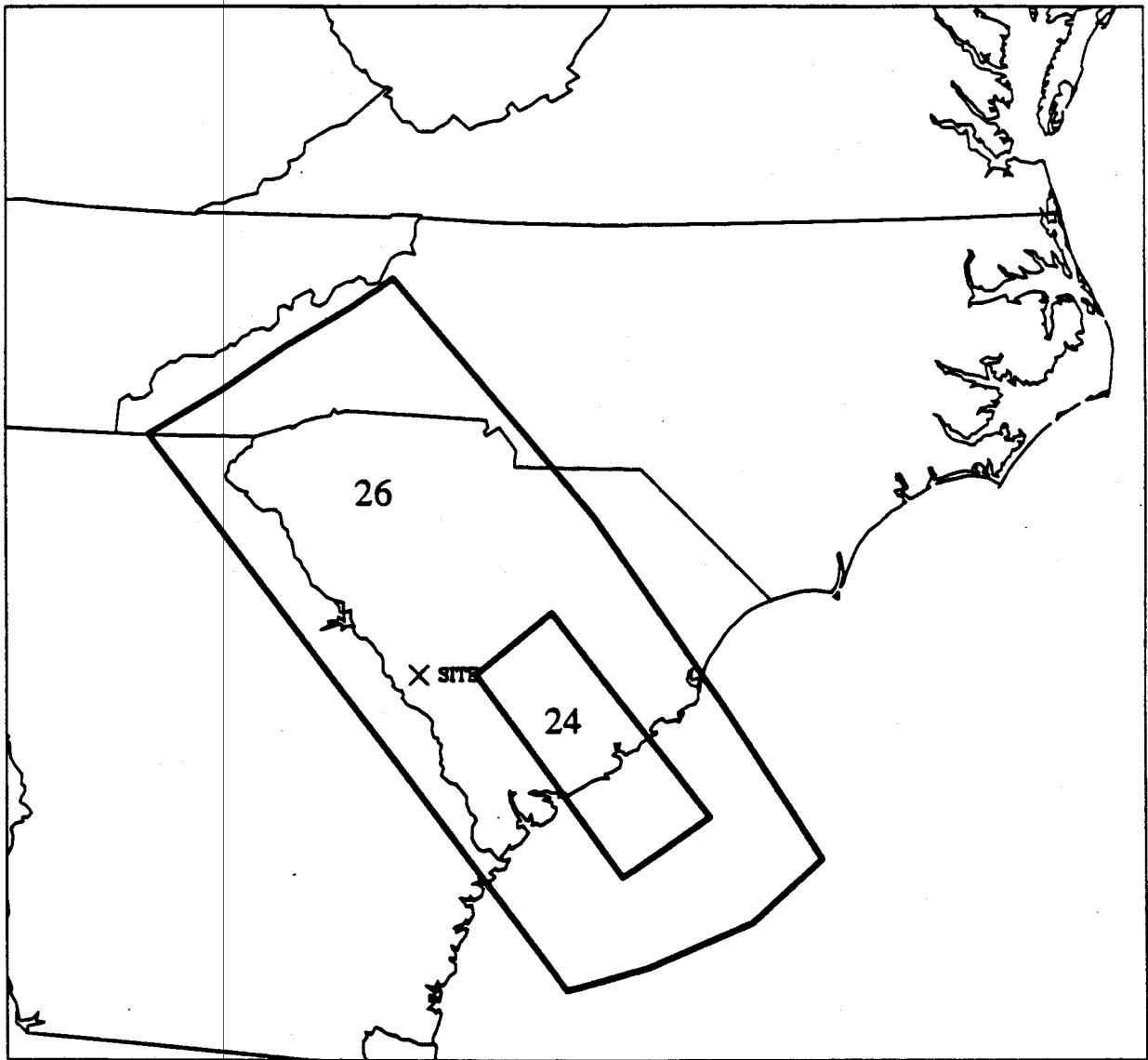


Figure 2-16. Seismic sources that dominate the calculated hazard at the SRP site; Ron-dout Team.

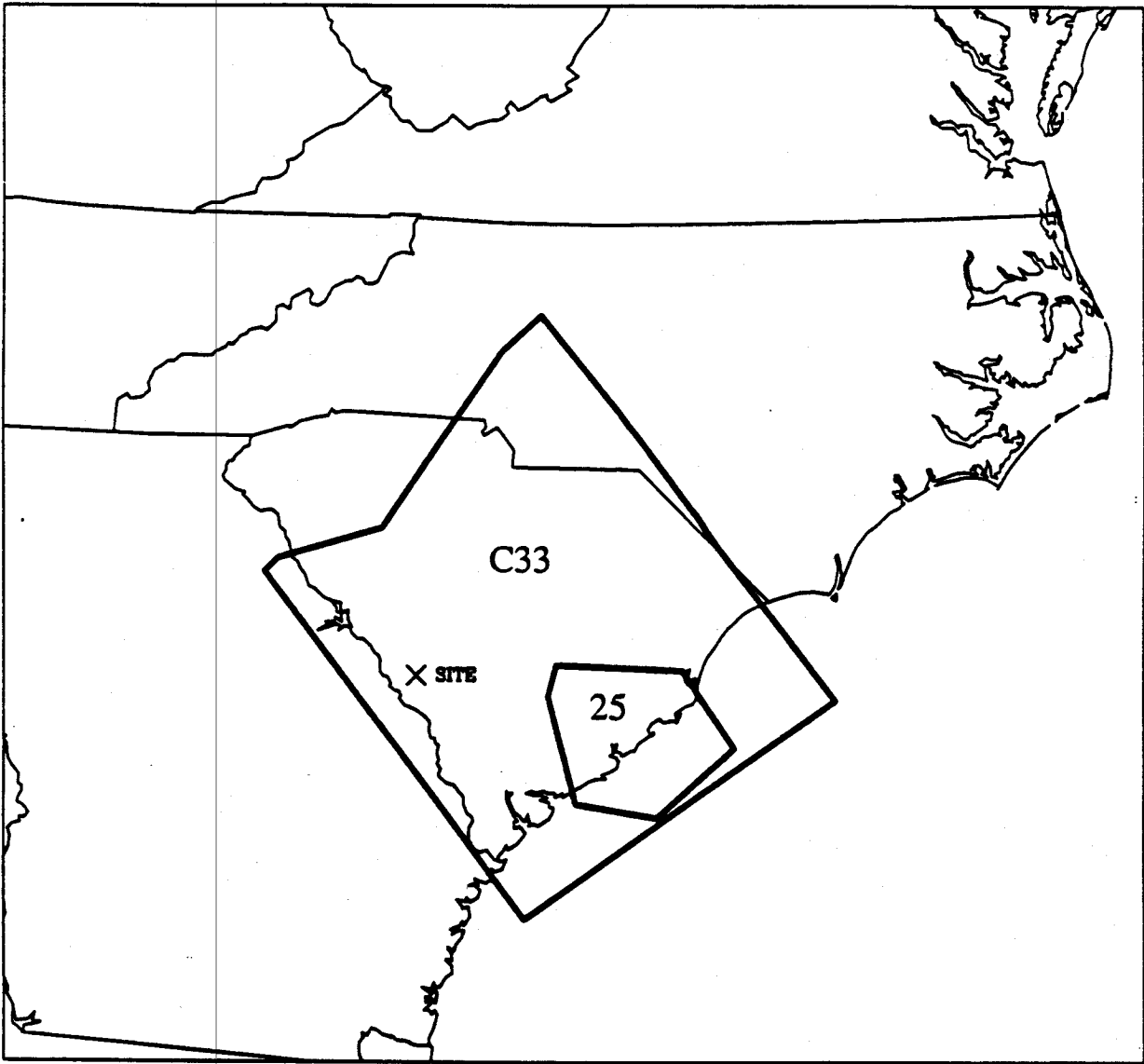


Figure 2-17. Seismic sources that dominate the calculated hazard at the SRP site; Weston Team.

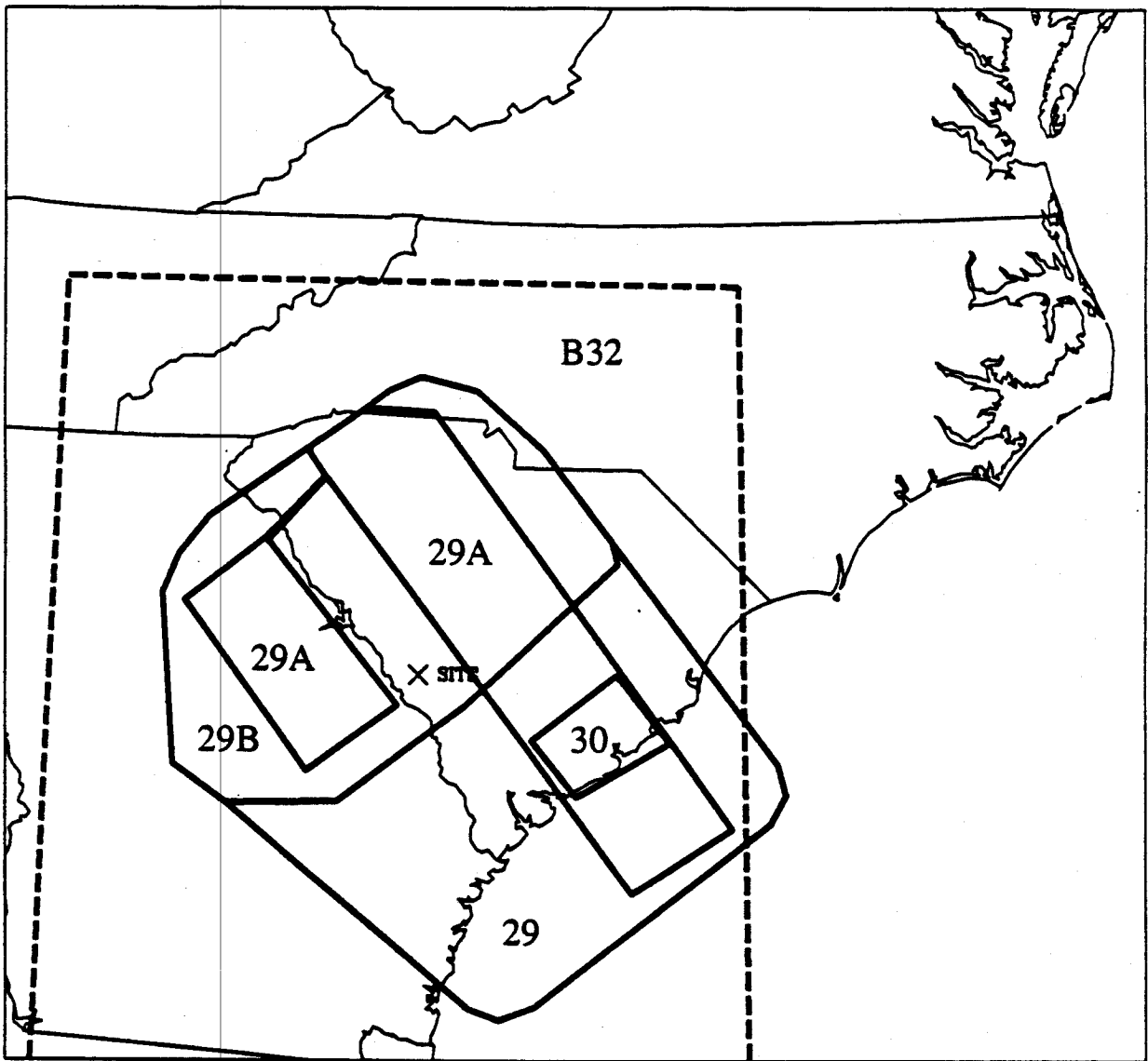


Figure 2-18. Seismic sources that dominate the calculated hazard at the SRP site; Woodward-Clyde Team.

SAVANNAH RIVER PLANT
MEDIAN HAZARDS FROM TEAMS

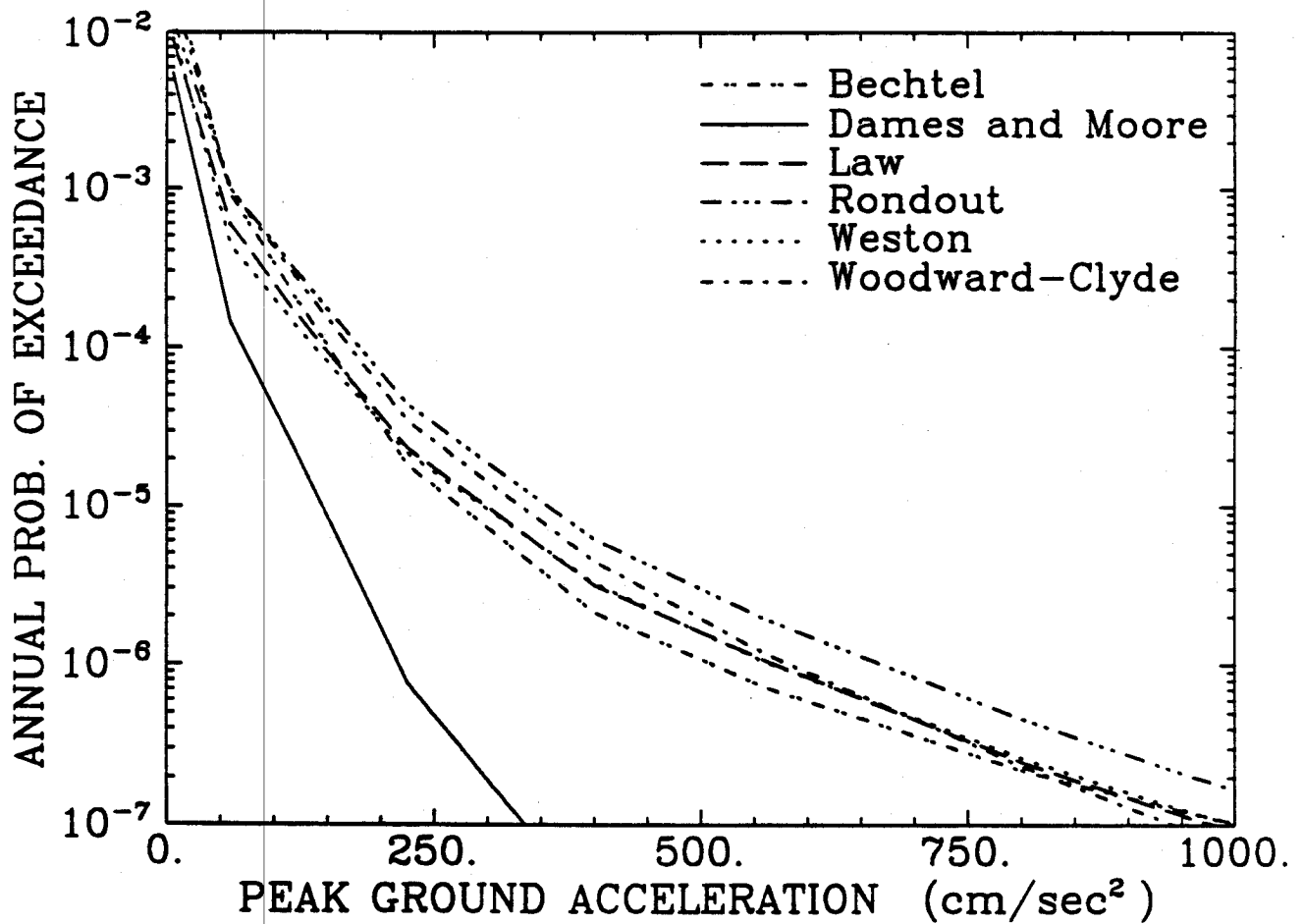


Figure 2-19. Median hazard curves for the the EPRI Teams; SRP site.

Section 3 GROUND-MOTION ATTENUATION

3.1 INTRODUCTION

This section compares the ground-motion attenuation functions and site-amplification models used in the LLNL and EPRI calculations.

Section 3.2 compares the attenuation functions for rock sites. Section 3.3 compares the site-amplification factors for deep-soil sites. Finally, Section 3.4 shows the differences in calculated hazard resulting using the LLNL or EPRI attenuation models (while using the same seismic sources and seismicity parameters).

3.2 ATTENUATION FUNCTIONS FOR GROUND MOTIONS ON ROCK

3.2.1 LLNL Attenuation Functions

The LLNL models were selected by a panel of 5 experts (the G-Experts), from among models in the literature and models proposed by the panel members. Each panelist assigned weights to the different attenuation models, and specified source depth, truncation, and standard deviation of residuals. These models are summarized in Tables 3-1 and 3-2, which are based on information in (1).

3.2.2 EPRI Attenuation Functions

The attenuation functions used in the EPRI calculations were selected by a consultant to EPRI, after extensive research and discussions with other researchers in the field (7,8). These attenuation functions are based on simplified physical models of energy release at the seismic source and of wave propagation. Uncertainty on attenuation functions arises from uncertainty on the parameters of these models and on the derivation of peak time-domain amplitudes from Fourier spectra. The most important of these are uncertainty on source scaling, on the magnitude-moment relation, and on the spectra to time-domain derivation. These uncertainties are captured by considering three alternative formulations of these models, as follows:

1. The attenuation functions obtained by McGuire et al. (1) using an ω -square model with stress drop of 100 bars. This set of attenuation functions is assigned a weight of 0.5.

Table 3-1
LLNL Peak Acceleration Models

| Designation | Description | σ | Depth | Truncation | Weight |
|-------------|---|----------|------------------------|---------------|--------|
| RV1 | Boore & Atkinson (2), Toro and McGuire (3); ω^2 model, 100 bars. | 0.42 | 8 | None | 0.32 |
| RV5(x2) | ω^2 model; parameters specified by G-Expert 2 | 0.55 | Variable (10-14 km) | +2.5 σ | 0.06 |
| RV5(x3) | ω^2 model; parameters specified by G-Expert 3 | 0.50 | 8 | None | 0.06 |
| G16-A3 | Trifunac (1976) + modif. Gupta-Nuttli + $I_o = 2m_b - 3.5$ | 0.70 | 0 | +4 σ | 0.20 |
| SE1(x14) | Nuttli (4) model; $M_o f_o^4 = \text{const}$; G-Expert 2 | 0.42 | 8 | None | 0.10 |
| SE1(x2) | Nuttli (4) model; $M_o f_o^4 = \text{const}$; G-Expert 2 | 0.55 | 12 | 2.5 σ | 0.09 |
| SE-2A | Nuttli (4) model; $M_o f_o^3 = \text{Const}$ | 0.42 | 8 | None | 0.10 |
| Comb-1A | Veneziano (1986), Intensity-based | 0.55 | 8 | 2.5 σ | 0.07 |

Table 3-2
LLNL Spectral Velocity Models

| Name | Description | σ | Depth | Truncation | Weight |
|-------------|--|----------|----------|--------------|--------|
| RV1 | Boore & Atkinson (2), Toro and McGuire (3), ω^2 model, 100 bars | 0.48 | 8 | None | 0.32 |
| RV5(x2) | ω^2 model; parameters specified by G-Expert 2 | 0.55 | Variable | 2.5 σ | 0.06 |
| RV5(x3) | ω^2 model; parameters specified by G-Expert 3 | 0.60 | Variable | None | 0.06 |
| TL | Trifunac and Lee (5) + Modif. Gupta-Nuttli + $I_o = 2m_b - 3.5$ | N/A | 0 | None | 0.20 |
| NH-SE1(x14) | Newmark-Hall (6) spectrum anchored to Nuttli (1986) ($M_0 f_0^4 = \text{const.}$) acceleration and velocity; G-Expert 1 and 4 | 0.42 | 8 | None | 0.1 |
| NH-SE1(x2) | Newmark-Hall (6) spectrum anchored to Nuttli (1986) ($M_0 f_0^4 = \text{const.}$) acceleration and velocity, G-Expert 2. | 0.5 | Variable | 2.5 σ | 0.09 |
| NH-SE2 | Newmark-Hall (6) spectrum anchored to Nuttli (1986) ($M_0 f_0^3 = \text{const.}$) acceleration and velocity. | 0.42 | 8 | None | 0.10 |
| NH-RV5 | Newmark-Hall (6) spectrum anchored to acceleration and velocity from ω^2 model (G-Expert 2). | 0.55 | Variable | 2.5 σ | 0.07 |

2. The attenuation functions obtained by Boore and Atkinson (2) using an ω -square model. This set of attenuation functions is assigned a weight of 0.25.
3. The attenuation function obtained from the velocity and acceleration attenuation equations obtained by Nuttli (4) using the "increasing stress-drop" assumption coupled with the dynamic amplification factors by Newmark and Hall (6). The attenuation functions in (4) were derived using a procedure analogous to that of Herrmann and Nuttli (9). This set of attenuation functions is given a weight of 0.25.

Table 3-2 contains the coefficients of these models.

3.2.3 Comparison

There is overlap between the EPRI and LLNL sets of attenuation equations. EPRI model 2 (Boore and Atkinson) is the same as LLNL model RV1. EPRI model 3 (Nuttli) is the same as LLNL model SE1 (for acceleration) and NHSE1 (for spectra).

Figures 3-1 and 3-2 compare median rock-site predictions by the EPRI and LLNL attenuation equations. Figure 3-1 compares peak acceleration versus distance curves for m_b 5 and 7. Figure 3-2 compares response spectra for 25 km epicentral distance and m_b 5 and 7.

Figure 3-1 shows that both sets of models predict similar accelerations at distances less than 10 km. The EPRI models predict roughly the same decay of acceleration with distance as the majority of the LLNL models, especially for large magnitudes. LLNL model G16-A3, which was proposed by G-Expert 5, predicts a slower decay with distance. (Model G16-A3 also predicts a relatively strong scaling with magnitude; i.e., peak acceleration is proportional to $e^{1.34m_b}$.)

Figure 3-2 shows a difference in spectral shapes between the random-vibration models, which contain considerable energy above 15 Hz, and models that use spectral shapes based on data from moderate and large California earthquakes. This difference is largest in predictions at 1 Hz and 25 Hz. Most models show reasonable agreement at 10 Hz. One significant difference between the TL (Trifunac-Lee) model and other models is the decay with distance. For instance, the TL model predicts that 25-Hz spectral velocity decays as roughly $R^{-0.56}$ for $R < 100$ km. This difference is not shown by Figure 3-2 but would become very clear had we calculate spectra at larger distances.

Table 3-3
EPRI Ground Motion Attenuation Models

$$(\ln[Y] = a + bm_b + c \ln[R] + dR)$$

| MODEL | WEIGHT | Y † | a | b | c | d |
|---|--------|-------------------------------------|---|------|-------|---------|
| McGuire et al. (7) | 0.5 | PSV(1 Hz) | -7.95 | 2.14 | -1.00 | -0.0018 |
| | | PSV(2.5 Hz) | -3.82 | 1.49 | -1.00 | -0.0024 |
| | | PSV(5 Hz) | -2.11 | 1.20 | -1.00 | -0.0031 |
| | | PSV(10 Hz) | -1.55 | 1.05 | -1.00 | -0.0039 |
| | | PSV(25 Hz) | -1.63 | 0.98 | -1.00 | -0.0053 |
| | | Accel. | 2.55 | 1.00 | -1.00 | -0.0046 |
| Boore and Atkinson (2) | 0.25 | All Frequencies and Acceleration | More complicated functional form; see Equations 12 and 13 and Table 3 of (2). | | | |
| Nuttli (4), Newmark-Hall Amplification Factors | 0.25 | PSV(1 Hz) ‡ | 0.29 | 1.15 | -0.83 | -0.0028 |
| | | PSV(2.5 Hz) ‡ | -0.62 | 1.15 | -0.83 | -0.0028 |
| | | PSV(5 Hz) ‡ | -1.32 | 1.15 | -0.83 | -0.0028 |
| | | PSV(10 Hz) ‡ | -2.13 | 1.15 | -0.83 | -0.0028 |
| | | PSV(25 Hz) ‡ | -3.53 | 1.15 | -0.83 | -0.0028 |
| | | Accel. | 1.38 | 1.15 | -0.83 | -0.0028 |

† Spectral velocities have units of cm/sec ; acceleration has units of cm/sec^2 ; R has units of km. Variability of $\ln[Y]$ around the predicted value is characterized by a normal distribution with $\sigma = 0.5$.

‡ For given m_b and R , $\ln[Y]$ is the smaller of $a + bm_b + c \ln[R] + dR$ and $-8.3 + 2.3m_b - 0.83 \ln[R] - 0.0012R$.

| MODEL | WT. | MODEL | WT. | | |
|----------------------|------------------------------------|-------|-------------|----------|------|
| — (thick) | RV1 | 0.32 | | SE1(X14) | 0.10 |
| - - - (medium) | RV5(X2) | 0.06 | - · - · - · | SE1(X2) | 0.09 |
| - · - · - · (medium) | RV5(X3) | 0.06 | - - - | SE2 | 0.10 |
| - - - (thin) | G16-A3 | 0.20 | — (thin) | COMB-1A | 0.07 |
| — (thick) | EPRI 100 BARS, THEOR. MAGN. MOMENT | | | | |

EPRI AND LLNL PGA MODELS (m_{Lg} 5 and 7)

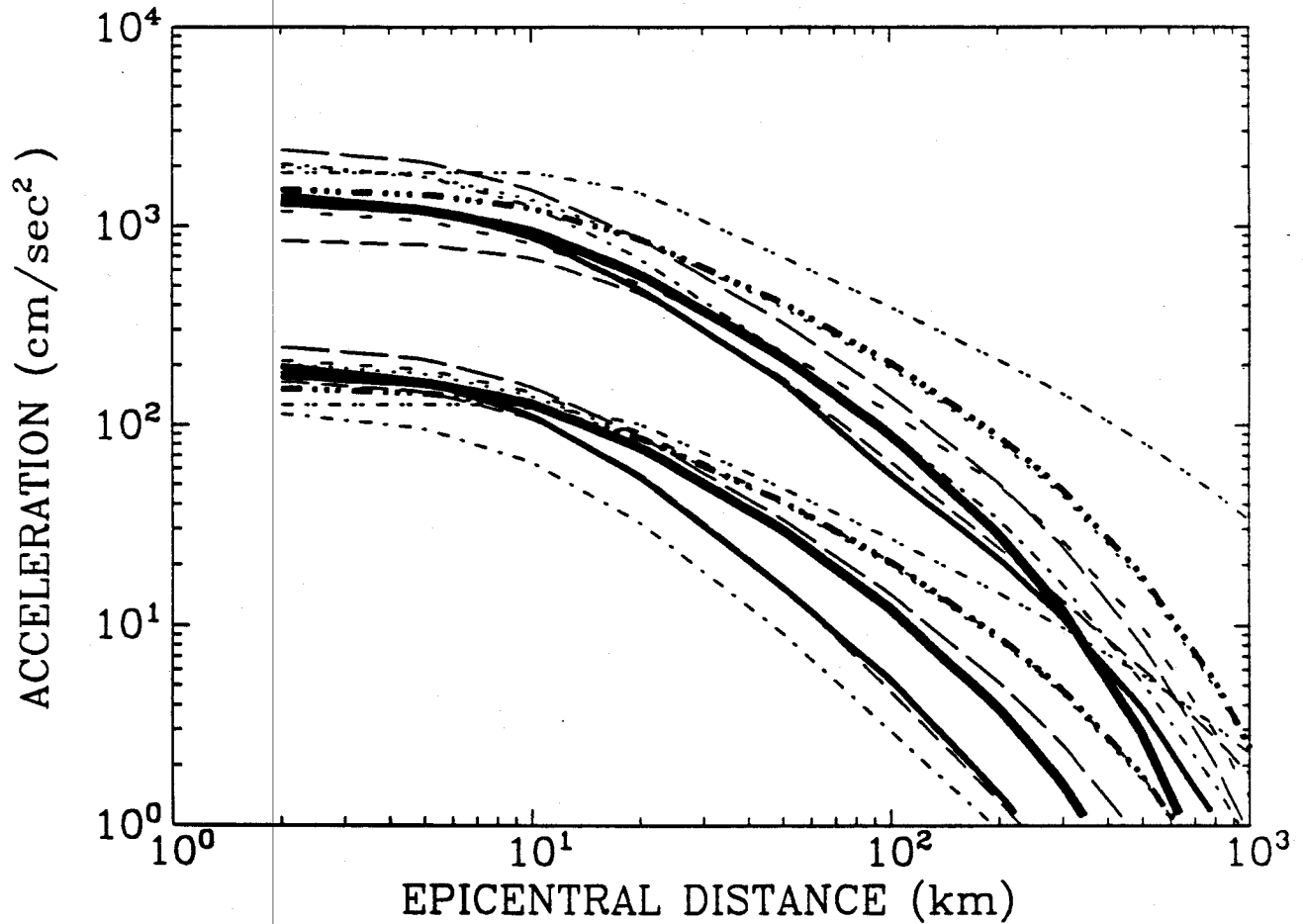


Figure 3-1. Comparison of predicted peak acceleration by the LLNL and EPRI attenuation equations. Predictions are shown for m_b 5 and 7. Predictions by McGuire et al. (7) are shown as thick lines. Predictions by Boore-Atkinson (RV1) and by Nuttli (SE1) are shown as medium lines; predictions by other LLNL models are shown as thin lines.

| MODEL | WT. | MODEL | WT. |
|------------------------------------|------|----------|------|
| RV1 | 0.32 | SE1(X14) | 0.10 |
| RV5(X2) | 0.06 | SE1(X2) | 0.09 |
| RV5(X3) | 0.06 | SE2 | 0.10 |
| G16-A3 | 0.20 | COMB-1A | 0.07 |
| EPRI 100 BARS, THEOR. MAGN. MOMENT | | | |

EPRI AND LLNL SPECTRA (m_b 5 and 7, $R=25\text{km}$)

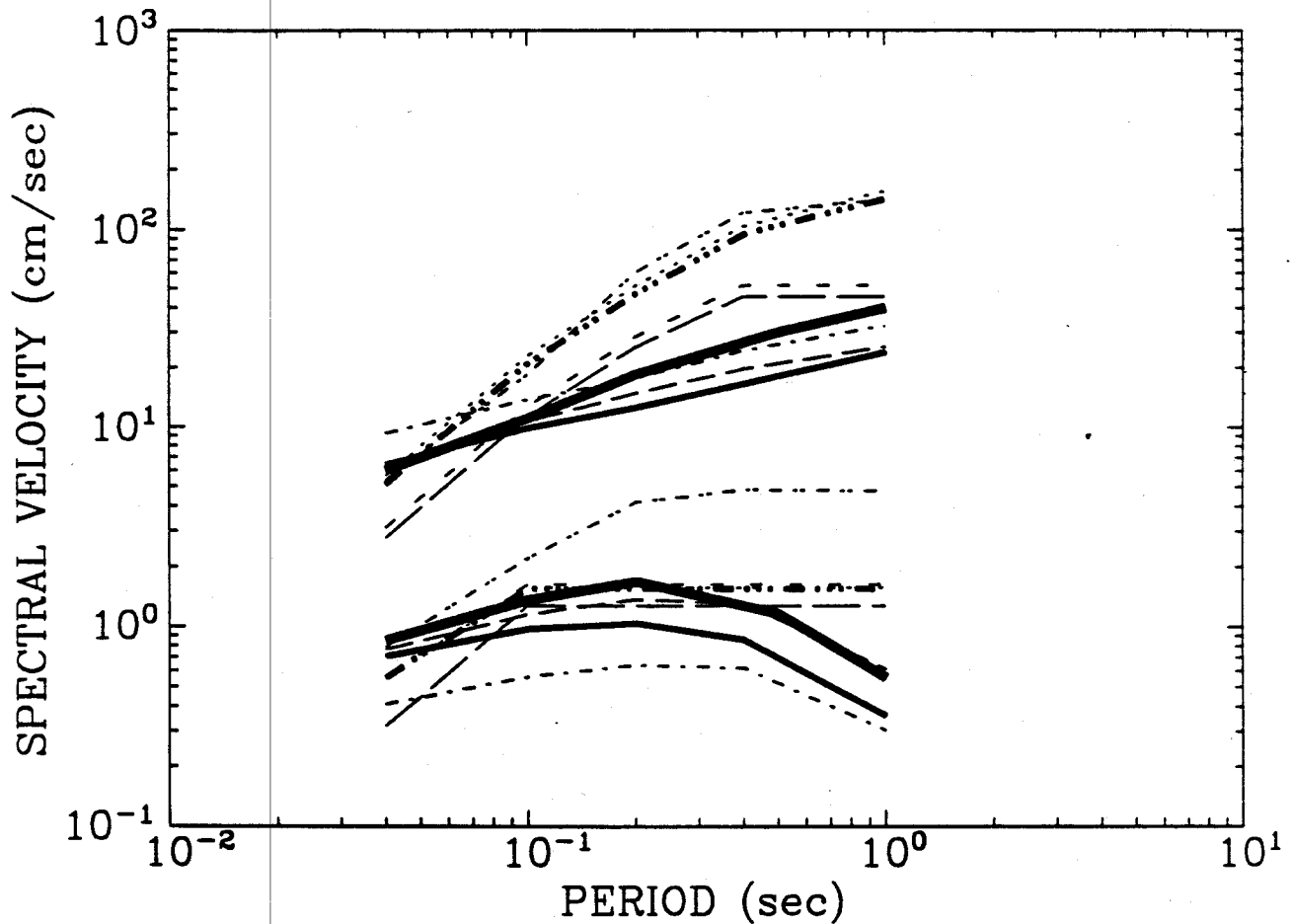


Figure 3-2. Comparison of response spectra predicted by the SOG and LLNL attenuation equations. Predictions are shown for an epicentral distance of 25 km and for m_b 5 and 7. Predictions by McGuire et al. (Z) are shown as thick lines. Predictions by Boore-Atkinson (RV1) and by Nuttli-Newmark-Hall (SE1) are shown as medium lines; predictions by other LLNL models are shown as thin lines.

3.3 SOIL AMPLIFICATION MODELS

3.3.1 LLNL Models

LLNL computed soil-amplification factors from SHAKE analyses using predominantly western-US outcrop motions with eastern-US soil profiles (10). Uncertainty was modeled by varying the properties of the profiles. Figure 3-3 shows the median amplification factors for the 7 soil categories. Uncertainty about these median values is characterized by a log-normal distribution with $\sigma = 0.5$.

These amplification factors were adopted by four of the five G-Experts. G-Expert 5 adopted the amplification factors shown in Figure 3-4. Thus, the attenuation equations by G-experts 1 through 4 are combined with the LLNL site-amplification factors, whereas the attenuation equation by G-Expert 5 is combined with the factors in Figure 3-4.

3.3.2 EPRI Models

The EPRI amplification factors were computed using a frequency-domain procedure analogous to the SHAKE analysis. The EPRI computations (1) differ from the LLNL computations in two main aspects: (1) they consider ground-motions typical of eastern-US earthquakes, and (2) they consider strain-dependent soil stiffness and damping, resulting in amplitude-dependent amplification factors.

Figures 3-5 through 3-10 show the EPRI amplification factors for peak acceleration and spectral velocity. Uncertainty in these amplification factors is modeled as lognormal with a coefficient of variation of 0.3.

3.3.3 Comparisons

The LLNL and EPRI site-amplification models predict similar amplification factors for deep soil sites. Typically, the EPRI amplification factors are higher than the LLNL factors at low amplitudes, but they become nearly identical at intermediate and high amplitudes.

G-Expert 5 uses a deep-soil amplification factor of 0.5 for peak acceleration, whereas the other G-experts use 1.0 and EPRI uses 1.2 to 0.8 (depending on amplitude). As a consequence, the difference between PGA predictions by G-Expert 5 and by other models is smaller for deep-soil sites than for rock sites.

3.4 EFFECT OF ATTENUATION FUNCTIONS AND SITE FACTORS ON CALCULATED HAZARD

In order to understand and quantify the effect of the LLNL and EPRI attenuation functions, we calculate seismic hazards at SRP using one set of zonations and seismicity parameters, but alternatively using the two sets of attenuation equations and site-amplification factors.

The first analysis uses the seismological inputs by the six EPRI Teams. Results are shown in Figures 3-11 (LLNL) and 3-12 (EPRI), in the form of median hazard curves for the various attenuation functions. The LLNL attenuation functions produce a wider scatter in predicted hazard than the EPRI attenuation function. The ratio of hazards between the highest LLNL and the highest EPRI curve is approximately 2.5 at 0.5g, 3 at 1g and 4 and 2g. The differences are largely due to the site-amplification factors. LLNL G-Experts use a PGA amplification factor of 1.0, whereas EPRI uses a value of 0.8 for accelerations of 0.3g or higher. If the same amplification factors had been used, there would be close agreement between the two sets of curves.

The second analysis uses the dominant source in the zonation by LLNL S-Expert 6 and his best-estimate values of seismicity parameters (see Table 2-1; recall that the zonation by S-Expert 6 yields the highest calculated hazard). Results are shown in Figures 3-13 and 3-14. The hazard curves show the same pattern as those obtained with the EPRI zonations, although the calculated hazards are now much higher.

The third analysis uses the dominant sources in the zonation by LLNL S-Expert 2 and his best-estimate values of seismicity parameters (recall that the zonation by S-Expert 2 yields the second highest calculated hazard). This Expert assigns a maximum magnitude of 7.5 to the Charleston source, which is the dominant source. Results are shown in Figures 3-15 and 3-16. The hazard curve obtained with model G16-A3 (G-Expert 5) is much higher than all other hazard curves, in spite of the amplification factor of 0.5 specified by this expert, because this attenuation function predicts significantly stronger magnitude dependence and weaker distance dependence than other attenuation functions.

Results in (11) indicate the effect of removing G-Expert 5 on the hazard calculated by LLNL (considering the assumptions by all S-Experts). Table 3-4 contains the mean and median hazard calculated with and without G-Expert 5, and the corresponding hazard ratios.

These three sets of results show that differences between the LLNL and EPRI attenuation functions have a significant effect in calculated hazards. These differences are due to two

main factors: (1) differences between the attenuation functions selected by G-Expert 5 and all other LLNL and EPRI attenuation functions, especially for high magnitudes and far distances; and (2) differences between LLNL and EPRI amplification factors for deep-soil sites.

Table 3-4
Effect of G-Expert 5 on Hazard Calculated by LLNL

| Quantity | Including G-Expert 5 | Excluding G-Expert 5 | Hazard Ratio |
|--------------|-------------------------|-------------------------|-----------------|
| Mean 0.25g | 1.3×10^{-3} | 6.0×10^{-4} | 4.6 |
| Mean 0.50g | 2.5×10^{-4} | 1.0×10^{-4} | 4.0 |
| Median 0.25g | 5.0×10^{-5} | 2.0×10^{-5} | 2.5 |
| Median 0.50g | 5.5×10^{-6} | 2.8×10^{-6} | 2.0 |

3.5 REFERENCES

1. D. L. Bernreuter, J. B. Savy, R. W. Mensing, and J. C. Chen. *Seismic Hazard Characterization of 69 Plant Sites East of the Rocky Mountains: Methodology, Input Data and Comparisons to Previous Results for Ten Test Sites*. Technical Report NUREG/CR5250, UCID-21517, U. S. Nuclear Regulatory Commission, 1989. Volume 1, Prepared by Lawrence Livermore National Laboratory.
2. D. M. Boore and G. M. Atkinson. "Stochastic Prediction of Ground Motion and Spectral Response Parameters at Hard-Rock Sites in Eastern North America". *Bulletin of the Seismological Society of America*, 77(2):440-467, 1987.
3. G. R. Toro and R. K. McGuire. "An Investigation into Earthquake Ground Motion Characteristics in Eastern North America". *Bulletin of the Seismological Society of America*, 77(2):468-489, April 1987.
4. O. W. Nuttli. Letter dated September 19, 1986 to J. B. Savy. Reproduced in: D. Bernreuter, J. Savy, R. Mensing, J. Chen, and B. Davis. *Seismic Hazard Characterization of 69 Nuclear Plant Sites East of the Rocky Mountains: Questionnaires*. U. S. Nuclear Regulatory Commission, Technical Report NUREG/CR-5250, UCID-21517, Volume 7, 1989. Prepared by the Lawrence Livermore National Laboratory.
5. M. Trifunac and V. W. Lee. *Frequency-Dependent Attenuation of Strong Earthquake Ground Motion*. Technical Report 86-02, University of Southern California, Department of Civil Engineering, 1986.
6. N. M. Newmark and W. J. Hall. *Earthquake Spectra and Design*. Earthquake Engineering Research Institute, Berkeley, CA, 1982.
7. R. K. McGuire, G. R. Toro, and W. J. Silva. *Engineering Model of Earthquake Ground Motion for Eastern North America*. Technical Report NP-6074, Electric Power Research Institute, 1988.
8. R. K. McGuire, G. R. Toro, J. P. Jacobson, T. F. O'Hara, and W. J. Silva. *Probabilistic Seismic Hazard Evaluations in the Central and Eastern United States: Resolution of the Charleston Earthquake Issue*. Special Report NP-6395-D, Electric Power Research Institute, April 1989.
9. R. B. Herrmann and O. W. Nuttli. "Strong Motion Investigations in the Central United States". In *Proceedings: 7th World Conference on Earthquake Engineering, Istanbul*, pp. 533-536, 1980.
10. D. L. Bernreuter, J. B. Savy, R. W. Mensing, and J. C. Chen. *Seismic Hazard Characterization of 69 Plant Sites East of the Rocky Mountains*. Technical Report NUREG/CR5250, UCID-21517, U. S. Nuclear Regulatory Commission, 1988.
11. J. B. Savy. *Seismic Hazard Characterization of the Savannah River Plant (SRP)*. Technical Report UCID-21596, Lawrence Livermore National Laboratory, November 1988.

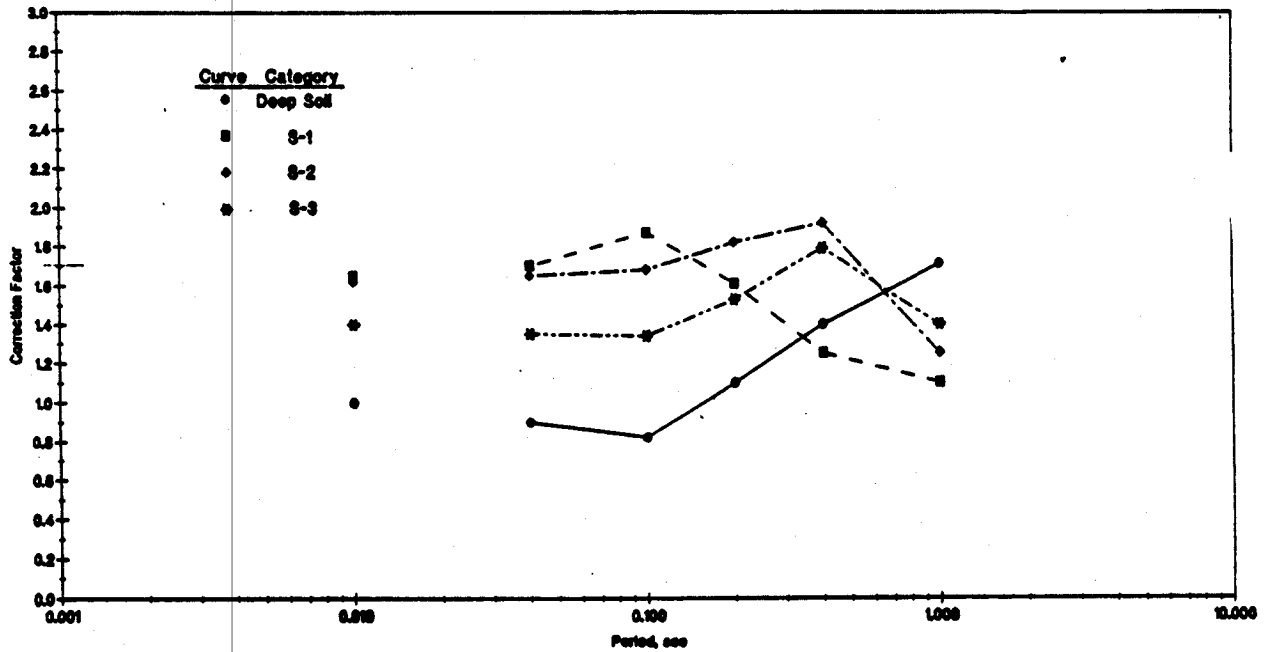
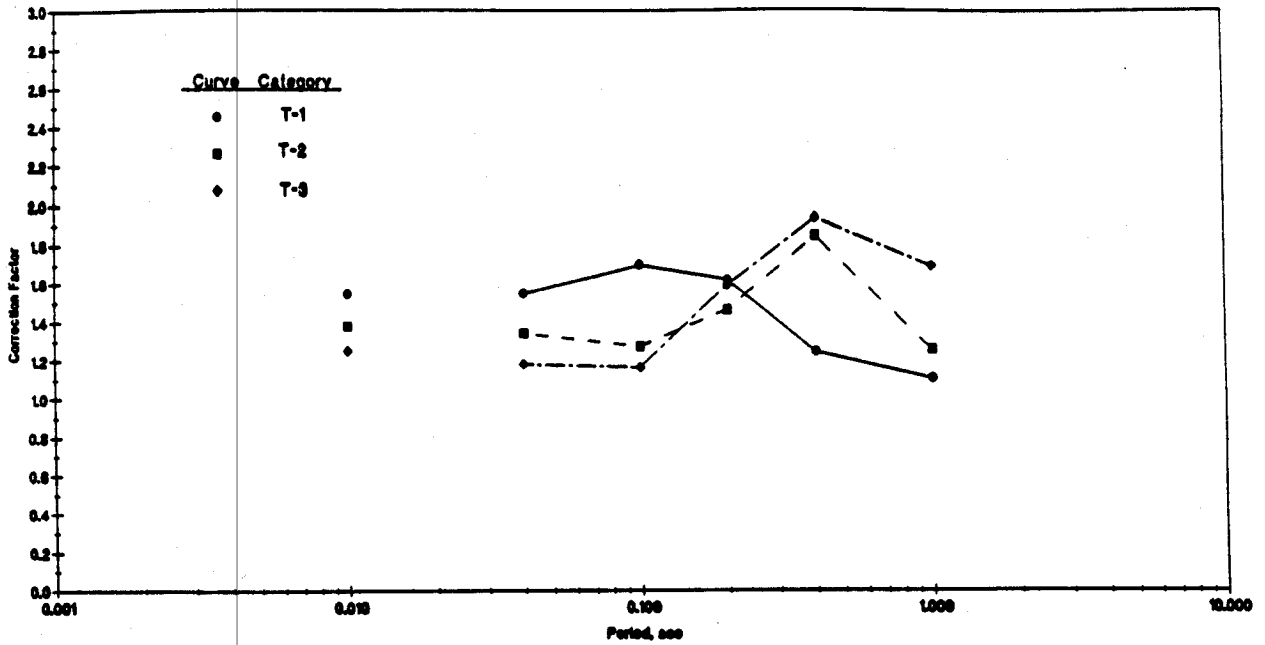


Figure 3-3. LLNL median site-amplification factors. The PGA factors are plotted at 0.01 sec. Site categories are defined according soil stiffness (T: till-like, S: sand-like) and depth to bedrock (1: 25-80 ft, 2: 80-180 ft, 3: 180-300 ft). Source: (10).

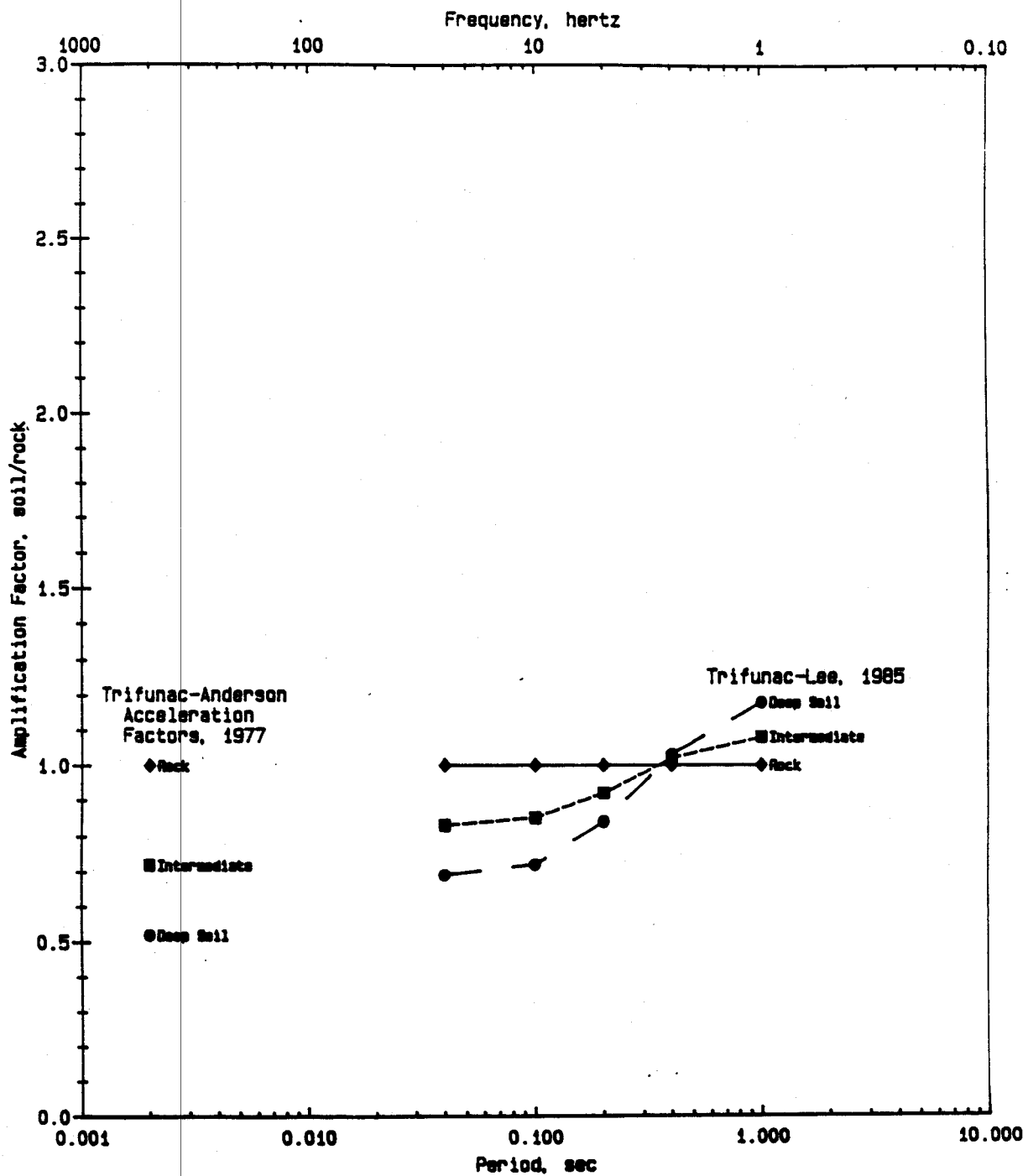


Figure 3-4. Site-amplification factors used by G-Expert 5. Source: (10).

SOIL/ROCK AMPLIFICATION FACTOR (1Hz)

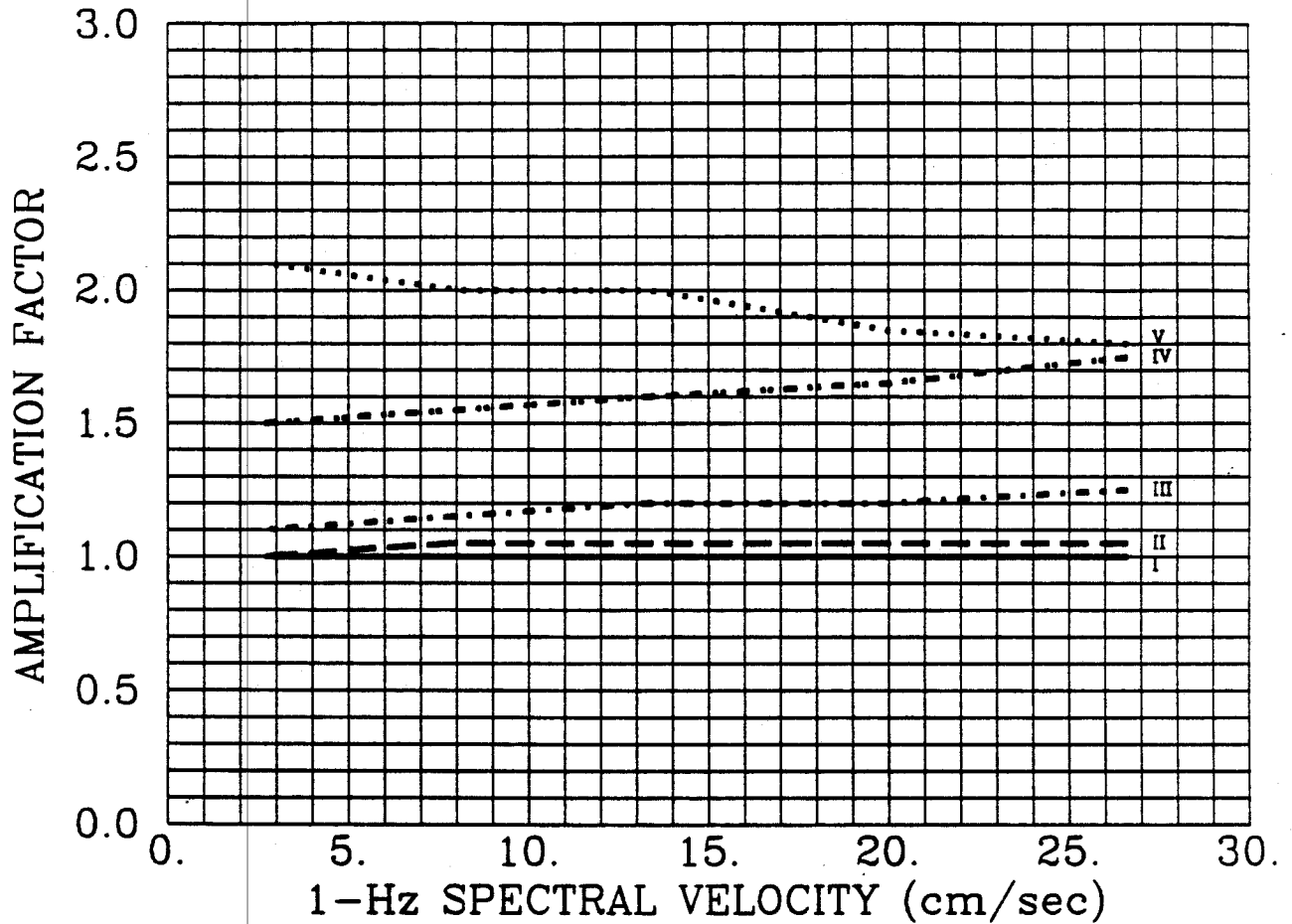


Figure 3-5. Site amplification factors for 1-Hz spectral velocity (5% damping). Site categories are defined based on depth to bedrock, as follows: I: 10-30 ft, II: 30-80 ft, III: 80-180 ft, IV: 180-400 ft, V: >500 ft.

SOIL/ROCK AMPLIFICATION FACTOR (2.5 Hz)

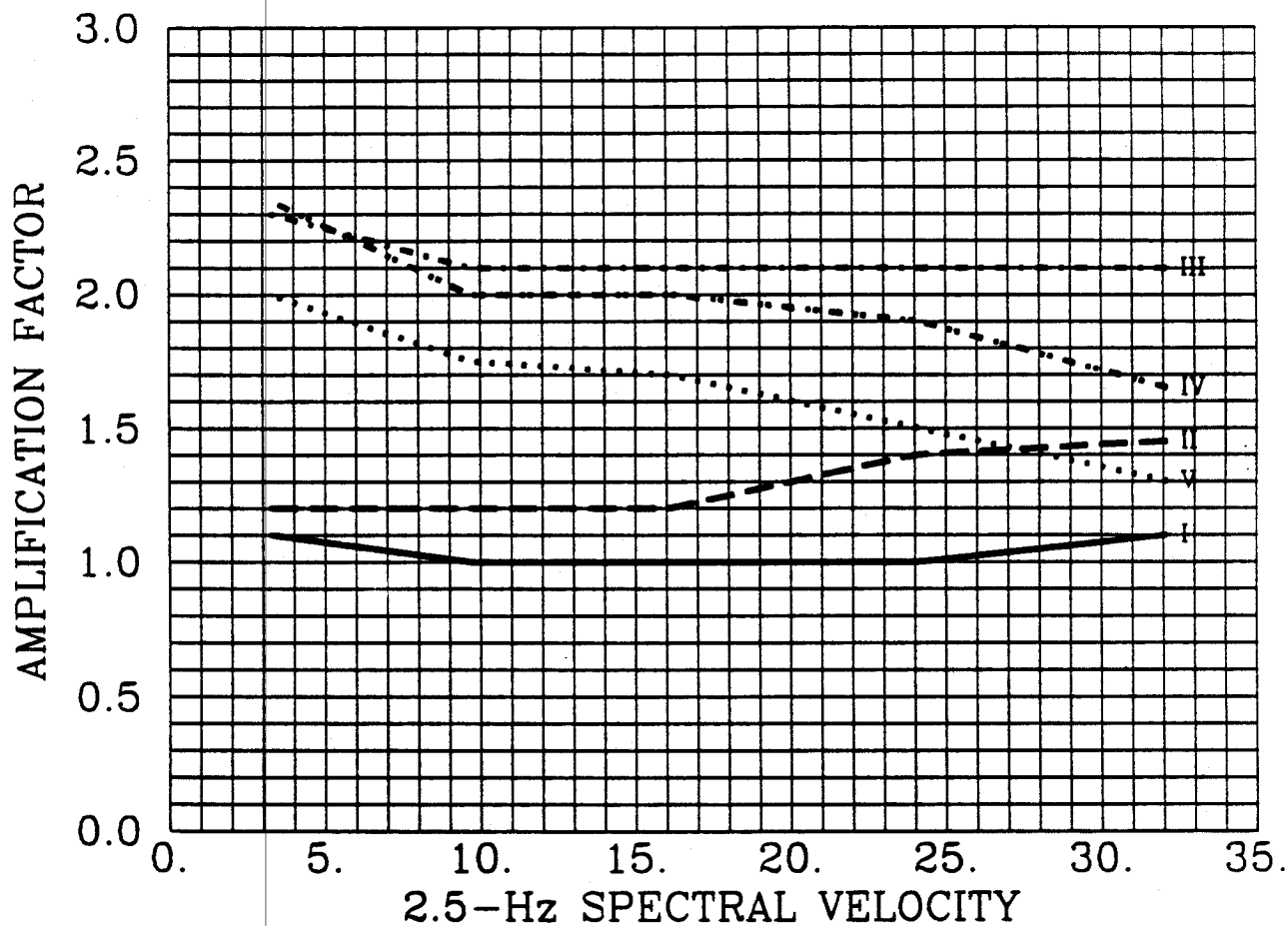


Figure 3-6. Site amplification factors for 2.5-Hz spectral velocity (5% damping). Site categories are defined based on depth to bedrock, as follows: I: 10-30 ft, II: 30-80 ft, III: 80-180 ft, IV: 180-400 ft, V: >500 ft.

SOIL/ROCK AMPLIFICATION FACTOR (5Hz)

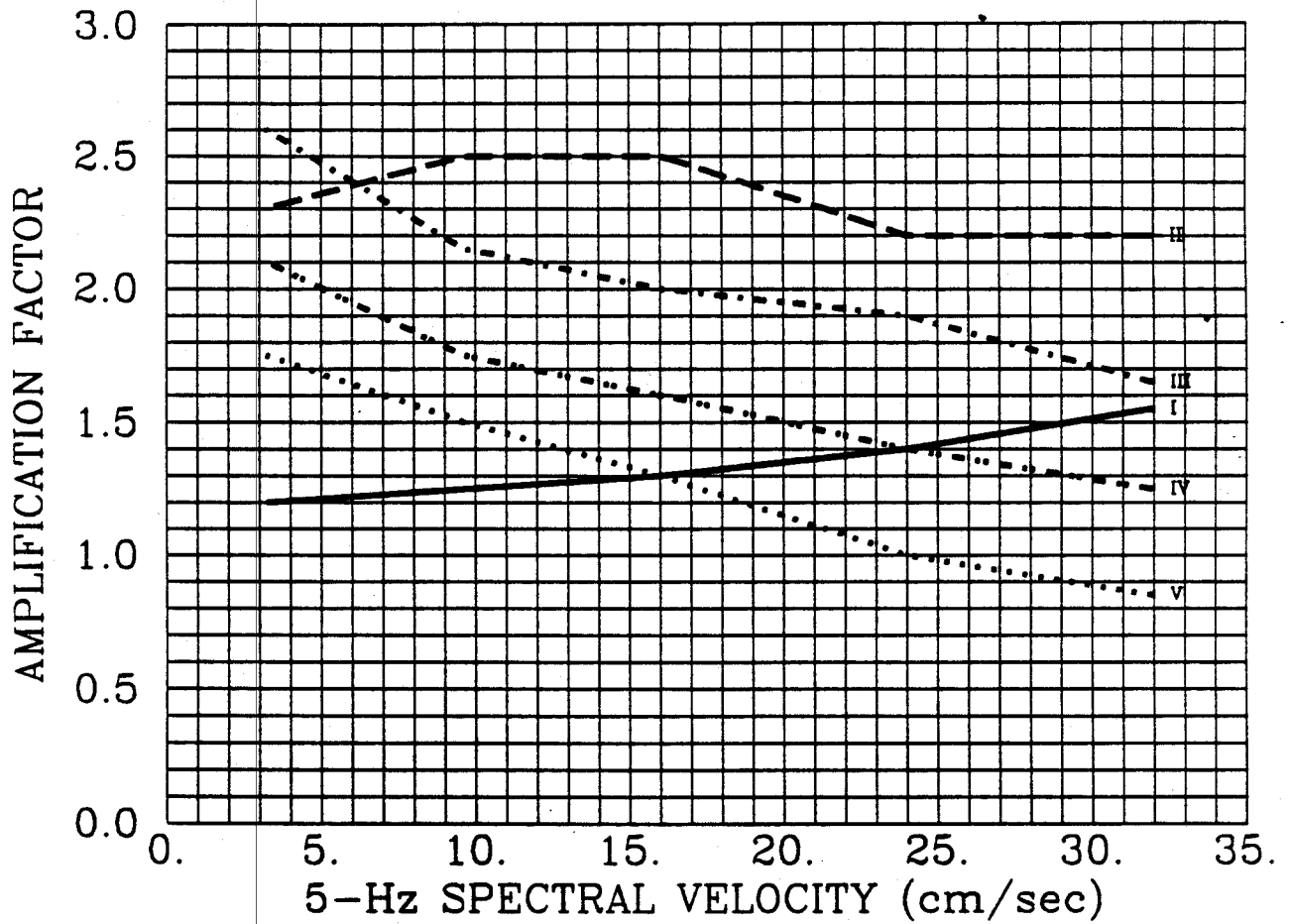


Figure 3-7. Site amplification factors for 5-Hz spectral velocity (5% damping). Site categories are defined based on depth to bedrock, as follows: I: 10-30 ft, II: 30-80 ft, III: 80-180 ft, IV: 180-400 ft, V: >500 ft.

SOIL/ROCK AMPLIFICATION FACTOR (10Hz)

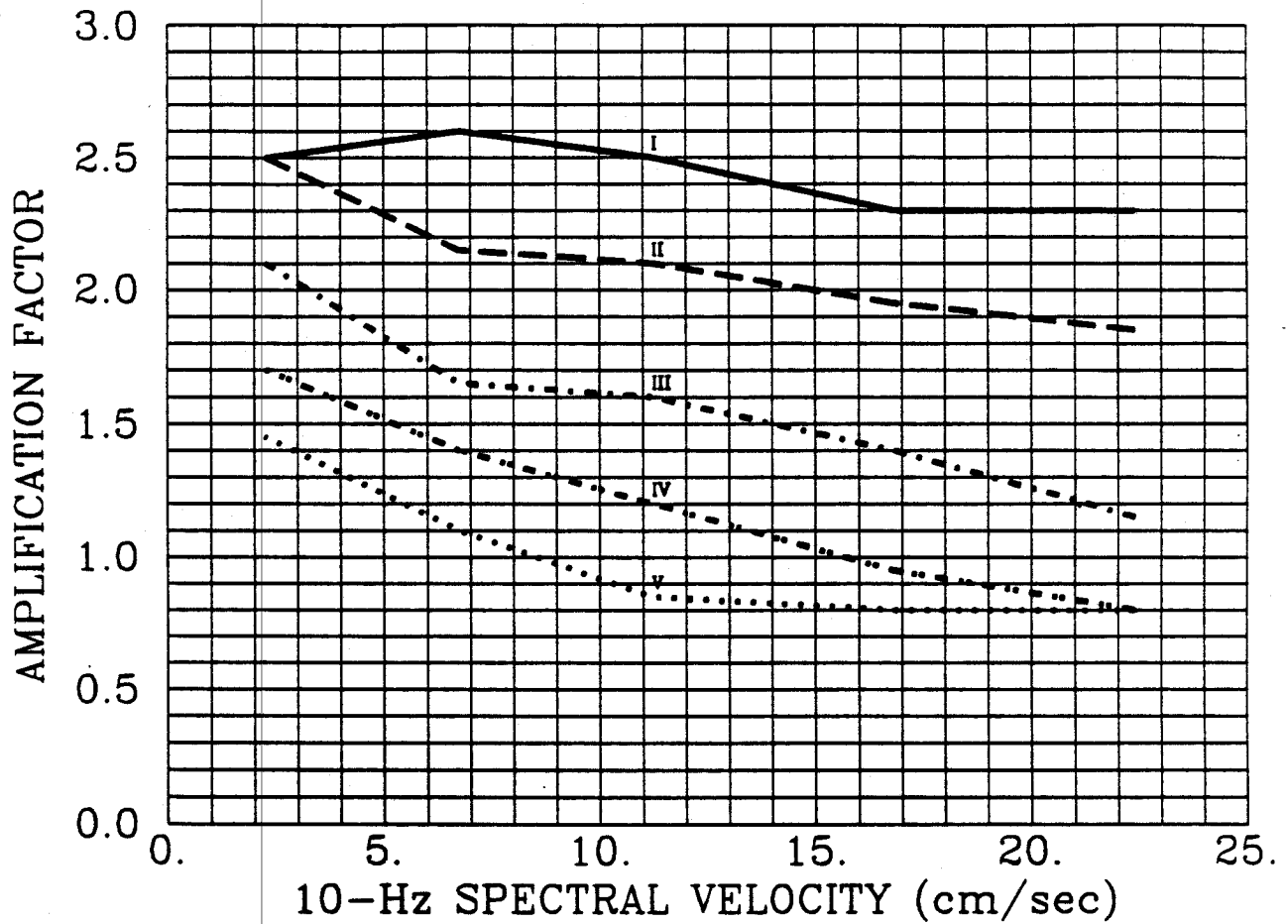


Figure 3-8. Site amplification factors for 10-Hz spectral velocity (5% damping). Site categories are defined based on depth to bedrock, as follows: I: 10-30 ft, II: 30-80 ft, III: 80-180 ft, IV: 180-400 ft, V: >500 ft.

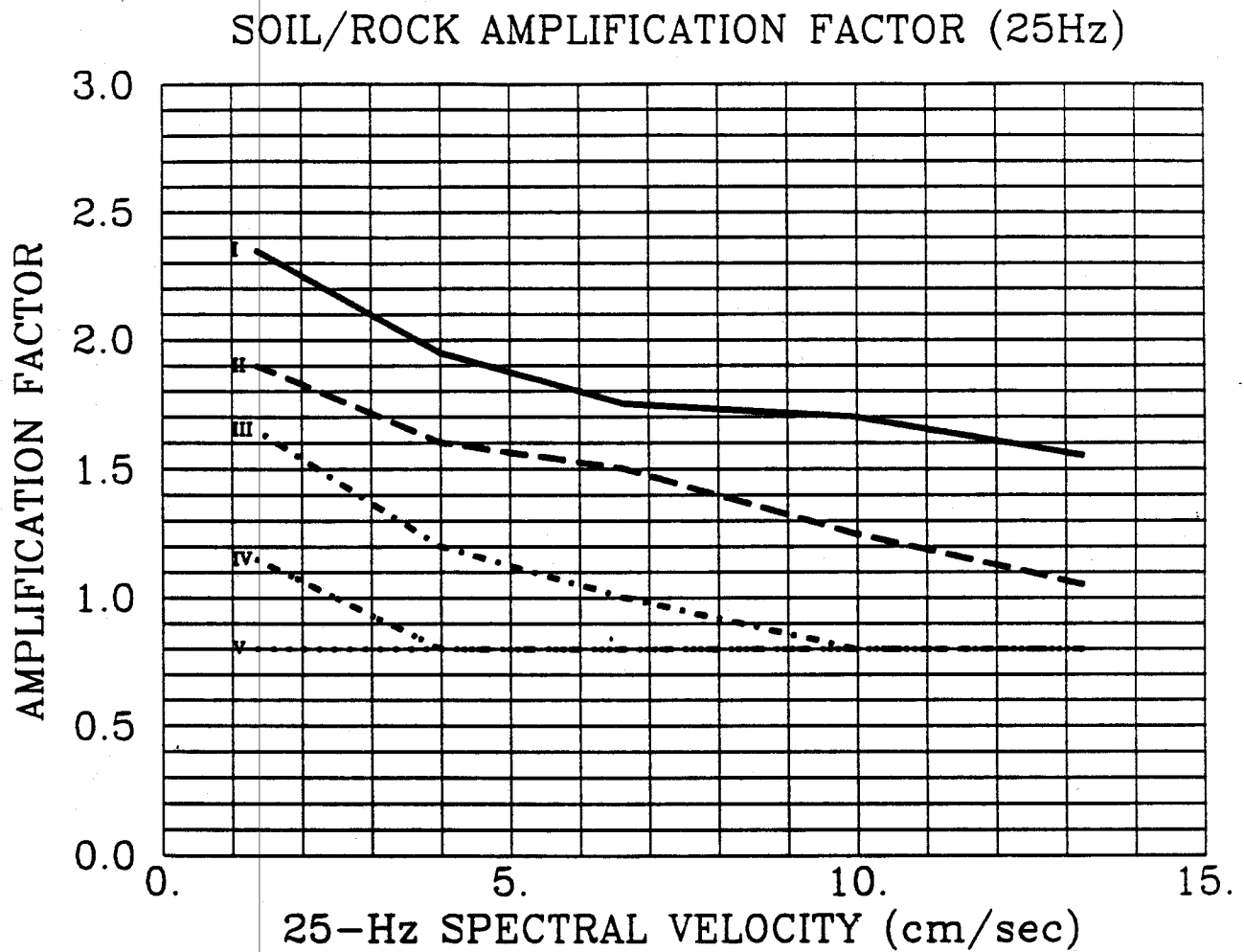


Figure 3-9. Site amplification factors for 25-Hz spectral velocity (5% damping). Site categories are defined based on depth to bedrock, as follows: I: 10-30 ft, II: 30-80 ft, III: 80-180 ft, IV: 180-400 ft, V: >500 ft.

SOIL/ROCK AMPLIFICATION FACTOR (PGA)

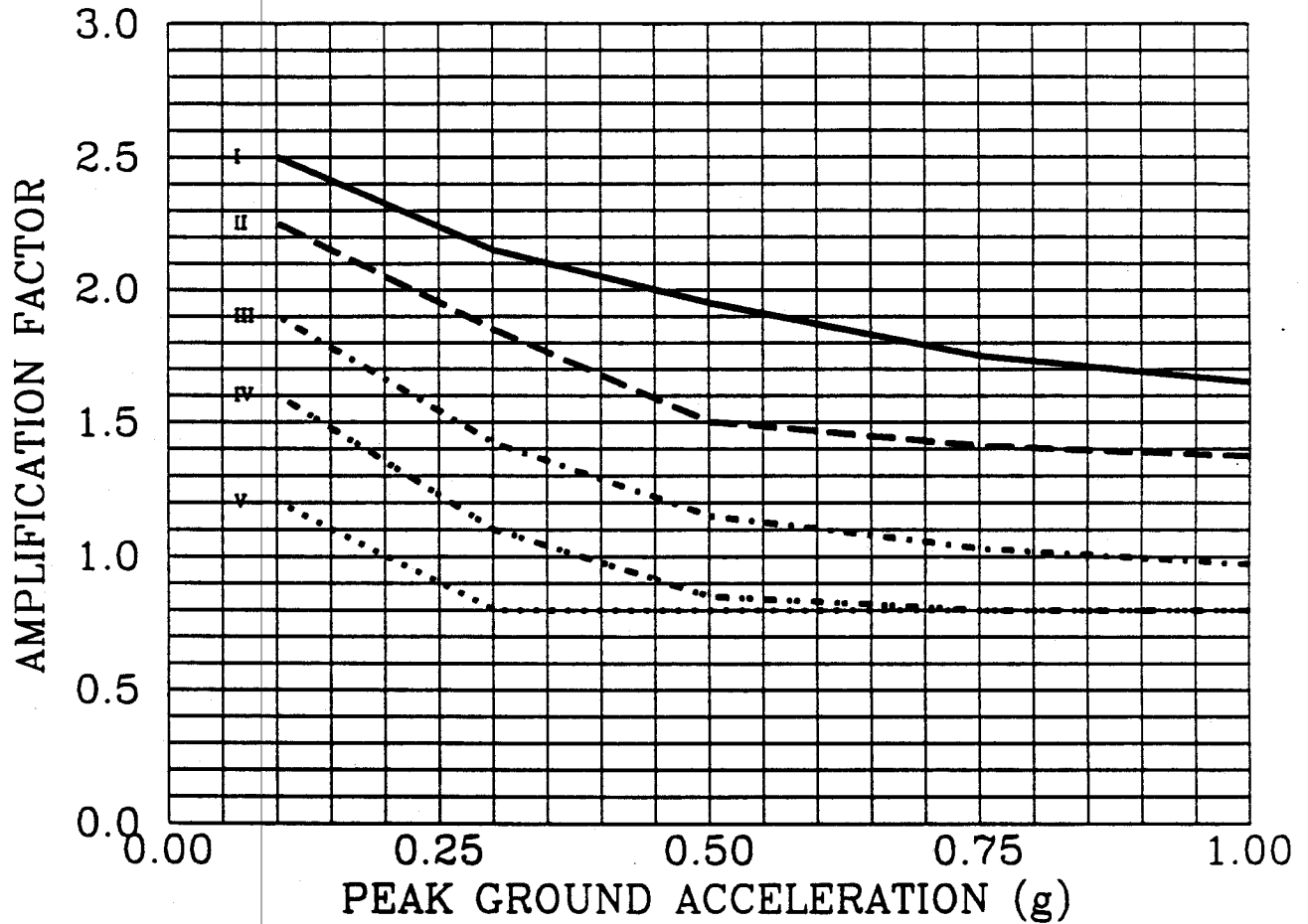


Figure 3-10. Site amplification factors for peak ground acceleration. Site categories are defined based on depth to bedrock, as follows: I: 10-30 ft, II: 30-80 ft, III: 80-180 ft, IV: 180-400 ft, V: >500 ft.

| MODEL | WT. | MODEL | WT. | | |
|-----------|---------|-------|-----------|----------|------|
| — | RV1 | 0.32 | | SE1(X14) | 0.10 |
| - - - | RV5(X2) | 0.06 | - · - · - | SE1(X2) | 0.09 |
| - · - · - | RV5(X3) | 0.06 | - - - | SE2 | 0.10 |
| - · - · - | G16-A3 | 0.20 | — | COMB-1A | 0.07 |

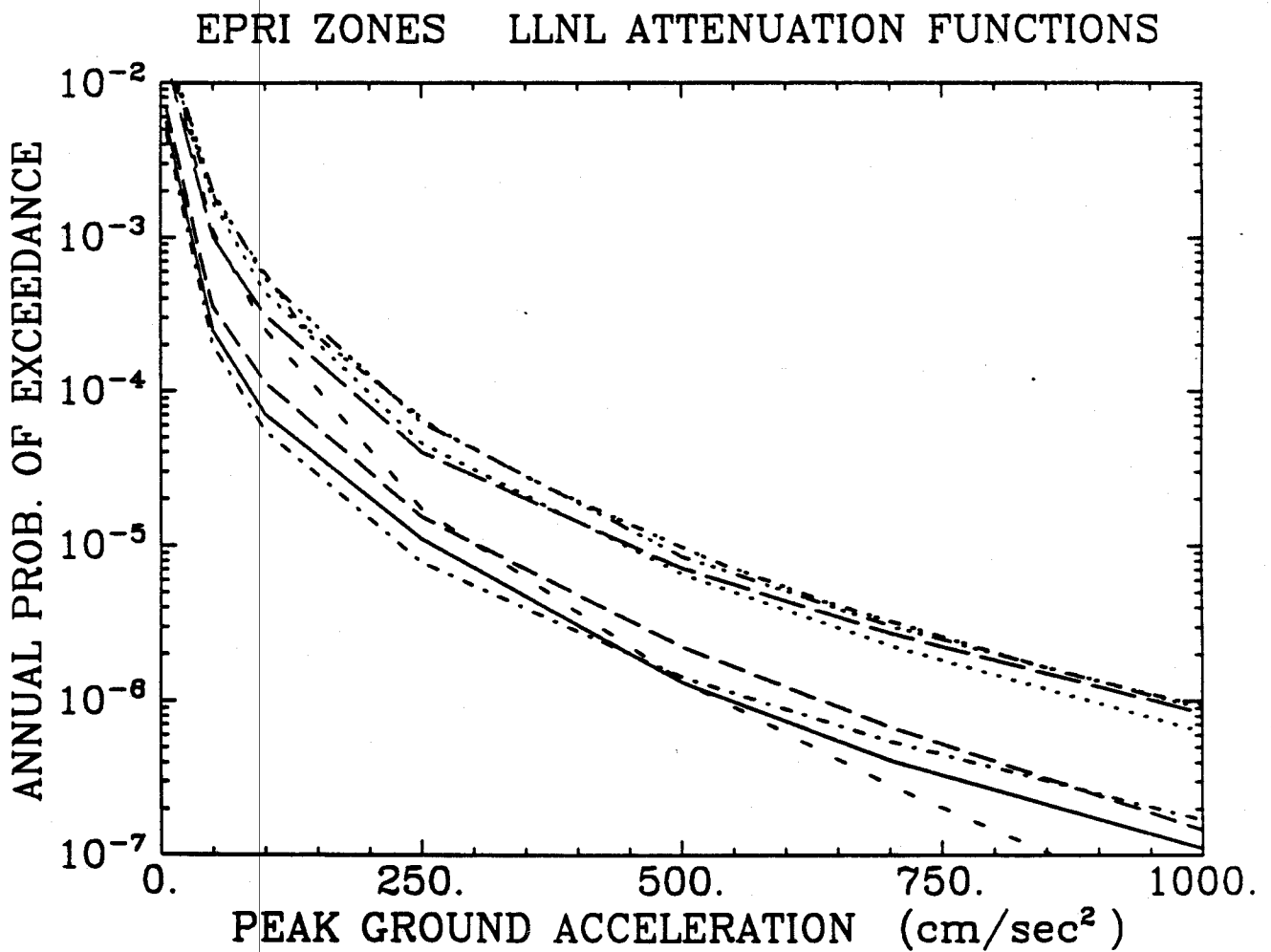


Figure 3-11. Median hazard curves for each LLNL attenuation function; SRP zonations and seismicity parameters by the EPRI Teams.

SAVANNAH RIVER PLANT
EPRI ZONES EPRI ATTENUATION FUNCTIONS

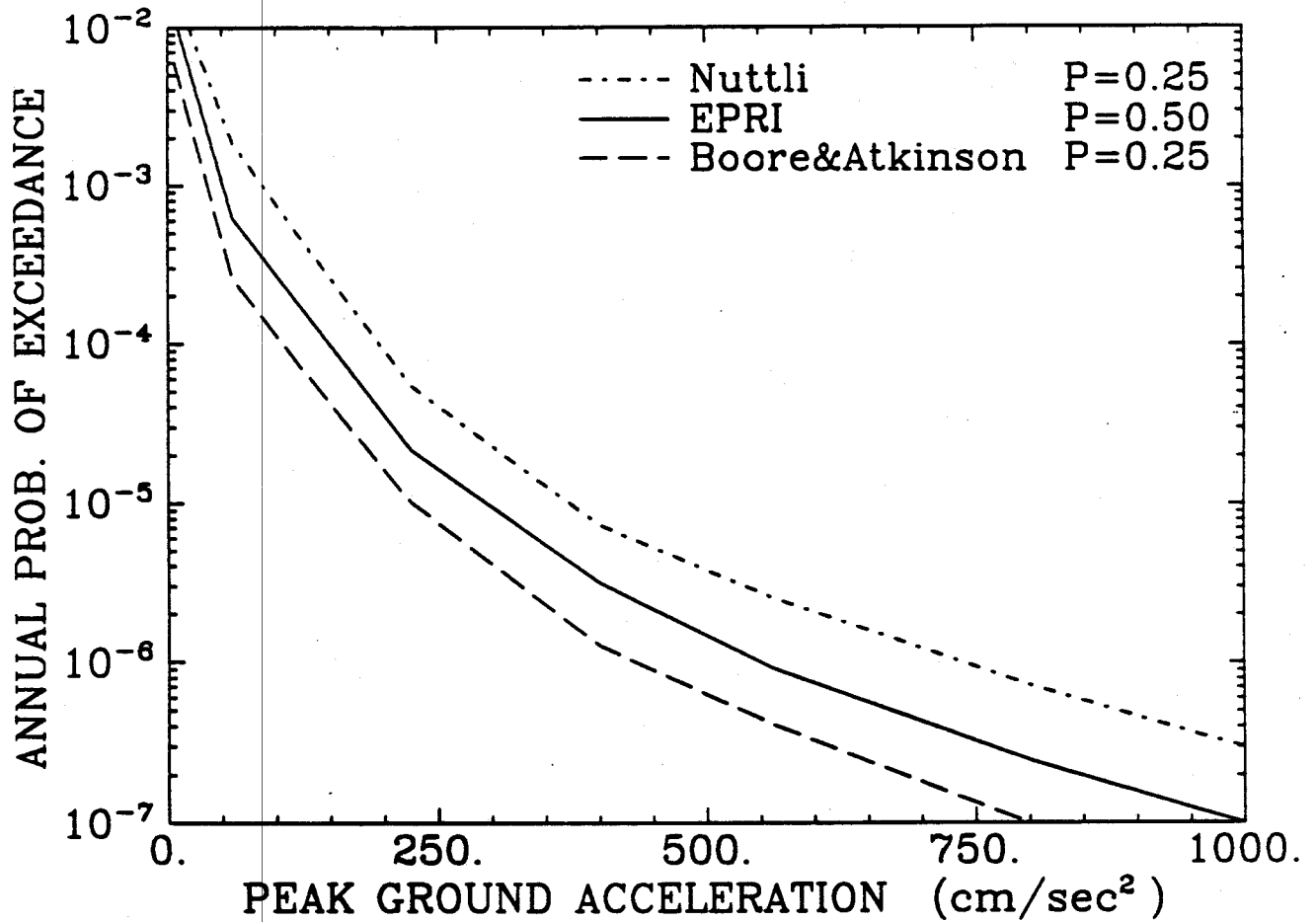


Figure 3-12. Median hazard curves for each EPRI attenuation function; SRP zonations and seismicity parameters by the EPRI Teams.

| MODEL | WT. | MODEL | WT. |
|---------|------|----------|------|
| RV1 | 0.32 | SE1(X14) | 0.10 |
| RV5(X2) | 0.06 | SE1(X2) | 0.09 |
| RV5(X3) | 0.06 | SE2 | 0.10 |
| G16-A3 | 0.20 | COMB-1A | 0.07 |

S EXPERT 6 LLNL ATTENUATION FUNCTIONS

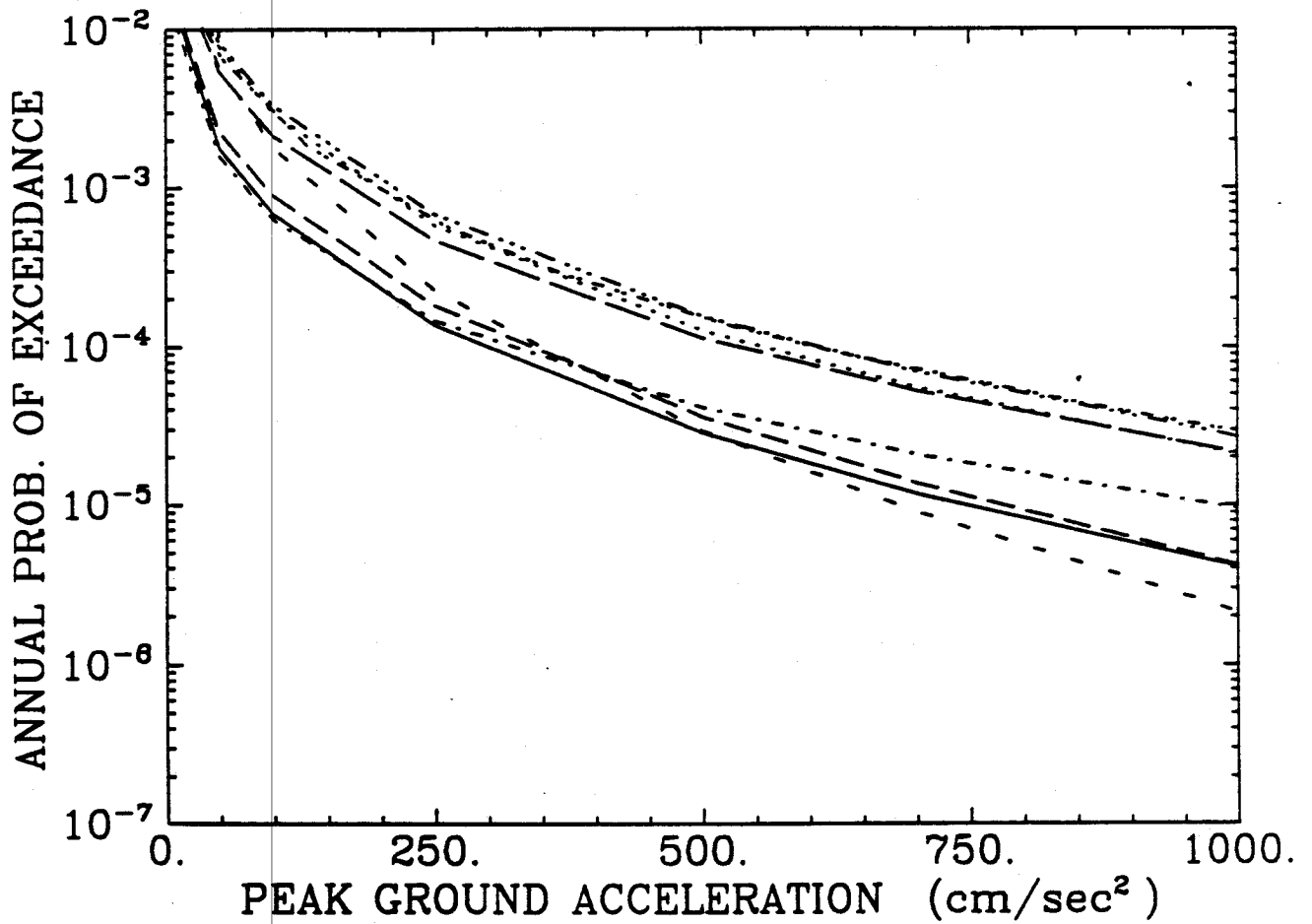


Figure 3-13. Hazard curves for each LLNL attenuation function; SRP zonation and best-estimate seismicity parameters by S-Expert 6.

SAVANNAH RIVER PLANT

LLNL S-EXPERT 6 EPRI ATTENUATION FUNCTIONS

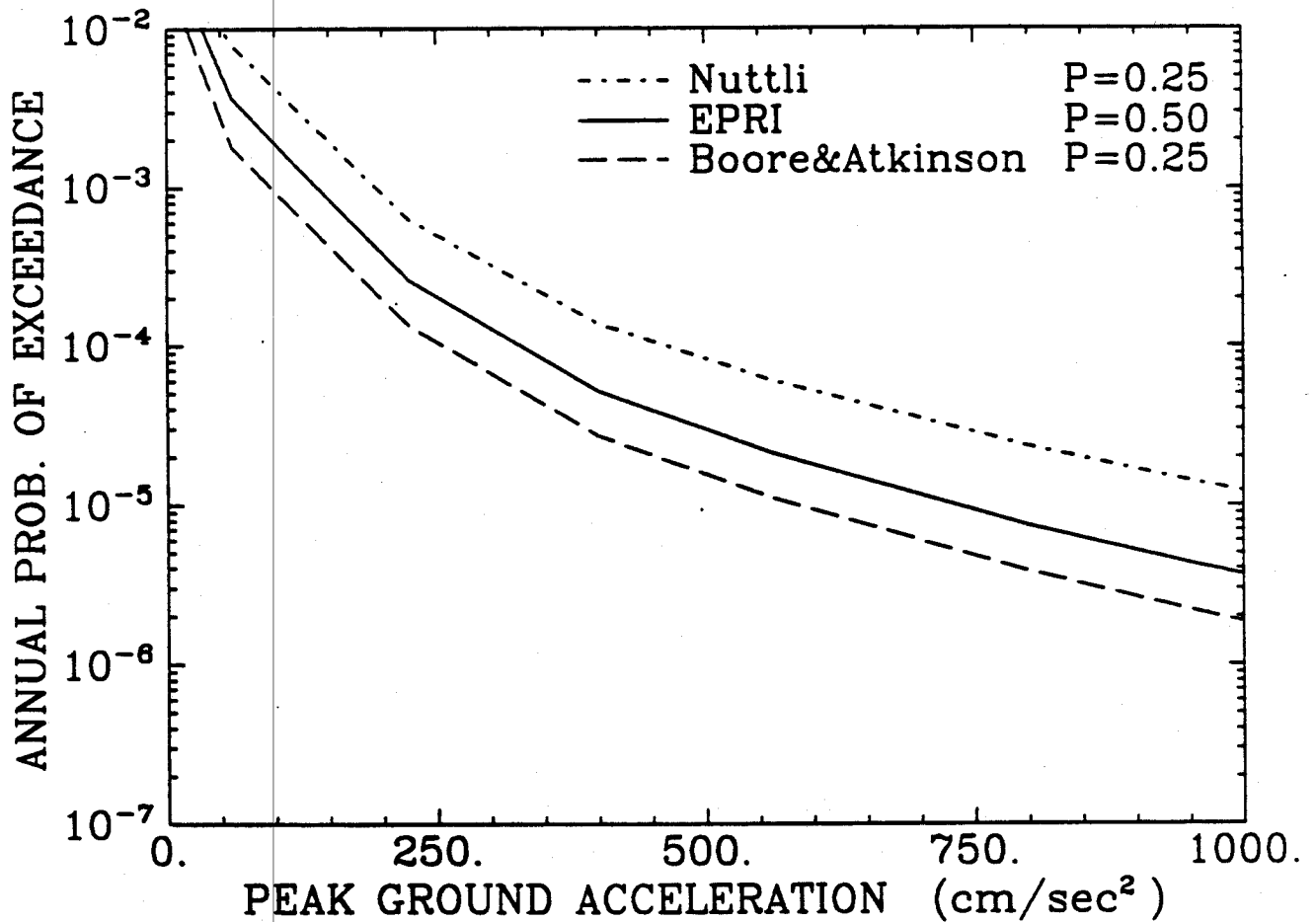


Figure 3-14. Hazard curves for each EPRI attenuation function; SRP zonation and best-estimate seismicity parameters by S-Expert 6.

| MODEL | WT. | MODEL | WT. | | |
|---------|---------|-------|---------|----------|------|
| — | RV1 | 0.32 | | SE1(X14) | 0.10 |
| - - - | RV5(X2) | 0.06 | - - - - | SE1(X2) | 0.09 |
| - - - - | RV5(X3) | 0.06 | - - - - | SE2 | 0.10 |
| - - - - | G16-A3 | 0.20 | — | COMB-1A | 0.07 |

S EXPERT 2 LLNL ATTENUATION FUNCTIONS

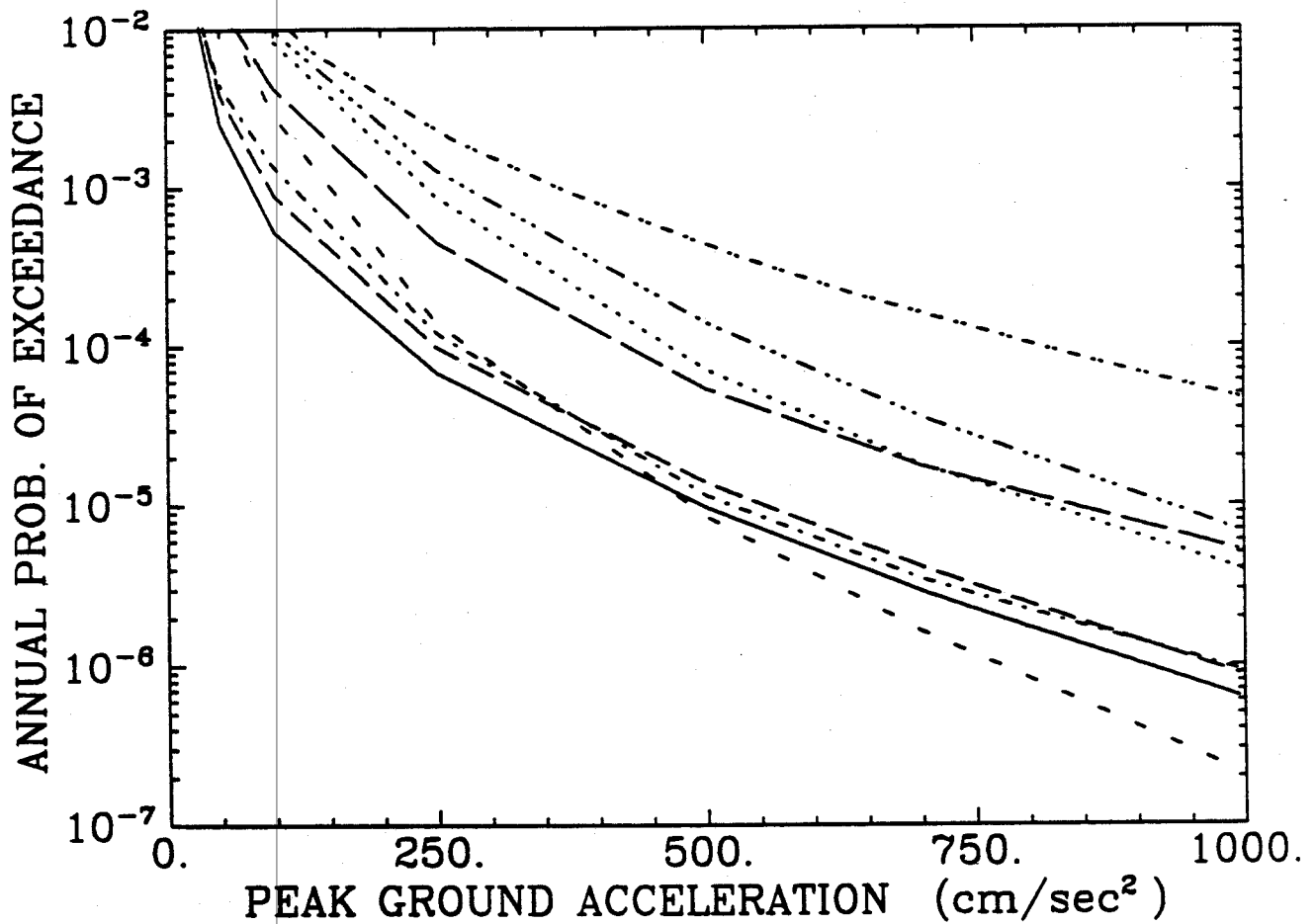


Figure 3-15. Hazard curves for each LLNL attenuation function; SRP zonation and best-estimate seismicity parameters by S-Expert 2.

SAVANNAH RIVER PLANT

LLNL S-EXPERT 2 EPRI ATTENUATION FUNCTIONS

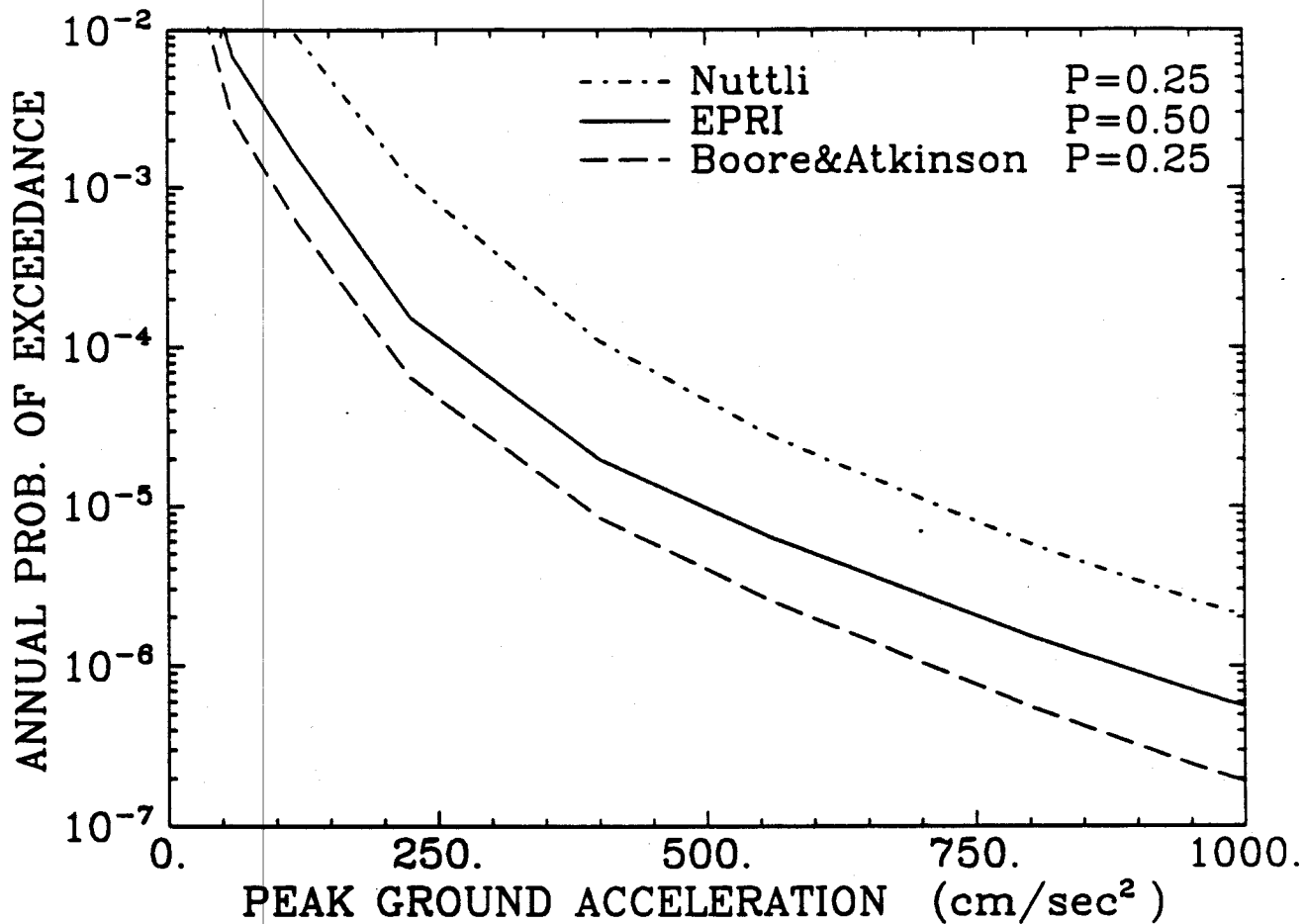


Figure 3-16. Hazard curves for each EPRI attenuation function; SRP zonation and best-estimate seismicity parameters by S-Expert 2.

Section 4

RECOMMENDATIONS

In this section we evaluate the differences in results presented in previous sections, and make recommendations regarding choices of seismic hazard curves for the Savannah River site. These recommendations are based on differences in input assumptions that are perceived to have the greatest effect on calculated seismic hazard at the site.

4.1 SEISMICITY MODELS

As presented in Section 2, there are differences in the seismicity assumptions used by the LLNL and EPRI Experts in modeling the sources of earthquakes in South Carolina. These differences are large for models of the Charleston seismicity and are small for models of seismicity in the adjacent regions of the coastal plain. Summaries of specific parameters used in the two studies are presented in Tables 2-1 and 2-2 for the two studies, respectively.

To evaluate the effects of these differences on seismic hazard, we have constructed a base-case set of parameters for the Charleston source and for the host source. We computed the hazard for the activity rate, *b*-value, and maximum magnitude assumed by each seismicity Expert or Team. We also computed the hazard by setting one parameter to its base-case value, while using the Expert or Team's values for the other parameters. We then calculated the effect of each Expert's or Team's assumptions by forming the ratio of these two hazards. The changes in assumptions were made and computed individually so that the individual effect of activity rate, *b*-value, and maximum magnitude could be presented.

Tables 2-4 and 2-5 show the effects of changing each Expert's or Team's assumptions regarding seismicity parameters for the source that dominates the hazard at the SRP site. For the Charleston source the factors for LLNL Experts are generally greater than unity, reflecting the more conservative choices made by those Experts on activity rates, *b*-values, and maximum magnitudes. Conversely the factors for EPRI Teams are generally less than unity, reflecting generally lower estimates of the rate of activity, higher (steeper) *b*-values, and lower maximum magnitude estimates. For the coastal plain sources the differences are not as large, as shown by the values closer to unity in Table 2-5. Thus the differences between the LLNL and EPRI hazard results derive primarily from modeling of the Charleston

seismicity. This is reflected also in Tables 2-1 and 2-2, which show that for the majority of LLNL Experts the Charleston source dominates the hazard at the site, whereas for the EPRI Teams the host source always dominates the hazard.

To evaluate these differences and reach some recommendations, we summarized historical earthquake data in the Charleston region, using the catalog of eastern US earthquakes derived during the EPRI study. The data are shown in Figure 4-1; historical earthquakes within 50 km of Charleston were analyzed, and are presented in Table 4-1. The derivation of seismicity parameters in this region is, of course, problematic, because of the few numbers of events at different magnitude levels and because of problems of incomplete reporting in the early history of the region.

One can see from Table 4-1 that assigning completeness intervals and computing rates of activity is difficult. In the EPRI study an automated methodology was developed for this that accounted for non-zero and non-unity probabilities of earthquake detection, thus taking into account events that occurred prior to the time that complete reporting of events occurred. In the LLNL study completeness estimates and activity rates were derived a more subjective way by each Expert, which is the traditional way such assessments are made.

To illustrate and compare empirical rates of activity, we have chosen two sets of time intervals and resulting activity rates. Table 4-2 gives the details of these assumptions. They are not the only ones that could be made, but they are useful for illustration purposes. Option 1 assumes that low-level seismicity (m_b between 3.3 and 5.1) has been completely reported since 1945, and that events above m_b 5.7 have been completely reported since 1800. Option 2 assumes that earthquakes between m_b 3.3 and 4.5 are complete only since 1970, and that the Charleston earthquake has an average recurrence period of 500 years. The recurrence period in option 2 may be still too high; paleoseismic evidence suggests a recurrence period of 1500 to 2000 years (1).

Figure 4-2 shows a comparison of these observed rates of occurrence with the models of seismicity specified by ten of the eleven LLNL Experts (one Expert, No. 11, used a much larger region representing the southeastern coastal plain as shown in Figure 2-9, so this Expert's interpretations were not included in this comparison). Five of the ten LLNL Experts have interpretations that lie above the data points for magnitudes 5.7 and less.

For comparison, Figure 4-3 compares the observed rates of occurrence with models of seismicity derived by the six EPRI Teams for their Charleston sources. For magnitudes below

Table 4-1

Summary of Historical Earthquakes in the
Charleston Region (50 km radius)
by Decade, 5-year Interval, and Year

| MAG. | 3.30 | 3.90 | 4.50 | 5.10 | 5.70 | 6.30 | 6.90 | 7.50 |
|---------|------|------|------|------|------|------|------|------|
| RANGE: | 3.90 | 4.50 | 5.10 | 5.70 | 6.30 | 6.90 | 7.50 | 8.10 |
| 1790 | . | 1 | . | . | . | . | . | . |
| 1800 | . | . | . | . | . | . | . | . |
| 1810 | . | . | . | . | . | . | . | . |
| 1820 | . | . | . | . | . | . | . | . |
| 1830 | . | . | . | . | . | . | . | . |
| 1840 | . | . | . | . | . | . | . | . |
| 1850 | . | 1 | . | . | . | . | . | . |
| 1860 | 1 | 1 | . | . | . | . | . | . |
| 1870 | 1 | . | . | . | . | . | . | . |
| 1880 | . | . | . | . | . | 1 | . | . |
| 1890 | 5 | . | . | . | . | . | . | . |
| 1900 | 2 | . | . | . | . | . | . | . |
| 1905 | . | 1 | . | . | . | . | . | . |
| 1910 | . | . | . | 1 | . | . | . | . |
| 1915 | . | . | . | . | . | . | . | . |
| 1920 | . | . | . | . | . | . | . | . |
| 1925 | . | . | . | . | . | . | . | . |
| 1930 | . | 1 | . | . | . | . | . | . |
| 1935 | . | . | . | . | . | . | . | . |
| 1940 | 1 | . | . | . | . | . | . | . |
| 1945 | 2 | . | . | . | . | . | . | . |
| 1950 | 2 | 1 | . | . | . | . | . | . |
| 1955 | . | 1 | . | . | . | . | . | . |
| 1960 | . | . | . | . | . | . | . | . |
| 1965 | 2 | . | . | . | . | . | . | . |
| 1970 | . | . | . | . | . | . | . | . |
| 1971 | . | . | . | . | . | . | . | . |
| 1972 | . | . | . | . | . | . | . | . |
| 1973 | . | . | . | . | . | . | . | . |
| 1974 | . | 1 | . | . | . | . | . | . |
| 1975 | . | . | . | . | . | . | . | . |
| 1976 | . | . | . | . | . | . | . | . |
| 1977 | . | 1 | . | . | . | . | . | . |
| 1978 | . | . | . | . | . | . | . | . |
| 1979 | . | . | . | . | . | . | . | . |
| 1980 | 1 | . | . | . | . | . | . | . |
| 1981 | . | . | . | . | . | . | . | . |
| 1982 | . | . | . | . | . | . | . | . |
| 1983 | 1 | . | . | . | . | . | . | . |
| TOTALS: | 18 | 9 | 0 | 1 | 0 | 1 | 0 | 0 |

Table 4-2
Completeness Period and Activity Rates
for the Charleston Source

| | Magnitudes | | | | | |
|-----------------------|------------|---------|---------|---------|---------|---------|
| | 3.3-3.9 | 3.9-4.5 | 4.5-5.1 | 5.1-5.7 | 5.7-6.3 | 6.3-6.9 |
| OPTION 1: | | | | | | |
| Complete from: | 1945 | 1945 | 1945 | 1860 | 1800 | 1800 |
| No. events thru 1983: | 8 | 4 | 0 | 1 | 0 | 1 |
| No. years: | 39 | 39 | 39 | 124 | 184 | 184 |
| Annual rate: | 0.205 | 0.103 | 0.0 | 0.008 | 0.0 | 0.008 |
| Cum. annual rate: | 0.321 | 0.116 | 0.0135 | 0.0135 | 0.0054 | 0.0054 |
| OPTION 2: | | | | | | |
| Complete from: | 1970 | 1970 | 1950 | 1860 | 1800 | ? |
| No. events thru 1983: | 2 | 2 | 0 | 1 | 0 | 1 |
| No. years: | 14 | 14 | 34 | 124 | 184 | 500 |
| Annual rate: | 0.143 | 0.143 | 0.0 | 0.008 | 0.0 | 0.002 |
| Cum. annual rate: | 0.296 | 0.153 | 0.010 | 0.010 | 0.002 | 0.002 |

5.0, five of the six EPRI Teams match the data and one is below them. At higher magnitudes all EPRI curves lie below the data. It is important to understand that the highest four data points are controlled by only two earthquakes and by the assumptions surrounding their interpretation. Thus there is substantial uncertainty on the vertical locations of these points, especially on the lower side. In particular for the occurrence of Charleston-size earthquakes, represented in the plots at magnitude 6.3, it is unlikely that the average rate of occurrence of such events exceeds 1 in 100 years, but it is likely that the rate is lower than the 1 in 500 rate indicated by the "x" on the figures.

It should be pointed out that the seismicity interpretations of Charleston made by participants in the LLNL and EPRI studies were rather more complicated than can be handled accurately by a simple comparison. The geometries of the Charleston source varied widely, as illustrated in the figures of seismic sources shown in Section 2. Neither study required a comparison of seismicity assumptions with observations for every source, although both studies based estimates on empirical data. In the EPRI case, more elaborate procedures were used than illustrated here for calculation of parameters; in the LLNL case different earthquake catalogs were used for estimation of parameters. For both studies multiple parameter values were allowed and, in fact, encouraged; we have used only the most likely central values in deriving the comparisons of Figures 4-2 and 4-3. Thus it is not surprising that there are some differences evident in the figures.

In spite of these points, it is possible to draw some conclusions on the seismicity parameter assumptions made in the LLNL and EPRI studies, and to derive some recommendations regarding seismic hazard at the Savannah River site. First, at least three of the LLNL Experts appear to have over-estimated low-level seismicity for Charleston to a degree; estimates of more than one event per year with $m_b > 3.5$ do not seem to be substantiated by observations. The only apparent cause for this discrepancy is that these four LLNL Experts were attempting to fit a rate for large magnitudes, and they also selected a reasonable b-value which, when extrapolated back to magnitude 3.5 gave high rates. This could arguably be of little concern if the hazard is dominated by the large events. Second, all of the EPRI Teams appear to have under-estimated the rate of occurrence of Charleston-size earthquakes in Charleston, if the long-term average rate is on the order of 1 per 500 years or higher. This point was discussed at length during development of the EPRI methodology, and the EPRI Teams were aware of it. The stated interpretation was that the rate of occurrence of Charleston-size earthquakes on the east coast could certainly be 1 in 100 years, and this was accurately modeled by the sum of activity rates of all earthquake sources specified by each Team on the east coast. If all of that rate were taken up by the Charleston source,

there could be no similar activity anywhere else, which the Teams thought was not a proper interpretation. Thus the Teams selected distributions of the type illustrated in Figure 4-3.

An alternate assumption that is appropriate for the Savannah River site is that a characteristic magnitude distribution is appropriate to consider. This distribution has achieved some credibility in California (2,3) and may apply to active faults in other areas (although it likely does not apply to a region; many studies of historical seismicity, even in parts of California, indicate that the distribution of magnitudes is exponential over a region, up to the maximum possible magnitude.

If we assume a characteristic magnitude model for the Charleston earthquake of the type proposed by (4), fit to the empirical data shown on Figures 4-2 and 4-3 (see Figure 4-4), we obtain the seismic hazard curves shown in Figure 4-5. This calculation used the Rondout seismic sources and parameters and the EPRI ground motion models. The effect of the characteristic magnitude model is to increase the hazard somewhat at low ground motion levels, but there is little influence for PGA levels of 0.5g and higher. That is, the hazard will not be as high as shown on Figure 2-12 for the highest five LLNL Experts.

Table 2-3 also indicates that the assumption by Experts 6 and 13 that the Charleston source (i.e., a source with high activity rate and maximum magnitude near 7) extends to the site causes a large increase in the calculated hazard. To evaluate the validity of this assumption, we examined the geographic distribution of seismicity within the Charleston source defined by Expert 6 (source 13; see Figures 2-6 and 4-1).

The EPRI computer program EQPARAM (5,6) can perform statistical tests to determine whether the assumption of a homogeneous seismic source (with a given geometry) is consistent with the geographic distribution of seismicity within that source. This is done by comparing the observed earthquake counts in each 1-degree cell to the expected counts (adjusted for incompleteness), given the assumption of a homogeneous source. Cells where the difference between observed and expected counts is statistically significant are flagged. The number of flagged cells and their geographic distribution provide an indication of whether the geometry of the source is consistent with historic seismicity.

We performed this analysis for source 13, using the EPRI catalog and completeness assumptions. Parameter b was fixed at 0.85 (the value specified by Expert 6) and the program was allowed to evaluate the activity rate for the source. Figure 4-6 shows the 1-degree cells that were flagged by the program. The distribution of flags in Figure 4-6 indicates that the assumption of a large, homogeneous Charleston source that extends to the site is inconsistent with the geographic distribution of historic seismicity.

The above comparison, although significant, is not definitive. This is because the comparison relies on the EPRI assumptions about catalog completeness. As mentioned earlier, the determination of completeness times and detection probabilities is problematic. The EPRI methodology uses a sophisticated statistical method to determine completeness parameters, but there is always uncertainty about these parameters and their geographical variation. Therefore, the zonations by LLNL Experts 6 and 11 should not be discarded as invalid. They should, however, be given lower weights than those assumptions that are more consistent with the data.

As a result of the sensitivity analyses and comparisons presented here, and with the purpose of deriving a synthesized set of seismic hazard curves for SRP, it is appropriate to use a subset of the interpretations by the LLNL Experts and the EPRI Teams, with weights as given in Table 4-3. These form a set of interpretations that are reasonably consistent with the data.

Table 4-3
Recommended LLNL and EPRI Seismicity Models

| <u>Expert/Team</u> | <u>Weight</u> |
|--------------------|---|
| LLNL Expert 1 | 0.072 |
| LLNL Expert 3 | 0.071 |
| LLNL Expert 6 | 0.036 |
| LLNL Expert 7 | 0.071 |
| LLNL Expert 10 | 0.071 |
| LLNL Expert 11 | 0.036 |
| LLNL Expert 12 | 0.071 |
| LLNL Expert 13 | 0.072 |
| | <hr style="width: 50%; margin-left: auto; margin-right: 0;"/> 0.500 |
| Bechtel | 0.100 |
| Law | 0.100 |
| Rondout | 0.100 |
| Weston | 0.100 |
| Woodward-Clyde | 0.100 |
| | <hr style="width: 50%; margin-left: auto; margin-right: 0;"/> 0.500 |

4.2 ATTENUATION FUNCTIONS FOR GROUND MOTIONS ON ROCK

The LLNL and EPRI rock-site attenuation functions were compared in Figures 3-1 and 3-2. With the exception of the models proposed by LLNL Expert 5, there is general agreement between the two sets of models.

Figures 3-3 through 3-8 contain comparisons in terms of the hazard calculated with the two sets of attenuation models, while using the same zonations and seismicity parameters. With the EPRI and Expert 6 zonations and seismicity parameters, differences in calculated hazards are largely due to differences in the LLNL and EPRI soil-amplification factors, not to differences in the rock-site attenuation functions. With the Expert 2 zonation and seismicity parameters, differences are due to G-Expert 5 and to the site-amplification factors.

Regarding G-Expert 5, Table 3-4 shows that the mean and median hazards predicted by LLNL change substantially if the attenuation functions by this expert are not included.

The models proposed by G-Expert 5 predict substantially higher ground motion estimates than the other models, especially for high magnitudes and far distances. These models are obtained by combining of two equations: a correlation between instrumental ground motion and MM intensity published by Trifunac from California data, and an MM intensity attenuation equation published by Gupta and Nuttli. This selection received 100% weight from G-Expert 5, and zero weight from the other LLNL G-Experts. Comparing the predictions from these equations to data available from EUS seismographs and accelerographs indicates that the models preferred by G-Expert 5 severely over-estimates ground motions in the EUS, particularly at distances greater than 20 km from the earthquake source. [See Figures 5-123 through 5-125 of (7) for these comparisons.]

There are good reasons why the attenuation functions proposed by G-Expert 5 might lead to poor estimates of ground motion in the EUS. These function were obtained by substitution of a stochastic relationship between instrumental ground-motion and intensity into a stochastic intensity-attenuation relation. This type of substitution of one regression into another is mathematically incorrect and has been demonstrated to produce significant biases when applied to intensity-attenuation data (8). In particular, after such a substitution the dependent variable does not appear to be as strongly correlated to the independent variable as it should be, which is the behavior evident in comparisons of data with estimates from these attenuation functions. For example, the data in Figures 5-123 through 5-125 of (7) show a much stronger dependence on distance than do the estimates. Further, these models were given zero weight by four of the five LLNL G-Experts (and 100% weight by the fifth),

an indication that the models have a small following in the scientific community [see Tables 3.5 and 3.6 in Volume 1 of (9)]. Because of the theoretical problems in their derivation, and their lack of agreement with available data from the eastern US, we recommend that the models proposed by G-Expert 5 not be used in the evaluation of seismic hazard at SRP.

The remaining LLNL attenuation models predict essentially the same range of ground-motion amplitudes as the EPRI models, and either set could be used to evaluate seismic hazard at SRP. We suggest that the EPRI attenuation models be used, because of their smaller number and mathematical simplicity.

4.3 SOIL AMPLIFICATION MODEL

The LLNL and EPRI methods to develop site amplification factors differ in one main aspect: the EPRI method takes credit for increased energy dissipation due to nonlinear soil behavior. There is considerable evidence to suggest that soils behave nonlinearly for moderate and high ground-motion amplitudes (10). The EPRI method predicts PGA amplification factors smaller than unity for deep soils and accelerations higher than 0.3 g. In fact, the soil-response calculations predict PGA amplification factors of 0.7 for 0.5g, but 0.8 is the smallest value used in the EPRI methodology.

The LLNL and EPRI methods also differ in that they consider ground motions with different frequency contents. Frequency content has a moderate effect on the calculated amplification factors.

Because the EPRI soil amplification factors consider soil nonlinearity and use input ground motions typical of eastern-US earthquakes at short and moderate distances, we recommend that the EPRI soil amplification factors be used to evaluate the hazard at SRP due to local earthquakes (i.e., the hazard contributed by the host source). For the evaluation of hazard due to the Charleston source (this hazard is significant for LLNL Experts 3, 7, and 13), the EPRI amplification factors may not be appropriate. This is because the rock-site ground motions from a large, distant earthquake have frequency contents different from those of the ground motions considered in the development of the EPRI soil-amplification factors.

4.4 REFERENCES

1. P. Talwani and K. Collinsworth. "Recurrence Intervals for Intraplate Earthquakes in Eastern North America from Paleoseismic Data". *Seismological Research Letters*, 59(4):207-212, 1988.
2. D. Schwartz and K. J. Coppersmith. "Fault Behavior and Characteristic Earthquakes: Examples from the Wasatch and San Andreas Fault Zones". *Journal of Geophysical Research*, 89:5681-5698, 1984.
3. U.S. Geological Survey. *Probabilities of Large Earthquakes Occurring in California on the San Andreas Fault*. Open-File Report 88-398, U. S. Geological Survey, 1988.
4. R. J. Youngs and K. J. Coppersmith. "Implications of Fault Slip Rates and Earthquake Recurrence Models to Probabilistic Seismic Hazard Estimates". *Bulletin of the Seismological Society of America*, 75:939-964, 1985.
5. *Seismic Hazard Methodology for the Central and Eastern United States*. Technical Report NP-4726-A, Electric Power Research Institute, July 1986. Revised, 1988. Vol. 1, Part 1: Methodology, Vol. 1, Part 2: Theory, Vol. 2: EQHAZARD Programmer's Manual, Vol. 3: EQHAZARD User's Manual, Vol. 4: Applications, Vols. 5 through 10: Tectonic Interpretations, Vol. 11: Nuclear Regulatory Commission Safety Review.
6. R. K. McGuire, G. R. Toro, and M. W. McCann, Jr. *EQHAZARD Primer*. Special Report NP101-46, Electric Power Research Institute, June 1989.
7. R. K. McGuire, G. R. Toro, and W. J. Silva. *Probabilistic Seismic Hazard Evaluations in the Central and Eastern United States — Appendix A: Model of Earthquake Ground Motion for the Central and Eastern United States*. Technical Report, Electric Power Research Institute, 1989. EPRI Project RP101-53, prepared by Risk Engineering, Inc.
8. C. A. Cornell, H. Banon, and A. F. Shakal. "Seismic Motion and Response Prediction Alternatives". *Earthquake Engineering and Structural Dynamics*, 7:295-315, 1979.
9. D. L. Bernreuter, J. B. Savy, R. W. Mensing, and J. C. Chen. *Seismic Hazard Characterization of 69 Plant Sites East of the Rocky Mountains*. Technical Report NUREG/CR5250, UCID-21517, U. S. Nuclear Regulatory Commission, 1988.
10. R. K. McGuire, G. R. Toro, and W. J. Silva. *Engineering Model of Earthquake Ground Motion for Eastern North America*. Technical Report NP-6074, Electric Power Research Institute, 1988.

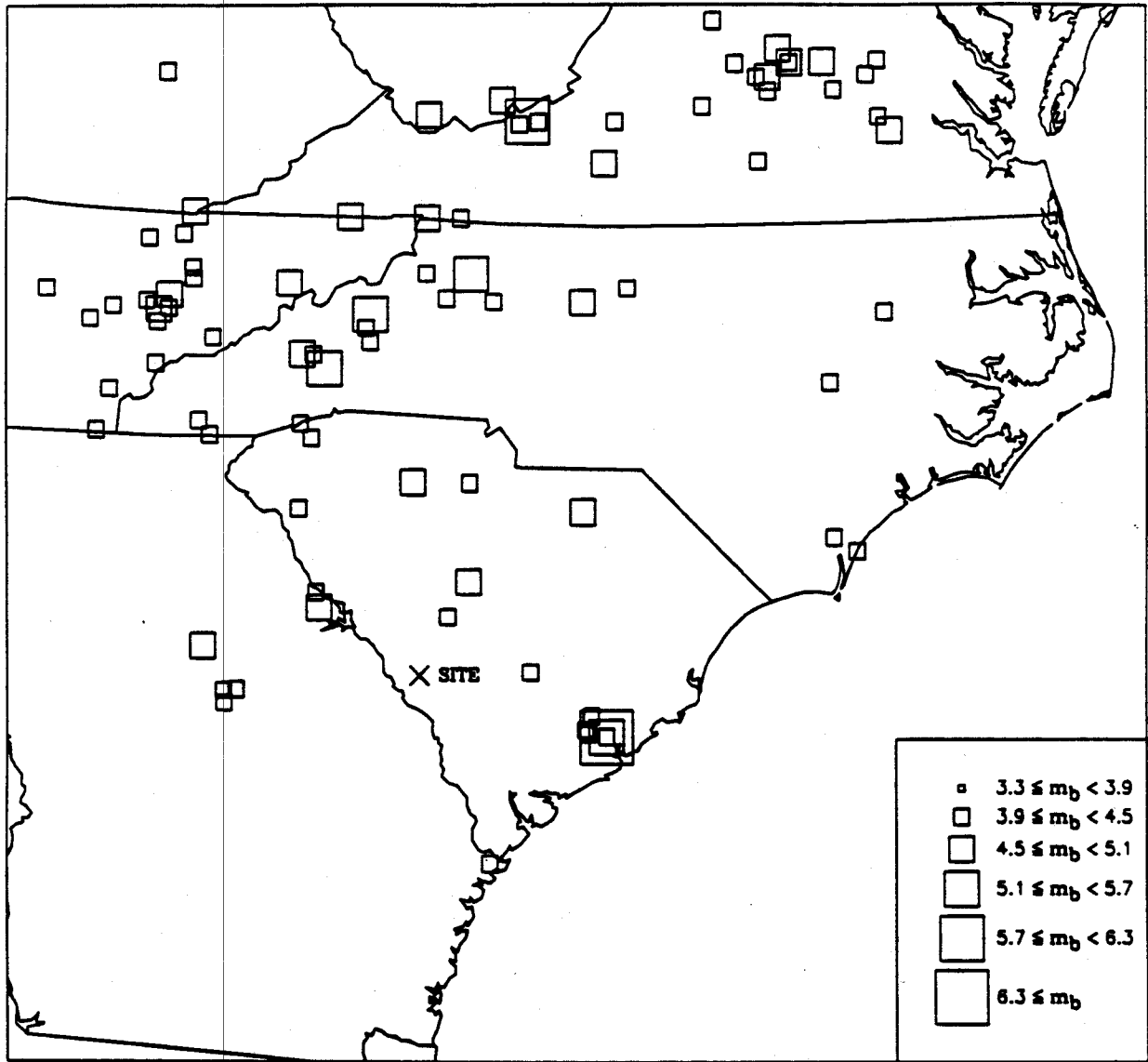


Figure 4-1. Seismicity of region around SRP, as contained in the EPRI catalog

CHARLESTON SEISMICITY RATES; LLNL EXPERTS

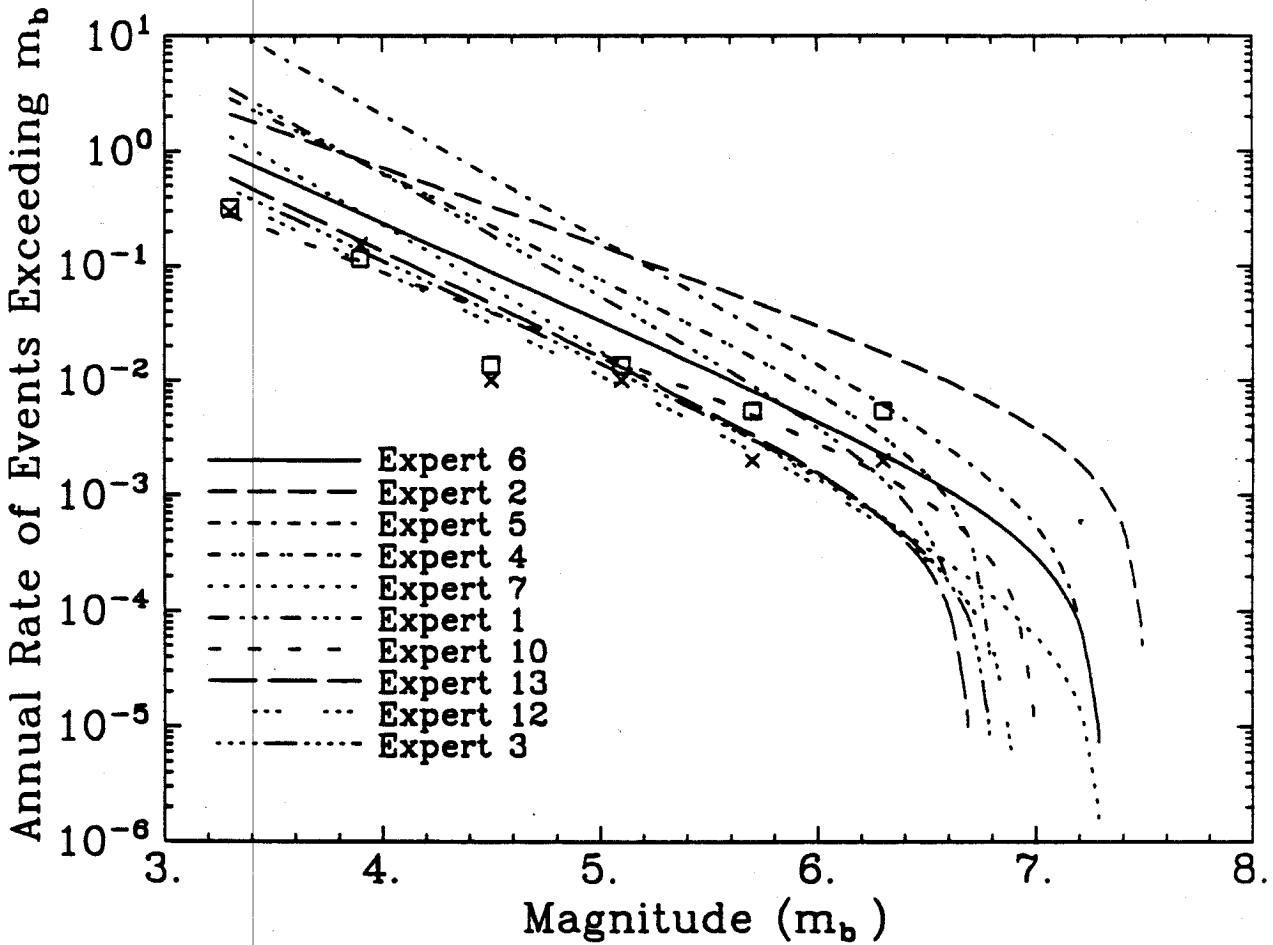


Figure 4-2. Comparison of observed seismicity in the Charleston area (50 km radius) with the models of seismicity specified by the LLNL Experts. Squares represent observed seismicity for completeness option 1; \times represent observed seismicity for completeness option 2.

CHARLESTON SEISMICITY RATES; EPRI TEAMS

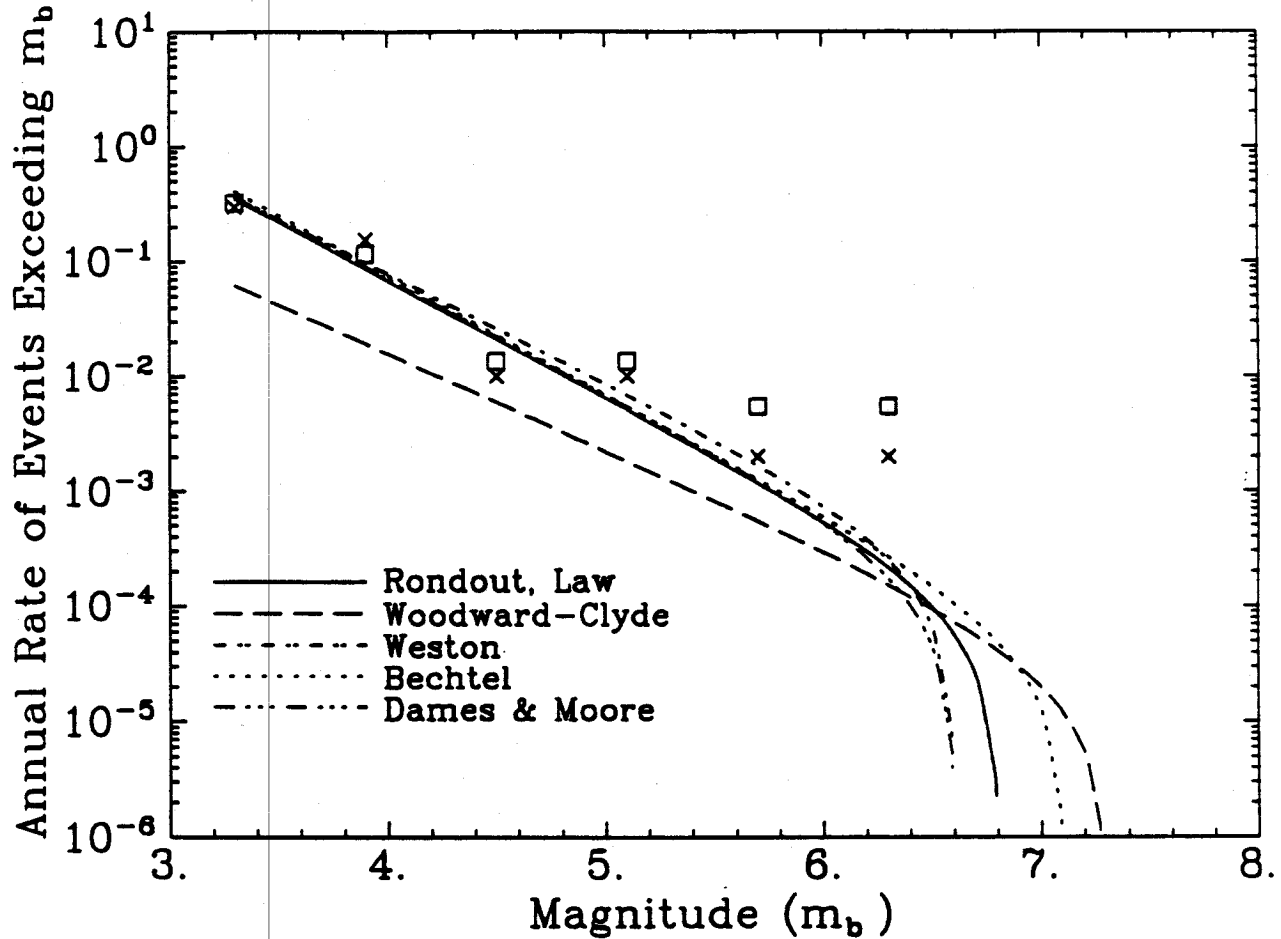


Figure 4-3. Comparison of observed seismicity in the Charleston area (50 km radius) with the models of seismicity specified by the EPRI Teams. Squares represent observed seismicity for completeness option 1; \times represent observed seismicity for completeness option 2.

CHARLESTON SEISMICITY RATES EXPONENTIAL AND CHARACTERISTIC MODELS

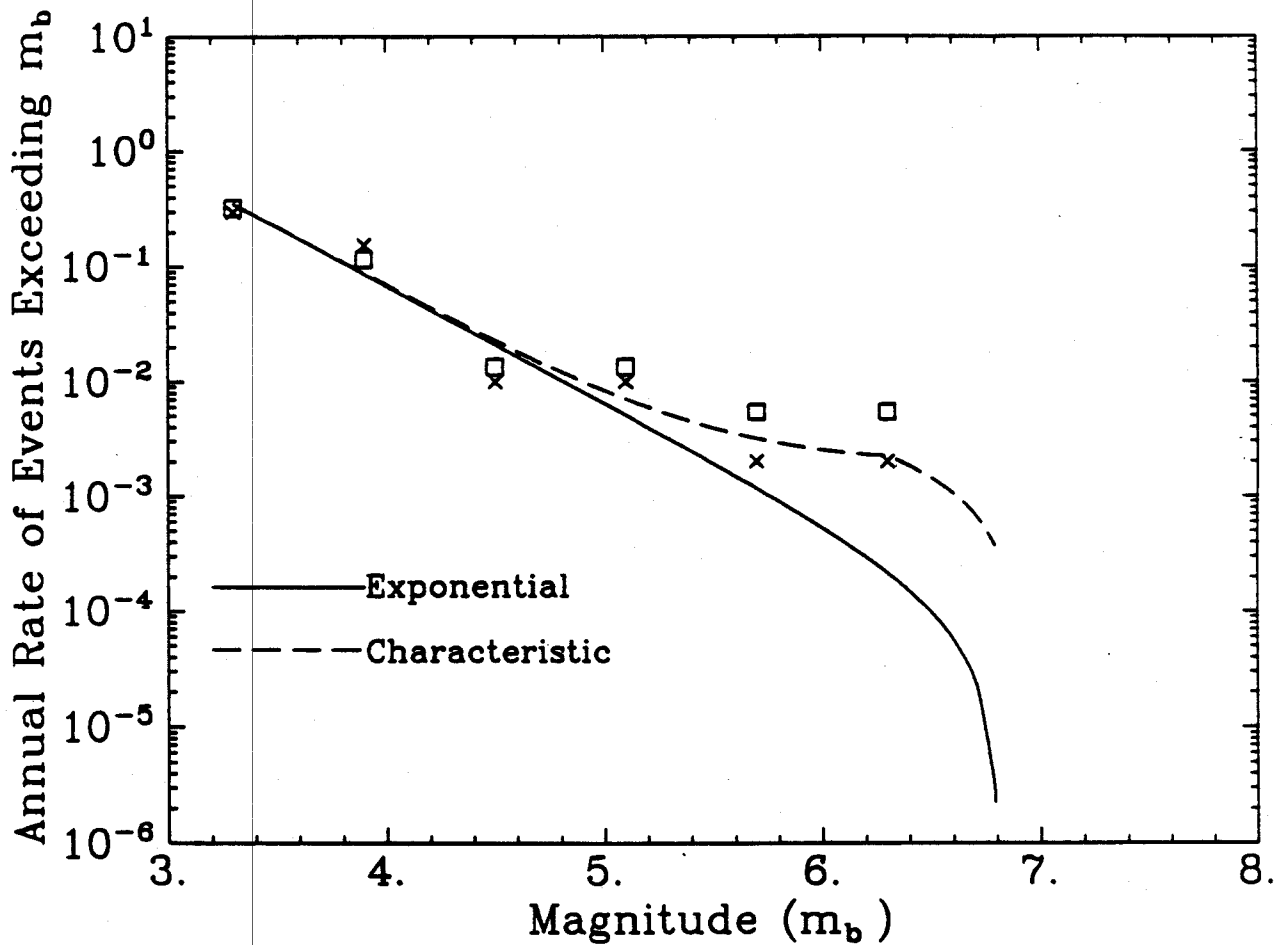


Figure 4-4. Comparison of observed seismicity in the Charleston area (50 km radius) with the characteristic model of seismicity. Squares represent observed seismicity for completeness option 1; \times represent observed seismicity for completeness option 2.

SAVANNAH RIVER PLANT
EFFECT OF CHARACTERISTIC EARTHQUAKE

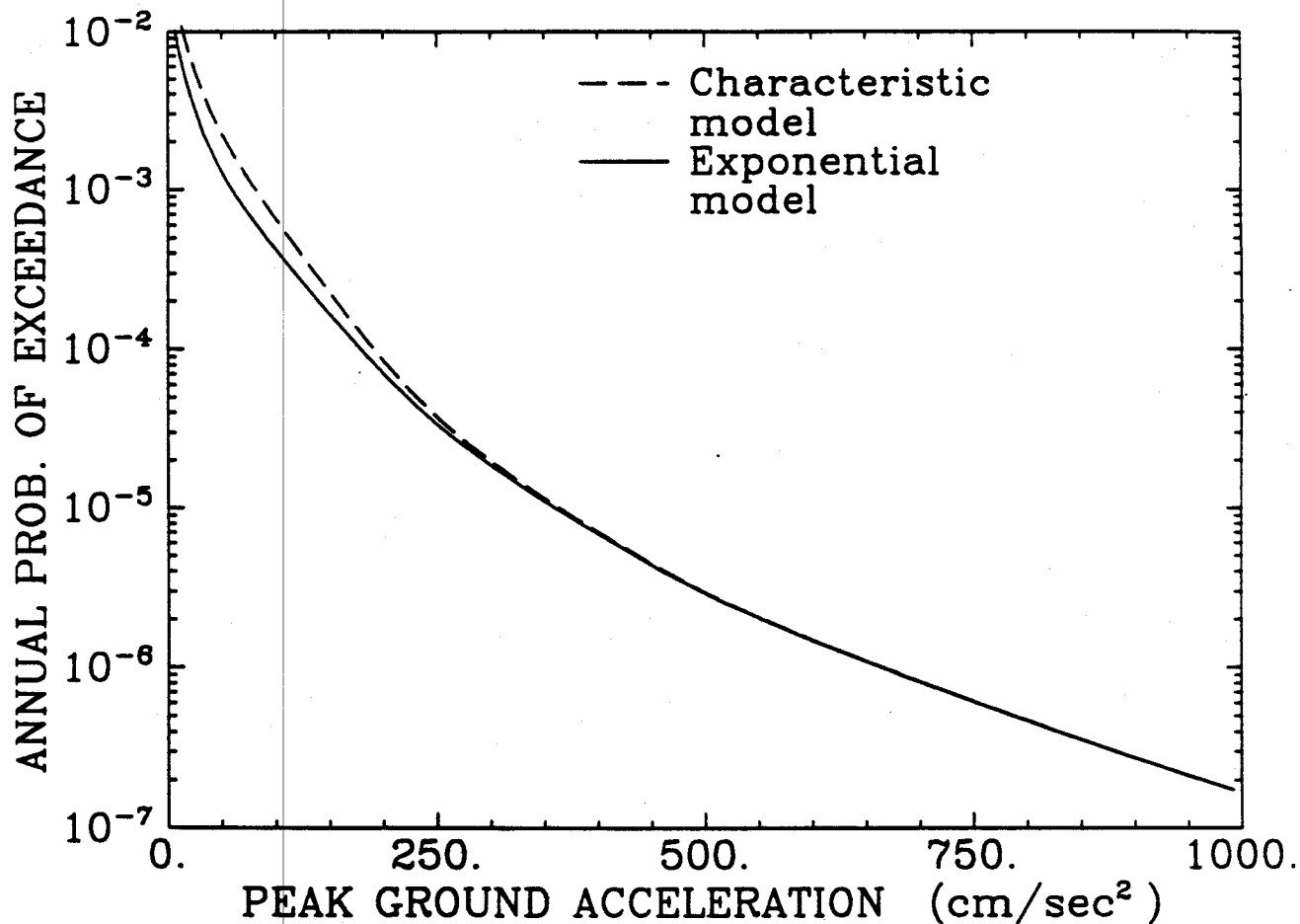


Figure 4-5. Effect of the characteristic magnitude distribution on the calculated hazard; Rondout Team.

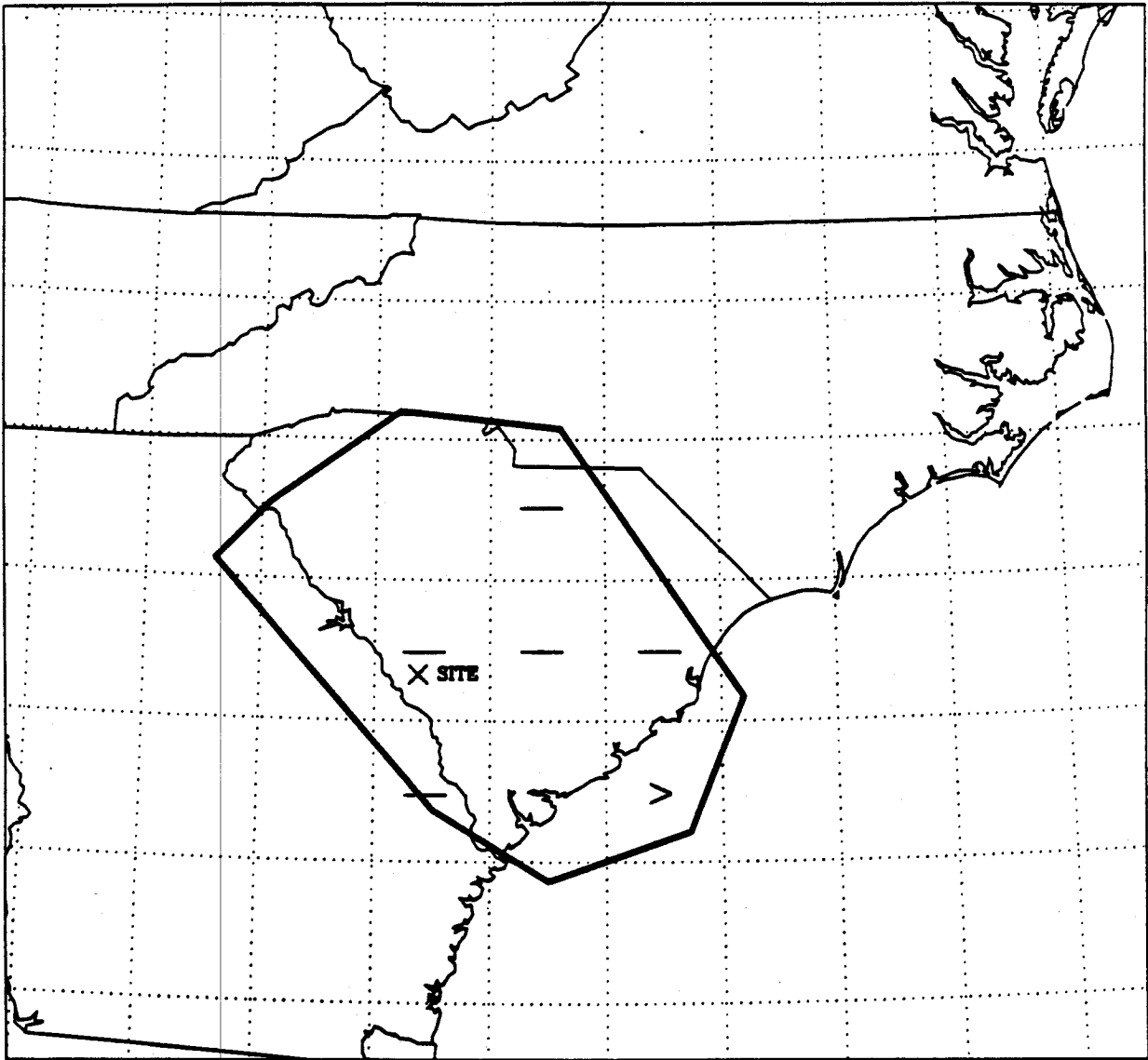


Figure 4-6. Results from the statistical analysis of the geographic distribution of earthquakes within source 18 of LLNL Expert 6. “-” indicates that the observed count in a 1-degree cell is significantly lower (at the 10% level) than the expected count. “>” indicates that the observed count is significantly higher (at the 2% level) than the expected count.

Section 5
CONCLUSIONS

This study has examined the causes of differences in seismic hazard results at the Savannah River site from applications of the LLNL and EPRI methodologies at that site. Differences in seismological interpretations are a large contributor to the differences in calculated seismic hazard. The two sets of ground-motion attenuation equations predict the same hazard under most seismological interpretations, but one of the LLNL attenuation equations predicts very different hazards under extreme seismological interpretations. The effect of soil amplification provides a difference: the LLNL study predicts that deep soil at the site will neither amplify nor de-amplify high frequencies of ground motion, but the EPRI study predicts that the amplitude of high-frequency motions will be reduced by 20% compared to rock sites.

A comparison of seismicity assumptions for the Charleston source shows that four of the LLNL experts over-estimate low-level seismic activity in the Charleston region, but provide a reasonable estimate of large earthquakes ($m_b > 6.5$). An alternative assumption is to use a characteristic magnitude distribution; a sensitivity study using this distribution, calibrated to the historical seismicity, shows it would have little effect on the seismic hazard at the Savannah River site.

An analysis of the geographic distribution of earthquakes in South Carolina suggests that this distribution is not consistent with the interpretations by two LLNL seismology experts. Each of these experts draw a large seismic source that contains the Charleston area and the Savannah River site.

A set of recommended seismological interpretations is developed by down-weighting or eliminating the LLNL experts whose interpretations are not consistent with the data, and eliminating one EPRI team that is inconsistent in its treatment of local seismicity.

With the exception of LLNL G-Expert 5, the LLNL and EPRI sets of rock-site attenuation functions predict similar ground motions. It is recommended that the models proposed by G-Expert 5 not be used because they were developed using an invalid substitution procedure and because their predictions do not agree with ground motions recorded in the eastern United States. It is also recommended that the EPRI site-amplification factors be used to calculate deep-soil ground motions from rock-site ground motions.

**EVALUATION OF SEISMIC HAZARD
AT THE SAVANNAH RIVER SITE
BASED ON THE LLNL AND EPRI
SEISMIC HAZARD STUDIES**

FINAL REPORT

Prepared for

**Westinghouse Savannah River Company
Aiken, South Carolina**

by

**Risk Engineering, Inc.
5255 Pine Ridge Road
Golden, Colorado**

April 4, 1991

Risk Engineering, Inc.

5255 Pine Ridge Road
Golden, Colorado 80403 USA
Telephone: 303-278-9800
Telefax: 303-278-9803

April 5, 1991

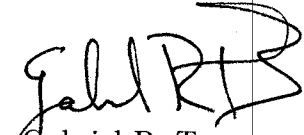
Mr. Dale E. Stephenson
Bldg. 773-42A
Westinghouse Savannah River Company
P.O. Box 616
Aiken, SC 29802

Dear Mr. Stephenson:

Enclosed please find three copies of the final report from contract AA46320, entitled "Evaluation of Seismic Hazard at the Savannah River Site Based on the LLNL and EPRI Seismic Hazard Studies."

Please contact me if you have any questions.

Sincerely yours,



Gabriel R. Toro
Senior Engineer

GRT/jc

CONTENTS

| <u>Section</u> | <u>Page</u> |
|---|-------------|
| 1 INTRODUCTION | 1-1 |
| 1.1 REFERENCES | 1-2 |
| 2 RECOMMENDATIONS FROM PREVIOUS STUDY | 2-1 |
| 2.1 SEISMOTECTONIC INTERPRETATIONS | 2-1 |
| 2.2 ATTENUATION FUNCTIONS | 2-1 |
| 2.3 REFERENCES | 2-3 |
| 3 CHARACTERISTIC MAGNITUDE MODEL FOR THE CHARLESTON SOURCE ZONE | 3-1 |
| 3.1 PALEOSEISMIC EVIDENCE | 3-1 |
| 3.2 QUANTIFICATION OF THE RATE OF CHARACTERISTIC EARTHQUAKES | 3-1 |
| 3.3 CHARACTERISTIC MAGNITUDE DISTRIBUTION AND ITS USE IN THE HAZARD CALCULATION | 3-2 |
| 3.4 REFERENCES | 3-4 |
| 4 CALCULATIONS AND RESULTS | 4-1 |
| 4.1 LLNL CALCULATIONS | 4-1 |
| 4.2 EPRI CALCULATIONS | 4-2 |
| 4.3 COMBINATION LLNL-EPRI RESULTS—DISCUSSION | 4-3 |
| 4.4 REFERENCES | 4-3 |
| 5 SUMMARY AND CONCLUSIONS | 5-1 |
| A EVALUATION OF UNCERTAINTIES | A-1 |
| A.1 REFERENCES | A-3 |

LIST OF FIGURES

| <u>Figure</u> | | <u>Page</u> |
|---------------|---|-------------|
| 3-1 | Schematic representation of the rate-density function for a characteristic magnitude-frequency law. | 3-3 |
| 3-2 | Charleston seismicity rates and characteristic magnitude-frequency law: LLNL seismicity expert 1 | 3-5 |
| 3-3 | Charleston seismicity rates and characteristic magnitude-frequency law: LLNL seismicity expert 3 | 3-6 |
| 3-4 | Charleston seismicity rates and characteristic magnitude-frequency law: LLNL seismicity expert 7 | 3-7 |
| 3-5 | Charleston seismicity rates and characteristic magnitude-frequency law: LLNL seismicity expert 10 | 3-8 |
| 3-6 | Charleston seismicity rates and characteristic magnitude-frequency law: LLNL seismicity expert 12 | 3-9 |
| 3-7 | Charleston seismicity rates and characteristic magnitude-frequency law: LLNL seismicity expert 13 | 3-10 |
| 3-8 | Charleston seismicity rates and characteristic magnitude-frequency law: Bechtel team | 3-11 |
| 3-9 | Charleston seismicity rates and characteristic magnitude-frequency law: Law team | 3-12 |
| 3-10 | Charleston seismicity rates and characteristic magnitude-frequency law: Rondout team | 3-13 |
| 3-11 | Charleston seismicity rates and characteristic magnitude-frequency law: Weston team | 3-14 |
| 3-12 | Charleston seismicity rates and characteristic magnitude-frequency law: Woodward-Clyde team | 3-15 |
| 4-1 | Mean and fractile hazard curves calculated for LLNL seismicity expert 1 | 4-5 |

| | | |
|------|--|------|
| 4-2 | Mean and fractile hazard curves calculated for LLNL seismicity expert 3 | 4-6 |
| 4-3 | Mean and fractile hazard curves calculated for LLNL seismicity expert 6 | 4-7 |
| 4-4 | Mean and fractile hazard curves calculated for LLNL seismicity expert 7 | 4-8 |
| 4-5 | Mean and fractile hazard curves calculated for LLNL seismicity expert 10 | 4-9 |
| 4-6 | Mean and fractile hazard curves calculated for LLNL seismicity expert 11 | 4-10 |
| 4-7 | Mean and fractile hazard curves calculated for LLNL seismicity expert 12 | 4-11 |
| 4-8 | Mean and fractile hazard curves calculated for LLNL seismicity expert 13 | 4-12 |
| 4-9 | Mean and fractile hazard curves calculated by combining results from the LLNL seismicity experts, using the weights in Table 2-1. | 4-13 |
| 4-10 | Mean and fractile hazard curves calculated for EPRI team Bechtel. | 4-14 |
| 4-11 | Mean and fractile hazard curves calculated for EPRI team Law. | 4-15 |
| 4-12 | Mean and fractile hazard curves calculated for EPRI team Rondout. | 4-16 |
| 4-13 | Mean and fractile hazard curves calculated for EPRI team Weston. | 4-17 |
| 4-14 | Mean and fractile hazard curves calculated for EPRI team Woodward-Clyde. | 4-18 |
| 4-15 | Mean and fractile hazard curves calculated by combining results from the EPRI teams, using the weights in Table 2-1. | 4-19 |
| 4-16 | Mean and fractile hazard curves calculated by combining results from the LLNL experts and the EPRI teams, using the weights in Table 2-1 | 4-20 |
| 4-17 | Mean and fractile hazard curves calculated by combining results from the LLNL experts and the EPRI teams—additional fractiles shown | 4-21 |
| 4-18 | Mean and fractile hazard curves calculated by combining results from LLNL seismicity experts 1, 3, 10, and 12. | 4-22 |
| 4-19 | Mean and fractile hazard curves calculated by combining results from LLNL (experts 1, 3, 10, and 12) and the EPRI teams | 4-23 |

| | | |
|------|--|------|
| 4-20 | Mean and fractile hazard curves calculated by combining results from LLNL (experts 1, 3, 10, and 12) and the EPRI teams—additional fractiles shown | 4-24 |
| A-1 | Magnitude-recurrence model specified by LLNL expert 1 for seismic source 1 | A-4 |
| A-2 | Magnitude-recurrence model specified by LLNL expert 3 for seismic source 9 | A-5 |
| A-3 | Magnitude-recurrence model specified by LLNL expert 6 for seismic source 13 | A-6 |
| A-4 | Magnitude-recurrence model specified by LLNL expert 7 for seismic source 10 | A-7 |
| A-5 | Magnitude-recurrence model specified by LLNL expert 10 for seismic source 4 | A-8 |
| A-6 | Magnitude-recurrence model specified by LLNL expert 11 for seismic source 8 | A-9 |
| A-7 | Magnitude-recurrence model specified by LLNL expert 12 for seismic source 23 | A-10 |
| A-8 | Magnitude-recurrence model specified by LLNL expert 13 for seismic source 9 | A-11 |
| A-9 | Mean and fractile hazard curves calculated by combining results from LLNL seismicity experts 1, 3, 10, and 12. | A-12 |
| A-10 | Mean and fractile hazard curves calculated by combining results from LLNL (experts 1, 3, 10, and 12) and the EPRI teams | A-13 |
| A-11 | Mean and fractile hazard curves calculated by combining results from LLNL (experts 1, 3, 10, and 12) and the EPRI teams—additional fractiles shown | A-14 |

Section 1
INTRODUCTION

Two state-of-the art seismic hazard studies have recently been performed for the Savannah River Site (SRS). One study was performed by the Lawrence Livermore National Laboratory (1) and used the inputs and methodology developed by LLNL (supported by the U.S. Nuclear Regulatory Commission). The other study was performed by the firm of Jack Benjamin and Associates (2) and used the inputs and methodology developed by the Electric Power Research Institute (EPRI; sponsored by the Seismic Owners' Group, a group of eastern U.S. electric utilities.)

A study by Risk Engineering, Inc. (3, REI) compared the key assumptions in the above studies, quantified the effects of the various assumptions on the calculated hazard, and recommended a set of assumptions to use in the evaluation of seismic hazard at SRS. The REI study also suggested that a characteristic-magnitude model be considered for the Charleston seismic source. The present study uses these recommended assumptions to calculate a composite hazard at SRS.

Section 2 of this report contains a summary of the recommendations in (3). Section 2 summarizes the paleoseismic evidence on large earthquakes in the Charleston area and presents a characteristic-magnitude model for the Charleston seismic source. Section 3 documents the LLNL and EPRI calculations and presents the results. Finally, Section 4 presents the conclusions from this study.

1.1 REFERENCES

1. J. B. Savy. *Seismic Hazard Characterization of the Savannah River Plant (SRP)*. Technical Report UCID-21596, Lawrence Livermore National Laboratory, November 1988.
2. *Probabilistic Seismic Hazard Evaluation for the Savannah River site, Aiken, South Carolina*. Report to Westinghouse Savannah River Company, Aiken, South Carolina, Jack Benjamin and Associates, 1989.
3. *Comparison and Analysis of Assumptions in LLNL and EPRI Seismic Hazard Studies for the Savannah River Site*. Report to Westinghouse Savannah River Company, Aiken, South Carolina, Risk Engineering, Inc., 1990.

Section 2

RECOMMENDATIONS FROM PREVIOUS STUDY

2.1 SEISMOTECTONIC INTERPRETATIONS

The study by Risk Engineering, Inc. (1, REI) compared the various assumptions by the LLNL experts and the EPRI teams and quantified the effects of these assumptions on the calculated hazards. The study concluded that two large contributors to differences between the LLNL and EPRI study (and to differences among the seismological interpretations in the two studies) were the assumptions about the activity rate and about the geographic extent of the Charleston source.

A comparison of activity rates specified in the two studies to the historic seismicity in the southeastern U.S. indicates that the rates specified by LLNL seismicity experts 2, 4, and 5 are inconsistent with the data, and that the EPRI Dames & Moore team does not fully account for seismicity, using a probability of activity of 0.26 in the vicinity of the SRS. In addition, a statistical analysis of the geographic pattern of historic seismicity in South Carolina indicates that the large Charleston sources specified by LLNL seismicity experts 6 and 11 are inconsistent with the geographic pattern of historical earthquake occurrences. Stated another way, using a large earthquake source in South Carolina assumes that earthquakes occur in a spatially-homogenous manner throughout the area. This spatial homogeneity has not been observed historically. This result, though significant, is not definitive because the observation of non-homogeneity in the region relies on the assumption that catalog completeness is homogeneous throughout the region. As a consequence of the above comparisons, the weights in Table 2-1 were recommended for the LLNL experts and EPRI teams.

The REI study also noted that a characteristic magnitude distribution may be appropriate for the Charleston source. This distribution is discussed in detail in Section 3.

2.2 ATTENUATION FUNCTIONS

The REI study noted that the only major difference between the LLNL and EPRI attenuation functions for peak acceleration is the model selected by LLNL ground-motion expert 5 [see (2, Appendix A) for a detailed discussion and hazard results with and without expert 5]. If the attenuation functions selected by ground-motion expert 5 is excluded from the LLNL

Table 2-1
 Recommended LLNL and EPRI Seismicity Models
 Source: (1)

| <u>Expert/Team</u> | <u>Weight</u> |
|--------------------|---|
| LLNL Expert 1 | 0.072 |
| LLNL Expert 3 | 0.071 |
| LLNL Expert 6 | 0.036 |
| LLNL Expert 7 | 0.071 |
| LLNL Expert 10 | 0.071 |
| LLNL Expert 11 | 0.036 |
| LLNL Expert 12 | 0.071 |
| LLNL Expert 13 | 0.072 |
| | <hr style="width: 50%; margin-left: auto; margin-right: 0;"/> 0.500 |
| Bechtel | 0.100 |
| Law | 0.100 |
| Rondout | 0.100 |
| Weston | 0.100 |
| Woodward-Clyde | 0.100 |
| | <hr style="width: 50%; margin-left: auto; margin-right: 0;"/> 0.500 |

set of attenuation functions, the LLNL and EPRI sets predict essentially the same range of ground motions.

The attenuation function selected by expert 5 shows poor agreement with eastern U.S. accelerograph and seismograph data. Furthermore, this attenuation function was obtained using a substitution procedure that is invalid and known to produce biased results (3). As a consequence, the REI study recommended that the attenuation function selected by LLNL ground-motion expert 5 not be used in the evaluation of seismic hazard at the Savannah River site.

2.3 REFERENCES

1. *Comparison and Analysis of Assumptions in LLNL and EPRI Seismic Hazard Studies for the Savannah River Site*. Report to Westinghouse Savannah River Company, Aiken, South Carolina, Risk Engineering, Inc., 1990.
2. R. K. McGuire, G. R. Toro, J. P. Jacobson, T. F. O'Hara, and W. J. Silva. *Probabilistic Seismic Hazard Evaluations in the Central and Eastern United States: Resolution of the Charleston Earthquake Issue*. Special Report NP-6395-D, Electric Power Research Institute, April 1989.
3. C. A. Cornell, H. Banon, and A. F. Shakal. "Seismic Motion and Response Prediction Alternatives". *Earthquake Engineering and Structural Dynamics*, 7:295-315, 1979.

Section 3

CHARACTERISTIC MAGNITUDE MODEL FOR THE CHARLESTON SOURCE ZONE

This Section summarizes the paleoseismic evidence on large earthquakes in the Charleston area and uses this evidence to quantify the rate of earthquakes similar to the 1886 Charleston event. This rate is then used to define a characteristic magnitude-recurrence law similar to that introduced by Youngs and Coppersmith (1).

3.1 PALEOSEISMIC EVIDENCE

The paleoseismicity studies available for the Charleston area are summarized by Talwani and Collinsworth (2). Talwani and Cox (3) obtained ages of organic material found in and near liquefaction sandblows, and observed the appearance of the sand in the various sandblows. Based on the ages of roots in the blowholes and roots disturbed by faulting or liquefaction, they concluded that three Charleston-size earthquakes (including the 1886 event) have occurred in the last 3060 to 3740 years.

Weems et al. (4) obtained ages of humate clasts, wood fragments, and roots at a number of liquefaction craters. Based on the dates of these materials, they conclude that four Charleston-size earthquakes (including the 1886 event) have occurred in the last 7200 years.

3.2 QUANTIFICATION OF THE RATE OF CHARACTERISTIC EARTHQUAKES

One can obtain estimates of the rate of Charleston-size earthquakes in the Charleston source, and the uncertainty associated with that rate, using the paleoseismic evidence summarized above and simple statistical concepts.

For the sake of simplicity and consistency with the LLNL and EPRI studies, it is assumed that Charleston-size earthquakes occur as a Poisson process, even if the source has a magnitude distribution that exhibits a "characteristic" magnitude. This assumption is consistent with the model used by Youngs and Coppersmith (1), but may not be consistent with our physical intuition about characteristic earthquakes. The Poisson assumption is also conservative in comparison to any periodic process that might be fit to the data, since the probability of occurrence soon after an event has occurred (within several hundred years for

an event with a 1000-year recurrence interval, for example) is lower for a periodic process than for a Poisson process.

Using the result of three occurrences in 3740 years, and assuming a Poisson process, we estimate a mean recurrence rate of $3/3740 = 8.0 \times 10^{-4} \text{ years}^{-1}$ (or 1 in 1247 years). The associated standard error is $8.0 \times 10^{-4}/\sqrt{3} = 4.6 \times 10^{-4} \text{ years}^{-1}$.

Similarly, using the result of four occurrences in 7200 years, we estimate a mean rate of $4/7200 = 5.6 \times 10^{-4} \text{ years}^{-1}$, with an associated standard error of $2.8 \times 10^{-4} \text{ years}^{-1}$.

Giving equal weights to these two results, we obtain a combined estimate of $6.8 \times 10^{-4} \text{ years}^{-1}$ (1 in 1500 years), with a standard error of $4.0 \times 10^{-4} \text{ years}^{-1}$ (or a coefficient of variation of 59%). Note that the average rate of 1 event per 1500 years is virtually identical to the observations of Talwani and Cox (3) that 3 events have occurred in 3060 years, if one assumes that those observations represent two repeat times of large events in a periodic process.

The large statistical uncertainty in the estimate obtained above will be represented in the calculations by considering two alternative values of the Charleston rate, associated with the combined estimate \pm its standard error. These values are 1.1×10^{-3} and $2.8 \times 10^{-4} \text{ years}^{-1}$, and are given equal weights.

3.3 CHARACTERISTIC MAGNITUDE DISTRIBUTION AND ITS USE IN THE HAZARD CALCULATION

For each LLNL seismicity expert and each EPRI team, we construct two magnitude distributions for the Charleston source using the expert's or team's best-estimate seismicity parameters and the two rates of large earthquakes obtained from paleoseismic studies.

The large characteristic earthquakes are assumed to have uniformly distributed magnitudes between $M_{\text{max,ch}} - 0.6$ and $M_{\text{max,ch}}$, where $M_{\text{max,ch}}$ is the expert's or team's best-estimate maximum magnitude for the Charleston source (or 6.9, whichever is larger).

The resulting rate-density function is shown in Figure 3-1¹. At magnitudes smaller than $M_{\text{max,ch}} - 0.6$, the activity rate is given by an exponential model with parameters given by

¹The rate density at magnitude m is define as

$$\lim_{dm \rightarrow 0} \frac{\text{Rate of earthquakes between magnitudes } m \text{ and } m + dm}{dm}$$

The rate density is, therefore, different from the cumulative rate of earthquakes (even though the two look similar for the familiar untruncated exponential model).

the expert or team. At magnitudes $M_{\max, \text{ch}} - 0.6$ to $M_{\max, \text{ch}}$, the activity rate (per unit magnitude) is equal to the rate of characteristic earthquakes divided by 0.6.

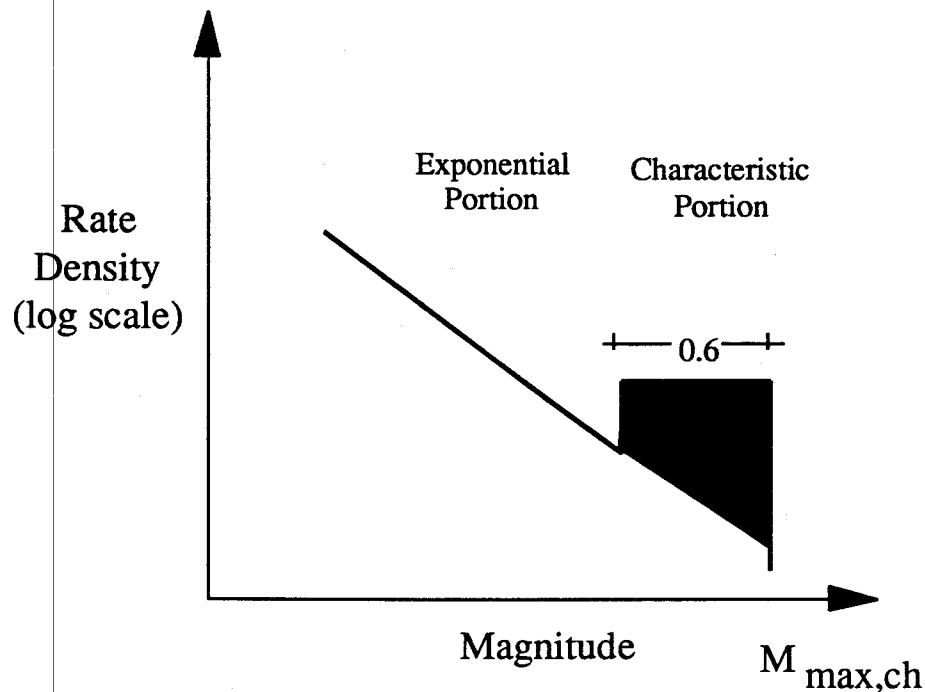


Figure 3-1. Schematic representation of the rate-density function for a characteristic magnitude-frequency law.

For the calculations, it was found convenient to quantify the increment in activity introduced by the characteristic-magnitude model. This increment is shown as the shaded portion in Figure 3-1. The hazard from the Charleston source therefore is computed by summing the hazard obtained using exponential magnitude distributions (i.e., using the standard LLNL and EPRI seismicity parameters) and the hazard contributed by the increment in the rate of large earthquakes. The latter hazard is computed separately for the two values of the characteristic activity rate described in Section 3.2.

Figures 3-2 through 3-12 show the cumulative magnitude-frequency curves for the LLNL experts and EPRI teams considered in this study, and compare these curves to the seismicity and paleoseismic data. No figures are included for LLNL experts 6 and 11, because the characteristic model is not applicable to their interpretations that a large seismic source covering South Carolina is appropriate (characteristic magnitude models have been proposed for specific faults or tectonic zones but not for large areas). Note that where experts or teams use a model that predicts a rate of events with $m_b > 6.3$ greater than 1×10^{-3} , the addition of a characteristic magnitude model adds little (e.g. Figure 3-2). On the other hand, when predicted seismicity is much lower and/or m_{\max} is much higher, the characteristic model makes a large difference (see for example Figure 3-12).

3.4 REFERENCES

1. R. J. Youngs and K. J. Coppersmith. "Implications of Fault Slip Rates and Earthquake Recurrence Models to Probabilistic Seismic Hazard Estimates". *Bulletin of the Seismological Society of America*, 75:939-964, 1985.
2. P. Talwani and K. Collinsworth. "Recurrence Intervals for Intraplate Earthquakes in Eastern North America from Paleoseismic Data". *Seismological Research Letters*, 59(4):207-212, 1988.
3. P. Talwani and J. Cox. "Paleoseismic Evidence for Recurrence of Earthquakes Near Charleston, South Carolina". *Science*, 229:379-381, 1985.
4. R. Weems, S. Obermeier, M. Pavich, G. Gohn, M. Rubin, R. Phipps, and R. Jacobson. "Evidence for Three Moderate to Large Prehistoric Holocene Earthquakes Near Charleston, South Carolina". In *Proceedings of the Third U.S. National Conference on Earthquake Engineering*, Charleston, SC, 1986.
5. *Comparison and Analysis of Assumptions in LLNL and EPRI Seismic Hazard Studies for the Savannah River Site*. Report to Westinghouse Savannah River Company, Aiken, South Carolina, Risk Engineering, Inc., 1990.

CHARLESTON SEISMICITY RATES AND
CHARACTERISTIC MODELS - LLNL EXPERT 1

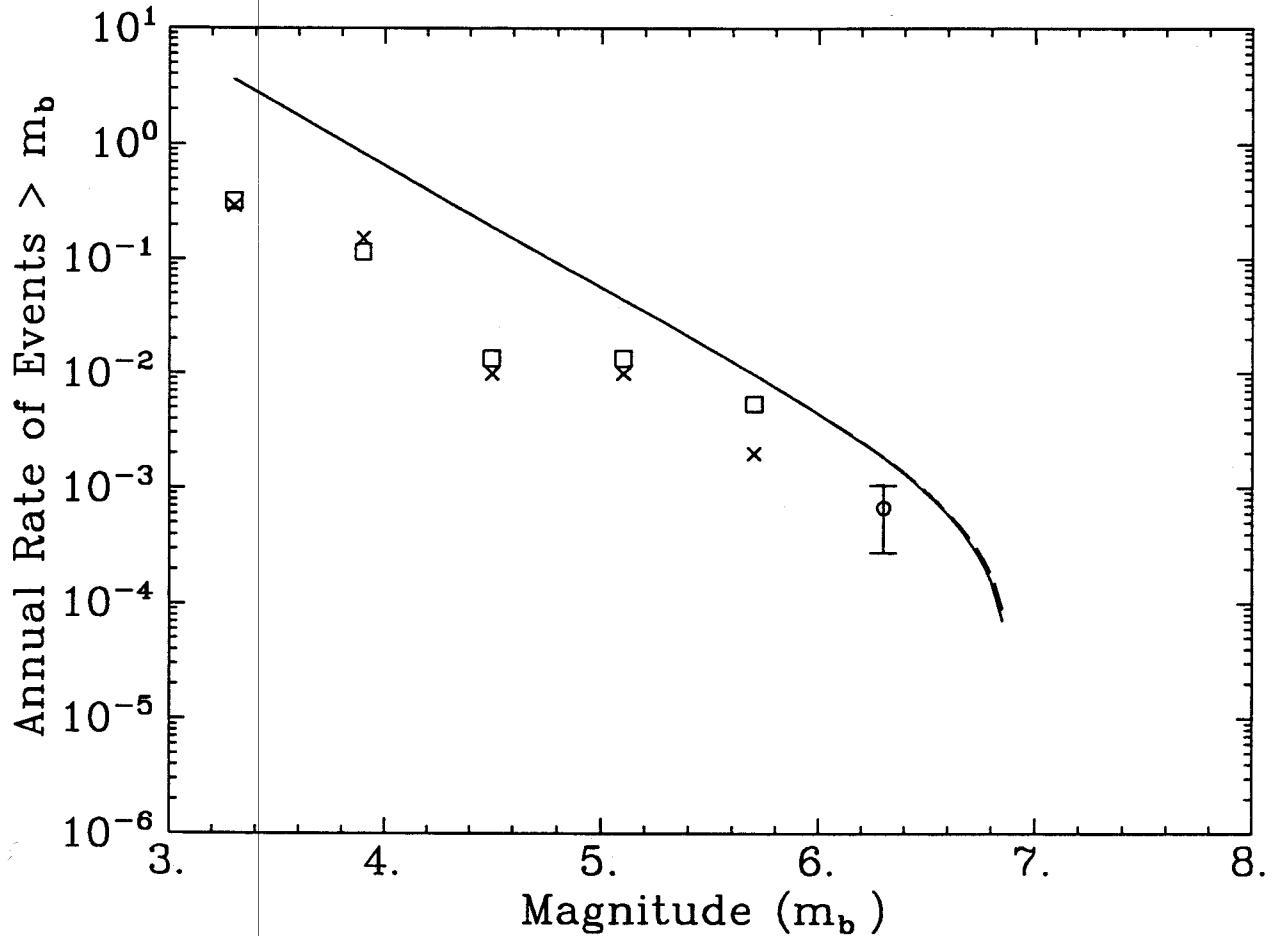


Figure 3-2. Charleston seismicity rates and characteristic magnitude-frequency law: LLNL seismicity expert 1. The two curves were obtained using the two equally likely values for the rate of Charleston-size earthquakes (i.e, 2.8×10^{-4} and 1.1×10^{-3}). The □ and × symbols represent observed seismicity in the Charleston area under two assumptions of completeness [see (5)]. The circle and error bar represent the rate of Charleston-size earthquakes and its 1σ bounds.

CHARLESTON SEISMICITY RATES AND CHARACTERISTIC MODELS - LLNL EXPERT 3

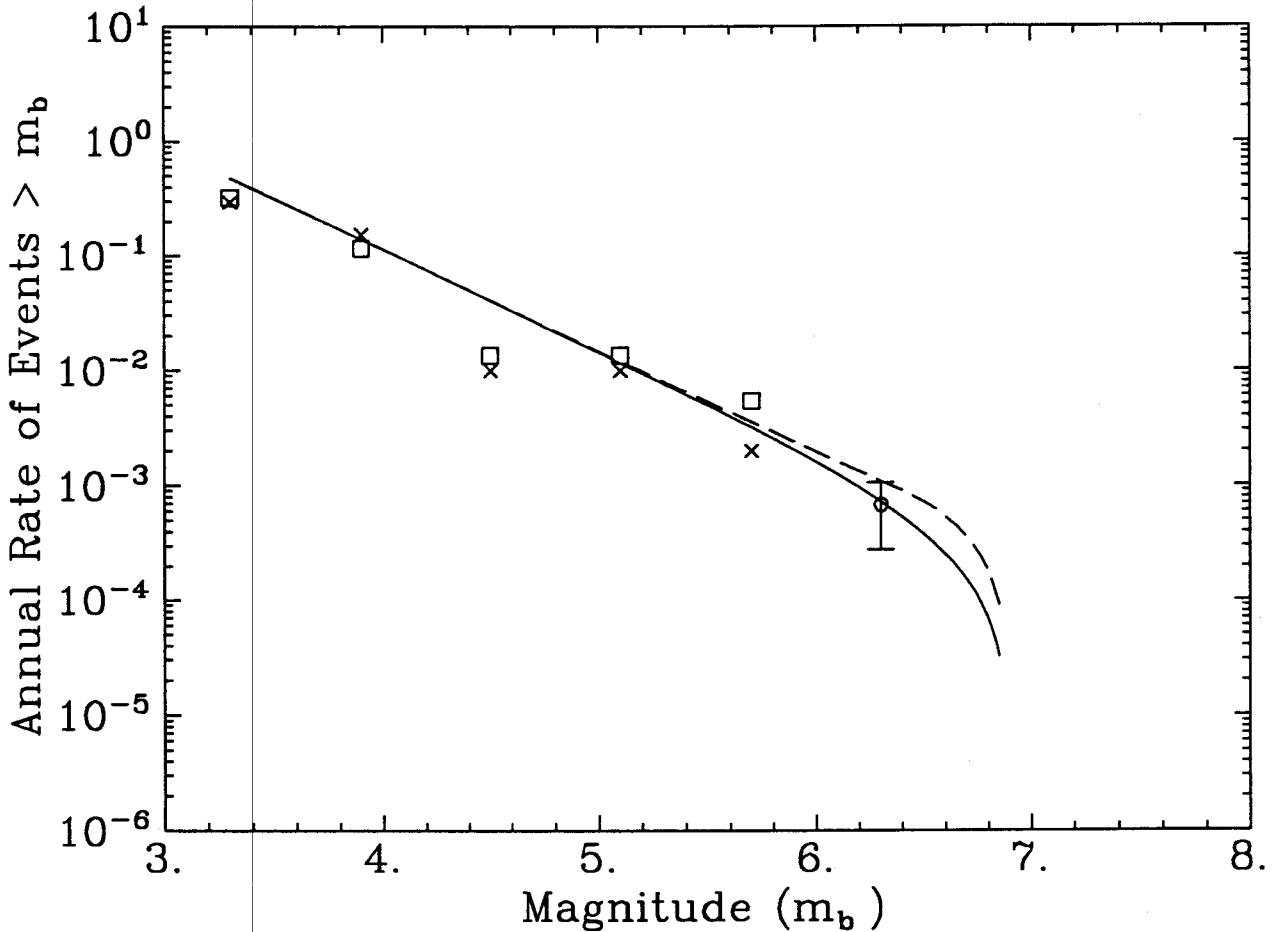


Figure 3-3. Charleston seismicity rates and characteristic magnitude-frequency law: LLNL seismicity expert 3. The two curves were obtained using the two equally likely values for the rate of Charleston-size earthquakes (i.e, 2.8×10^{-4} and 1.1×10^{-3}). The \square and \times symbols represent observed seismicity in the Charleston area under two assumptions of completeness [see (5)]. The circle and error bar represent the rate of Charleston-size earthquakes and its 1σ bounds.

CHARLESTON SEISMICITY RATES AND
CHARACTERISTIC MODELS - LLNL EXPERT 7

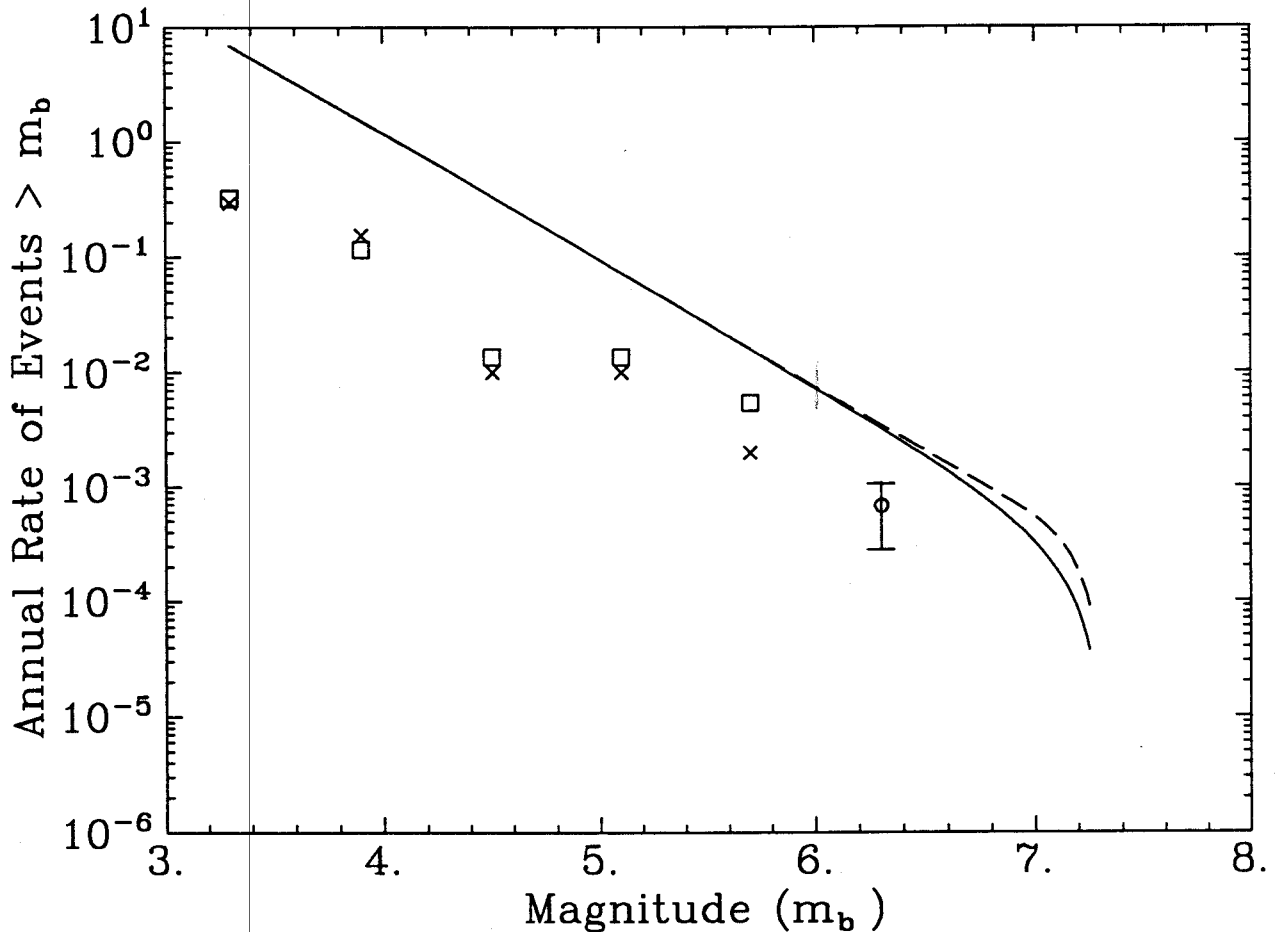


Figure 3-4. Charleston seismicity rates and characteristic magnitude-frequency law: LLNL seismicity expert 7. The two curves were obtained using the two equally likely values for the rate of Charleston-size earthquakes (i.e., 2.8×10^{-4} and 1.1×10^{-3}). The \square and \times symbols represent observed seismicity in the Charleston area under two assumptions of completeness [see (5)]. The circle and error bar represent the rate of Charleston-size earthquakes and its 1σ bounds.

CHARLESTON SEISMICITY RATES AND CHARACTERISTIC MODELS - LLNL EXPERT 10

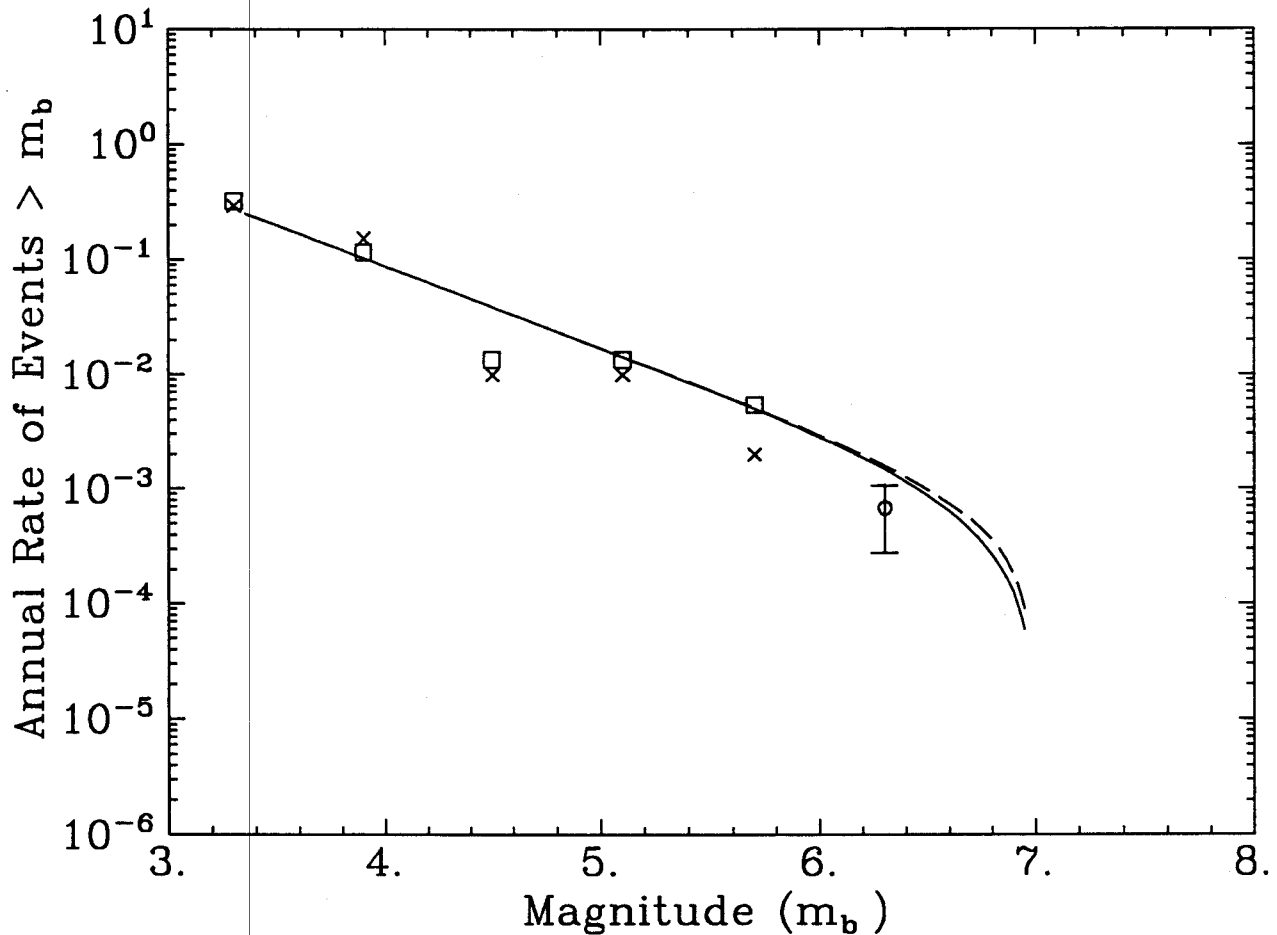


Figure 3-5. Charleston seismicity rates and characteristic magnitude-frequency law: LLNL seismicity expert 10. The two curves were obtained using the two equally likely values for the rate of Charleston-size earthquakes (i.e., 2.8×10^{-4} and 1.1×10^{-3}). The □ and × symbols represent observed seismicity in the Charleston area under two assumptions of completeness [see (5)]. The circle and error bar represent the rate of Charleston-size earthquakes and its 1σ bounds.

CHARLESTON SEISMICITY RATES AND CHARACTERISTIC MODELS - LLNL EXPERT 12

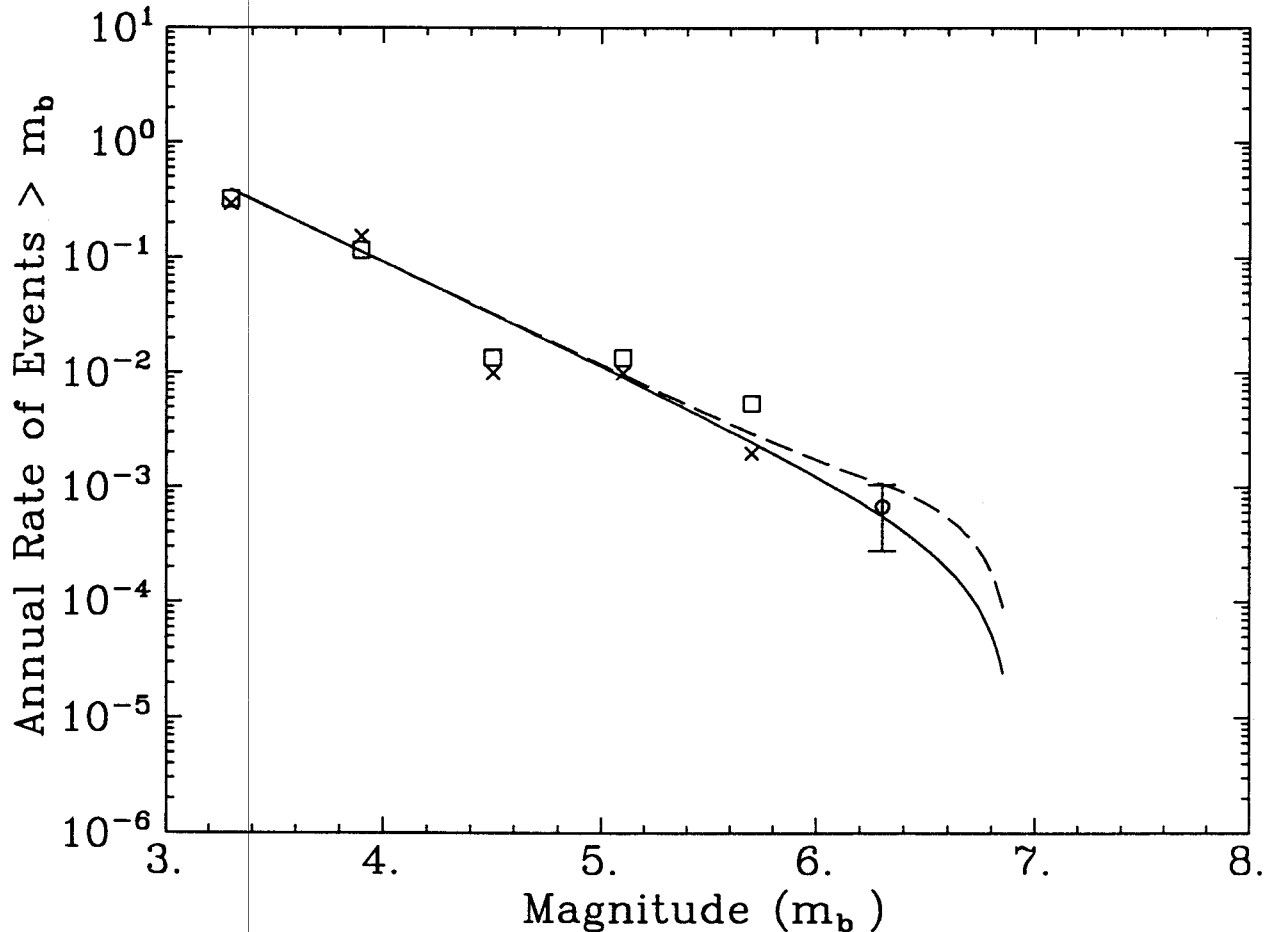


Figure 3-6. Charleston seismicity rates and characteristic magnitude-frequency law: LLNL seismicity expert 12. The two curves were obtained using the two equally likely values for the rate of Charleston-size earthquakes (i.e, 2.8×10^{-4} and 1.1×10^{-3}). The \square and \times symbols represent observed seismicity in the Charleston area under two assumptions of completeness [see (5)]. The circle and error bar represent the rate of Charleston-size earthquakes and its 1σ bounds.

CHARLESTON SEISMICITY RATES AND CHARACTERISTIC MODELS - LLNL EXPERT 13

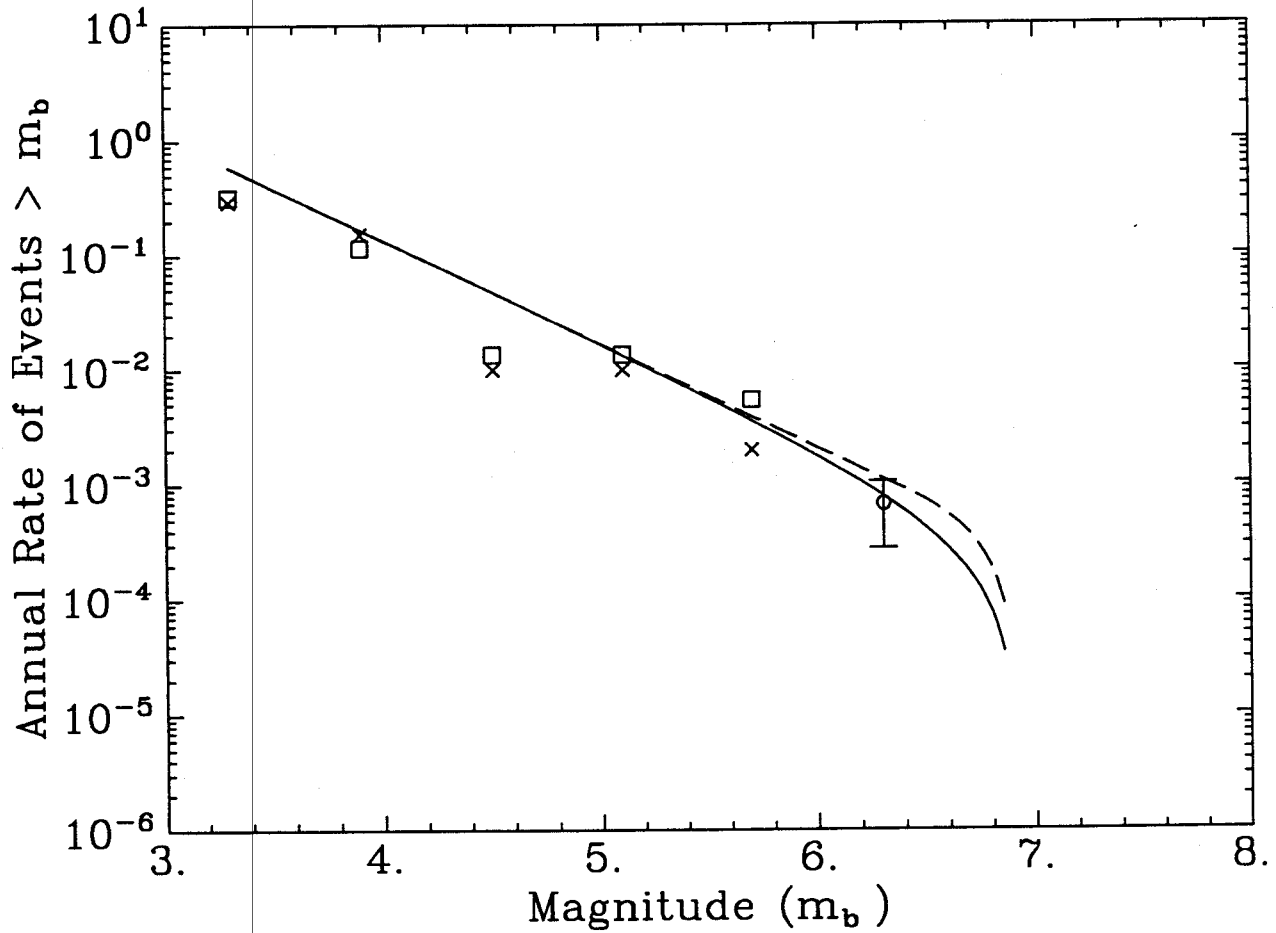


Figure 3-7. Charleston seismicity rates and characteristic magnitude-frequency law: LLNL seismicity expert 13. The two curves were obtained using the two equally likely values for the rate of Charleston-size earthquakes (i.e., 2.8×10^{-4} and 1.1×10^{-3}). The \square and \times symbols represent observed seismicity in the Charleston area under two assumptions of completeness [see (5)]. The circle and error bar represent the rate of Charleston-size earthquakes and its 1σ bounds.

CHARLESTON SEISMICITY RATES AND CHARACTERISTIC MODELS - BECHTEL TEAM

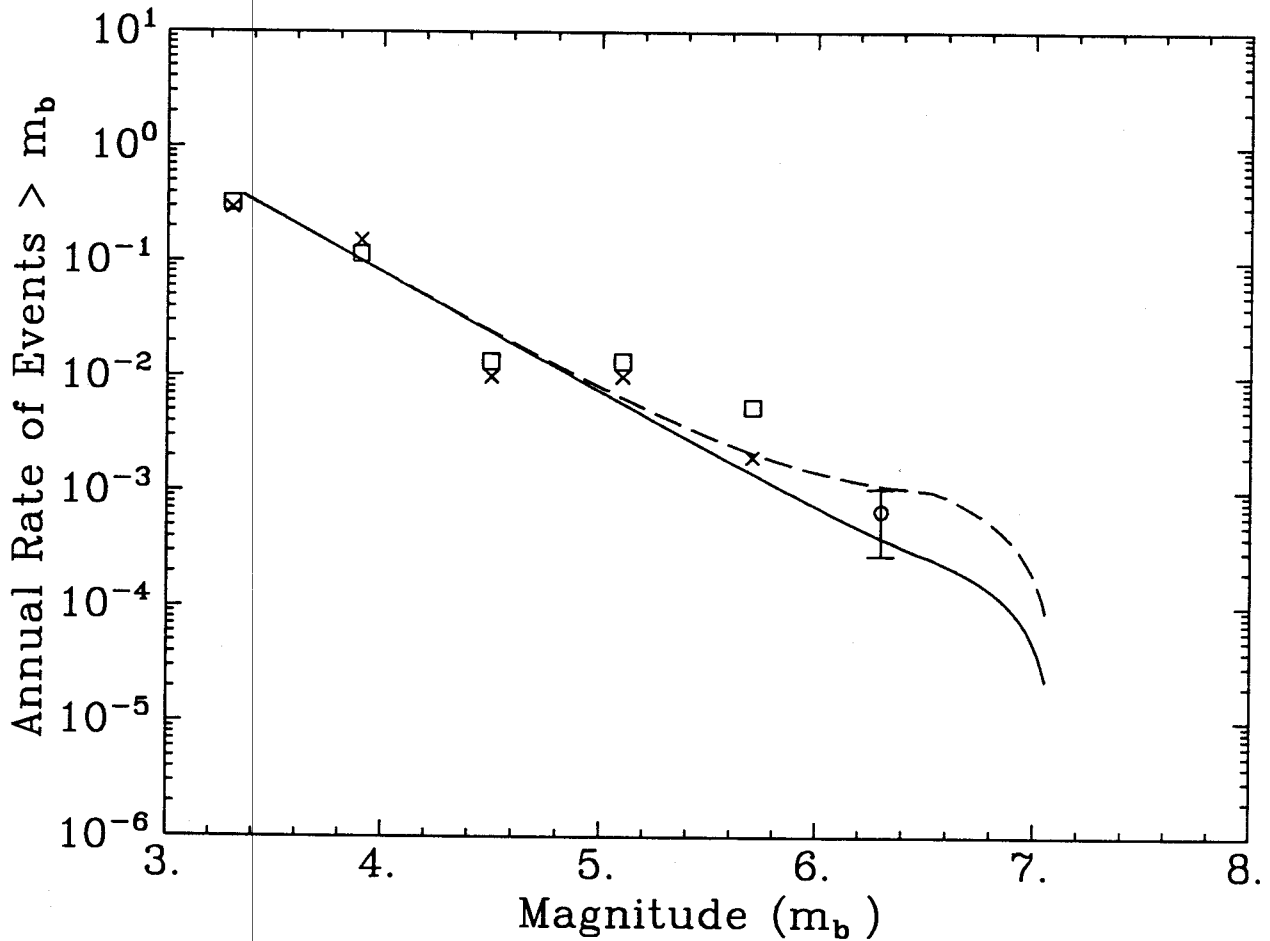


Figure 3-8. Charleston seismicity rates and characteristic magnitude-frequency law: Bechtel team. The two curves were obtained using the two equally likely values for the rate of Charleston-size earthquakes (i.e., 2.8×10^{-4} and 1.1×10^{-3}). The \square and \times symbols represent observed seismicity in the Charleston area under two assumptions of completeness [see (5)]. The circle and error bar represent the rate of Charleston-size earthquakes and its 1σ bounds.

CHARLESTON SEISMICITY RATES AND CHARACTERISTIC MODELS - LAW TEAM

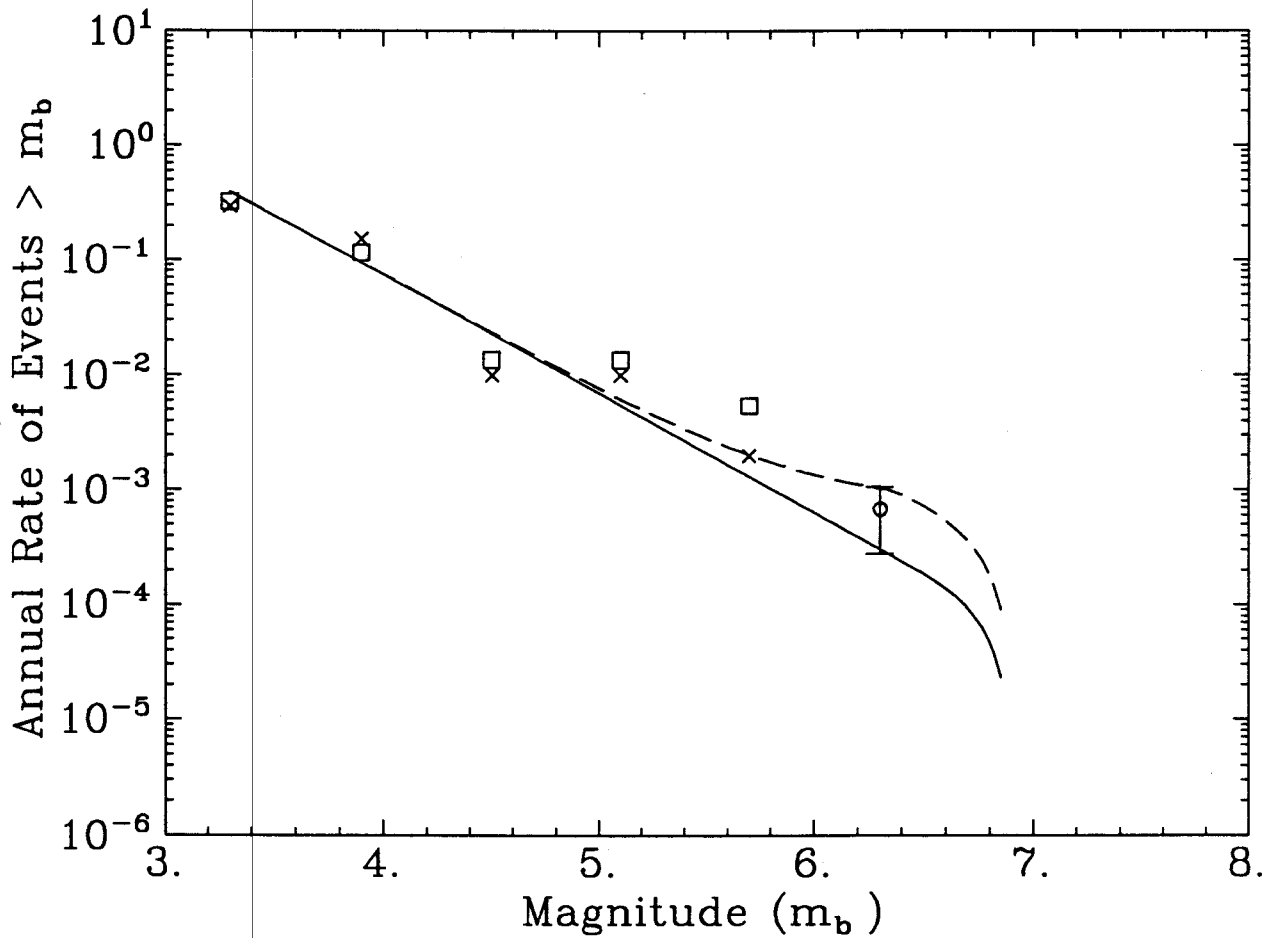


Figure 3-9. Charleston seismicity rates and characteristic magnitude-frequency law: Law team. The two curves were obtained using the two equally likely values for the rate of Charleston-size earthquakes (i.e, 2.8×10^{-4} and 1.1×10^{-3}). The \square and \times symbols represent observed seismicity in the Charleston area under two assumptions of completeness [see (5)]. The circle and error bar represent the rate of Charleston-size earthquakes and its 1σ bounds.

CHARLESTON SEISMICITY RATES AND CHARACTERISTIC MODELS – RONDOUT TEAM

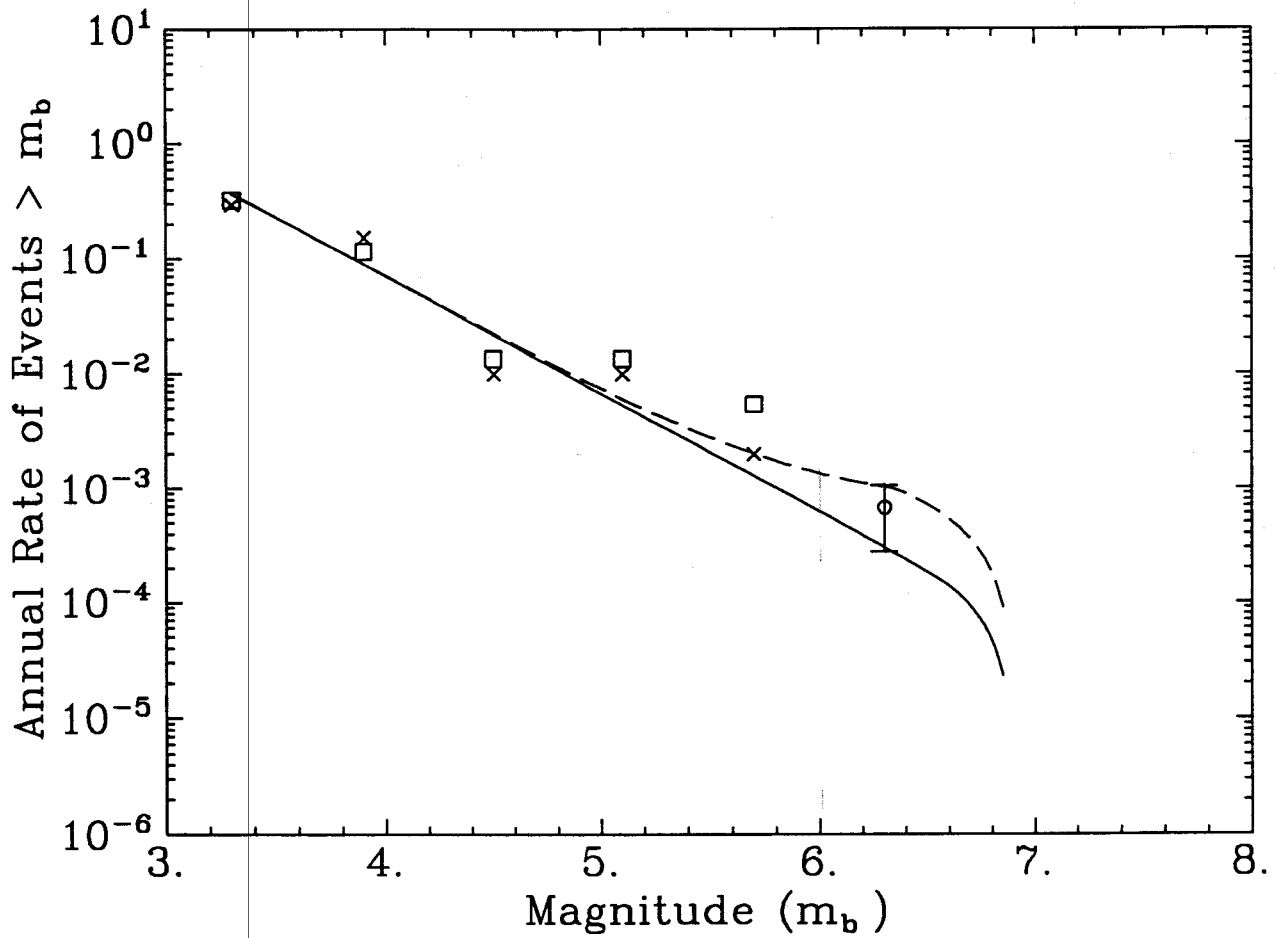


Figure 3-10. Charleston seismicity rates and characteristic magnitude-frequency law: Rondout team. The two curves were obtained using the two equally likely values for the rate of Charleston-size earthquakes (i.e., 2.8×10^{-4} and 1.1×10^{-3}). The \square and \times symbols represent observed seismicity in the Charleston area under two assumptions of completeness [see (5)]. The circle and error bar represent the rate of Charleston-size earthquakes and its 1σ bounds.

CHARLESTON SEISMICITY RATES AND CHARACTERISTIC MODELS – WESTON TEAM

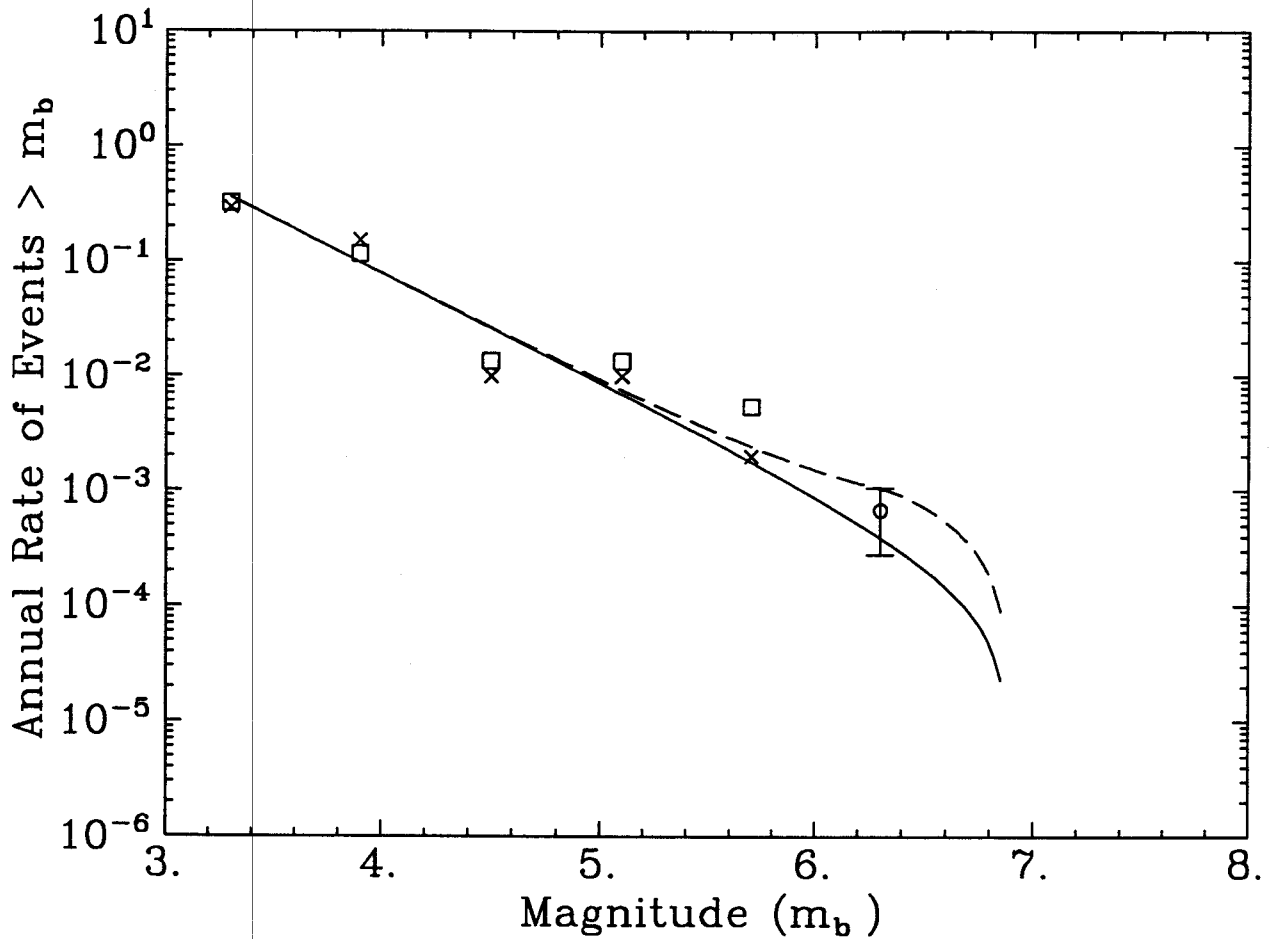


Figure 3-11. Charleston seismicity rates and characteristic magnitude-frequency law: Weston team. The two curves were obtained using the two equally likely values for the rate of Charleston-size earthquakes (i.e., 2.8×10^{-4} and 1.1×10^{-3}). The \square and \times symbols represent observed seismicity in the Charleston area under two assumptions of completeness [see (5)]. The circle and error bar represent the rate of Charleston-size earthquakes and its 1σ bounds.

CHARLESTON SEISMICITY RATES AND
CHARACTERISTIC MODELS - WOODWARD-CLYDE TEAM

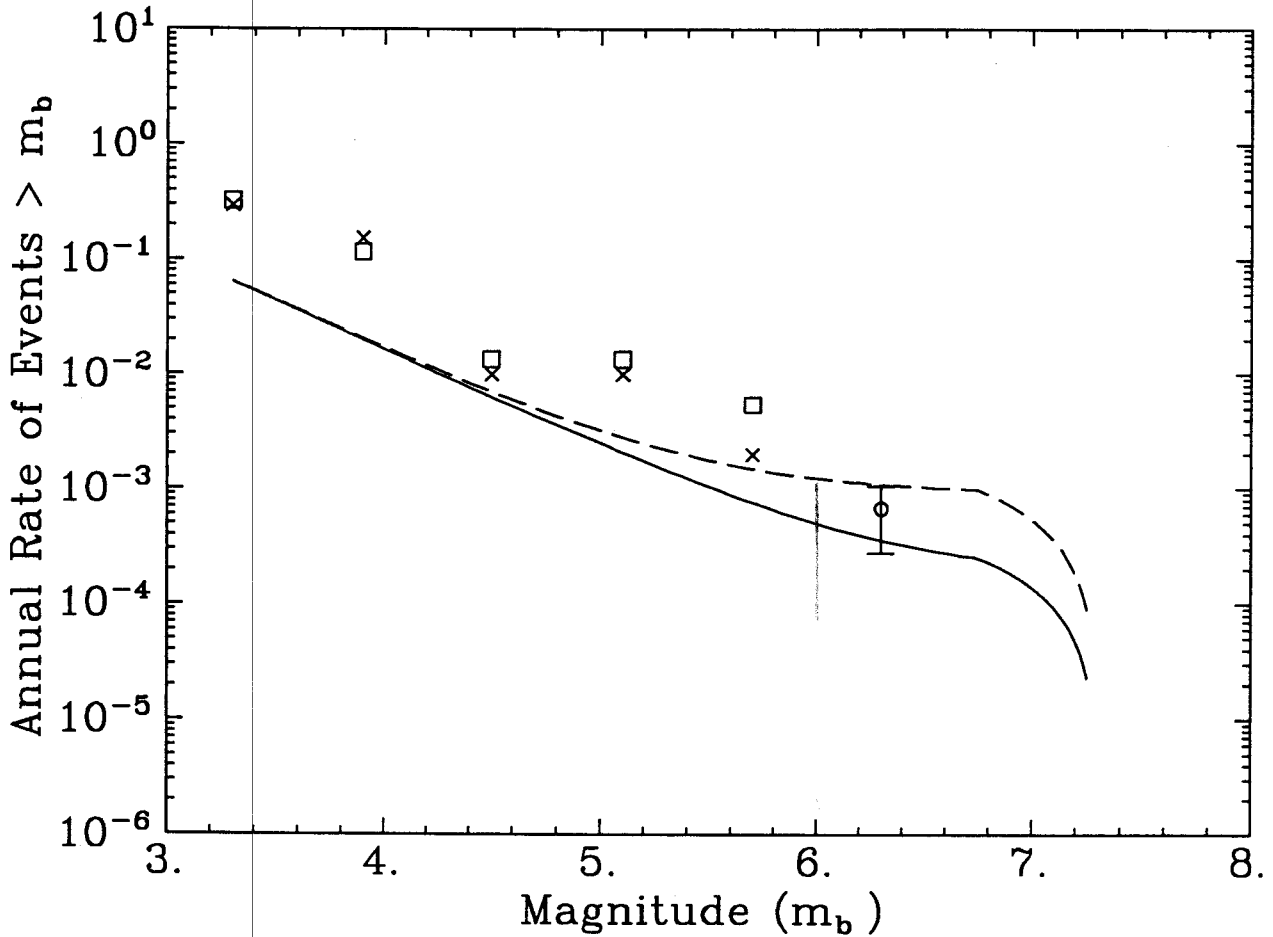


Figure 3-12. Charleston seismicity rates and characteristic magnitude-frequency law: Woodward-Clyde team. The two curves were obtained using the two equally likely values for the rate of Charleston-size earthquakes (i.e, 2.8×10^{-4} and 1.1×10^{-3}). The □ and × symbols represent observed seismicity in the Charleston area under two assumptions of completeness [see (5)]. The circle and error bar represent the rate of Charleston-size earthquakes and its 1σ bounds.

Section 4
CALCULATIONS AND RESULTS

4.1 LLNL CALCULATIONS

We obtained from LLNL the computer files containing the raw results from LLNL's analysis of seismic hazard at the SRS ¹. These results consist of 50 equally likely hazard curves for each combination of seismicity expert and ground-motion expert.

The steps used to obtain the LLNL hazard, including the characteristic magnitude model and excluding ground-motion expert 5, are as follows:

1. For each combination of seismicity and ground-motion expert, evaluate the hazard introduced by the increased rate of large earthquakes in the Charleston source. This calculation considers the two alternative values for the rate of large earthquakes in the Charleston source. This calculation uses the seismicity expert best-estimate recurrence parameters and geometry for the Charleston source. This calculation also considers uncertainty in attenuation functions and in site-amplification factors ². Uncertainty is represented by multiple hazard curves (typically 36 or 48 curves) with associated weights.
2. For each combination of seismicity and ground-motion expert, convolve the 50 hazard curves from the standard LLNL results with the multiple hazard curves obtained in step 1. In this calculation, each pair of hazard curves (one curve from the standard LLNL calculations, one curve from step 1 above) are summed to obtain the total hazard. The weight associated with the resulting hazard curve is the product of the weights associated with the two hazard curves.
3. For each seismicity expert, combine the hazard curves obtained in step 2 for the various ground-motion experts (excluding ground-motion expert 5); compute summary statistics (i.e., mean and fractile hazard curves).

¹We call these the standard LLNL results.

²Each LLNL ground-motion expert, with the exception of expert 5, specified multiple attenuation functions [see Table 3.5 in Volume 1 of (1)]. The LLNL amplification factor for deep soil has a median value of 1, but it has a lognormal uncertainty with $\sigma_{\ln[\text{ampl.factor}]} = 0.5$ [see Section 3.7 in (1)].

4. Combine the hazard curves from multiple LLNL seismicity experts using the weights in Table 2-1; compute summary statistics.

Seismicity experts 6 and 11 used large seismic sources (which include Charleston) to model seismicity in the southeastern United States. A characteristic model is not appropriate for sources of this size. Therefore, the standard LLNL results for these experts (without ground-motion expert 5) were used in steps 3 and 4 above.

Figures 4-1 through 4-8 show the mean and fractile hazard curves obtained from the interpretations of each LLNL expert. Two sets of results are drawn (except for experts 6 and 11) representing the hazard with and without the characteristic-magnitude assumption. These results show that the effect of the characteristic-magnitude assumption is always small, and sometimes imperceptible.

Figure 4-9 shows the mean and fractile hazard curves obtained by combining the LLNL seismicity experts using the weights in Table 2-1. These hazard curves include the effect of the characteristic-magnitude assumption.

4.2 EPRI CALCULATIONS

For the EPRI calculations, we considered the seismic sources used in the Jack Benjamin and Associates study (2), which are the same sources used in (3) for the Vogtle site. A description of these sources is contained in the former reference and is not repeated here.

We also calculated the hazard introduced by the increased rate of large earthquakes in the Charleston source (due to the characteristic-magnitude assumption). This calculation was performed separately for each team, considering the team's geometry, maximum magnitude, and seismicity parameters for the Charleston source. This calculation considers uncertainty in the rate of characteristic earthquakes, uncertainty in attenuation functions, and uncertainty in site-amplification factors.

To include the characteristic-magnitude assumption in the calculation of the total hazard, a fictitious seismic source—representing the additional hazard computed above—was added to all the EPRI source combinations used in (2).

Figures 4-10 through 4-14 show the median hazard curves from each of the EPRI teams included in Table 2-1 with and without the characteristic-magnitude assumption. As was

the case with the LLNL calculations, the characteristic-magnitude assumption has a small effect on the hazard.

Figure 4-15 shows the mean and fractile hazard curves obtained by combining the results from the five EPRI teams considered in this study. These hazard curves include the effect of the characteristic-magnitude assumption.

4.3 COMBINATION LLNL-EPRI RESULTS—DISCUSSION

The hazard results obtained using the LLNL interpretations (excluding ground-motion expert 5) and the EPRI interpretations were combined using the weights in Table 2-1, and summary statistics were computed. Results are presented in Figures 4-16 and 4-17.

Comparison of Figures 4-9 and 4-15 indicates that the results obtained here from the LLNL and EPRI studies show good agreement in the median hazard curves. Differences remain in the uncertainties, and this causes the mean and 85% fractile hazard curves from the LLNL study (Figure 4-9) to exceed those of the EPRI study (Figure 4-15) by a substantial margin. To understand the causes of these larger uncertainties, an investigation was made into the range of seismicity parameters specified by the LLNL S-experts. Details of the study are presented in Appendix A; it is concluded that unrealistically large uncertainty bands on the seismicity parameters for four of the LLNL S-experts leads to unrealistically large uncertainties in seismic hazard.

As a result, a modified set of LLNL S-experts (numbers 1, 3, 10, and 12) were used to derive a modified set of LLNL seismic hazard curves (these four LLNL S-experts were given equal weights). Again, details are presented in Appendix A. The resulting set of modified LLNL hazard curves are shown in Figure 4-18. Comparing these curves to the equivalent EPRI set (Figure 4-9) shows good agreement between the median, mean, and 85% fractile (these curves all agree within a factor of 3.6 at all ground motion levels). Figures 4-19 and 4-20 present the combined (modified) LLNL and EPRI analyses.

Because some of the LLNL S-experts interpretations have uncertainties on parameters that are unrealistically large, as discussed in Appendix A, we believe the combined, modified set of curves (Figures 4-18 and 4-19) are the best set of curves to use for seismic decisions at the SRS.

4.4 REFERENCES

1. D. L. Bernreuter, J. B. Savy, R. W. Mensing, and J. C. Chen. *Seismic Hazard Characterization of 69 Plant Sites East of the Rocky Mountains*. Technical Report NUREG/CR5250, UCID-21517, U. S. Nuclear Regulatory Commission, 1988.

2. *Probabilistic Seismic Hazard Evaluation for the Savannah River site, Aiken, South Carolina.* Report to Westinghouse Savannah River Company, Aiken, South Carolina, Jack Benjamin and Associates, 1989.
3. R. K. McGuire, G. R. Toro, J. P. Jacobson, T. F. O'Hara, and W. J. Silva. *Probabilistic Seismic Hazard Evaluations in the Central and Eastern United States: Resolution of the Charleston Earthquake Issue.* Special Report NP-6395-D, Electric Power Research Institute, April 1989.

SAVANNAH RIVER SITE
LLNL EXPERT 1

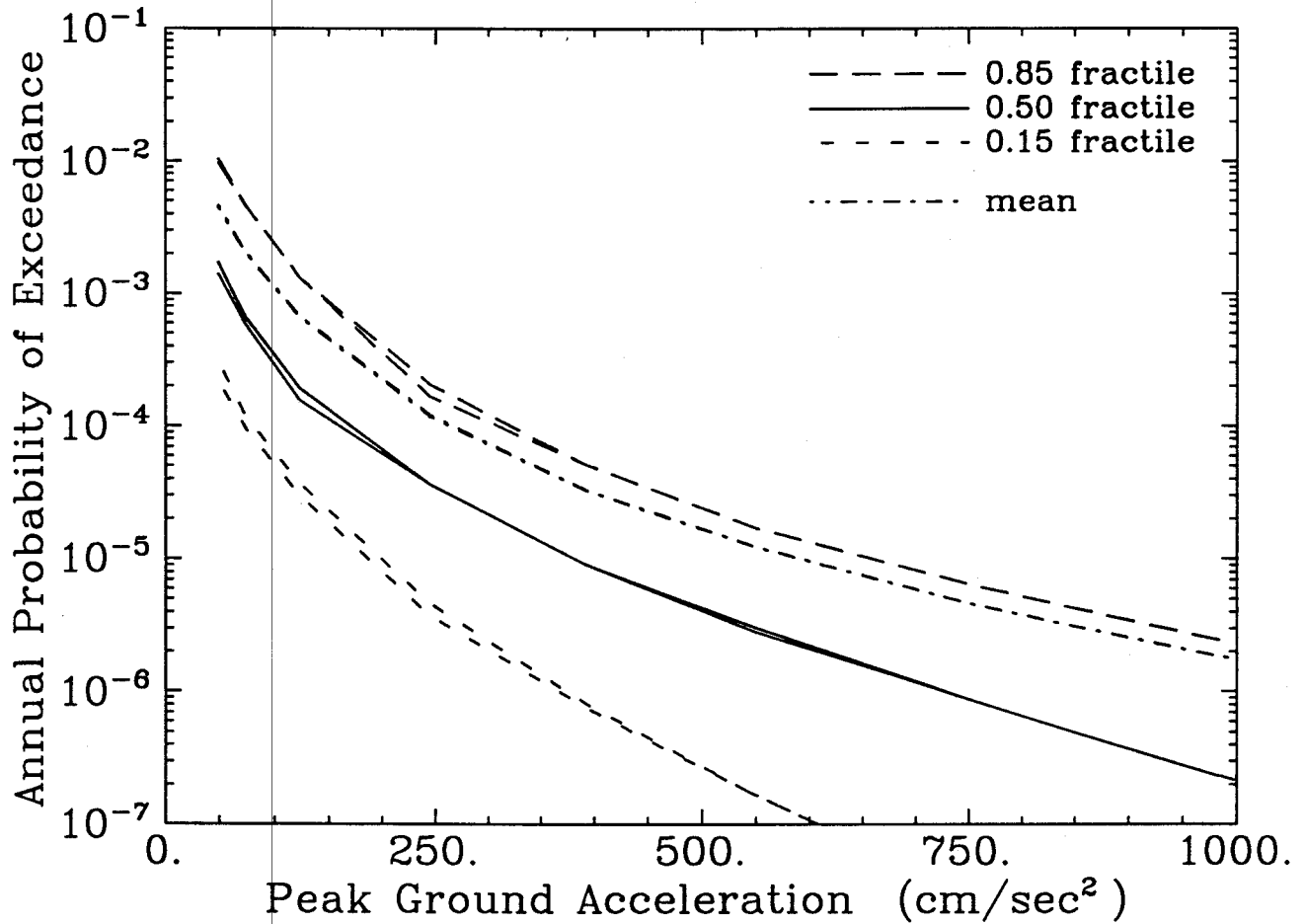


Figure 4-1. Mean and fractile hazard curves calculated for LLNL seismicity expert 1. Two sets of curves are shown, representing results with and without the characteristic-magnitude assumption.

SAVANNAH RIVER SITE
LLNL EXPERT 3

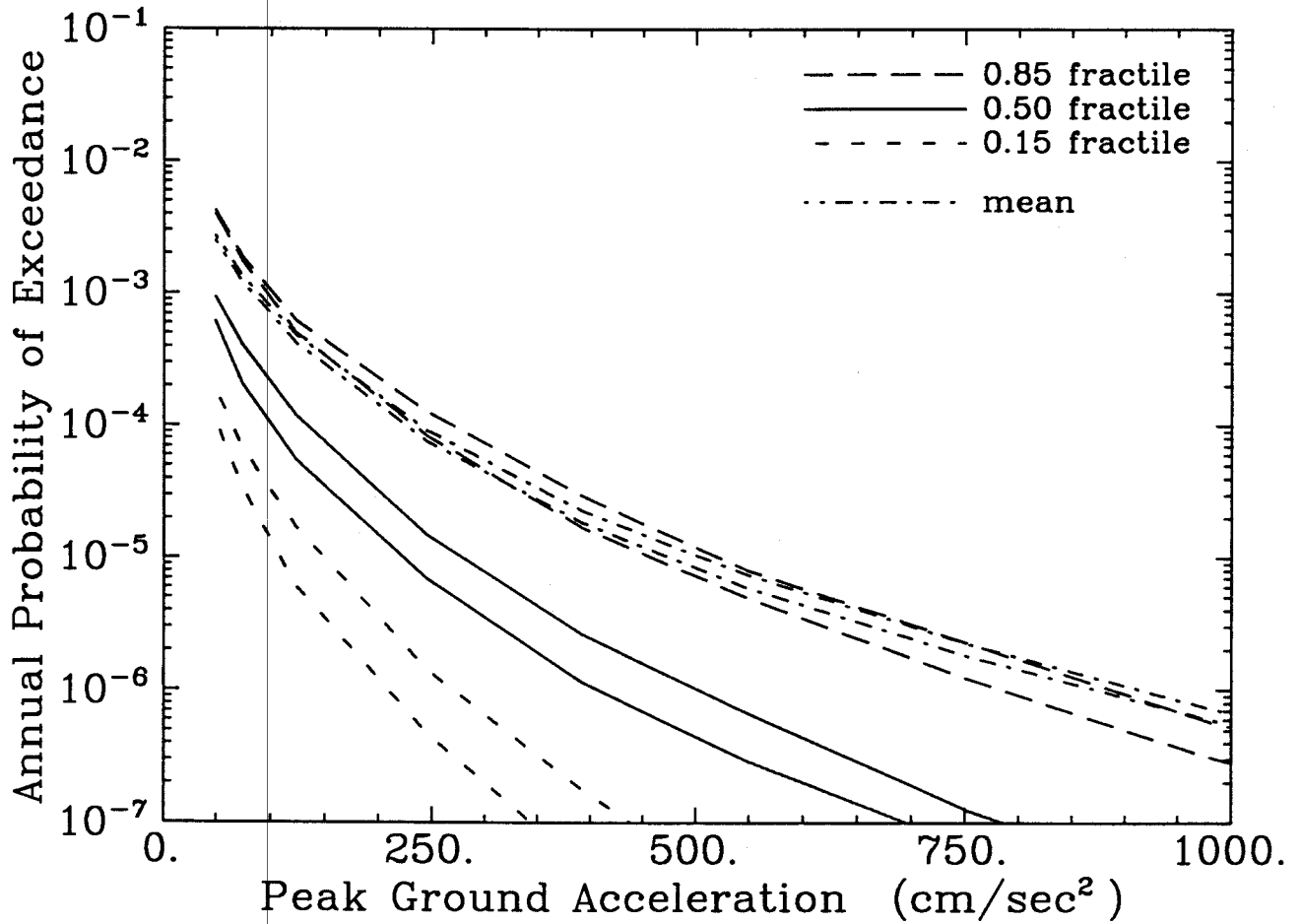


Figure 4-2. Mean and fractile hazard curves calculated for LLNL seismicity expert 3. Two sets of curves are shown, representing results with and without the characteristic-magnitude assumption.

SAVANNAH RIVER SITE
LLNL EXPERT 6

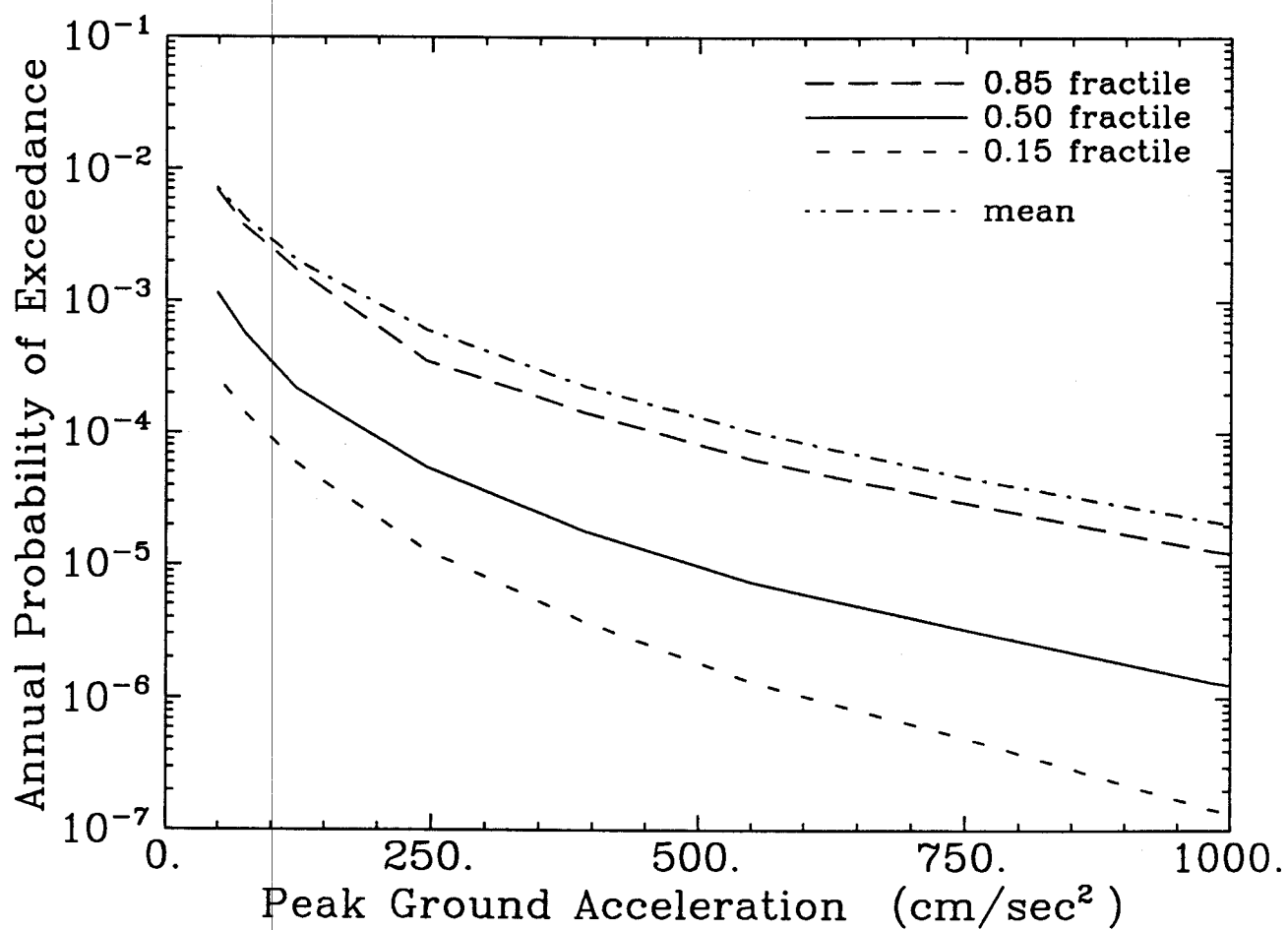


Figure 4-3. Mean and fractile hazard curves calculated for LLNL seismicity expert 6.

SAVANNAH RIVER SITE
LLNL EXPERT 7

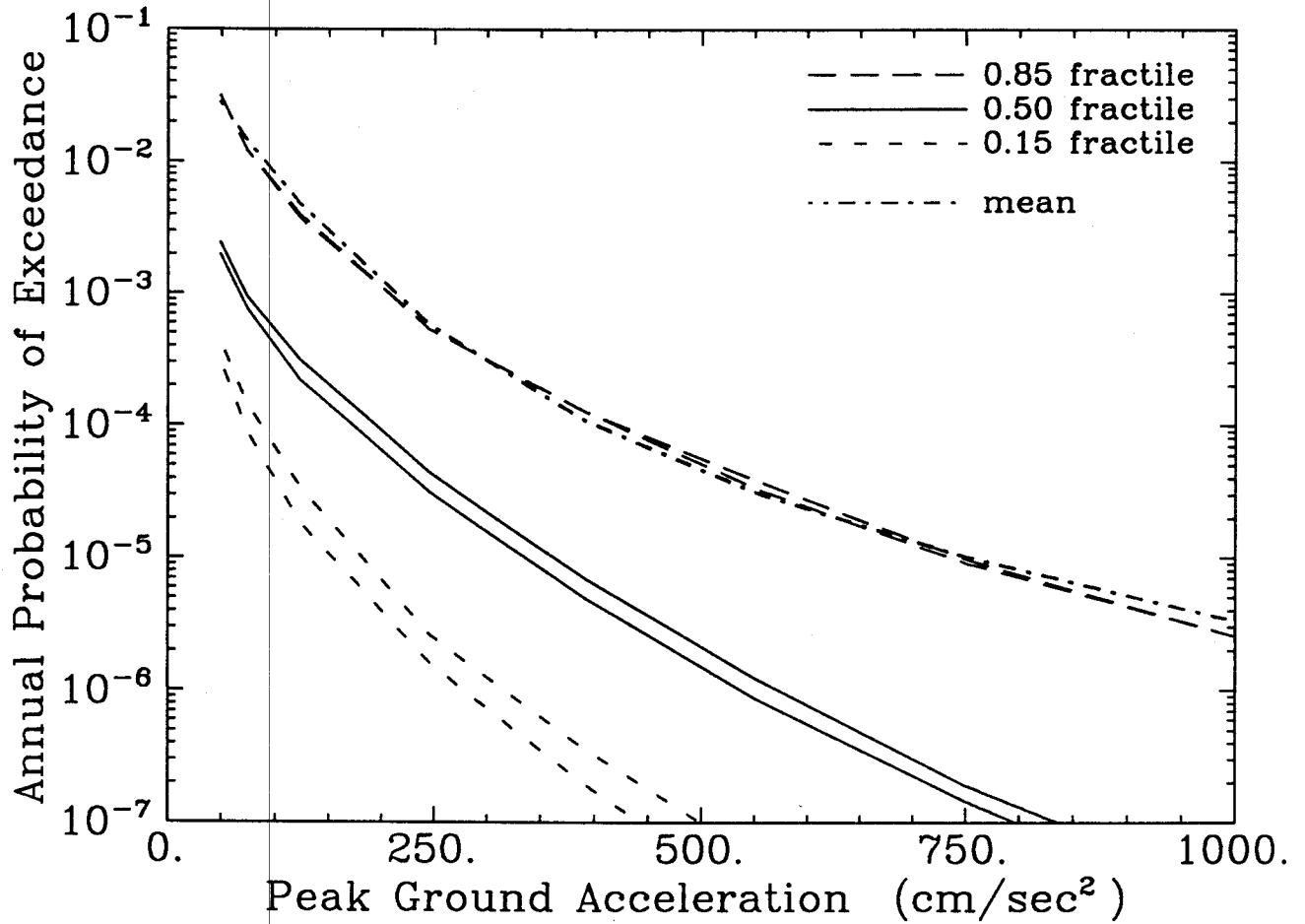


Figure 4-4. Mean and fractile hazard curves calculated for LLNL seismicity expert 7. Two sets of curves are shown, representing results with and without the characteristic-magnitude assumption.

SAVANNAH RIVER SITE
LLNL EXPERT 10

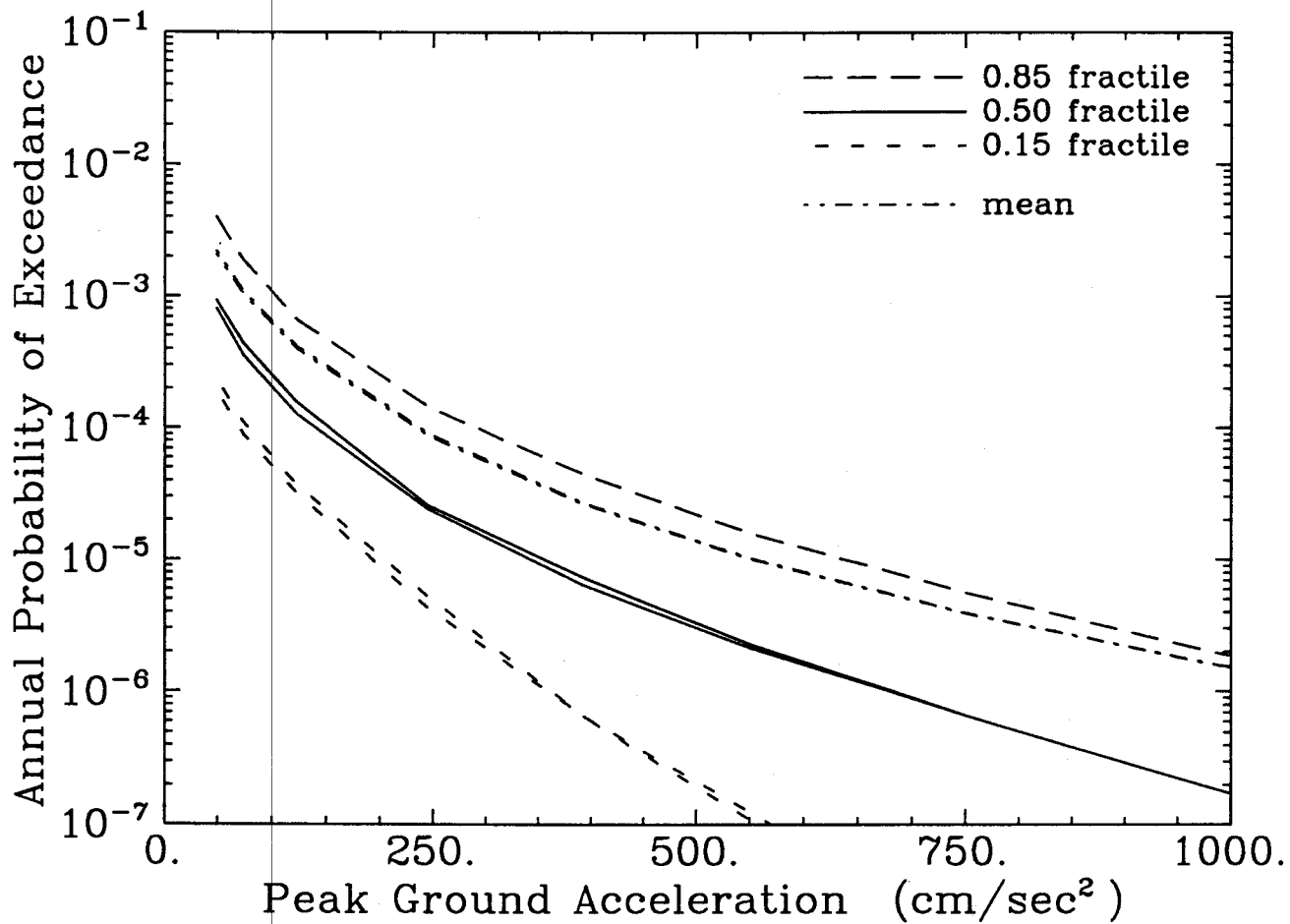


Figure 4-5. Mean and fractile hazard curves calculated for LLNL seismicity expert 10. Two sets of curves are shown, representing results with and without the characteristic-magnitude assumption.

SAVANNAH RIVER SITE
LLNL EXPERT 11

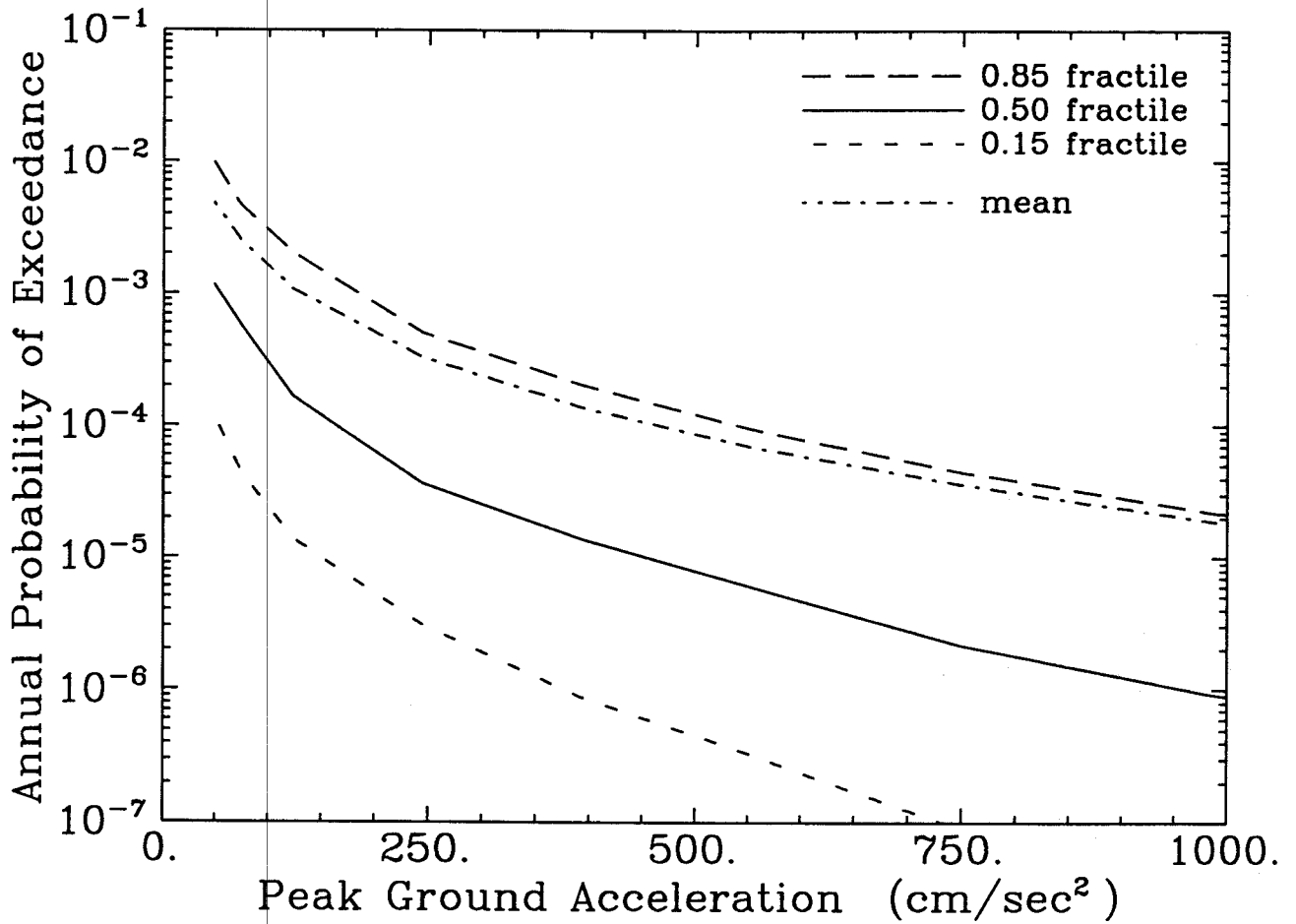


Figure 4-6. Mean and fractile hazard curves calculated for LLNL seismicity expert 11.

SAVANNAH RIVER SITE
LLNL EXPERT 12

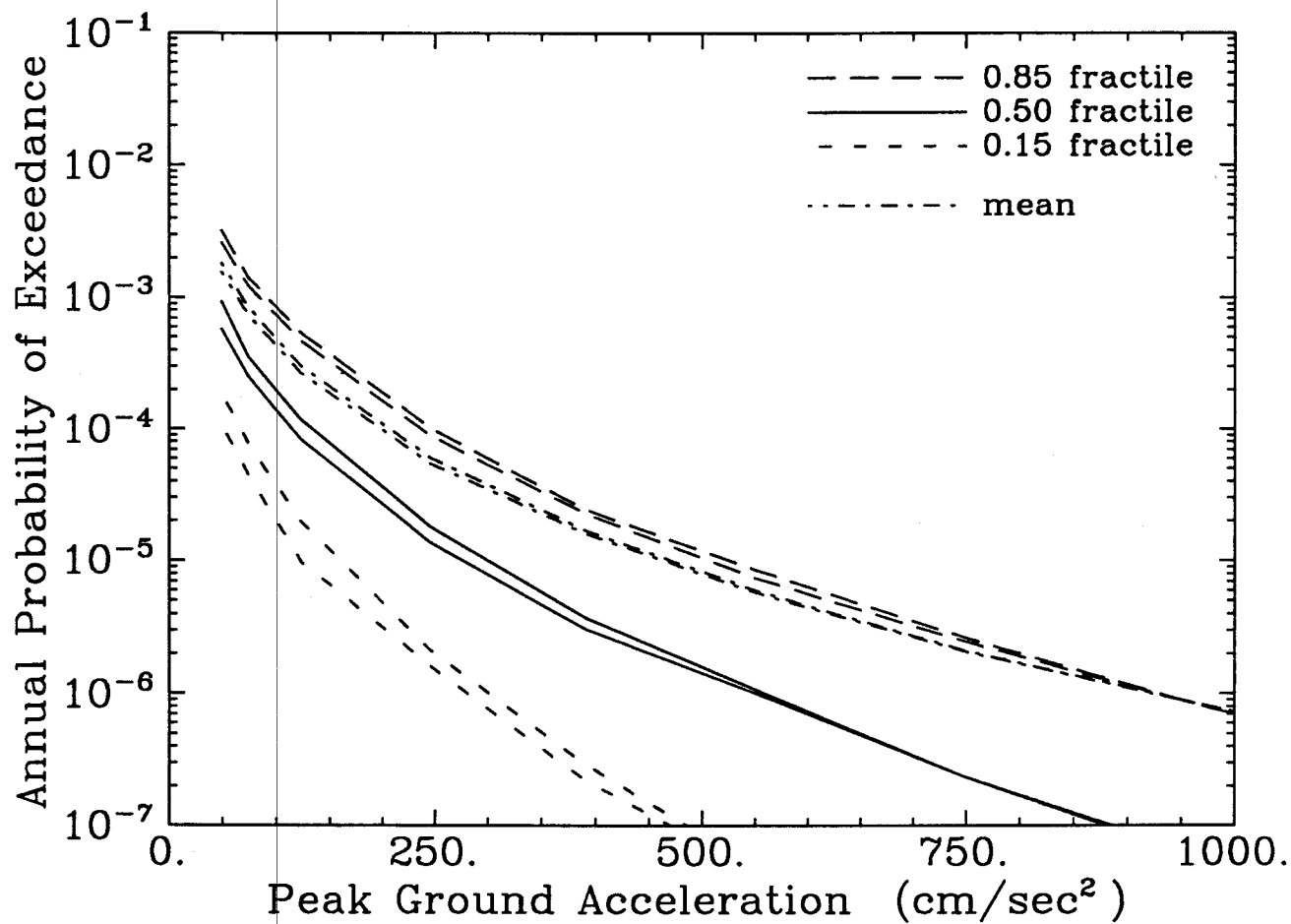


Figure 4-7. Mean and fractile hazard curves calculated for LLNL seismicity expert 12. Two sets of curves are shown, representing results with and without the characteristic-magnitude assumption.

SAVANNAH RIVER SITE
LLNL EXPERT 13

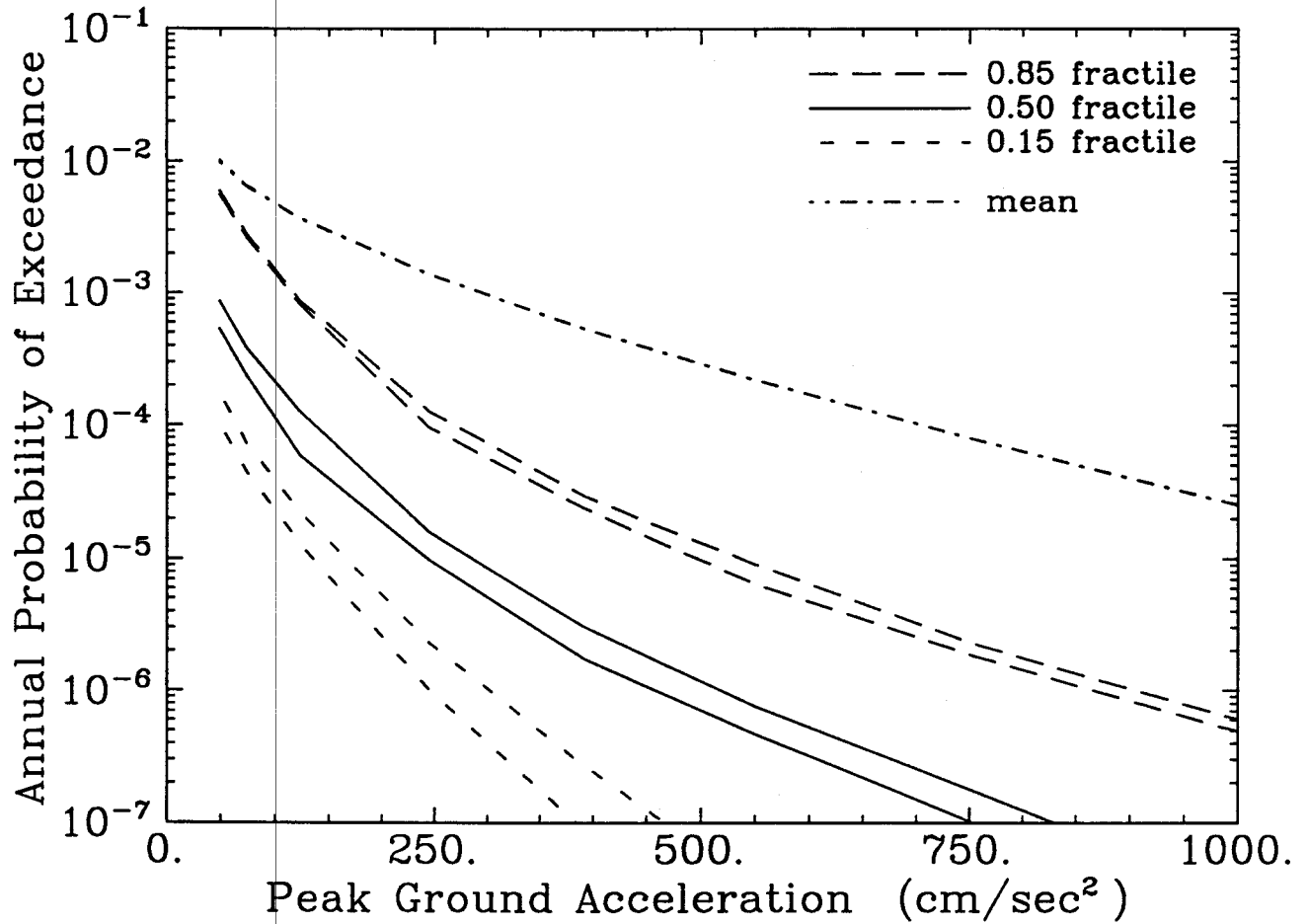


Figure 4-8. Mean and fractile hazard curves calculated for LLNL seismicity expert 13. Two sets of curves are shown, representing results with and without the characteristic-magnitude assumption.

SAVANNAH RIVER SITE
HAZARD USING SUBSET OF LLNL INTERPRETATIONS

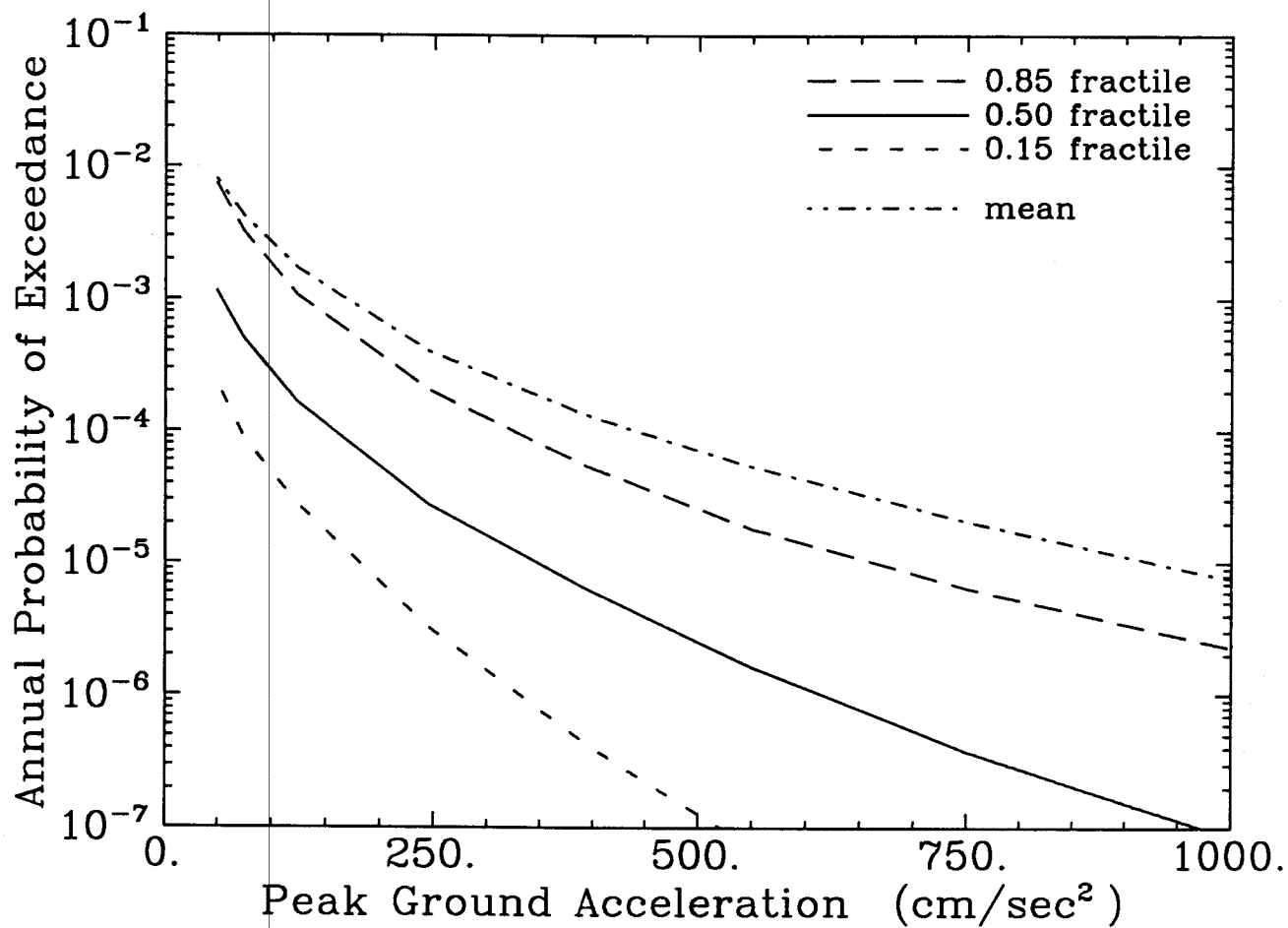


Figure 4-9. Mean and fractile hazard curves calculated by combining results from the LLNL seismicity experts, using the weights in Table 2-1.

SAVANNAH RIVER SITE
BECHTEL TEAM

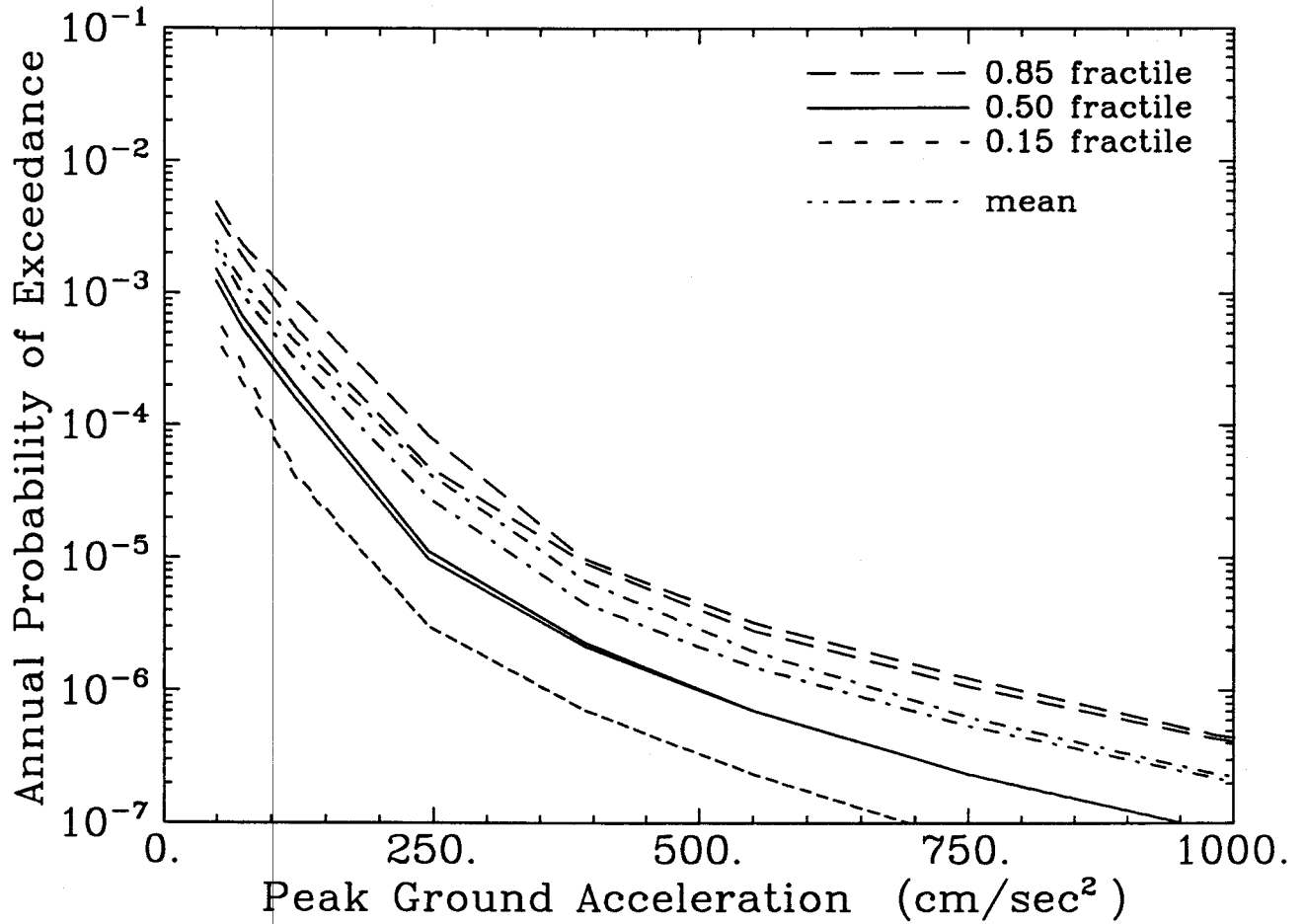


Figure 4-10. Mean and fractile hazard curves calculated for EPRI team Bechtel. Two sets of curves are shown, representing results with and without the characteristic-magnitude assumption.

SAVANNAH RIVER SITE
LAW TEAM

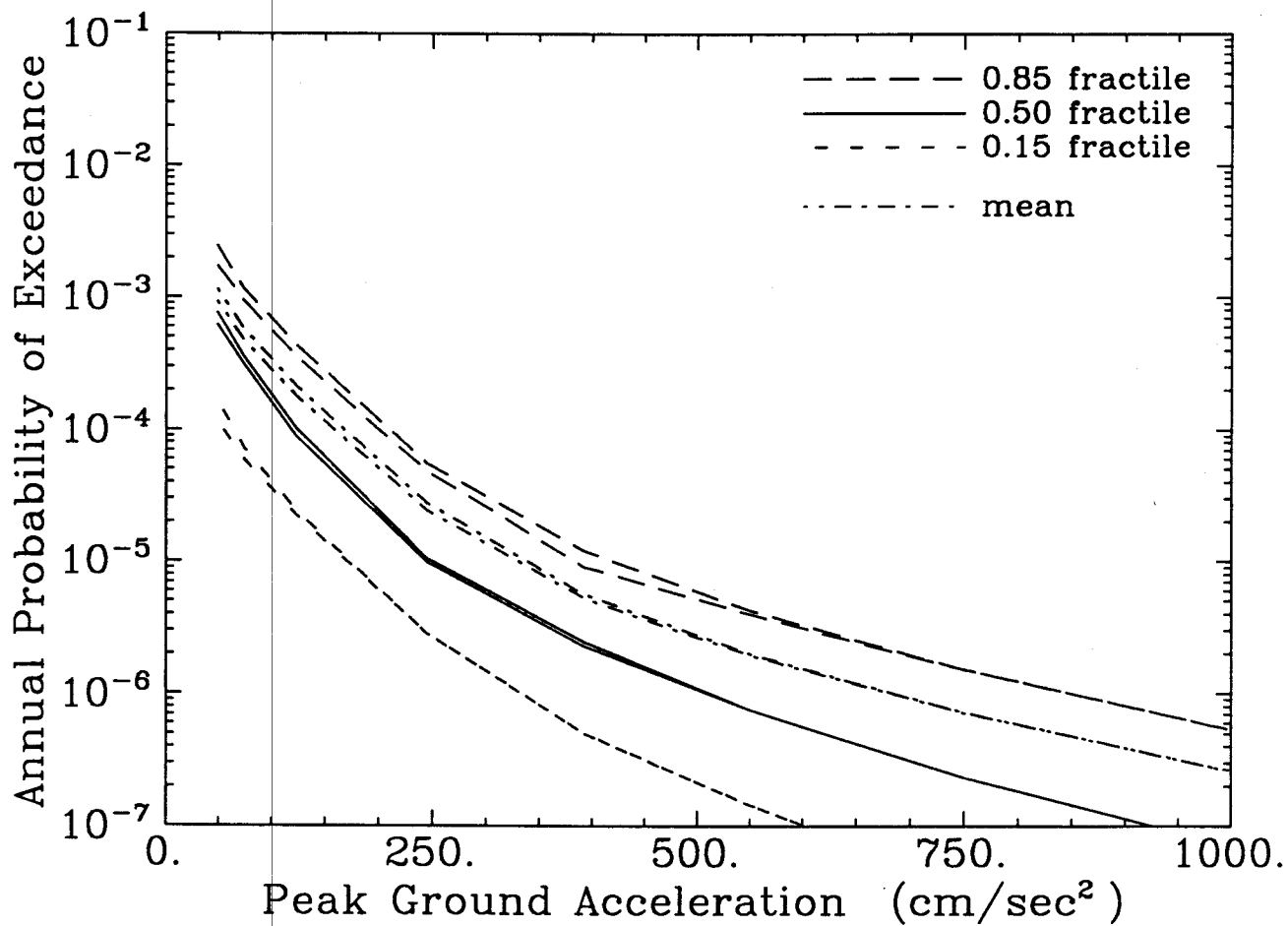


Figure 4-11. Mean and fractile hazard curves calculated for EPRI team Law. Two sets of curves are shown, representing results with and without the characteristic-magnitude assumption.

SAVANNAH RIVER SITE
 RONDOUT TEAM

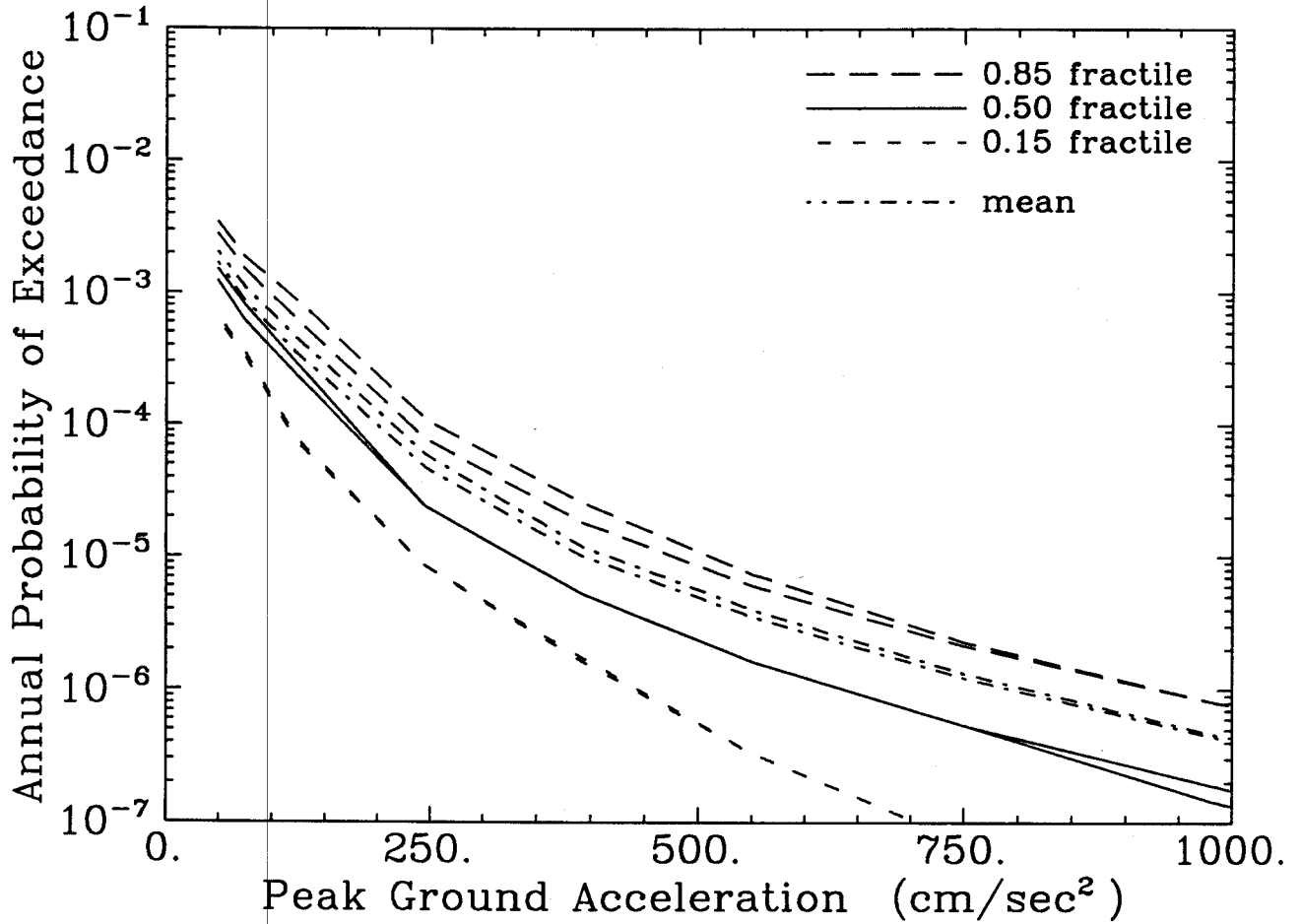


Figure 4-12. Mean and fractile hazard curves calculated for EPRI team Rondout. Two sets of curves are shown, representing results with and without the characteristic-magnitude assumption.

SAVANNAH RIVER SITE
WESTON TEAM

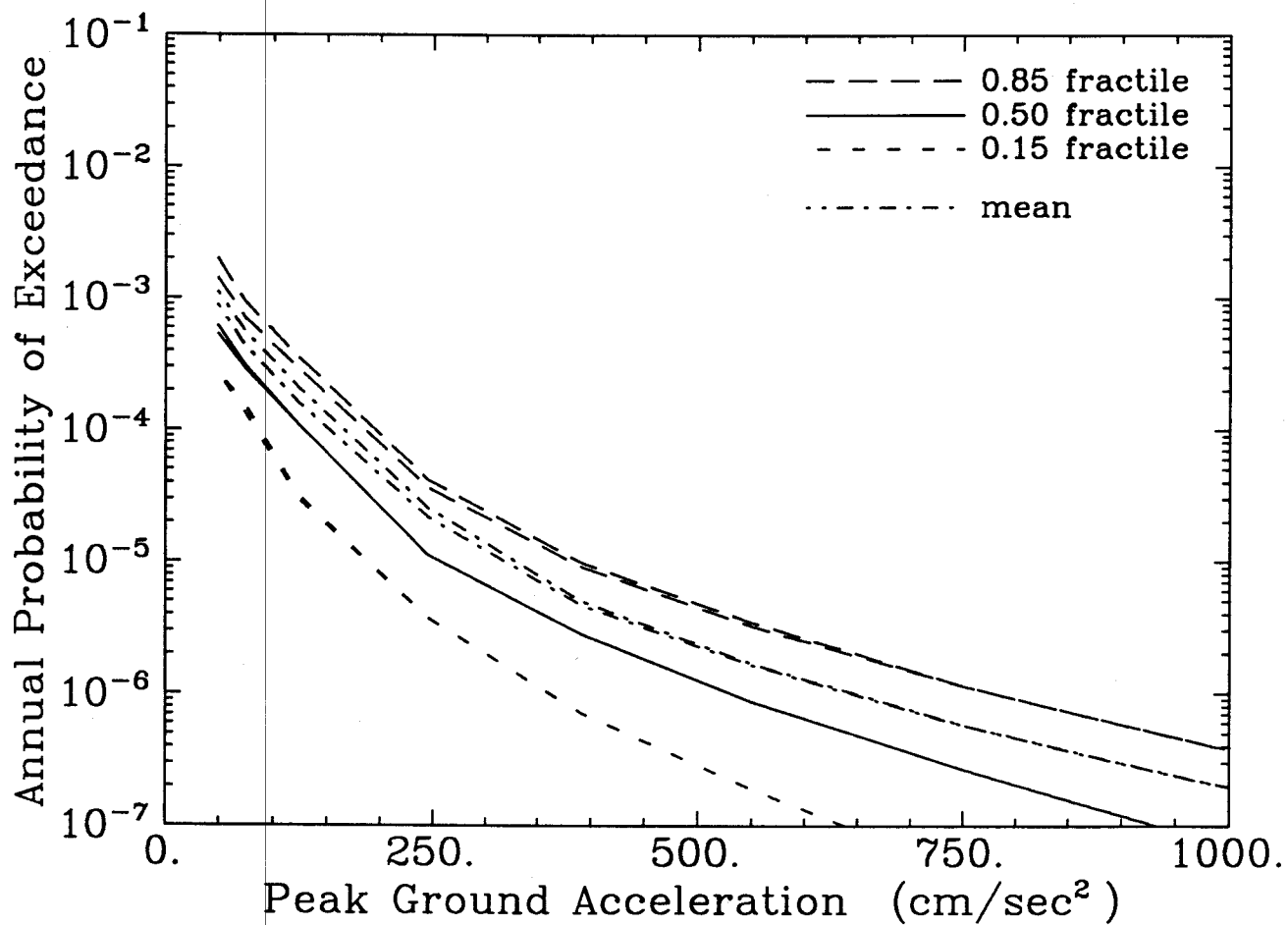


Figure 4-13. Mean and fractile hazard curves calculated for EPRI team Weston. Two sets of curves are shown, representing results with and without the characteristic-magnitude assumption.

SAVANNAH RIVER SITE
WOODWARD-CLYDE TEAM

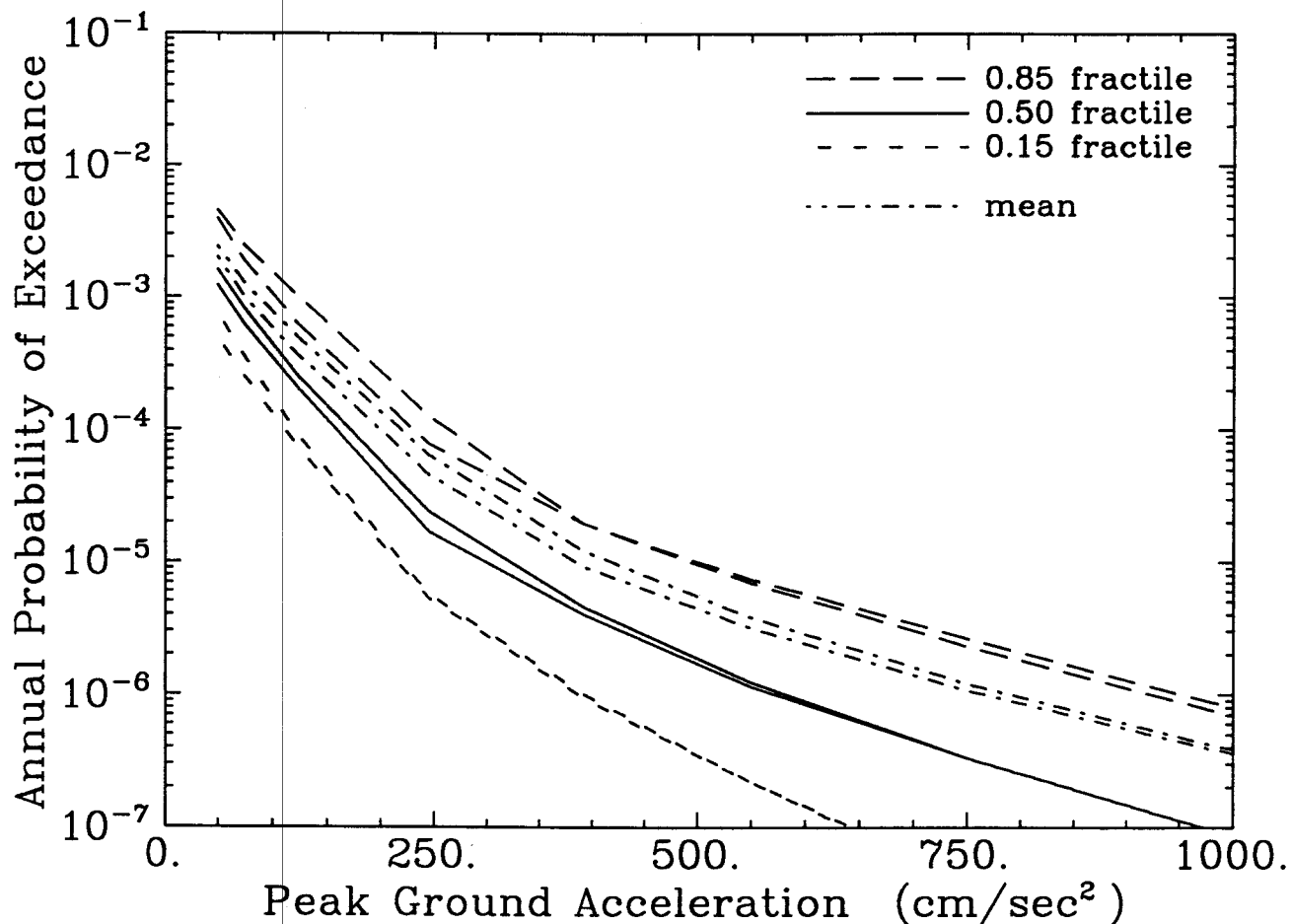


Figure 4-14. Mean and fractile hazard curves calculated for EPRI team Woodward-Clyde. Two sets of curves are shown, representing results with and without the characteristic-magnitude assumption.

SAVANNAH RIVER SITE
 EPRI RESULTS (5 TEAMS)

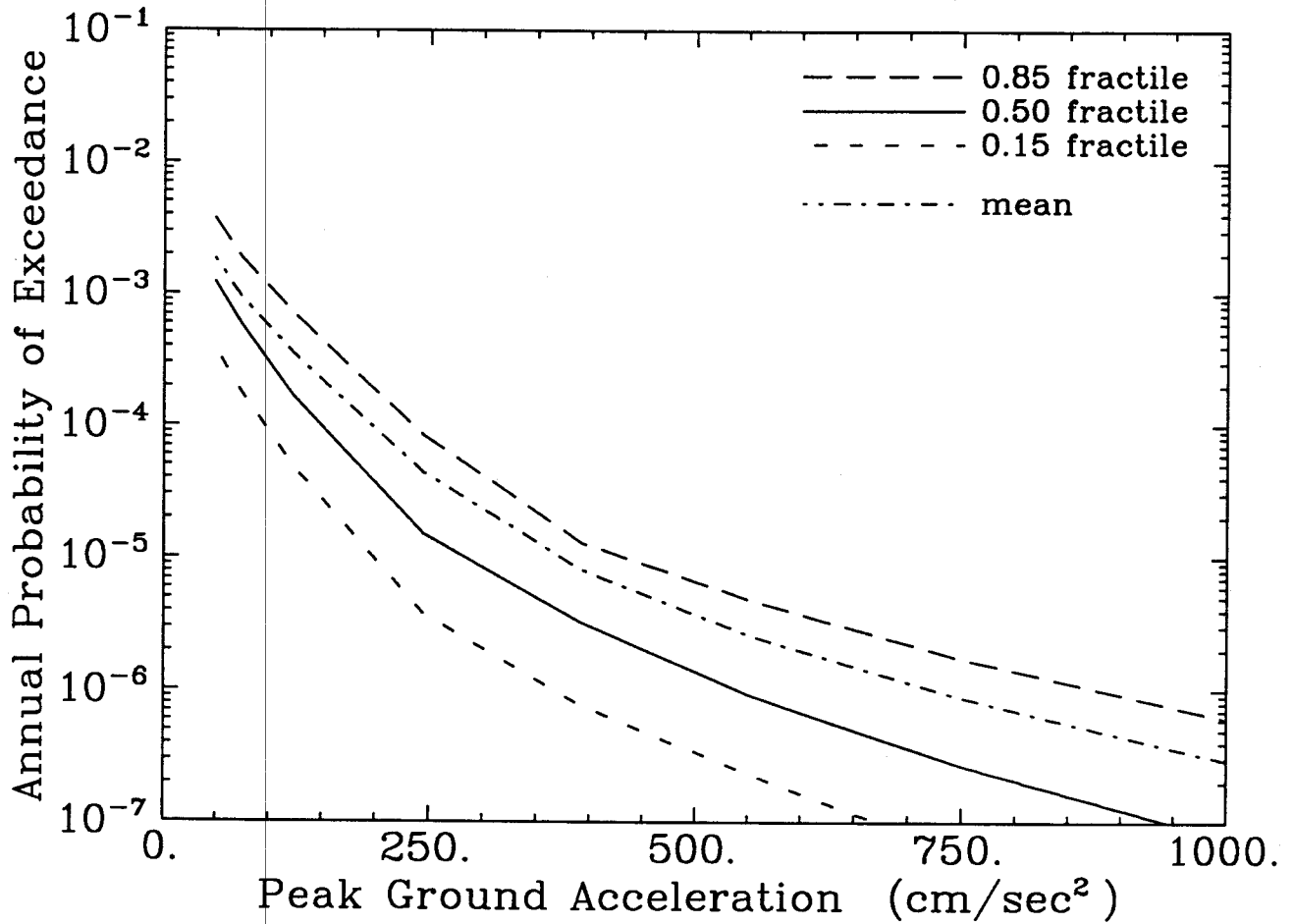


Figure 4-15. Mean and fractile hazard curves calculated by combining results from the EPRI teams, using the weights in Table 2-1.

SAVANNAH RIVER SITE
 COMBINED LLNL AND EPRI RESULTS

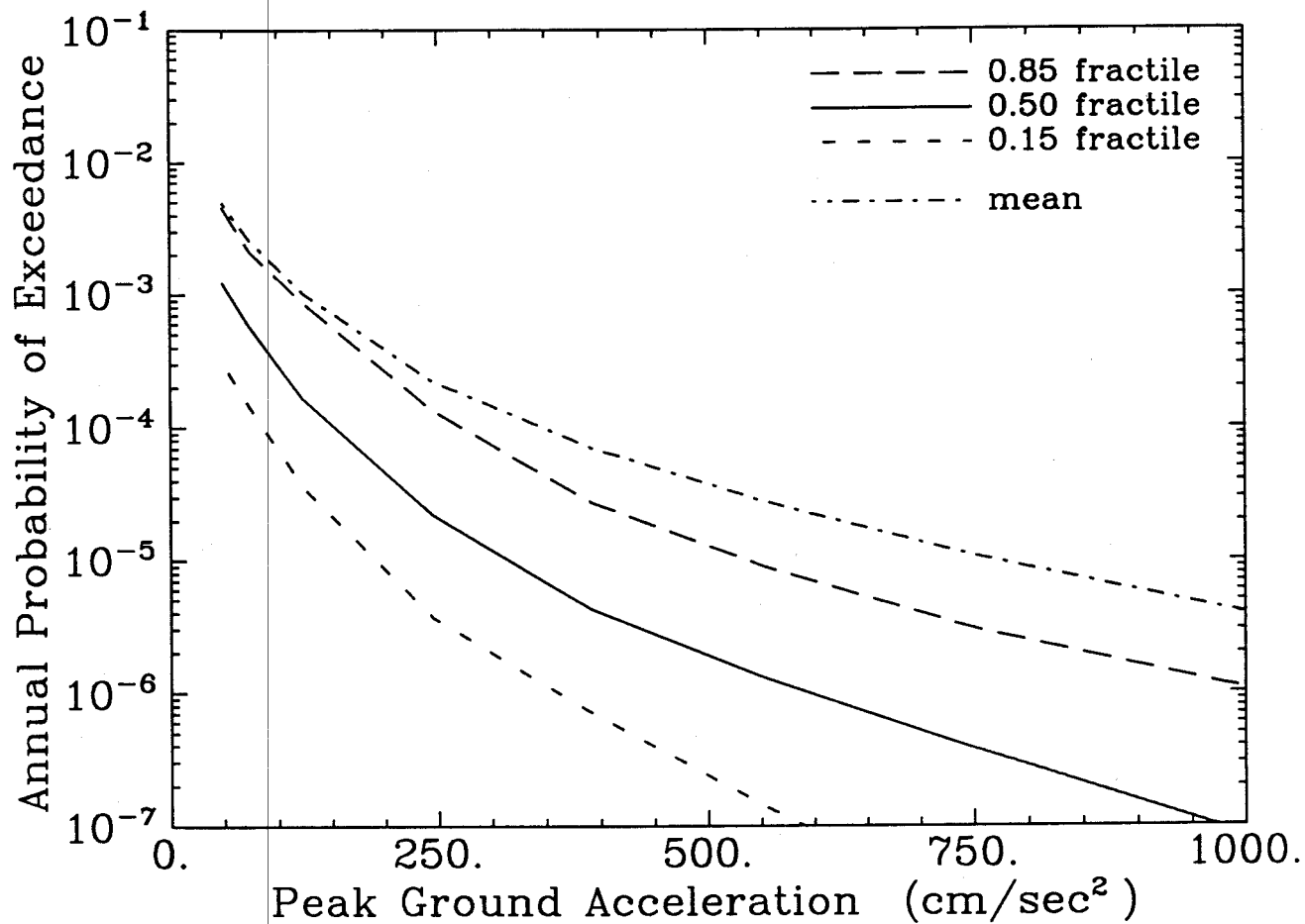


Figure 4-16. Mean and fractile hazard curves calculated by combining results from the LLNL experts and the EPRI teams, using the weights in Table 2-1.

SAVANNAH RIVER SITE
COMBINED LLNL AND EPRI RESULTS

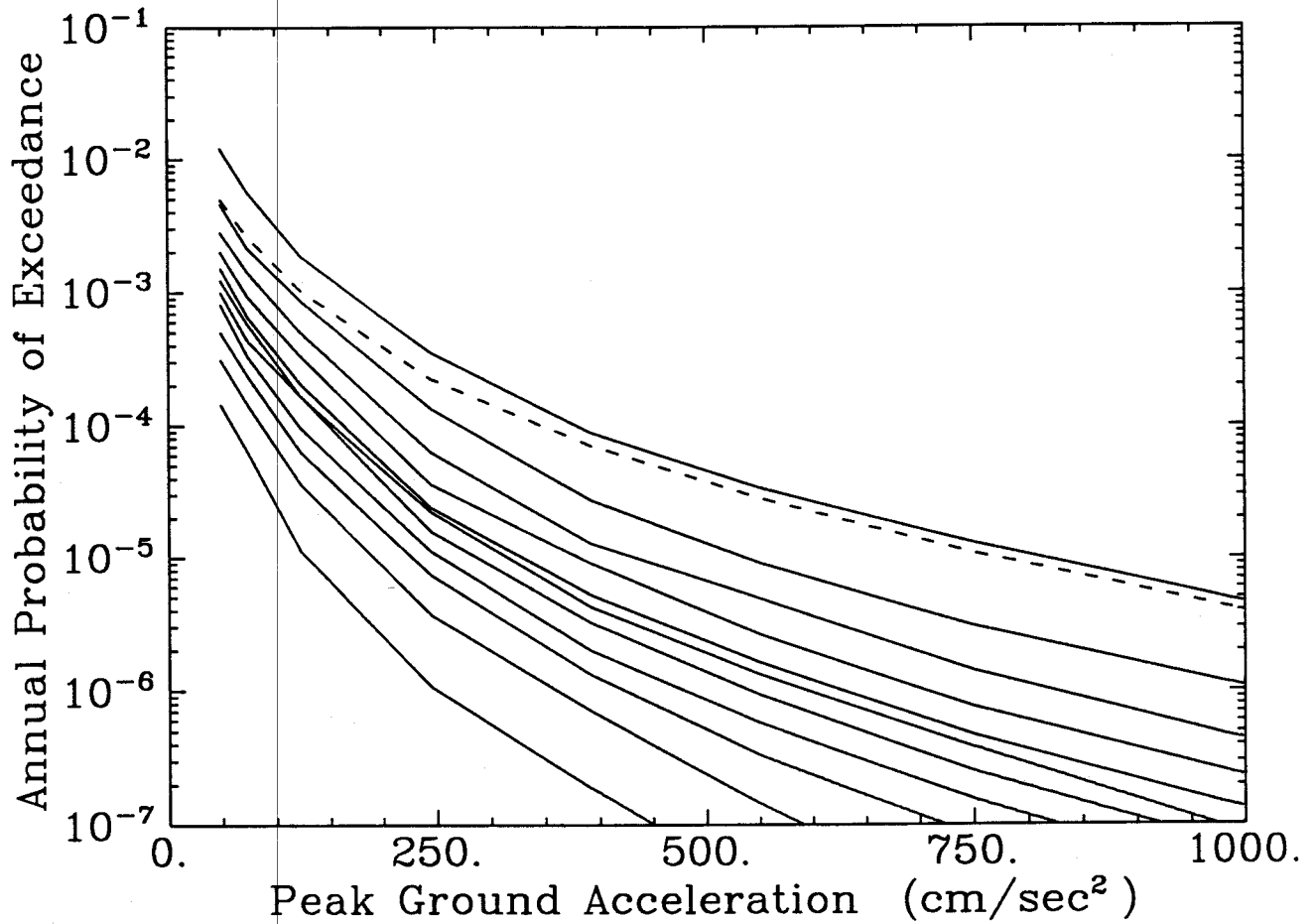


Figure 4-17. Mean and fractile hazard curves calculated by combining results from the LLNL experts and the EPRI teams—additional fractiles shown. The dashed line represents the mean hazard curve. The solid lines represent fractiles as follows: 0.05 (bottom), 0.15, 0.25, 0.35, 0.45, 0.50, 0.55, 0.65, 0.75, 0.85, 0.95 (top).

SAVANNAH RIVER SITE
HAZARD USING LLNL EXPERTS 1 3 10 AND 12

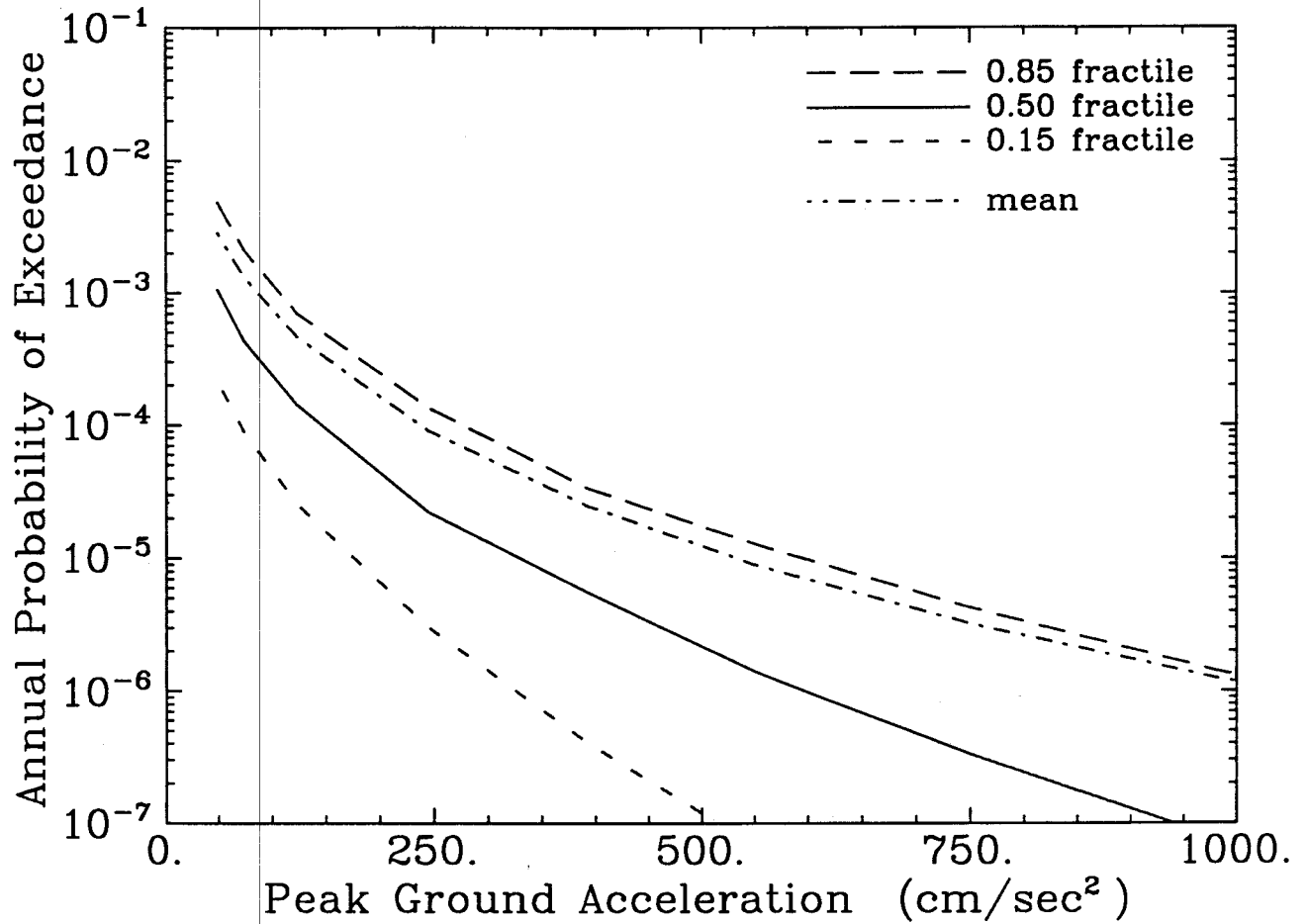


Figure 4-18. Mean and fractile hazard curves calculated by combining results from LLNL seismicity experts 1, 3, 10, and 12.

SAVANNAH RIVER SITE
COMBINED LLNL(1,3,10,12) AND EPRI RESULTS

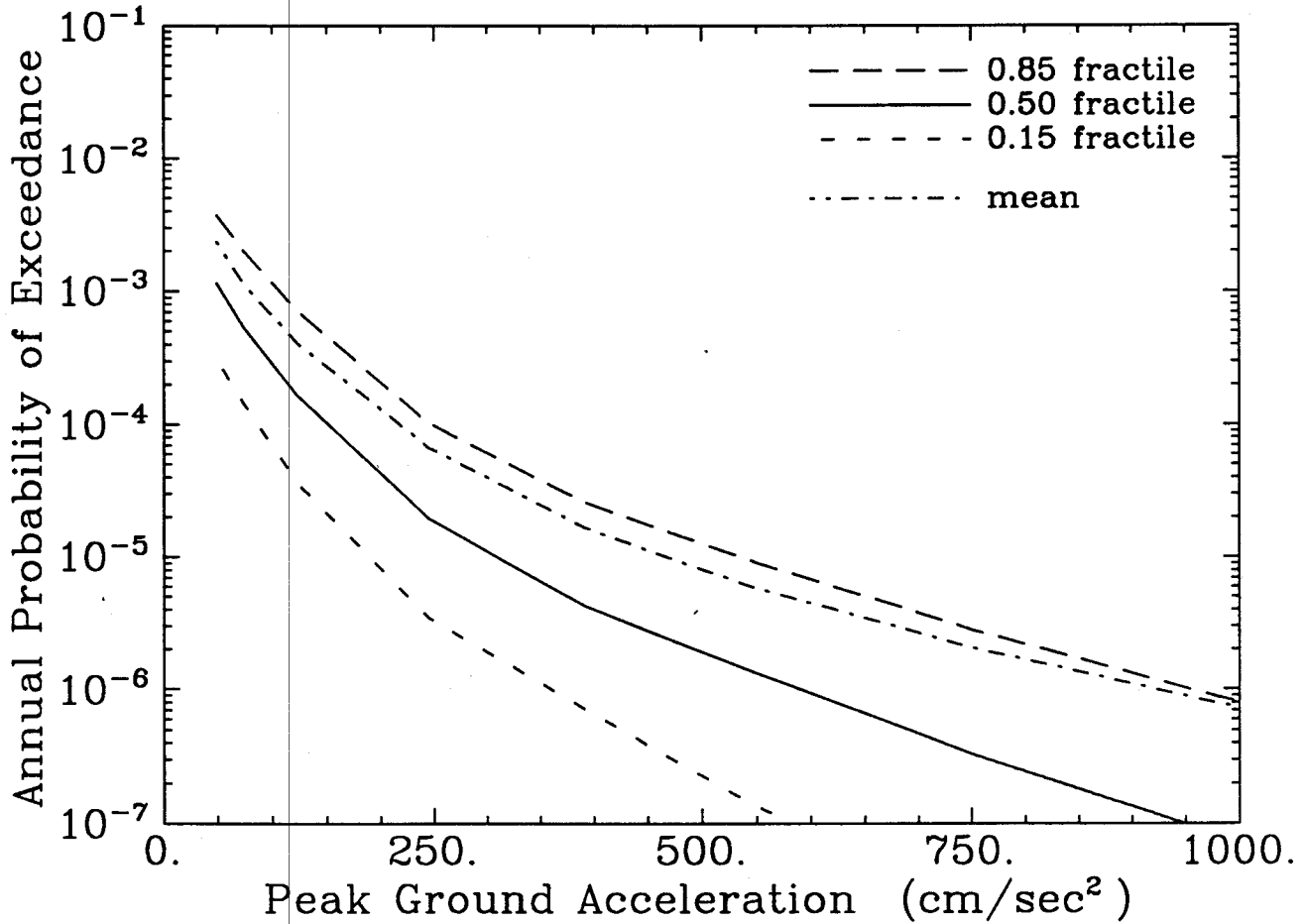


Figure 4-19. Mean and fractile hazard curves calculated by combining results from LLNL (experts 1, 3, 10, and 12) and the EPRI teams. Each LLNL expert gets a weight of 1/8; each EPRI team gets a weight of 1/10.

SAVANNAH RIVER SITE
COMBINED LLNL(1,3,10,12) AND EPRI RESULTS

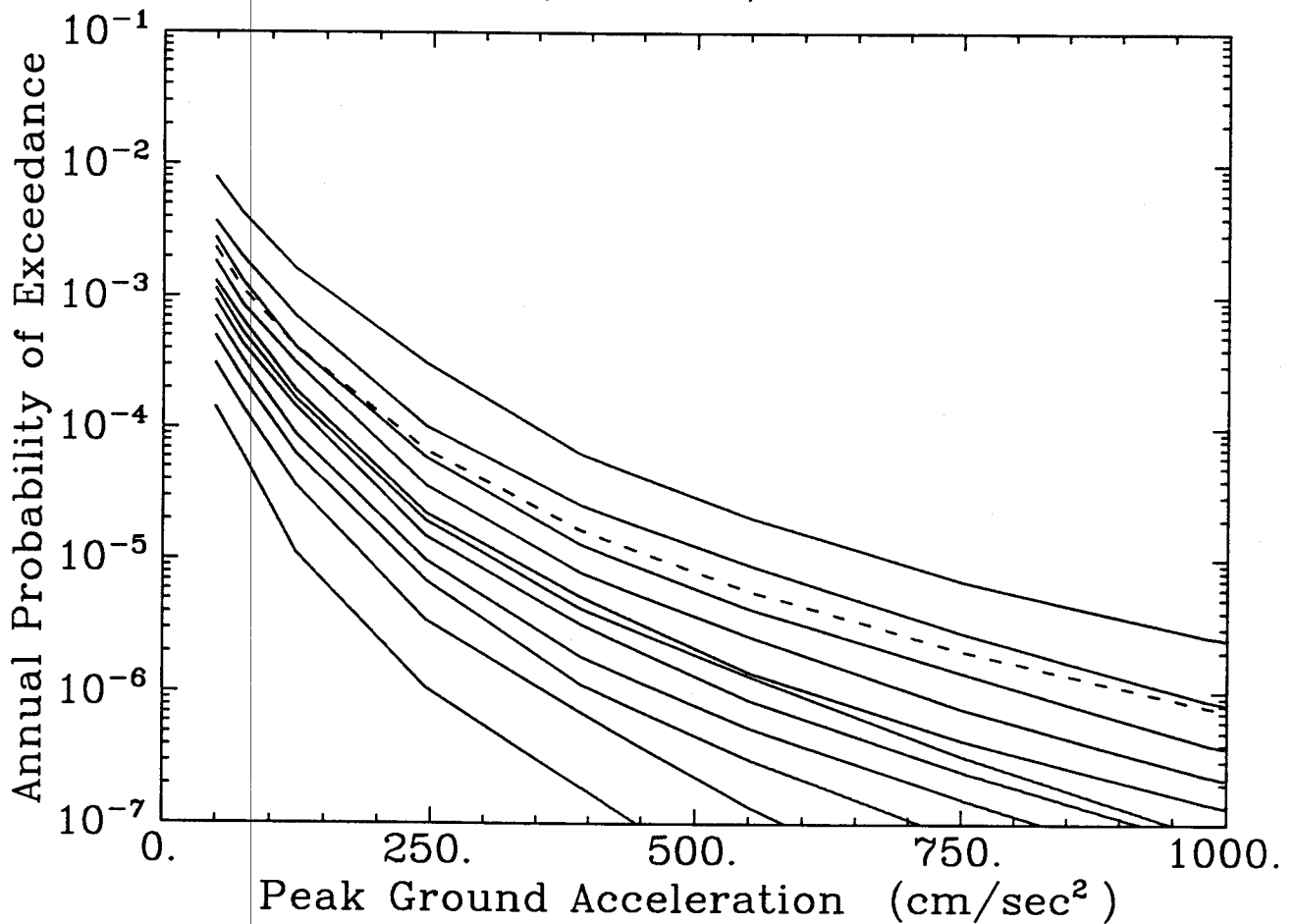


Figure 4-20. Mean and fractile hazard curves calculated by combining results from LLNL (experts 1, 3, 10, and 12) and the EPRI teams—additional fractiles shown. Each LLNL expert gets a weight of 1/8; each EPRI team gets a weight of 1/10. The dashed line represents the mean hazard curve. The solid lines represent fractiles as follows: 0.05 (bottom), 0.15, 0.25, 0.35, 0.45, 0.50, 0.55, 0.65, 0.75, 0.85, 0.95 (top).

Section 5

SUMMARY AND CONCLUSIONS

This study has obtained a combined LLNL-EPRI estimate of the seismic hazard at the SRS using those interpretations from the two studies specified by the project scope. The exclusion of two LLNL seismicity experts and one EPRI seismicity team is based on the poor agreement of their seismicity parameters with observed historic seismicity in the region. The exclusion of one LLNL ground-motion expert is based the poor agreement of his predictions with accelerograph and seismograph records from eastern North America and on the theoretically limitations of his methodology. These exclusion are justified, and they result in a significant decrease in uncertainty in seismic hazard at the SRS.

This study also assumes that earthquakes in the Charleston seismic source follow a characteristic magnitude-frequency law. The parameters of the characteristic portion are based on paleoseismic evidence. For all LLNL experts and EPRI teams, the effect of the characteristic-magnitude assumption is small. This effect would have been even smaller had we assumed that characteristic earthquakes have more regular inter-arrival times.

Results from the LLNL and EPRI inputs showed good agreement in the median hazard curve, but differences remained in the uncertainties inherent in the two studies, and in the mean and 85% fractile curves. As a result of these remaining differences, an investigation of the causes of the large uncertainties in the LLNL results was undertaken. The range of seismicity parameter values specified by many of the LLNL S-experts was large, in some cases unrealistically large, showing (in one extreme case) a possible recurrence interval of one event with $m_b > 5.0$ in the Charleston region every 77 days. Details of this comparison are given in Appendix A. Excluding four of the LLNL S-experts because of these unrealistically-large ranges of parameter values, and conducting a modified LLNL analysis, leads to results that are very quite consistent, in the medians, means, and 85% fractiles, with results from the EPRI analysis.

From these considerations, the combined seismic hazard curves using the modified LLNL results are recommended (Figures 4-19 and 4-20). These combined seismic-hazard curves constitute a solid basis for decisions related to seismic safety.

Appendix A
EVALUATION OF UNCERTAINTIES

The base case results produced by this study are presented in Section 4. These results show median results for the modified LLNL and EPRI analyses that are quite similar, but still indicate larger uncertainties and mean values for the modified LLNL results than are obtained from the EPRI results (see Figures 4-9 and 4-15).

In the interest of understanding what causes these remaining uncertainties, we have examined the seismicity assumptions for the eight LLNL S-experts. In particular, the ranges of activity rates and b-values specified by the experts were of concern. By way of background information, the LLNL experts were asked to specify best estimates, lower bounds, and upper bounds for the activity rates and b-values for each source, and were asked to designate any statistical correlation between these two parameters (most experts specified no correlation). For comparison purposes, these activity rates and b-values (and their ranges of uncertainty) can be used to calculate uncertainty in rate of occurrence of earthquakes above a certain magnitude.

Table A-1 presents the recurrence intervals for $m_b > 5.0$ that are obtained from the distributions of activity rates and b-values specified by each of the eight LLNL S-experts included in the present study. Figures A-1 through A-8 present the corresponding magnitude-recurrence relations and their uncertainty. It is apparent that the uncertainty bands from some of the LLNL S-experts are so wide as to lack credibility. For example, the range of recurrence intervals for $m_b > 5.0$ specified by expert 7 for his zone 10 ranges from 0.21 years (one event every 77 days) to 563 years. The ranges for experts 11 and 13 are similarly broad. Although these ranges represent extremes of the interpretations, they are possible ranges allowed by the methodology; recurrence intervals at these extreme values were used in generating the LLNL seismic hazard results.

We conclude that, although the LLNL S-experts were asked to specify their uncertainties on activity rates and b-values, there was insufficient feedback in the study to allow comparison of the resulting interpretations with data. If there were, we suspect strongly the experts would have modified their interpretations. This should be evident, for example, by comparison of

Table A-1

Range of Seismicity Interpretations from LLNL S-Experts

| Expert | Source No. | Correlation | Mean Recurrence interval for $m_b > 5.0$ (years) | | |
|--------|------------|-------------|---|---------------|-----------------|
| | | | 2.5 percentile | Best Estimate | 97.5 percentile |
| 1 | 1 and 2 | partial | 8.9 and 11 | 14 and 18 | 26 and 30 |
| 3 | 9 | none | 11 | 71 | 670 |
| 6 | 13 and 10 | full | 4.8 and 1.8 | 30.2 and 31.6 | 380 and 355 |
| 7 | 10 | none | 0.21† | 11.2 | 563 |
| 10 | 4 | none | 9.9 | 32 | 102 |
| 11 | 8 | none | 2.0 | 18 | 5120 |
| 12 | 23 | none | 55 | 347 | 2920 |
| 13 | 9 | none | 1.5 | 63 | 2840 |

†This recurrence interval corresponds to one $m_b > 5$ event every 77 days.

the rates shown in Table A-1 for experts 7 and 13 with the historical rates for Charleston presented in Section 3 (see Figures A-4 and A-8).

In regard to the other interpretations shown in Table A-1, it is unclear how recurrence intervals on the order of 10 years for $m_b > 5.0$ can be justified—either for the best estimate or for the 2.5 percentile—given that only two such earthquakes have occurred in historical times in South Carolina (see Figure 4-1 of (1)). We can only conclude again that little if any comparison of predicted and observed seismicity was made in the LLNL study. The result is a wide range of predicted seismicity and a wide range in seismic hazard, for the LLNL study.

In order to show the possible effects of these wide ranges in interpretations, we use a subset of four LLNL S-experts, excluding expert nos. 6, 7, 11, and 13. The last three are excluded because the range in their seismicity interpretations is extreme; expert 6 is excluded because this expert's interpretations lead to a recurrence interval of 4.8 or 1.8 years for $m_b > 5.0$, and the geometry of this expert's source allows events with this rate to occur at the SRS.

The resulting hazard curves for the remaining four LLNL experts are shown in Figure A-9; for this plot the curves from each expert have been weighted equally. Comparing these hazard curves with those from the five EPRI teams (Figure 4-15) shows consistency in the medians, means, and 85% fractiles (the means and 85% fractiles differ by a factor of 3.6 or

less at all ground motion levels). Figure A-10 shows the combined set of modified LLNL and EPRI hazard curves, and Figure A-11 shows the combined set for eleven fractiles plus the mean.

We conclude that the wide range of uncertainty evidenced by the LLNL hazard curves at the SRS is caused by large uncertainty in seismicity parameters specified by the LLNL S-experts, an uncertainty that is not justified by historical seismicity. Excluding a subset of interpretations from the four LLNL S-experts with the largest effect leads to results that are consistent with the EPRI results. The modified, combined set of results is recommended for use in seismic hazard decisions at the SRS.

A.1 REFERENCES

1. *Comparison and Analysis of Assumptions in LLNL and EPRI Seismic Hazard Studies for the Savannah River Site.* Report to Westinghouse Savannah River Company, Aiken, South Carolina, Risk Engineering, Inc., 1990.

SEISMICITY ASSUMPTIONS
BY LLNL EXPERT 1 (SOURCE 1)

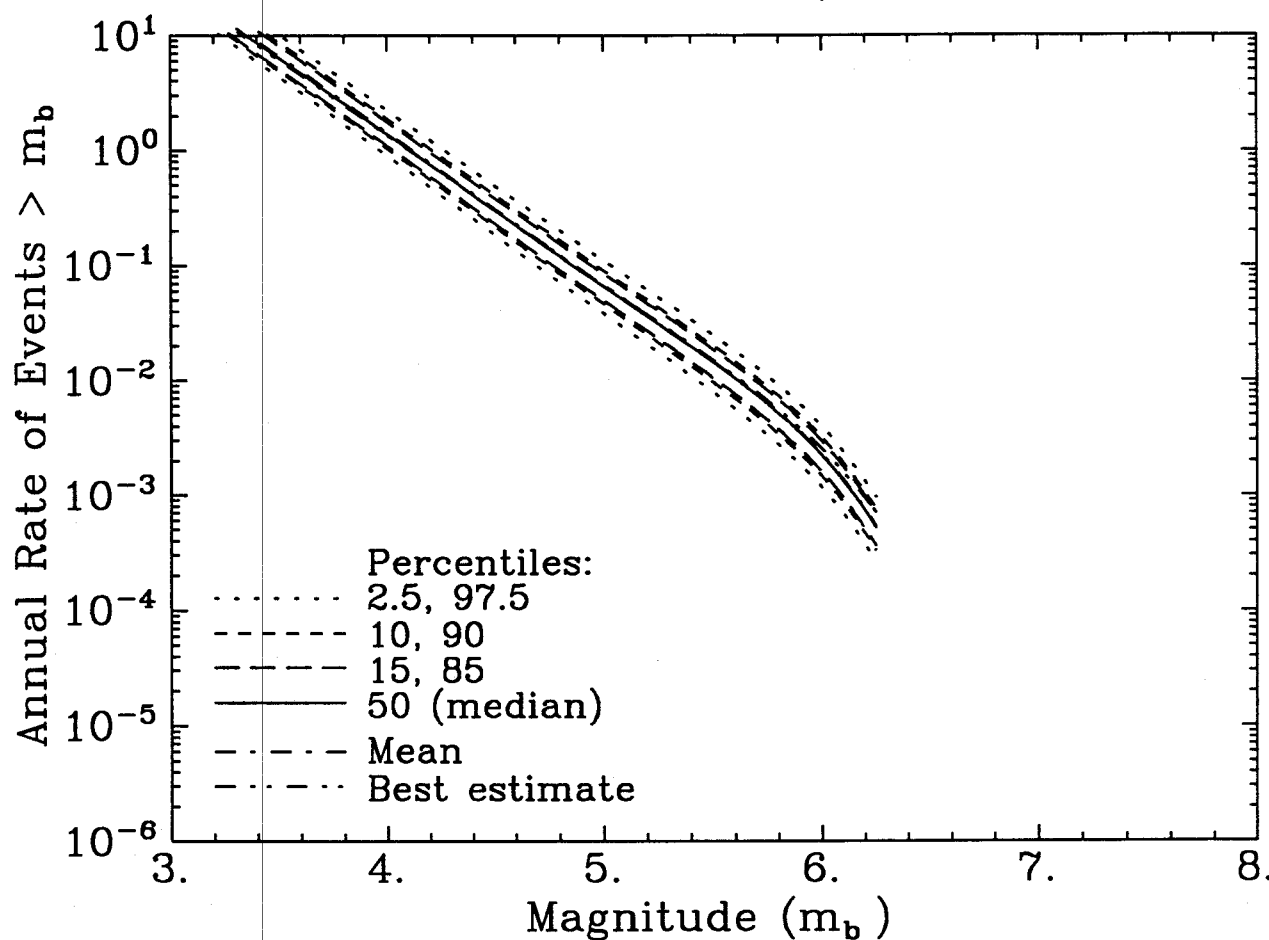


Figure A-1. Magnitude-recurrence model specified by LLNL expert 1 for seismic source 1; uncertainty is represented by the spread among fractile curves.

SEISMICITY ASSUMPTIONS
 BY LLNL EXPERT 3 (SOURCE 9)
 AND CHARLESTON SEISMICITY RATES

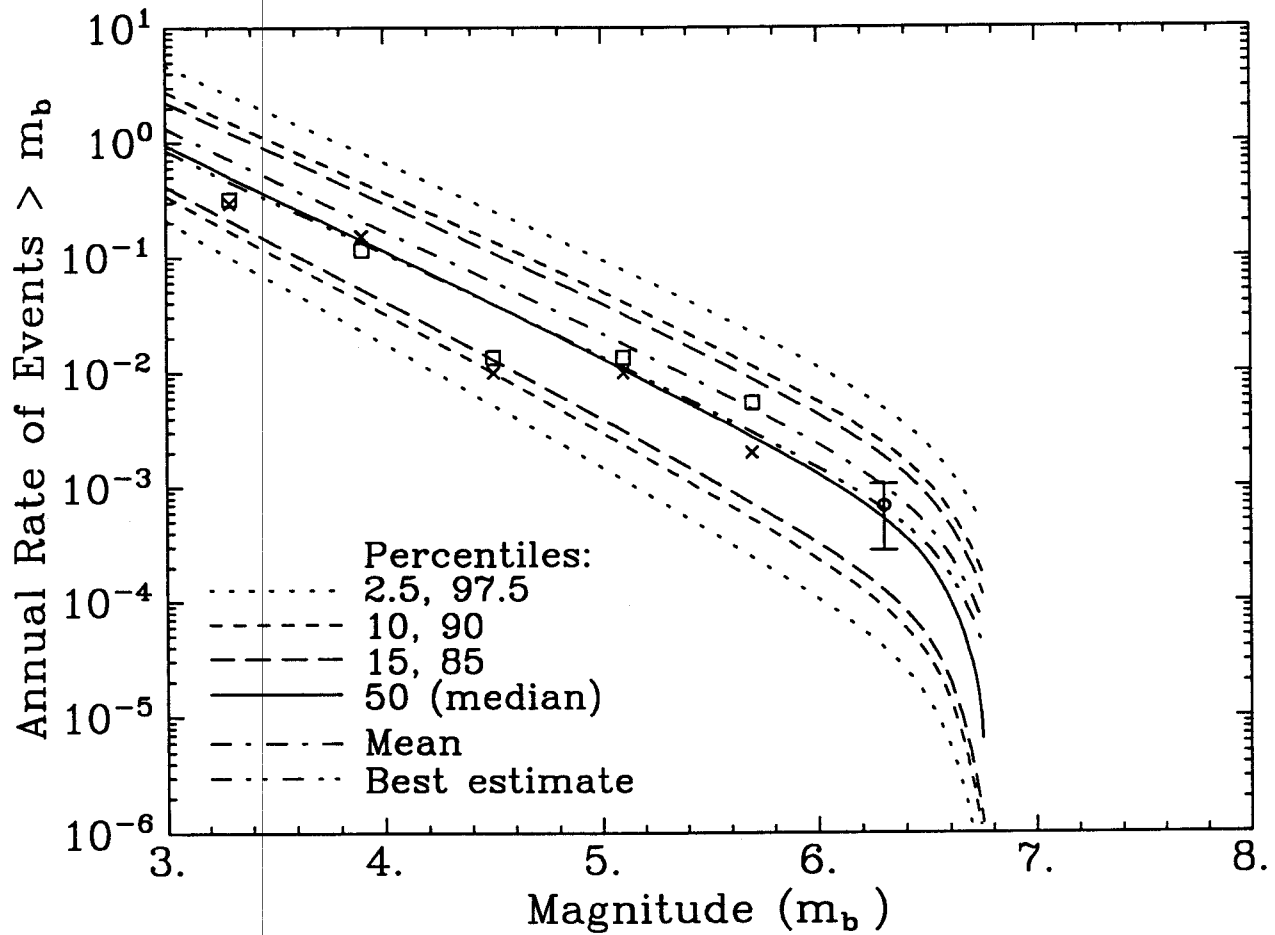


Figure A-2. Magnitude-recurrence model specified by LLNL expert 3 for seismic source 9; uncertainty is represented by the spread among fractile curves. Also shown are the activity rates in the Charleston region, as obtained from historical seismicity and from paleoseismicity studies. The \square and \times symbols represent observed seismicity in the Charleston area under two assumptions of completeness [see (1)]. The circle and error bar represent the rate of Charleston-size earthquakes and its 1σ bounds.

SEISMICITY ASSUMPTIONS
 BY LLNL EXPERT 6 (SOURCE 13)
 AND CHARLESTON SEISMICITY RATES

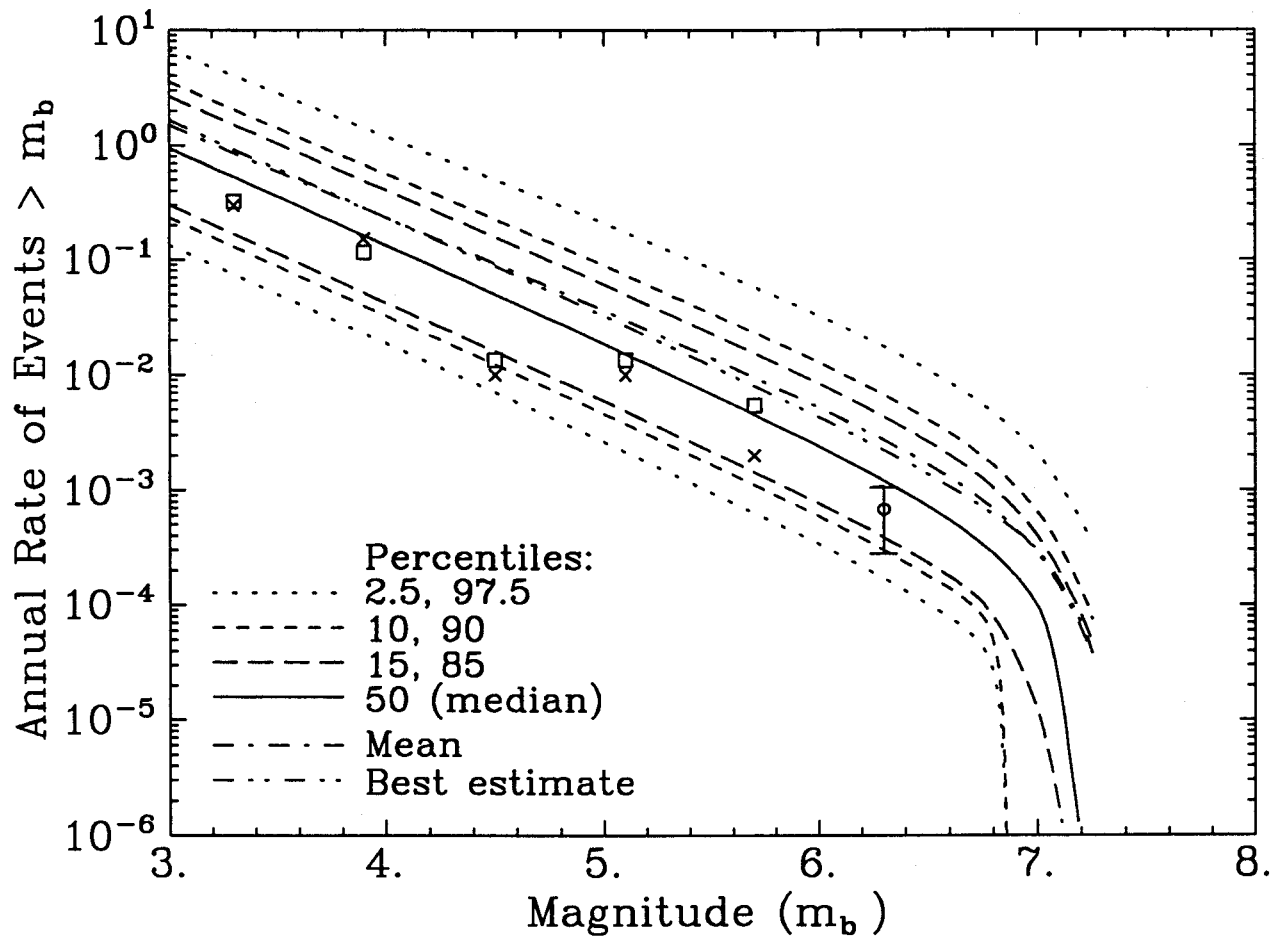


Figure A-3. Magnitude-recurrence model specified by LLNL expert 6 for seismic source 13; uncertainty is represented by the spread among fractile curves. Also shown are the activity rates in the Charleston region, as obtained from historical seismicity and from paleoseismicity studies. The \square and \times symbols represent observed seismicity in the Charleston area under two assumptions of completeness [see (1)]. The circle and error bar represent the rate of Charleston-size earthquakes and its 1σ bounds.

SEISMICITY ASSUMPTIONS
 BY LLNL EXPERT 7 (SOURCE 10)
 AND CHARLESTON SEISMICITY RATES

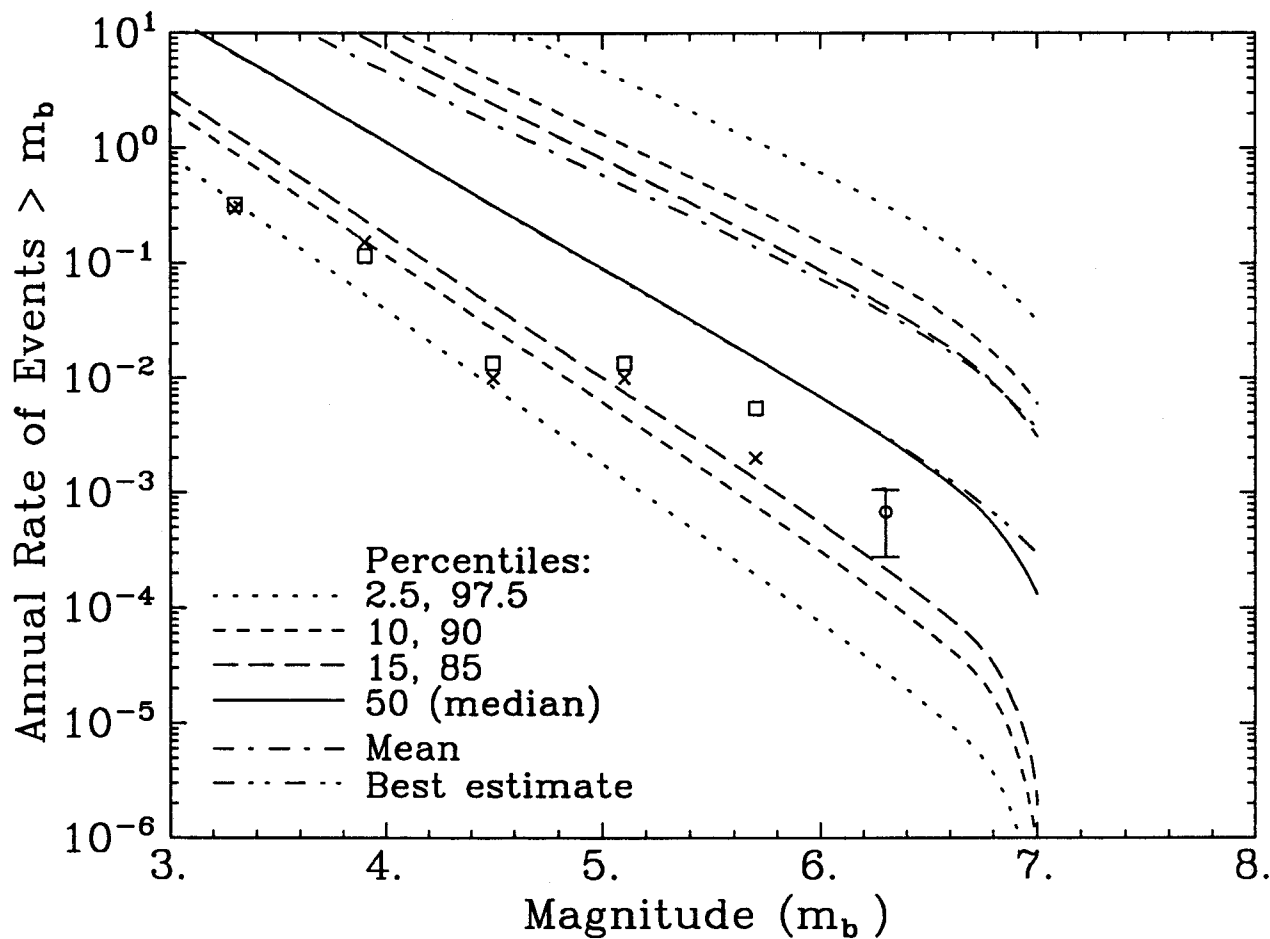


Figure A-4. Magnitude-recurrence model specified by LLNL expert 7 for seismic source 10; uncertainty is represented by the spread among fractile curves. Also shown are the activity rates in the Charleston region, as obtained from historical seismicity and from paleo-seismicity studies. The □ and × symbols represent observed seismicity in the Charleston area under two assumptions of completeness [see (1)]. The circle and error bar represent the rate of Charleston-size earthquakes and its 1σ bounds.

SEISMICITY ASSUMPTIONS
BY LLNL EXPERT 10 (SOURCE 4)

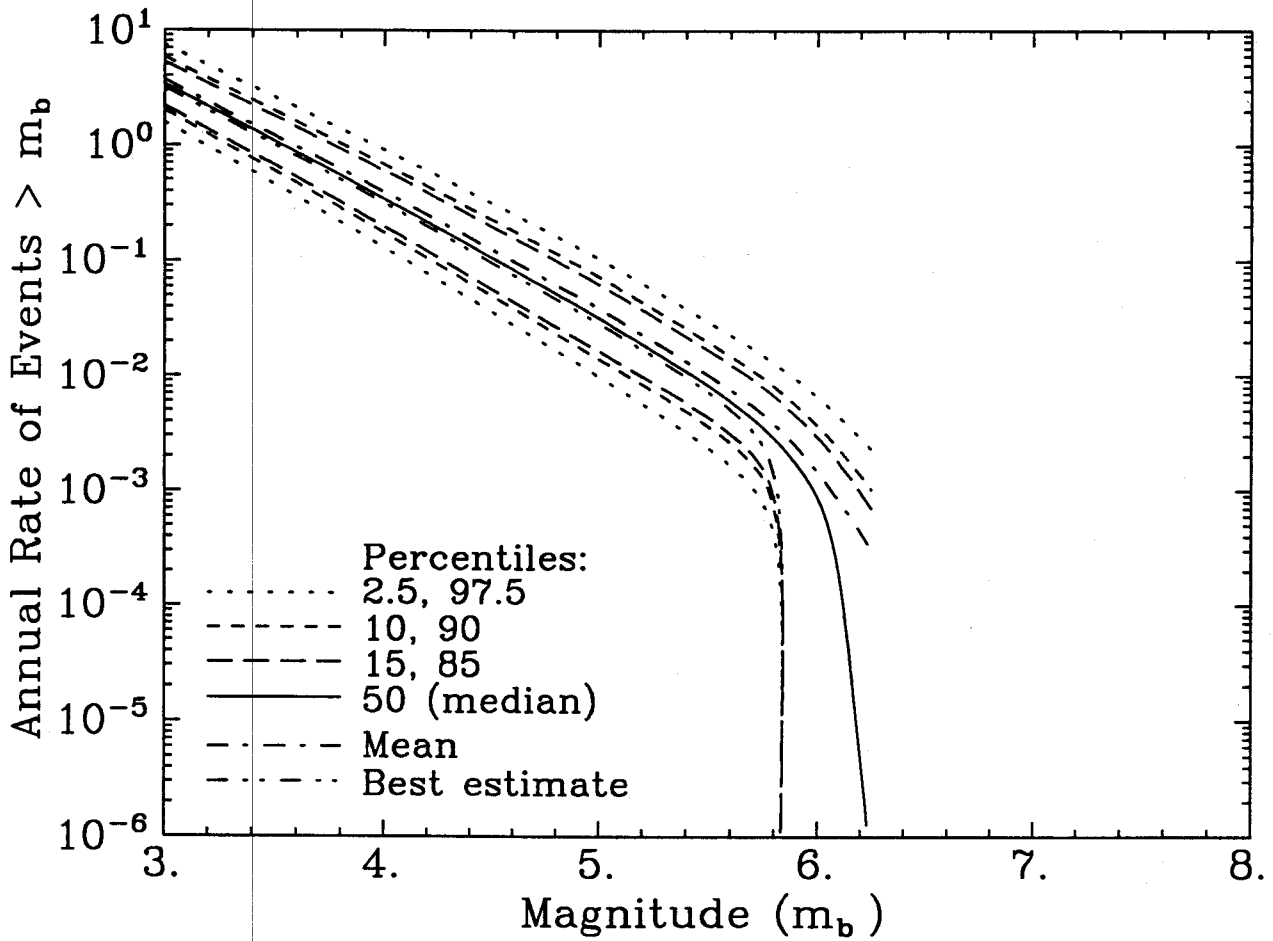


Figure A-5. Magnitude-recurrence model specified by LLNL expert 10 for seismic source 4; uncertainty is represented by the spread among fractile curves.

SEISMICITY ASSUMPTIONS
 BY LLNL EXPERT 11 (SOURCE 8)
 AND CHARLESTON SEISMICITY RATES

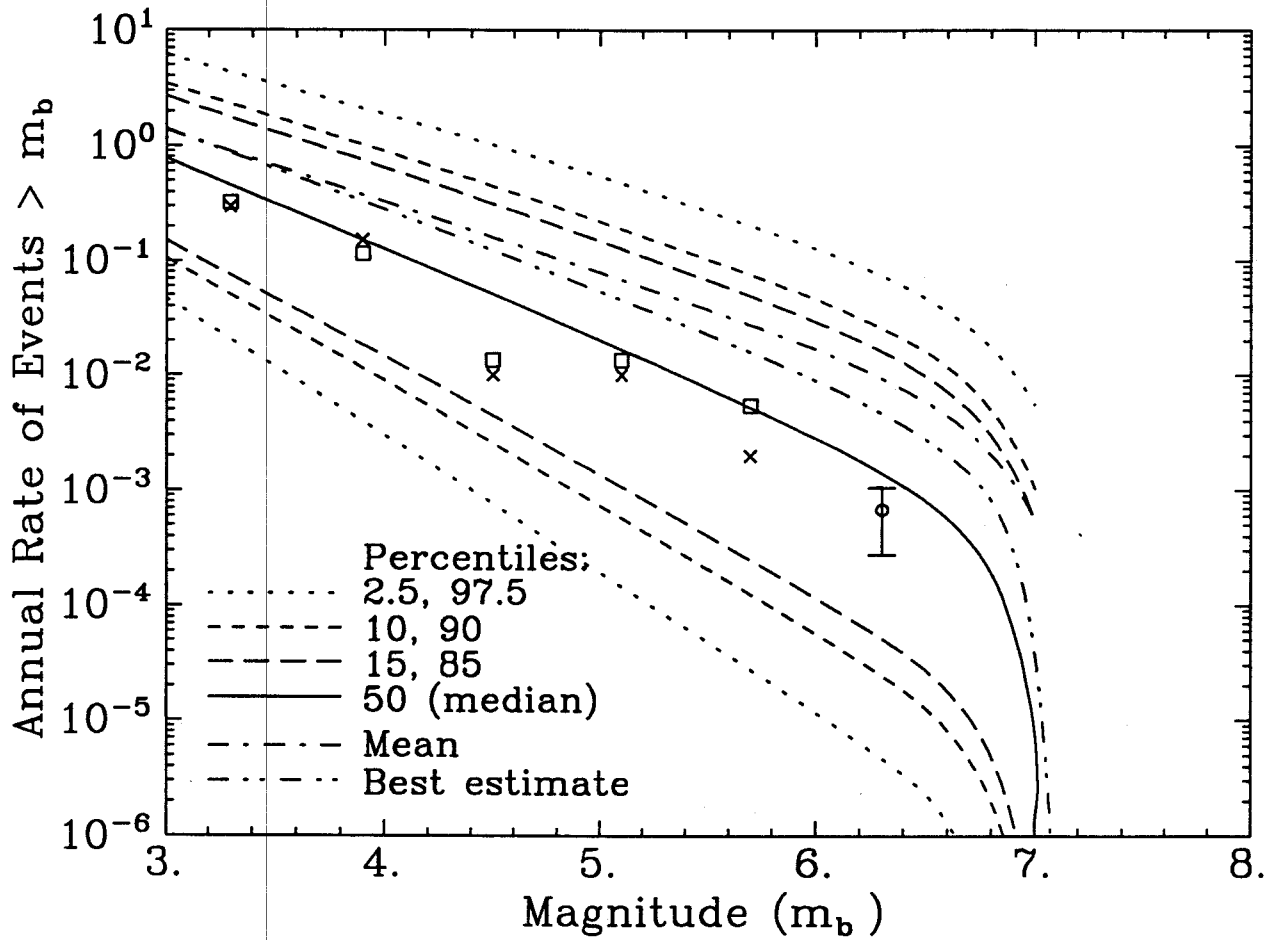


Figure A-6. Magnitude-recurrence model specified by LLNL expert 11 for seismic source 8; uncertainty is represented by the spread among fractile curves. Also shown are the activity rates in the Charleston region, as obtained from historical seismicity and from paleoseismicity studies. The \square and \times symbols represent observed seismicity in the Charleston area under two assumptions of completeness [see (1)]. The circle and error bar represent the rate of Charleston-size earthquakes and its 1σ bounds.

SEISMICITY ASSUMPTIONS
BY LLNL EXPERT 12 (SOURCE 23)

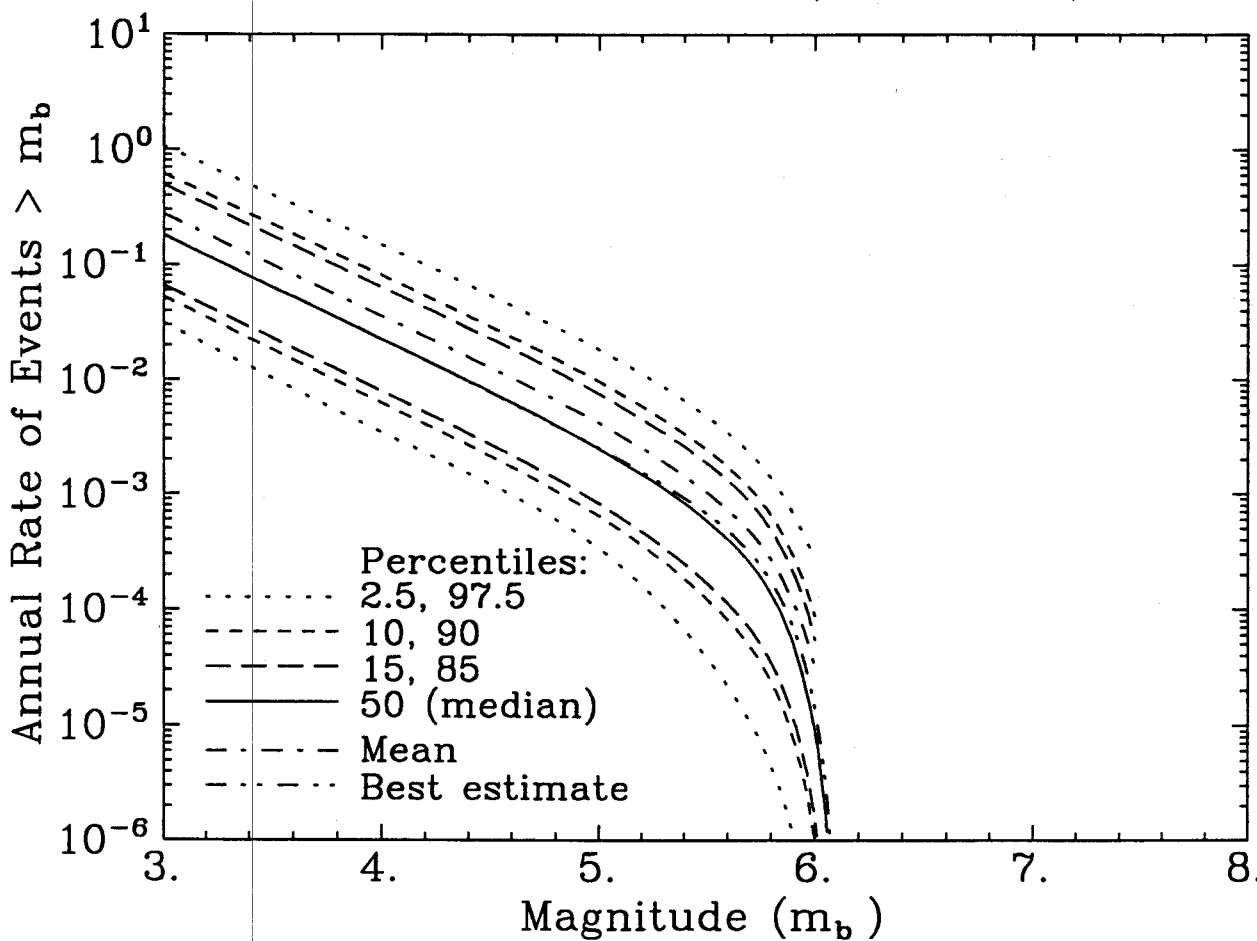


Figure A-7. Magnitude-recurrence model specified by LLNL expert 12 for seismic source 23; uncertainty is represented by the spread among fractile curves.

SEISMICITY ASSUMPTIONS
 BY LLNL EXPERT 13 (SOURCE 9)
 AND CHARLESTON SEISMICITY RATES

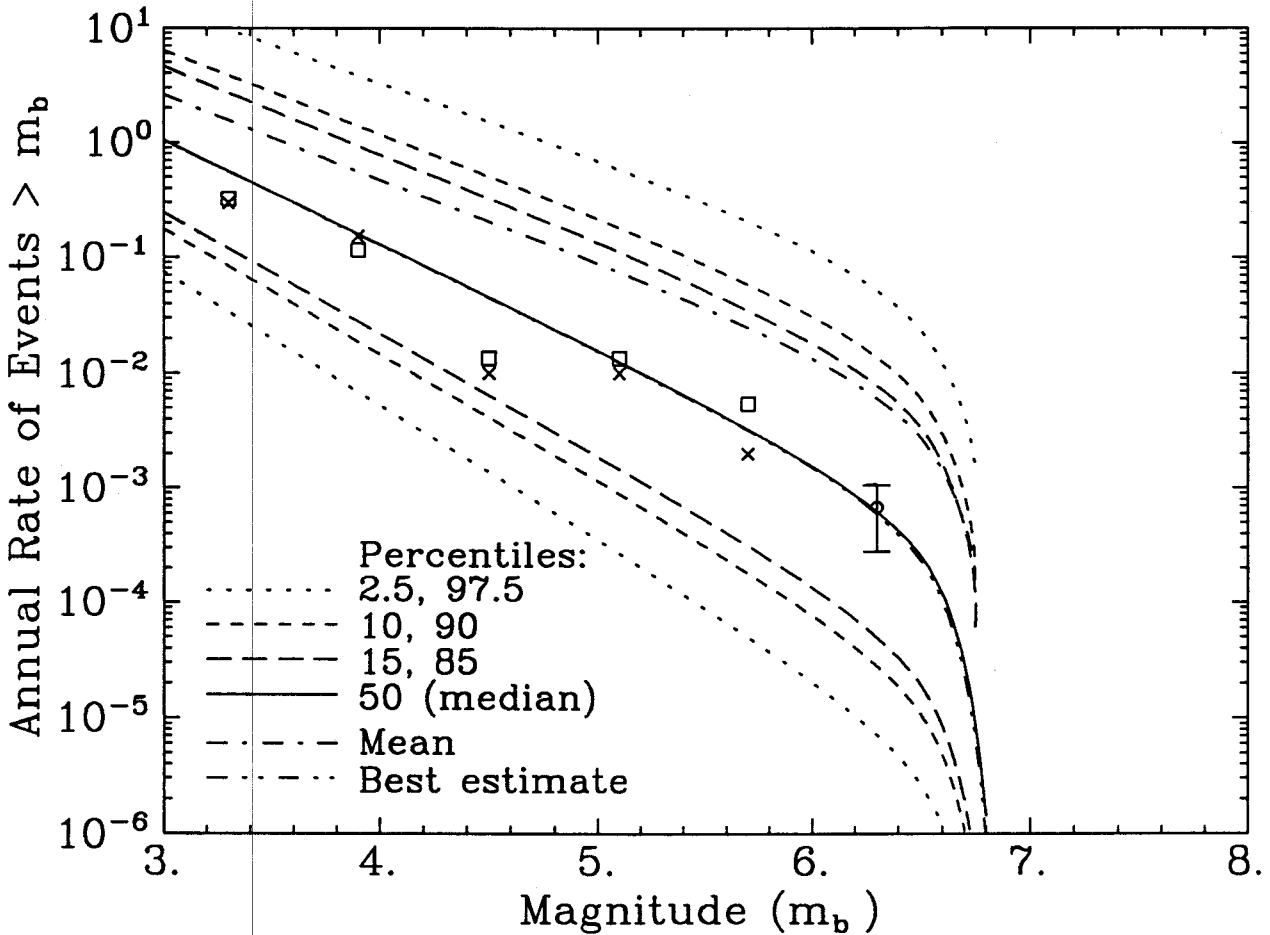


Figure A-8. Magnitude-recurrence model specified by LLNL expert 13 for seismic source 9; uncertainty is represented by the spread among fractile curves. Also shown are the activity rates in the Charleston region, as obtained from historical seismicity and from paleo-seismicity studies. The \square and \times symbols represent observed seismicity in the Charleston area under two assumptions of completeness [see (1)]. The circle and error bar represent the rate of Charleston-size earthquakes and its 1σ bounds.

SAVANNAH RIVER SITE
HAZARD USING LLNL EXPERTS 1 3 10 AND 12

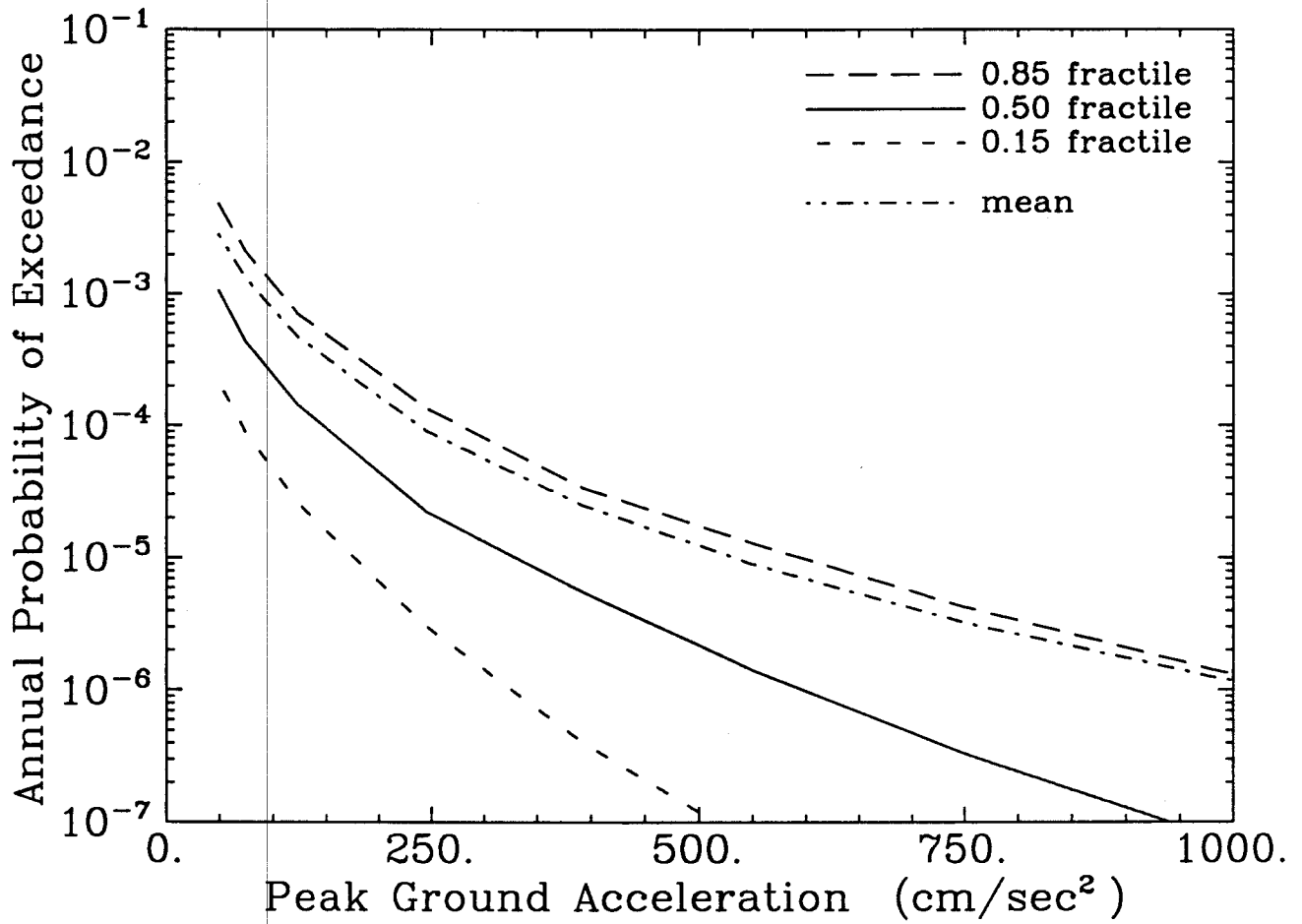


Figure A-9. Mean and fractile hazard curves calculated by combining results from LLNL seismicity experts 1, 3, 10, and 12.

SAVANNAH RIVER SITE
 COMBINED LLNL(1,3,10,12) AND EPRI RESULTS

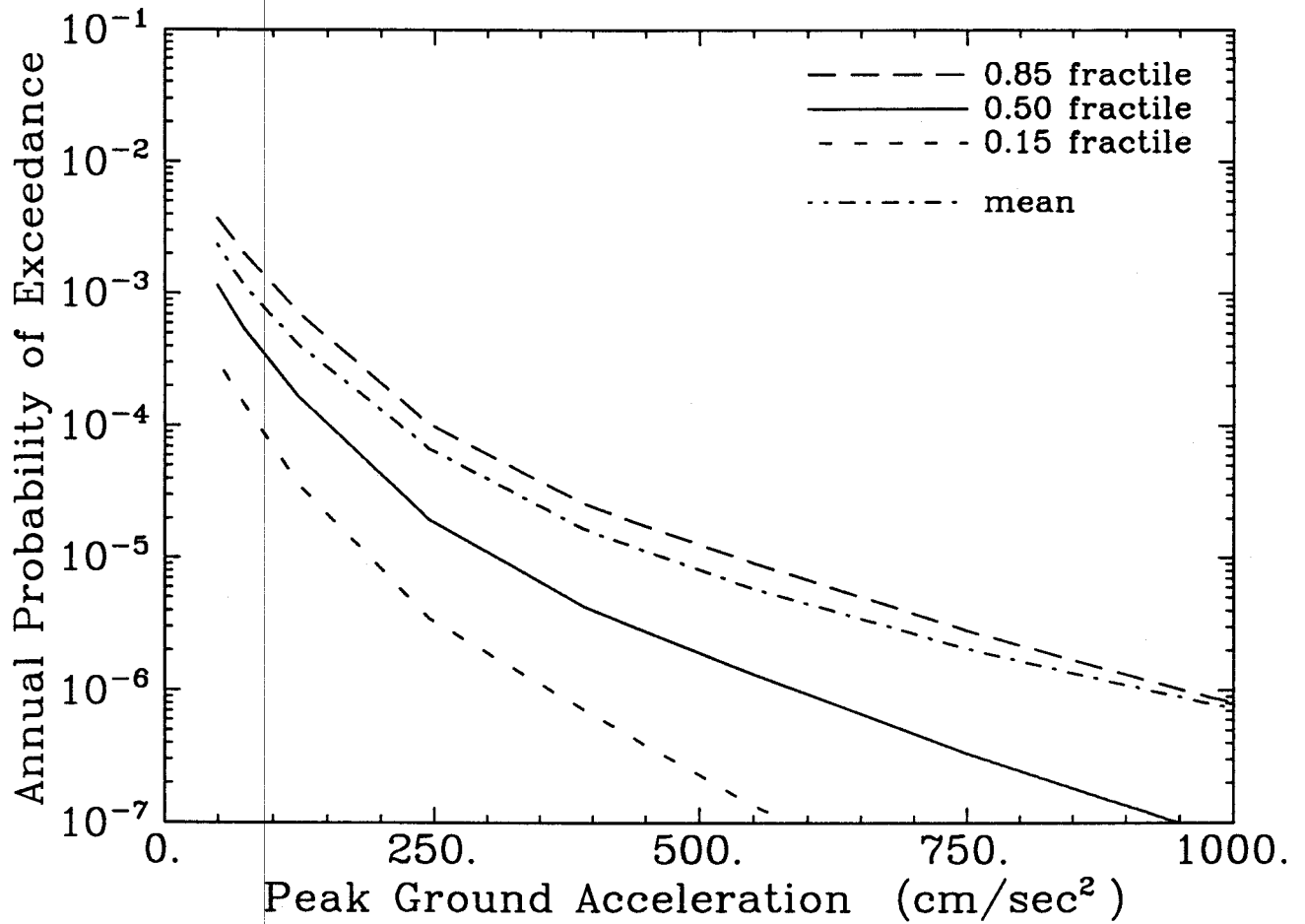


Figure A-10. Mean and fractile hazard curves calculated by combining results from LLNL (experts 1, 3, 10, and 12) and the EPRI teams. Each LLNL expert gets a weight of 1/8; each EPRI team gets a weight of 1/10.

SAVANNAH RIVER SITE
COMBINED LLNL(1,3,10,12) AND EPRI RESULTS

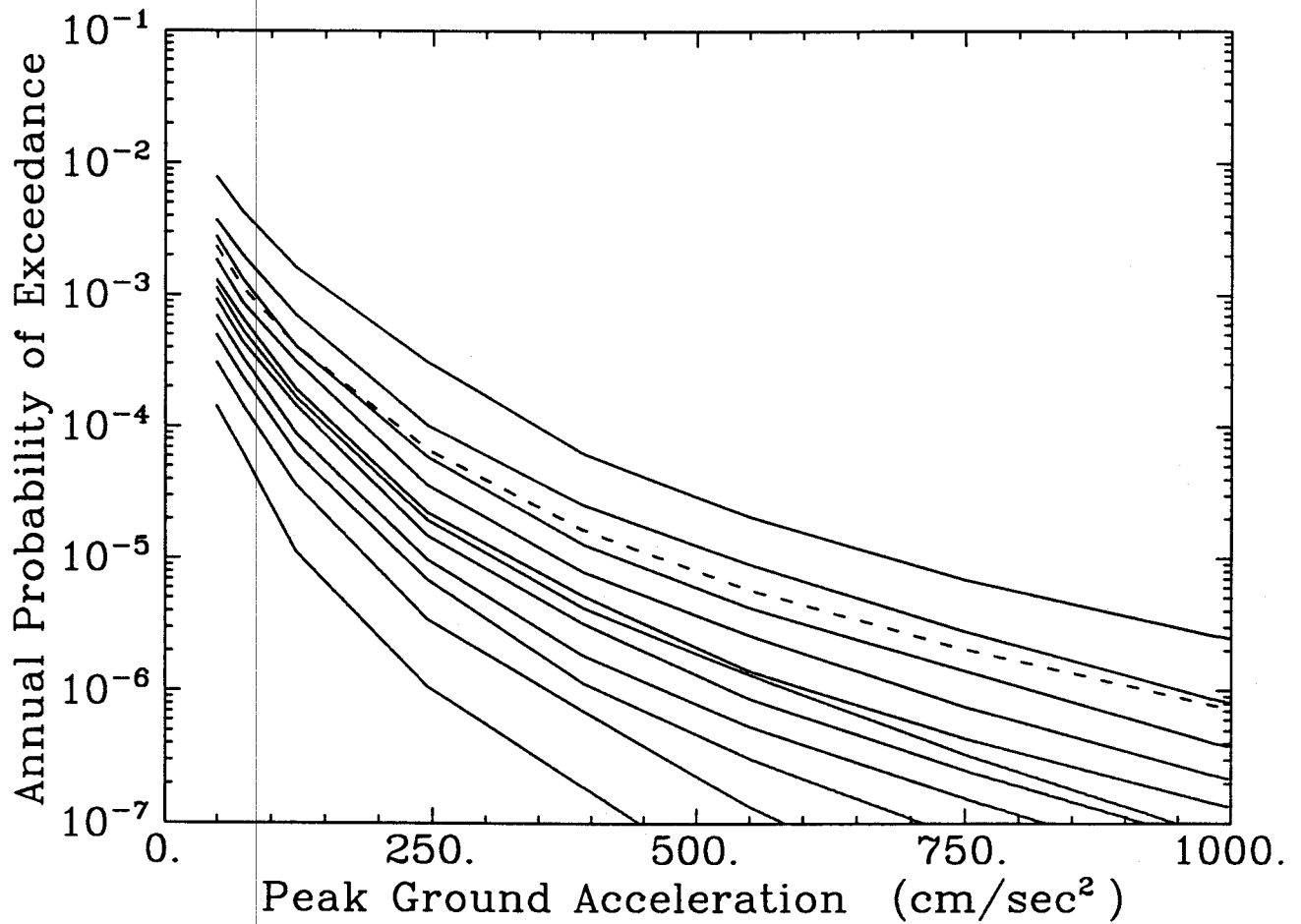


Figure A-11. Mean and fractile hazard curves calculated by combining results from LLNL (experts 1, 3, 10, and 12) and the EPRI teams—additional fractiles shown. Each LLNL expert gets a weight of 1/8; each EPRI team gets a weight of 1/10. The dashed line represents the mean hazard curve. The solid lines represent fractiles as follows: 0.05 (bottom), 0.15, 0.25, 0.35, 0.45, 0.50, 0.55, 0.65, 0.75, 0.85, 0.95 (top).